Adaptation of the South-Eastern drainage system under a changing climate
Water Availability

Matt Gibbs, Mahdi Montazeri, Bill Wang, Russell Crosbie, Ang Yang

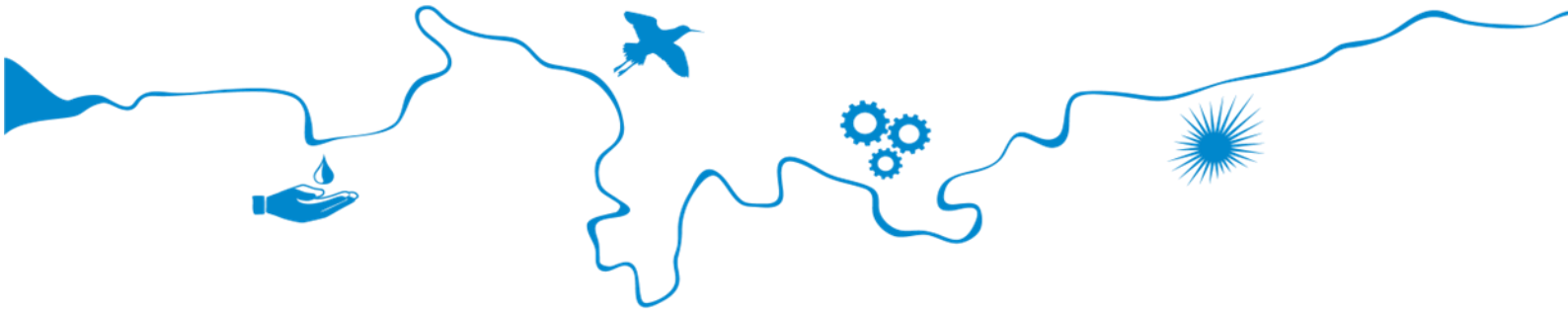

Goyder Institute for Water Research
Technical Report Series No. 25/3

www.goyderinstitute.org

Goyder Institute for Water Research Technical Report Series ISSN: 1839-2725

The Goyder Institute for Water Research is a research alliance between the South Australian Government through the Department for Environment and Water, CSIRO, Flinders University, the University of Adelaide and the University of South Australia. The Institute facilitates governments, industries, and leading researchers to collaboratively identify, develop and adopt innovative solutions for complex water management challenges to ensure a sustainable future.

This *Adaptation of the SE drainage system to a changing climate* project has been jointly funded by the Australian Government through the National Water Grid Fund, the Limestone Coast Landscape Board, and the South Australian Government. The project was delivered by the Goyder Institute for Water Research partners: CSIRO, the University of South Australia, Flinders University and the University of Adelaide in collaboration with the Limestone Coast Landscape Board, South Eastern Water Conservation and Drainage Board (SEWCD Board) and the Department for Environment and Water.

Enquires should be addressed to: Goyder Institute for Water Research
The University of Adelaide (Manager)
209A, Level 2 Darling Building, North Terrace,
Adelaide, SA 5000
tel: (08) 8313 5020
e-mail: enquiries@goyderinstitute.org

Citation

Gibbs MS, Montazeri M, Wang B, Crosbie R, Yang A (2025) *Adaptation of the South-Eastern drainage system under a changing climate - Water Availability for South East Drainage Adaptation*. Goyder Institute for Water Research Technical Report Series No. 25/3

Disclaimer

This report has been prepared by the CSIRO, Flinders University and the Lower Limestone Coast Landscape Board and reviewed in accordance with the publication protocols of the Goyder Institute for Water Research. The report contains independent scientific/technical advice to inform government decision-making. The independent findings and recommendations of this report are subject to separate and further consideration and decision-making processes and do not necessarily represent the views of the Australian Government or the South Australian Department for Environment and Water. The Goyder Institute and its partner organisations do not warrant or make any representation regarding the use, or results of the use, of the information contained herein about its correctness, accuracy, reliability, currency or otherwise and expressly disclaim all liability or responsibility to any person using the information or advice. Information contained in this document is, to the knowledge of the project partners, correct at the time of writing.

Contents

Figures

Tables

First Nations Respect and Reconciliation

The project partners, including CSIRO, Goyder Institute for Water Research and Limestone Coast Landscape Board, acknowledges the Traditional Custodians of the lands and waters of the Limestone Coast and South East region, where this project took place. Together we pay our respects to their Elders—past, present, and emerging—and recognise Aboriginal people as the First Peoples and Nations of South Australia, possessing and caring for these lands under their own laws and customs.

We respect the enduring cultural, spiritual, physical, and emotional connections that Aboriginal peoples maintain with their lands and waters. We recognise the diverse rights, interests, and obligations of First Nations and the deep cultural connections that exist between different First Nations communities. We seek to support their meaningful engagement and honour the continuation of their cultural heritage, economies, languages, and laws, which remain of ongoing importance.

We walk together with the First Nations of the South East and the Ngarrindjeri peoples through organisations such as Burrandies Aboriginal Corporation, Ngarrindjeri Aboriginal Corporation, the Ngarrindjeri Lands & Progress Aboriginal Corporation and South East Aboriginal Focus Group. For the work of generations past, and the benefit of generations future, we seek to be a voice for reconciliation in all that we do.

Project Summary

The Limestone Coast of South Australia is a highly modified landscape with an extensive cross-catchment drainage system converting what was once a wetland dominated landscape into one dominated by agricultural production. The region now has a diverse agricultural sector and extensive forestry plantations which are highly dependent on reliable rainfall and easy access to the region's substantial groundwater resources. However, as climatic conditions become hotter and drier it's important to understand impacts on ground and surface water resources and consequent risks to primary production and the environment to build a water secure future.

Achieving water security in the Limestone Coast region under a changing climate requires a more integrated and holistic approach to water resource management. In particular, the interactions between surface water and groundwater must be better understood, quantified, and managed to balance the seasonal demands—removing excess water from productive lands during winter while safeguarding groundwater-dependent agriculture and ecosystems during summer.

The "Adaptation of the South Eastern Drainage Network under a changing climate" project aims to inform opportunities to improve water management in the region - including potential use of water in the drainage network - to address risks to primary industries and groundwater dependent ecosystems. Delivered through the Goyder Institute for Water Research, research teams from the CSIRO, Flinders University and the University of South Australia have completed five separate but inter-connected tasks:

1. Quantifying the value of consumptive and non-consumptive uses of water
   This task assessed the value of additional water for key primary industries in the region, while also estimating the value of water for non-consumptive uses aimed at achieving ecological outcomes. Together, these valuations provide important context to the project's hydrological tasks, informing options to manage additional available water in the region.

2. Current and future water availability
   A water balance model for the region has been developed using the Bureau of Meteorology's Australian Water Resources Assessment – Landscape (AWRA-L) model. It integrates national and regional datasets to capture surface runoff, recharge, and soil moisture, while accounting for seasonal dynamics and regional variability. The model enables analysis of climate change impacts on the full water balance, providing insight into future water availability, supporting both short- and long-term water management decisions.

3. Groundwater and wetland modelling
   Site-specific models representing three-dimensional aquifer-wetland interactions have been developed for two key groundwater dependent sites. The models test the feasibility of changing the water distribution in the local landscape to improve ecosystem health and mitigate impacts of groundwater extraction. Options included redirecting / holding water back in drains, altering surface water inflows and reducing the extent of the wetland basin with levees. The learnings from modelling these two disparate sites will assist decisions to manage additional available water in the region.

4. Sea water intrusion risk
   The coastal area south of Mount Gambier is an area of high value irrigated agriculture and significant karst springs where the risk of seawater intrusion is of concern for both irrigators and environmental assets. This task set out to understand the extent and hydrodynamics of seawater intrusion in the region with an airborne electromagnetic survey of the south coast area, undertaken in October 2022, and construction of cross-sectional models to simulate seawater intrusion under different scenarios at different regional locations. This work provides the evidential basis to build on previous projects where reinstating wetlands by retaining water in drains appeared to effect some control over the seawater interface.

5. Groundwater, Ecology, Surface water and Wetland Assessment Tool (GESWAT)
   To enable opportunities to improve water management to be easily identified and investigated - including the potential use of water in the drainage network –a dynamic GIS tool (GESWAT) was built. GESWAT brings together outputs from the other project tasks integrating them in a tool with a range of other critical data (e.g. surface water flows, groundwater levels, and rainfall data, annual water use and allocation data, ecological information and other standard datasets). GESWAT provides the LC Landscape Board and its partner agencies a single platform with which to view, compare and interrogate the diversity of hydrological and ecological information available to inform policy and management decisions.

This report details results from Task 2 of the project.

Further results from this project are presented in the following reports:

Task 1

Cooper, C., Crase, L., Kandulu, J., and Subroy, V. (2025) *Adaptation of the South-Eastern drainage system under a changing climate – Quantifying the value of different water uses and future demands*. Goyder Institute for Water Research Technical Report Series No. 25/2

Task 2

Gibbs, M.S., Montazeri, M., Wang, B., Crosbie, R., Yang, A. (2025) *Adaptation of the South-Eastern drainage system under a changing climate - Water Availability for South East Drainage Adaptation*. Goyder Institute for Water Research Technical Report Series No. 25/3

Task 3

Gholami, A., Werner, A.D., Maskooni, E.K., Fan, H., Jazayeri, A., and Solórzano-Rivas, C. (2025) *Adaptation of the South-Eastern drainage system under a changing climate - Groundwater and wetland modelling*. Goyder Institute for Water Research Technical Report Series No. 25/4

Task 4

Davis A, Munday TJ, and Ibrahimi T (2025) *Adaptation of the South-Eastern drainage system under a changing climate - Limestone Coast Airborne Electromagnetic Survey: Acquisition, Processing and Modelling*. Goyder Institute for Water Research Technical Report Series No. 25/5.1

Davis A, Munday TJ, and Ibrahimi T (2025) *Adaptation of the South-Eastern drainage system under a changing climate - Limestone Coast Airborne Electromagnetic Survey: Conductivity-Depth Sections*. Goyder Institute for Water Research Technical Report Series No. 25/5.2

Gholami, A., Werner, A.D., Solórzano-Rivas, C., Jazayeri, A., Maskooni, E.K., and Fan, H. (2025) *Adaptation of the South-Eastern drainage system under a changing climate - Seawater intrusion risk*. Goyder Institute for Water Research Technical Report Series No. 25/5.3

Task 5

Gonzalez, D., Werner, A., Jazayeri, A., Pritchard, J., Fan, H., Botting, S., Judd, R. (2025) *Adaptation of the South-Eastern drainage system under a changing climate - Groundwater, Ecology, Surface water and Wetland Assessment Tool (GESWAT) Spatial Data Dictionary*. Goyder Institute for Water Research Technical Report Series No. 25/6

Executive summary

The Lower Limestone Coast region in South Australia contains a diverse and productive agricultural sector that supports the local economy and a number of regionally, nationally and internationally important wetlands. Over the past 160 years surface water drains have been constructed to remove water from the landscape that previously pooled against dune ranges to increase agricultural productivity and transportation, and more recently to manage dryland salinity. This extensive drainage led to a drastic reduction of wetland area which, in turn, minimised infiltration of recharge water to the unconfined aquifer. In the context of a future climate predicted to yield drier and warmer conditions, the historical drainage network may need to adapt.

In this context, this work aims at quantifying the water balance for the Lower Limestone Coast region, both historically and into the future. Previous water balances for the region have reported lumped annual averages for the region as a whole, or focused on specific components of the water balance, such as runoff or recharge. This work has developed an integrated water balance model that concurrently captures actual evapotranspiration, runoff and recharge, including seasonal dynamics and the variability across the region. The water balance outputs at a high spatial and temporal resolution are intended to help identify where there are opportunities to better manage water from the extensive drainage network in the region to address risks to primary industries and groundwater dependent ecosystems in the face of a changing climate.

The model selected for this study is the Australian Water Resources Assessment Landscape (AWRA-L) model that was developed to undertake water accounts and resource assessments in Australia. The model was designed to incorporate a broad range of observed and physical data, including climate, soil properties, topographic information and vegetation cover. The model configured to represent the water balance for the Lower Limestone Coast has a spatial resolution of 0.01° (approximately 1 km cell size), daily time step and represents five hydrological response units including deep and shallow rooted vegetation, irrigation areas, permanent water bodies, and impervious areas.

The model was calibrated to the high-quality streamflow gauges in the region that are not influenced by operation of the drainage network; remotely sensed leaf area index to provide an indication of actual evapotranspiration; remotely sensed soil moisture; and changes in recorded groundwater levels. The locally calibrated model was found to produce a suitable representation of annual runoff and recharge rates and calibrating to more than just streamflow data was found to improve the accuracy against all outputs, including streamflow in some cases.

Trends in the observed and modelled variables were analysed to set the context for projected future water availability. Trends of reducing rainfall and increased temperature have been observed in high quality datasets in the region and are in line with observations across the nation. 57 of 65 unconfined groundwater management zones had declining trends in recharge over time, with 31 of these statistically significant. All streamflow stations considered had declining trends identified, with 3 of 7 catchments producing statistically significant trends. This was not only driven by reduced rainfall, but the proportion of rainfall resulting in runoff was also observed to have reduced since the mid-1990s.

For future projections, a 2060 time horizon and medium emissions scenario (SSP 2-4.5) was considered, based on a time horizon not so distant that the assumptions represented by different SSPs have a substantial influence on the climate changes projected, and to be near enough to be within three iterations of water allocation plan reviews. 21 Global climate models (GCMs) from the IPCC's Sixth Assessment Report were identified that provide the outputs necessary for hydrological modelling and had been assessed as providing a suitable representation of past climate for the climate variables of interest in Australia. All GCMs selected projected a reduction in mean annual rainfall; Dry, Mid and Wet scenarios were selected to represent the range in projections. Despite a reduction in annual rainfall, the Wet scenario resulted in similar or increased runoff compared to the historical climate, due to the projected increase in winter rainfall from this GCM. The Mid and Dry GCMs resulted in relatively large reductions in runoff compared to the reduction in rainfall, with the slope of the relationship (or 'elasticity') of 4.2; that is, for a 1% reduction in rainfall on average, a 4.2% reduction in runoff was modelled. For recharge, the elasticity was lower at approximately 2 but possessed a

large variability in this result, with a range from 5-30% change in recharge for the Mid GCM rainfall reduction of 7%. This variability can be explained in part by the mean annual rainfall; the wettest zones above approximately 750 mm/year reduced by a proportion similar to the rainfall reduction, while in areas with a lower mean annual rainfall the proportional reduction in recharge increased.

Historical (1960-2021) and future water availability was represented as average water balances across different reporting zones. Actual evapotranspiration is by far the largest component of the water balance, with runoff the smallest at approximately 1 – 7% of mean annual rainfall. Gross recharge rates (all recharge to the groundwater store) were larger than the runoff in all zones, but net recharge rates (after evapotranspiration from groundwater) can be small, and in some zones negative, resulting in a declining storage level in the model.

Maps of mean annual runoff for the historical climate, represented by the 20th (dry), 50th (median) and 80th (wet) annual rainfall highlight the high annual variability of surface water availability in the region. Drought indices were used to investigate changes in the periods of low water availability, representing climatological, hydrological and agricultural droughts. Drought conditions were estimated to have occurred approximately 20% of the time historically across the catchments and drought variables, with the Wet future climate scenario remaining consistent with historical conditions for the drought indices. Drought conditions were projected to double to approximately 40% of the time for the Mid scenario, and over 50% of the time for the Dry scenario. Typically, hydrological (runoff) and agricultural (soil moisture) drought occur more frequently than climatological drought (rainfall) for the Mid and Dry future climate scenarios. In summary, trends in the observed data indicate water availability has been reducing in the region, and future climate projections indicate that this phenomenon is expected to continue. A dashboard has been developed to allow for further interrogation of the water balance and at specific wetlands across the region and throughout time.

Acknowledgments

This report covers one of five tasks undertaken as part of the *Adaptation of the SE drainage system to a changing climate* project. The project has been jointly funded by the Australian Government through the National Water Grid Fund, the Limestone Coast Landscape Board, and the South Australian Government. The project was delivered by the Goyder Institute for Water Research partners: CSIRO, the University of South Australia, Flinders University and the University of Adelaide in collaboration with the Limestone Coast Landscape Board, South Eastern Water Conservation and Drainage Board (SEWCD Board) and the Department for Environment and Water.

This work has relied on a significant amount of recorded data to investigate the water balance for the region, and a large number of people have supported the collection of these datasets. We would like to thank the following people for their time and effort to locate and provide these datasets and discuss their interpretation. Field measurements of actual evapotranspiration and soil moisture data were provided by Tanya Doody (CSIRO), Steve Gao (CSIRO), Edoardo Daly (WMAwater/Monash University) and Malcolm McCaskill (Victorian Department of Primary Industries). Insights and access to South Australian groundwater data was provided by Kent Inverarity (Department for Environment and Water) and surface water data by Peta Hansen (Department for Environment and Water). James Cameron (Department for Environment and Water) located the 2 m Digital Elevation Model for the region and associated hydrological processing of this dataset, and Cameron Wood (Department for Environment and Water) provided an early land use/land cover dataset. Discussions with Cameron Wood and Graham Green (Department for Environment and Water) were very informative to identify suitable climate projection scenarios.

Discussions with Sue Botting and Ryan Judd from the Limestone Coast Landscape Board have been instrumental to guide the direction and analysis of the results presented in this report. We also thank the leaders from other tasks involved in this project and their teams, Bethany Cooper, Adrian Werner and Tim Munday, as well as the support from Fiona Adamson and the Goyder Institute for Water Research.

This report was reviewed by Dr Julien Lerat (CSIRO), Dr Justin Hughes (CSIRO), Dr Daniel McCullough (Department for Environment and Water), Professor Holger Maier (The University of Adelaide), Sue Botting (Limestone Coast Landscape Board) and the Goyder Institute for Water Research Advisory Committee. Their comments and suggestions have greatly improved the rigour, clarity and interpretation of the work presented, and the authors are grateful for the time and insights provided.

1 Introduction

1.1 Adaptation of the South-Eastern drainage system under a changing climate project

The Limestone Coast Landscape region contains a diverse and productive agricultural sector that supports the local economy and a number of regionally, nationally and internationally important wetlands. These values are underpinned by the availability of good quality groundwater, but demand for good quality water is outstripping supply in some areas. The Lower Limestone Coast Water Allocation Plan (LLC WAP), which covers the southern part of the region, has reduced allocations for irrigators for some management areas to mitigate risks associated with the over-allocation of water resources and to achieve the broad environmental and social goals of the plan.

Climate change and increased water demand will put further pressure on existing water sources. Observations suggest that the Limestone Coast has already experienced a 1-5mm/year decrease in rainfall since 1960 compared to a mean annual recharge rate across the LLC WAP management areas of 106 mm/year. Declines in recharge rates in the order of 1 mm/year have been identified over the period 1970-2012 (Crosbie et al., 2013; Fu et al., 2019), which is expected to continue under future climate scenarios. Under an extreme wet scenario there may be no change to recharge, but under an extreme dry scenario there may be a 42% reduction by 2050, with similar patterns for surface water (Crosbie et al., 2013).

The Limestone Coast Landscape Board (LCLB) are seeking to identify whether there are opportunities to better manage water from the extensive drainage network in the region to address risks to primary industries and groundwater dependent ecosystems. The study area corresponds to the area of the Lower Limestone Coast and Padthaway Prescribed Wells Areas, as well as headwater catchments originating in Victoria, and collectively is referred to as the "region".

1.2 Current and future water availability task

Previous water balances for the region have reported lumped annual averages for the region as a whole (e.g. Harrington et al., 2015a), or focused on components of the water balance, such as runoff (Humphrey et al., 2016; Wood and Way, 2011) or recharge (Doble et al., 2015; Harrington et al., 2015a). A water balance that concurrently captures all significant output components, incorporating seasonal dynamics as well as the variability across the region, is a current knowledge gap limiting both short- and long-term management.

Studies on the effects of climate projections on water availability for the region are limited. Denny et al. (2015) considered wetland vulnerability to groundwater decline and a case study focused on the Drain L system, while national scale changes in recharge with climate projections have also been undertaken (Crosbie et al., 2013). Consequently, an analysis of the impact of contemporary climate projections for the complete water balance across the region is needed.

The key management questions that will be addressed in this report are:

- How do components of the water balance (runoff, recharge and actual evapotranspiration) vary over time and across the region?
- At which locations, and under which conditions, is there water available in the drainage network to support further water uses (e.g. diversion for environmental restoration or to maintain consumptive use)?
- How might the water availability change with future climate projections?

1.3 South-Eastern drainage system

Water availability in the southeast of SA has had a complex history. Across most of the region, there is not enough topographic gradient for channelised creeks to form naturally and instead wetlands formed along the eastern side of dune ranges, deposited by successive retreat of sea level over the past 700,000 years. This resulted in around 50% of the region being seasonally or permanently flooded wetland habitat. Drainage commenced in the 1860s to remove water for agricultural productivity and transportation, and more recently to manage dryland salinity. Following drainage, less than 6% of the original wetland extent remains, with most of the remnant wetlands in poor condition (South East Natural Resources Management Board and South Eastern Water Conservation and Drainage Board, 2019). Drainage has also minimised recharge to the unconfined aquifer in the vicinity of what was once wetland, and deeper drains were designed to increase groundwater discharge to manage dryland salinity.

A map of the drainage network and key wetlands is provided in Figure 1-1. The flow monitoring network (reviewed in Section 2) indicates that higher volumes of water available in the drainage network is concentrated in the downstream section of the main drainage catchments closer to the western coast. There is comparatively little surface water available in the eastern and southern portion of the region where water demand may be higher (IGS, 2023), with the predominant water uses of irrigation and plantation forestry (see Brookes et al., 2017) are also represented on Figure 1-1. The drainage catchments have already been extensively modified to support environmental water requirements over the past few decades, including:

- Blackford Drain - the South East Flow Restoration Project (toward the Taratap drain in Figure 1-1) constructed a drain to direct flow out of the Blackford Drain toward the Coorong, with the capability to also divert water to wetlands enroute (Taratap watercourse and Tilley Swamp). Also, drains in the north of the region have high salinity that may not be suitable for productive or environmental use, with the average salinity over 8500 and 12,500 EC in the Fairview Drain and the Blackford Drain, respectively.
- Drain L - a regulator is currently being constructed at the outlet of Lake Hawdon North, designed to maintain water in that wetland. The receiving system of the Robe Lakes at the end of Drain L also has water requirements to maintain water quality and aesthetic values. Numerous studies have investigated the feasibility of diverting water out of the Drain L catchment (and previously also Drain M) toward the Blackford Drain and in turn the Coorong, most recently the Healthy Coorong Healthy Basin Project (Tonkin, 2020). These studies have found the water available and resulting ecological benefit is unlikely to justify the construction and operation and maintenance costs.
- Drain M – Drain M has significant existing environmental water requirements associated with the Ramsar-listed Bool and Hacks Lagoons, as well as to maintain Lake George at the end of the drain, which has a nominal water requirement of 20 GL/year. This volume has passed the monitoring station at the end of Drain M upstream of Lake George (A2390512) eight times in the last 30 years. As part of the Restoring Flows to Wetlands in the Upper South East (REFLOWS) project, the Western Floodway was constructed in 2006 to divert excess flow from Drain M into the Bakers Range watercourse to the north, however there have been limited opportunities to use the drain since construction given existing environmental water requirements and the limited volumes available.
- Reedy Creek - Mount Hope Drain – has Lake Frome as a downstream receiving water. Diverting flow from this drain into Drain M to support the volume commitments to Lake George has been proposed (South East Natural Resources Management Board and South Eastern Water Conservation and Drainage Board, 2019).

To quantify the water balance components and water availability across the region, the Australian Water Resources Assessment Landscape (AWRA-L) model has been used. This model has been customised and calibrated to be applicable to the region, with a detailed review of the data used as inputs, or calibrate parameters based on outputs, in Section 2. The calibration approach and resulting model performance is presented in Section 3. The data available and model outputs are then used to quantify historical water availability and trends over time in Section 4, before future climate projections are selected and applied in Section 5. These results provide information to inform how the water management, and management of the drainage network, may need to continue to adapt with a changing climate.

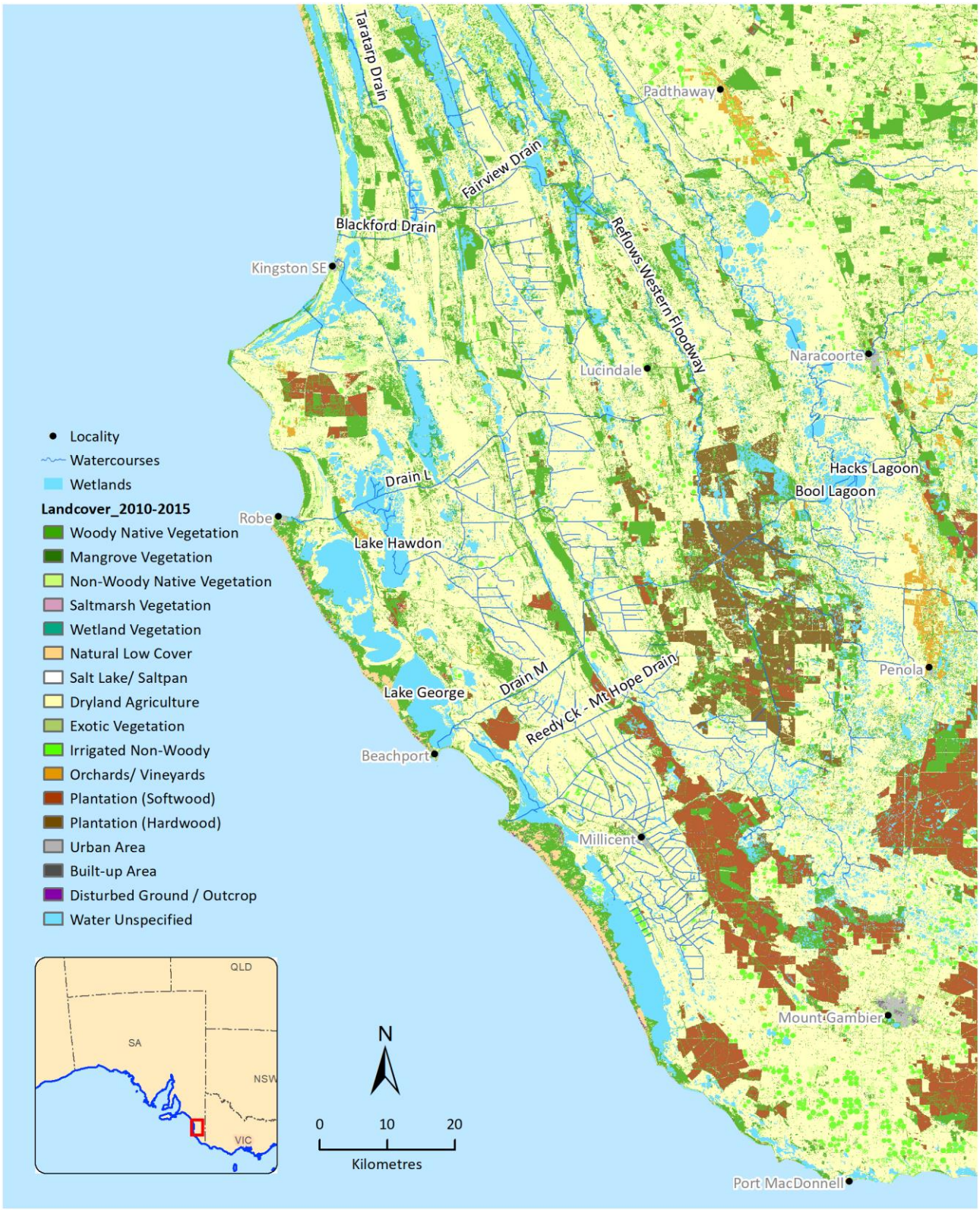

Figure 1-1 Map of the study region, including South-Eastern drainage system, wetlands and land cover as mapped over 2010-15 (Willoughby et al., 2018)

2 Data Review

This section first provides an overview of the AWRA-L model used in this study, to provide context for the datasets that are required to undertake the water balance. Then data sets available for the region that may be used to update the national scale datasets based on local scale information are evaluated. This section also reviews data available to use as targets to calibrate the water balance model outputs.

2.1 Australian Water Resources Assessment Landscape model

Landscape models provide consistent estimates of runoff, soil water content, deep drainage and evapotranspiration across a large region. The Australian Water Resources Assessment Landscape (AWRA-L) model has been developed for this purpose by the Bureau of Meteorology and CSIRO over the last decade (Frost et al., 2018; Van Dijk, 2010). The model was designed to support the Bureau's requirement to undertake national water accounts and resource assessments under the Water Act (2007). AWRA-L is a hybrid physical/conceptual model that accepts gridded inputs of climate, soil properties, topographic information and vegetation cover. The structure of AWRA-L is guided by the desire to incorporate a broad range of observed and physical data, thereby providing more robust water balance estimates. Outputs from AWRA-L include surface runoff, soil moisture, evapotranspiration, and deep drainage (recharge), which correspond to the water balance outputs of interest. The model has been developed for undertaking water resource assessment in Australia and has been adopted as the modelling system for this project.

The conceptual structure of AWRA-L is shown in Figure 2-1 (Frost et al., 2018). Runoff in AWRA-L is generated via infiltration excess overland flow, interflow between soil layers, groundwater flow from the groundwater store to the stream, and saturated overland flow from groundwater saturated areas. These processes are represented across three soil layers: Top 0-10 cm, Shallow 10-100 cm, and Deep 100-600 cm soil. The layers used in the national scale model, along with the units; brief description about source data from which each of the layers are derived; and the processing techniques used to generate the layers are outlined in Appendix A. The model has 21 calibration parameters that are used to scale the values of the spatial inputs.

At a national scale the model runs on a daily timestep and 0.05° grid (approximately 5 km cell size) simulating the landscape water balance for Australia from 1911 with results up to yesterday provided online (https://awo.bom.gov.au/). Vaze et al. (2018) developed a 0.01° grid model; while not practical to run at a national scale, the higher resolution model demonstrated improved performance for a case study in the Murrumbidgee catchment (Vaze et al., 2017). Vaze et al. (2016) increased the number of Hydrological Response Units (HRUs) from two—representing deep and shallow rooted vegetation—to five, adding irrigation areas, permanent water bodies, and impervious areas.

The five HRU model with the higher resolution grid has been used in this work given the region specific (as opposed to national) application; existence of irrigation areas in the region (predominantly vineyards and centre pivot); frequent changes in spatial model inputs (e.g., land cover); and improved process representation provided by the 0.01° grid model.

Topographic data is required to delineate catchments, to aggregate the cell-based output from AWRA-L to represent how runoff will accumulate. Identifying this direction of flow is non-trivial in the very flat and highly modified landscape of the region, and previous catchment delineation used in this work is summarised in Section 2.2. Each grid cell in AWRA-L has a hypsometric curve and mean slope specified, which has been updated based on the high-resolution topographic information available in the region. This is used with groundwater depth estimates to generate saturated overland flow within each grid cell.

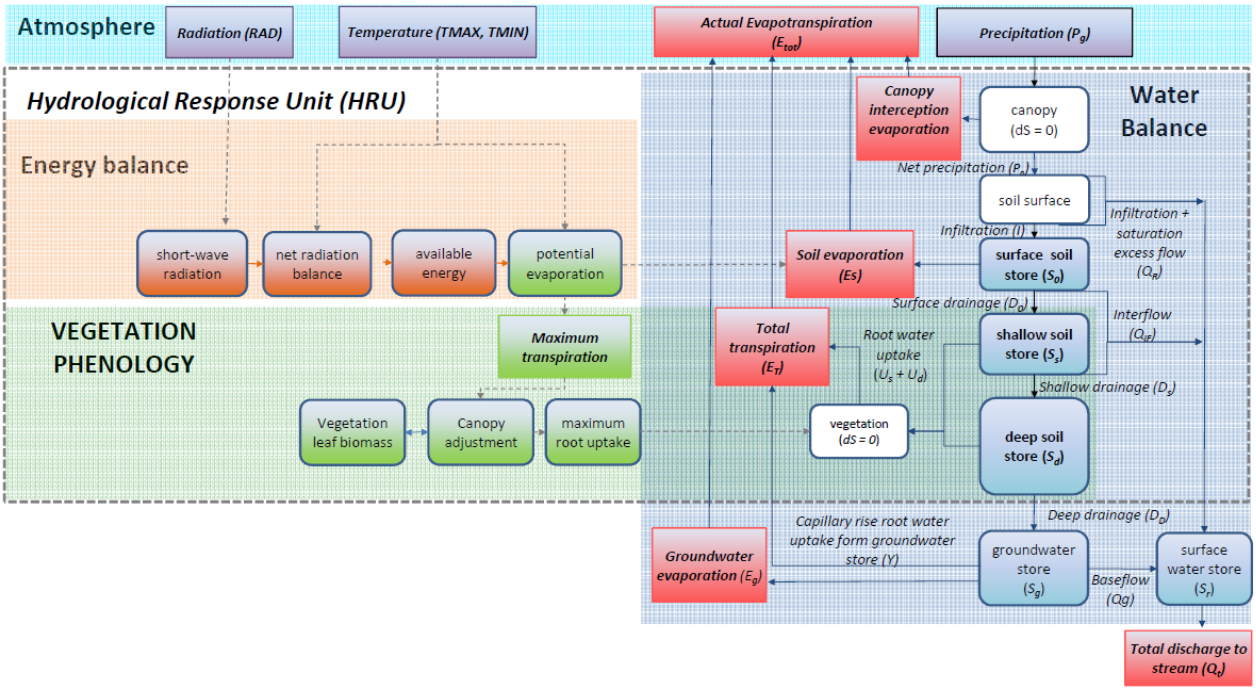

Figure 2-1 AWRA-L conceptual structure, reproduced from Frost et al. (2018). Purple boxes are climate inputs; blue rounded boxes represent water stores; red boxes are calculated water flux outputs; brown rounded boxes represent the energy balance; and green rounded boxes: vegetation processes.

Other AWRA-L input data can be classified as meteorological variables, vegetation variables, surface properties, and soil properties:

- Meteorological inputs (purple boxes in Figure 2-1) include precipitation, incoming shortwave radiation, maximum and minimum temperature, and wind speed. Precipitation is a significant driver of water availability and reviewed in Section 2.3.1.
- Vegetation properties include fraction of tree cover, leaf area index and vegetation height. These inputs are involved in the vegetation phenology component of the model, as well as specifying the proportions of the different hydrologic response units within each cell. Data to inform these components of the model are reviewed in Section 2.3.2.
- Soil properties are generally related to the saturated hydraulic conductivity and water storage capacity and clay content of each soil layer, reviewed in Section 2.3.3. These parameters are used to configure the water holding capacity and drainage rates between the water stores in the model (blue rounded boxes in Figure 2-1).

A number of studies have calibrated AWRA-L to multiple datasets concurrently. Azarnivand et al. (2022) used a multi-objective approach to calibrate the model to streamflow, remotely sensed actual evapotranspiration, and top layer soil moisture. In multi-objective optimisation there are trade-offs between the objective functions, where selecting parameter values that improve the model performance against one objective results in reduced model performance against another objective. Azarnivand et al. (2022) found the largest trade-off was between the runoff and soil moisture components, where selecting the best model for one component (e.g. total runoff) resulted in poorer performance for the other component (soil moisture, and vice-versa). Viney et al. (2015) applied a similar joint calibration to multiple components of AWRA-L and found a similar result that improving performance of all components of the model inevitably came at the expense of metrics representing streamflow accuracy. A more accurate representation of the full water balance may result in more valid extrapolations from the historical climate to scenarios considering climate projections. This concept will be explored further in this project, where there is expected to be value in an accurate representation of the full water balance for the region given the large component of recharge and groundwater use in the region. Datasets that can be compared to model states and outputs (see Figure 2-1) to calibrate parameter values are reviewed in Section 2.4, including:

- streamflow data, directly related to the total discharge to stream model output,
- groundwater level, related to the groundwater store and changes in groundwater level related to deep drainage,
- remotely sensed soil moisture is expected to represent the storage in the surface soil store,
- remotely sensed actual evapotranspiration could be related to the actual evapotranspiration model output, and
- remotely sensed leaf area index is a component of the vegetation leaf biomass (green rounded box in Figure 2-1), which then in turn influences the modelled transpiration and actual evapotranspiration.

2.2 Topographic data

2.2.1 Elevation data

AWRA-L contains input grids to represent the average slope within a grid cell, and to quantify the hypsometric curve, a cumulative density function of sub-grid elevation data. The hypsometric curve is used to determine the proportion of the groundwater storage that is connected to the lowest drainage point in the grid cell (Peeters et al., 2013). These AWRA-L input grids have been updated based on the 2 m Digital Elevation Model (DEM) available for the region.

The DEM of the South East (Figure 2-2) was developed from aerial LiDAR (Light Detection and Ranging) imagery flown by AAM Hatch as part of the National Water Initiative (NWI), which aimed to develop a flow strategy for the South East of South Australia. The LiDAR data was validated by a ground-based network of differential GPS stations. The accumulated data was processed into grid formats at 2 m with vertical accuracy of 0.15 m.

2.2.2 Catchment delineation

Wood and Way (2011) undertook a catchment delineation process using ArcGIS Hydro data model. A coarser 10 m South East DEM was pre-processed further in order to be used as input to Arc Hydro's terrain processing functions. The purpose of the pre-processing was to ensure that the physical features of the landscape that direct water flow such as the South East drainage network, embankments and bunds were adequately replicated in the DEM. Pre-processing included filling voids in the DEM to prevent artificial internally draining catchments; drainage lines were digitised and "burnt in" to the DEM; "walls" were built to reinforce the presence of embankments; and "sinks" were created to represent the terminus of known internally draining catchment systems.

Arc Hydro was used to derive flow direction and flow accumulation layers, which are integral to all subsequent analysis. Flow accumulation plays an important role in the derivation of stream networks. Figure 2-3 shows the flow accumulation raster layer for a section of the region (Way and Wood, 2011), which in turn was used to derive drainage lines. Segmentation of the drainage lines was undertaken to allow the identification of junctions in the drainage network and ensure calculations at locations of interest (e.g., at gauging stations). Once drainage lines have been delineated and segmented, catchment polygons can be defined. The flow direction raster and segmented drainage lines are required to perform this task, with an example shown in Figure 2-4.

2.2.1 Model domain

The catchment delineation outlined above was used to inform the domain for the AWRA-L model. The boundary of the LLC PWA was used as a starting point, extended to also include the adjacent groundwater management zones of Pathway PWA and the South Australia-Victoria Border Agreement Zone. The domain was further extended to include the full contributing catchments of Mosquito Creek, Naracoorte Creek, and Drain C. The resulting model domain is presented in Figure 2-5.

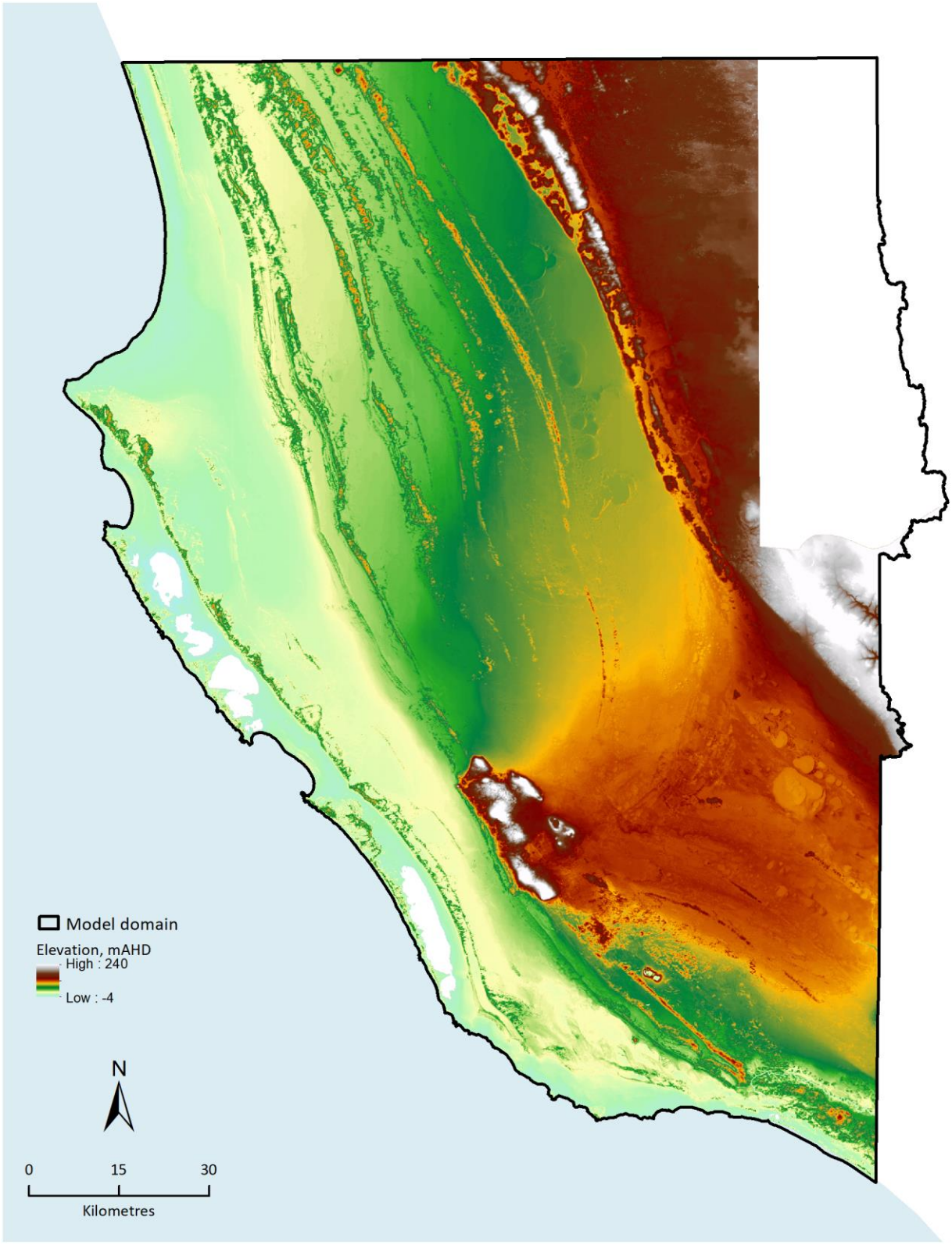

Figure 2-2 2m resolution Digital Elevation model (DEM) available for the region. In the north east of the domain data from Wimmera Catchment Management Authority was used for catchment delineation (Wood and Water, 2011).

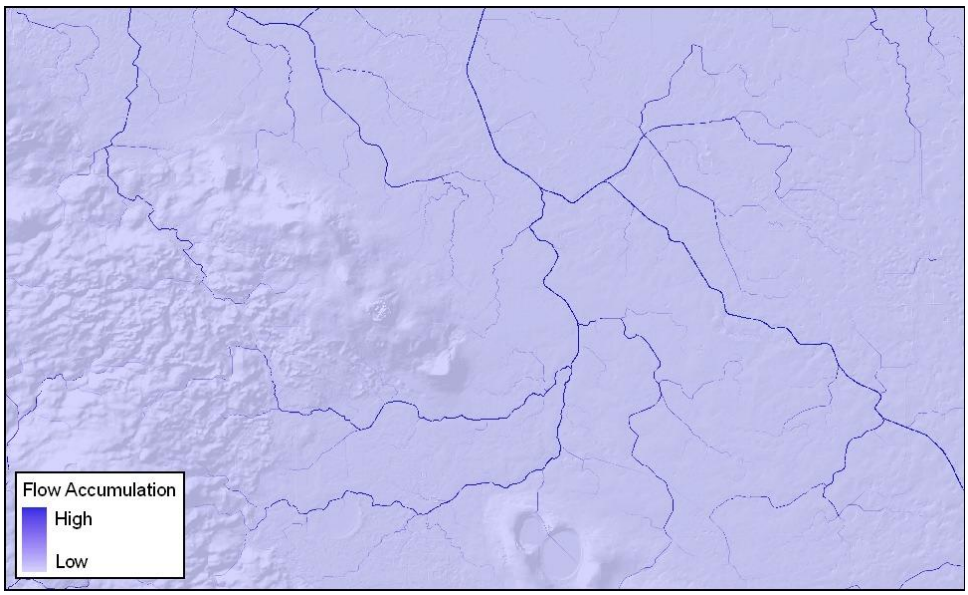

Figure 2-3 Sample flow accumulation derived from SE 10 metre DEM (Wood and Way, 2011)

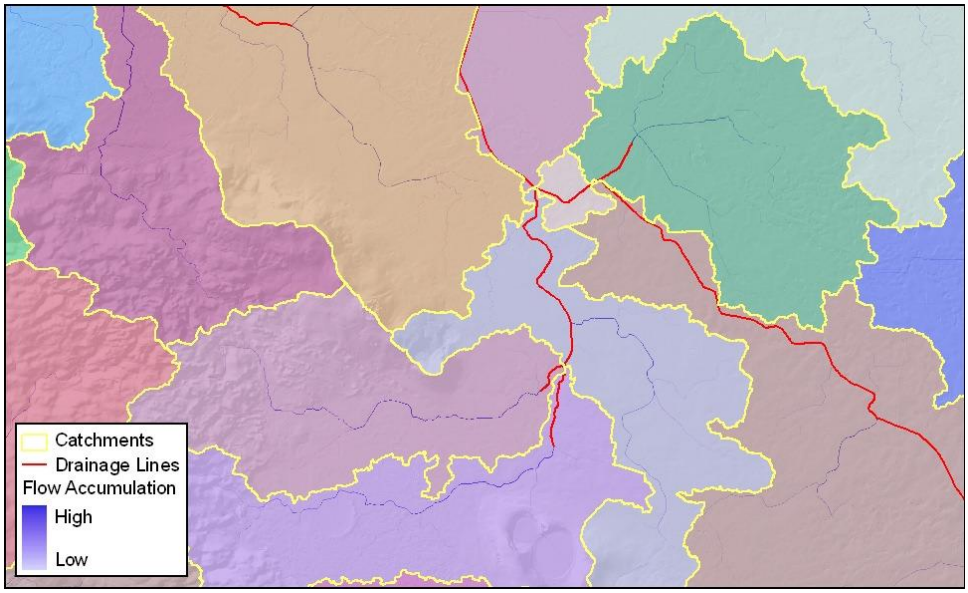

Figure 2-4 Derived catchments, drainage lines and flow accumulation (Wood and Way, 2011)

Figure 2-5 Adopted AWRA-L model domain, based on the Lower Limestone Coast Prescribed Wells Area, including the South Australia – Victoria Border Agreement Zone

2.3 Spatial AWRA-L inputs

2.3.1 CLIMATE

The South East of South Australia has good spatial and temporal coverage of rainfall stations (Figure 2-6), with daily rainfall records available from as early as 1860. For data review and quality assurance, rainfall data was sourced from the SILO patched point dataset (Jeffery et al., 2001). This dataset was derived from Bureau of Meteorology data, with missing data infilled using interpolated values. Analysis of daily rainfall data was carried out for this study using the *SWTools* R package to assess quality and homogeneity of data (Gibbs et al., 2024).

Table 2-1 lists 11 SILO stations selected for analysis that cover the region with long term observed data. The Robe and Mount Gambier Aero stations are part of the Bureau of Meteorology's high quality rainfall station network, suitable for climate change studies (see Section 4.1.2). Where a station was established post-1889 or closed, data has been interpolated using a nearby station. Interpolated data is shown with orange colour, and recorded data is shown with dark green colour in Figure 2-7.

Table 2-1 List of high-quality SILO stations within the model domain.

Site	Station	Percent missing	Mean annual rainfall (mm)	Elevation (m AHD)	Established	Closed
Beachport	26000	7.49	702	9	1881	-
Millicent	26018	12.22	748	20	1877	-
Robe	26026	1.04	636	3	1860	-
Kingston SE	26012	6.68	575	7	1875	-
Lucindale Post Office	26016	6.29	601	30	1879	-
Frances	26007	2.2	517	103	1889	-
Penola Post Office	26025	9.71	646	62	1861	-
Lake Leake (Kooeeyong)	26014	9.63	827	105	1892	-
Naracoorte	26023	17.81	566	58	1868	2001
Cape Northumberland	26005	14.44	715	5	1864	2006
Mount Gambier Aero	26021	34.84	729	63	1941	-

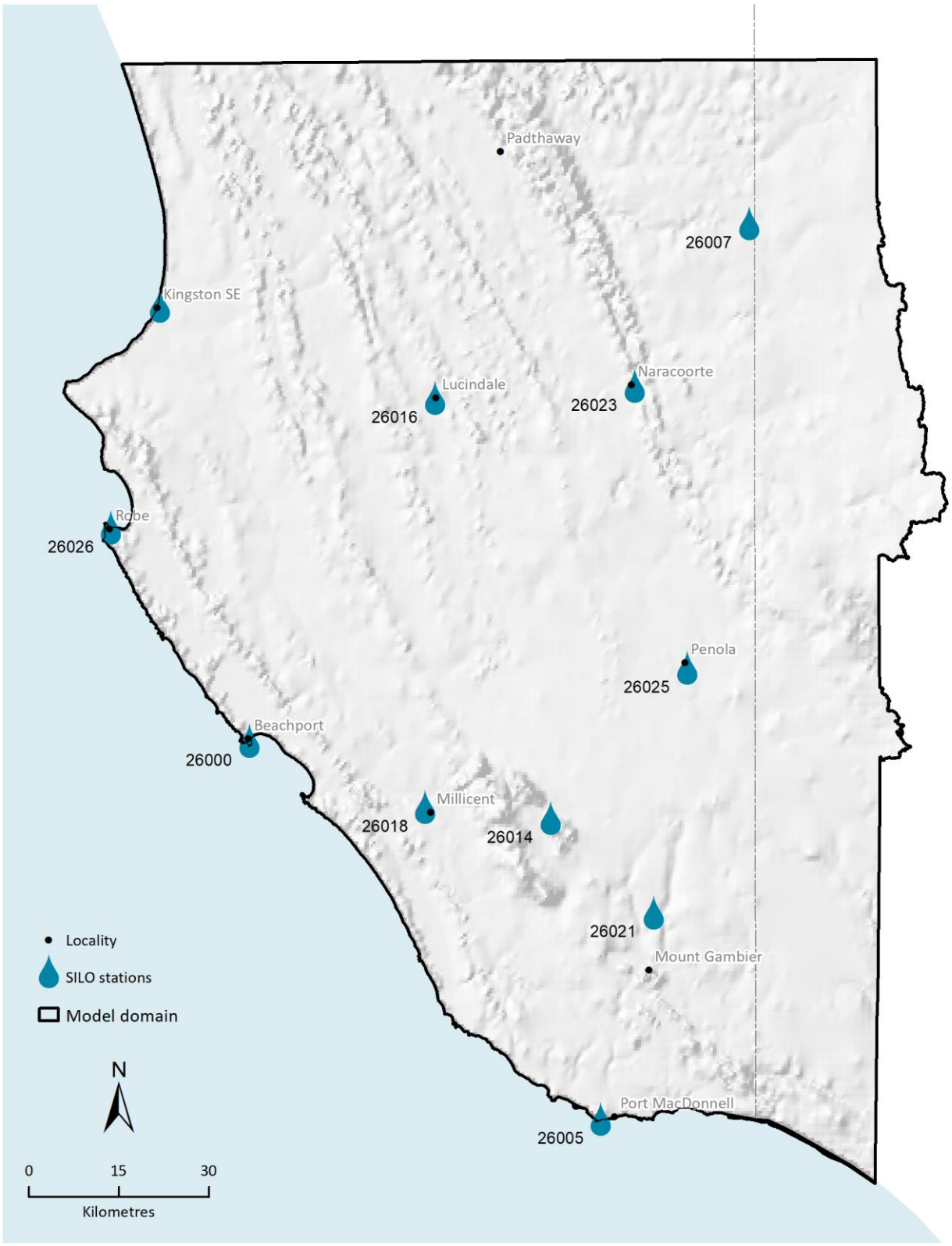

Figure 2-6 High quality rainfall stations across the region

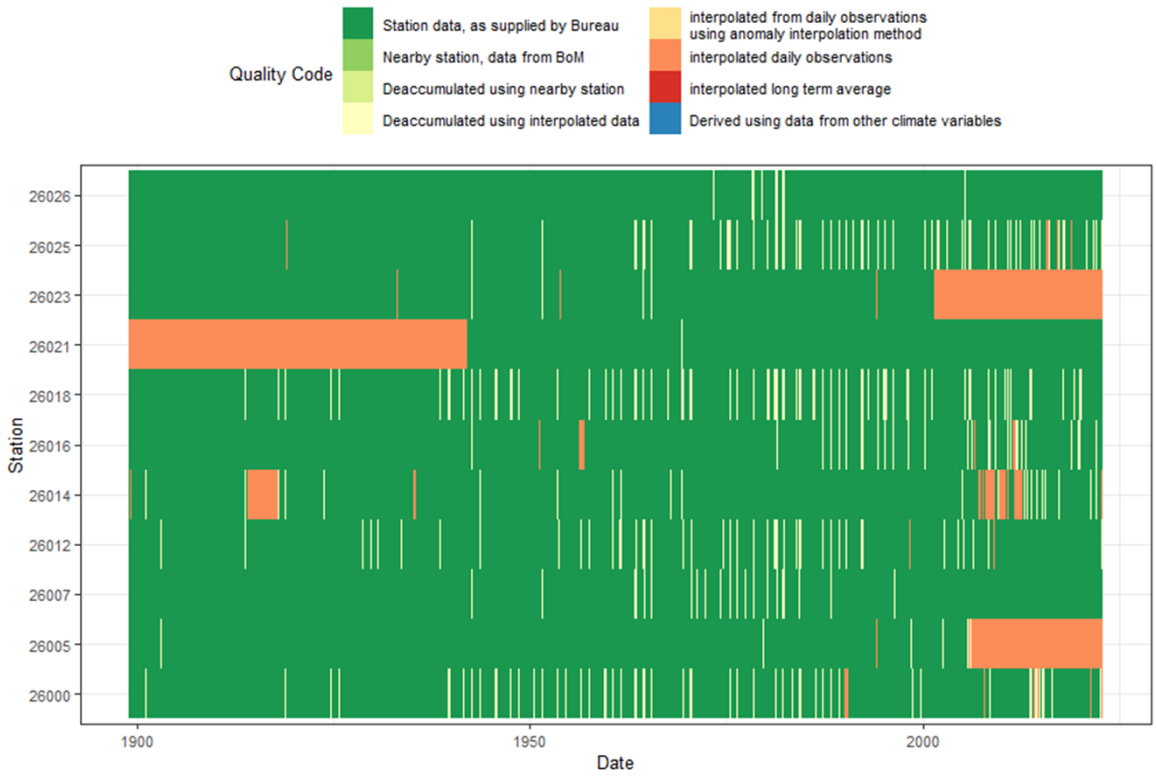

Figure 2-7 Data quality codes for each rainfall station

The monthly rainfall and Morton's wet environment areal potential evapotranspiration (PET) at 11 sites can be seen in Figure 2-8. The box plots represent the variability in monthly rainfall and solid lines the monthly average PET. The whole period of the SILO rainfall record (1889–2022, inclusive) was used to produce the plot in Figure 2-8, and all stations exhibiting the same trend over this period. Typically, rainfall exceeds PET from May to August-September, with the rest of the year typically water limited with more PET than rainfall.

The annual rainfall at each of the 11 sites is presented in Figure 2-9, including a 5-year rolling average trend. An overall decreasing trend of annual rainfall can be observed for 7 out of 11 sites. The biggest reduction in annual rainfall was observed at site 26012 (Kingstone SE) with the slope of -1.17 mm/year. A Mann-Kendall test has been used to test for any statistically significant monotonic trend over time, with the p value of the test included in Figure 2-9. Values of $p<0.05$ are typically accepted as statistically significant, indicating that following the hypothesis that there is no trend over time in the data that can be rejected at a 95% confidence level. Given the high variability in rainfall from year to year, most of the trends were not determined to be significant, but three stations across the northern part of the region including Kingston (26012), Lucindale (26016), and Naracoorte (26023) did have statistically significant trends, with reductions in rainfall of -0.7 to -1.2 mm/year based on the slope of a linear regression. Fu et al. (2019) found statistically significant negative correlations between time and both the amount of groundwater recharge as well as the percentage of annual rainfall that resulted in recharge, implying that both recharge and its percentage of rainfall had a decreasing trend over the period considered in that study (1970-2012).

For the purposes for inputs to AWRA-L, the 0.01° resolution Australian National University (ANU) Climate (GH70) v2 product has be used (https://dx.doi.org/10.25914/60a10aa56dd1b). This product is based on the rainfall station data presented in this section but has a resolution that matches the 0.01° AWRA-L model, compared to other coarser products available, such as SILO (Jeffrey et al., 2001) or AWAP (Jones et al., 2009).

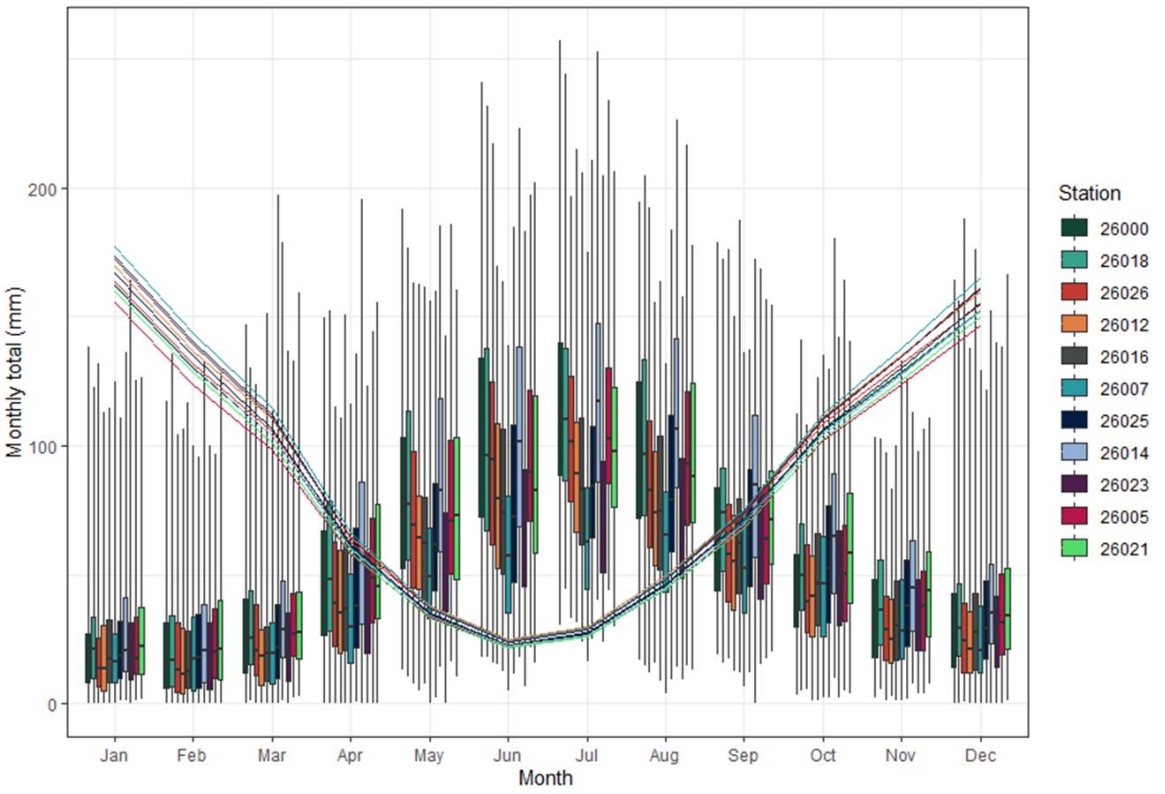

Figure 2-8 Monthly rainfall at each station as boxplots and the mean monthly potential evapotranspiration as a line

Figure 2-9 Annual rainfall (green) and 5 year rolling average (blue line) rainfall at each station

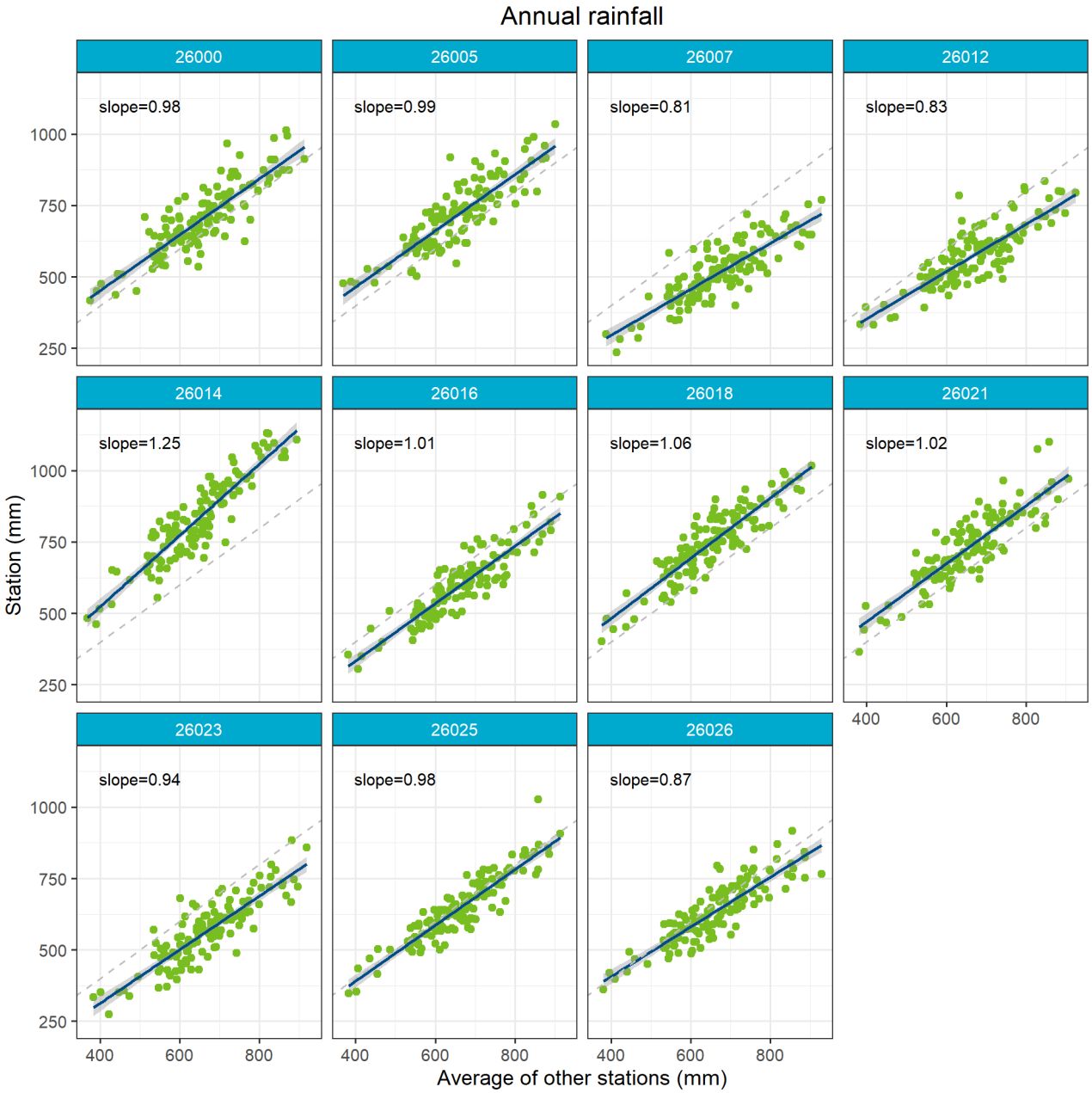

Figure 2-10 Comparison of annual rainfall at each station with the average of annual rainfall from other stations

2.3.2 HYDROLOGICAL RESPONSE UNITS

AWRA-L originally had two hydrological response units (HRUs), to represent the different streamflow responses of shallow and deep-rooted vegetation within each grid cell. The main difference between these two HRUs is that the shallow rooted vegetation has access to subsurface soil moisture in the two upper soil stores only (top 1m of soil in the current implementation), while the deep-rooted vegetation could also transpire moisture in the deep store (top 6m of soil). Vaze et al. (2016) extended the model to include three additional HRUs including impervious areas, irrigated agricultural areas, and large water bodies. Hydrologically, these five HRUs differ in their aerodynamic control of evaporation; in their interception capacities; and in their degree of access to different soil layers. The methods used to model the irrigated hydrological response unit are very similar to the shallow rooted hydrological response unit, however there is an additional provision in this HRU to apply irrigation water.

The proportion that is occupied by each of the 5 HRUs within an AWRA-L grid cell is set to a value obtained from a configuration layer. In reality, these proportions are not fixed as land use changes over time. Changes in land use have not been represented in AWRA-L previously, and this functionality has been developed as part of this project.

The South Australian Land Cover Layers (Willoughby et al., 2018) represent land cover in five-year epochs over the Landsat record from 1987 to 2020. These layers provide a consistent-through-time, whole-of-state, spatial land cover data set and include classifications related to each of the AWRA-L HRUs. Digital Earth Australia (DEA) have a similar land cover product based on Landsat imagery (Lucas et al., 2019). This data product is available at an annual time step, however, does not include an irrigated agriculture classification. Inspection of the annual layers also revealed the land cover classification in the DEA dataset had large, unrealistic changes in land cover from year to year, likely due to vegetation response to rainfall, resulting in different land cover classification. Hence, the SA land cover layers have been preferred as the land cover data source where available (i.e., in SA), and the DEA product is used in Victoria. For the DEA product, the median land cover for each 25m pixel in each 5-year period, corresponding to the SA land cover product, was taken to provide a consistent time step in the land cover layers and to remove some of the year-to-year variability. For the irrigated areas in the Victorian portion of the region, the national scale AWRA-L model was used and hence was assumed to not change over time. The mapping from each land cover classification to the proportion of HRU, based on 25 m land cover pixels to each 1km AWRA-L grid cell, is outlined in Table 2-2. For estimates of land use that predate the Landsat era, Harrington et al. (2015b) interpreted aerial photographs and irrigation bore drilling records to create a 1969 land use map. A 1983 land use map was also created, based on the 1969 map and modifying areas affected by bushfires in 1983. The 1983 map has not been used for the purpose of AWRA-L HRUs, given it is near the start of the Landsat satellite record (1987) and the satellite-based product is preferred to provide a consistent approach over the majority of the calibration period. The resulting HRU proportions over time are presented in Figures 13-16, where there are changes in the proportion of deep-rooted vegetation and irrigated areas in some pixels over the 1990-2020 period.

Table 2-2 Mapping from land cover product to proportion of AWRA-L hydrological response units

AWRA-L HRU	South Australian Land Cover	Digital Earth Australia Land Cover	1969 Land use
Water	water unspecified	water_seasonality = semi-permanent or permanent	water
Impervious	urban area, built-up area	level 3 = artificial surface or natural bare surface[1]	intensive uses (mainly urban), rural residential, mining and waste
Irrigated agriculture	irrigated non-woody, orchards or vineyards	none (existing AWRA-L)	irrigated cropping, irrigated pastures, irrigated horticulture, interpreted irrigation, crop or irrigation
Deep rooted vegetation	woody native vegetation, mangrove vegetation, plantation (softwood), plantation (hardwood)	Lifeform = woody vegetation	nature conservation, hardwood plantation, dryland horticulture, softwood plantation, native vegetation, scattered native vegetation, young forestry (seedling), production forestry, interpreted dryland vineyard, young forestry (almost closed canopy)
Shallow rooted vegetation	non-woody native vegetation, saltmarsh vegetation, wetland vegetation, natural low cover, salt lake or saltpan, dryland agriculture, exotic vegetation, disturbed ground or outcrop	remaining proportion not classified as other HRUs	other minimal use, grazing modified pastures, dryland cropping, cleared or modified pasture, interpreted crop, land in transition, intensive animal and plant production, grazing native vegetation, recently cleared, cleared for forestry, other protected areas

[1] On inspection of pixels within Mount Gambier and Millicent, the “natural bare surface” classification corresponded to areas expected to be impervious

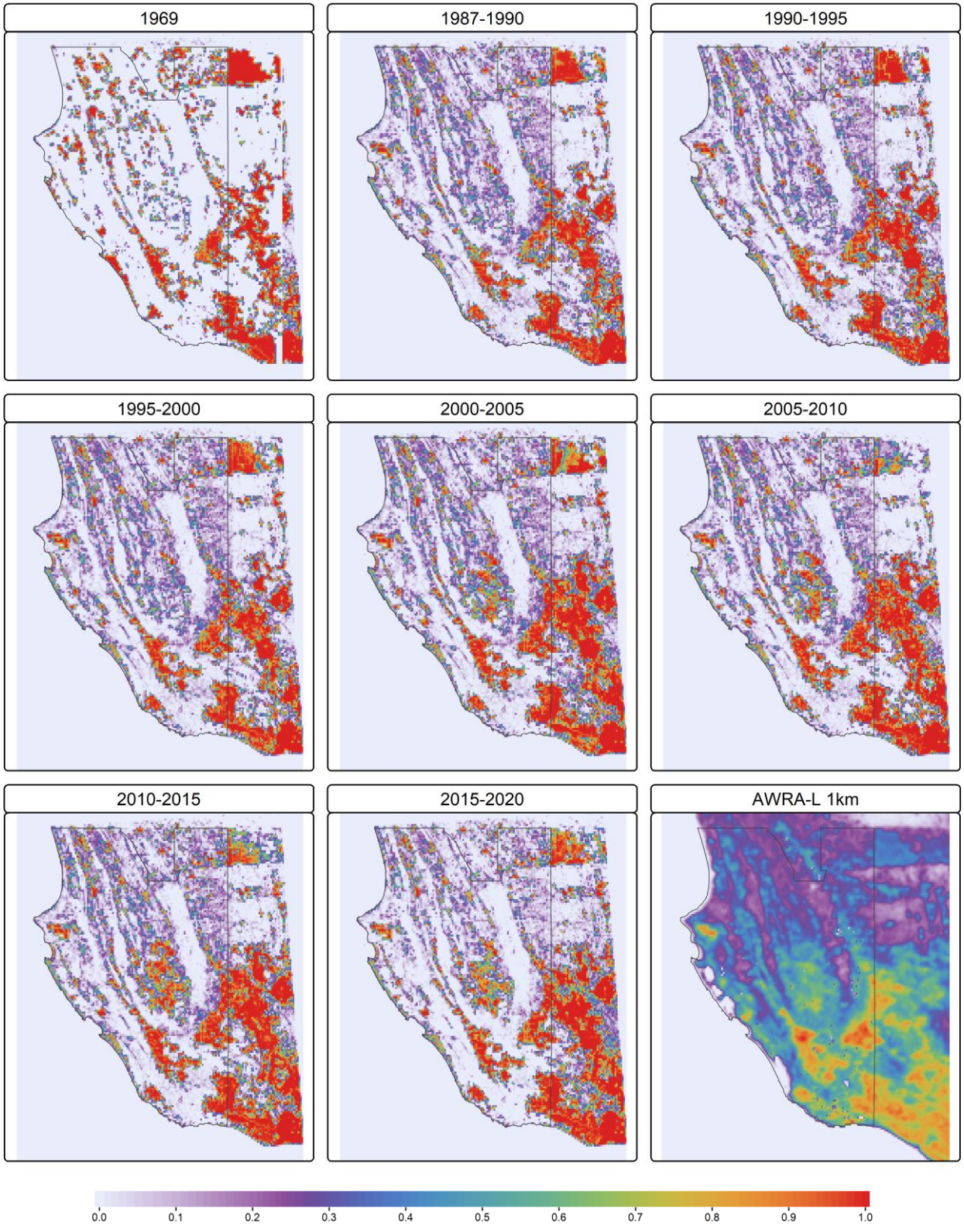

Figure 2-11 Proportion of deep-rooted vegetation in each 1km grid cell over time, with boundary of the Lower Limestone Coast Prescribed Wells area for reference

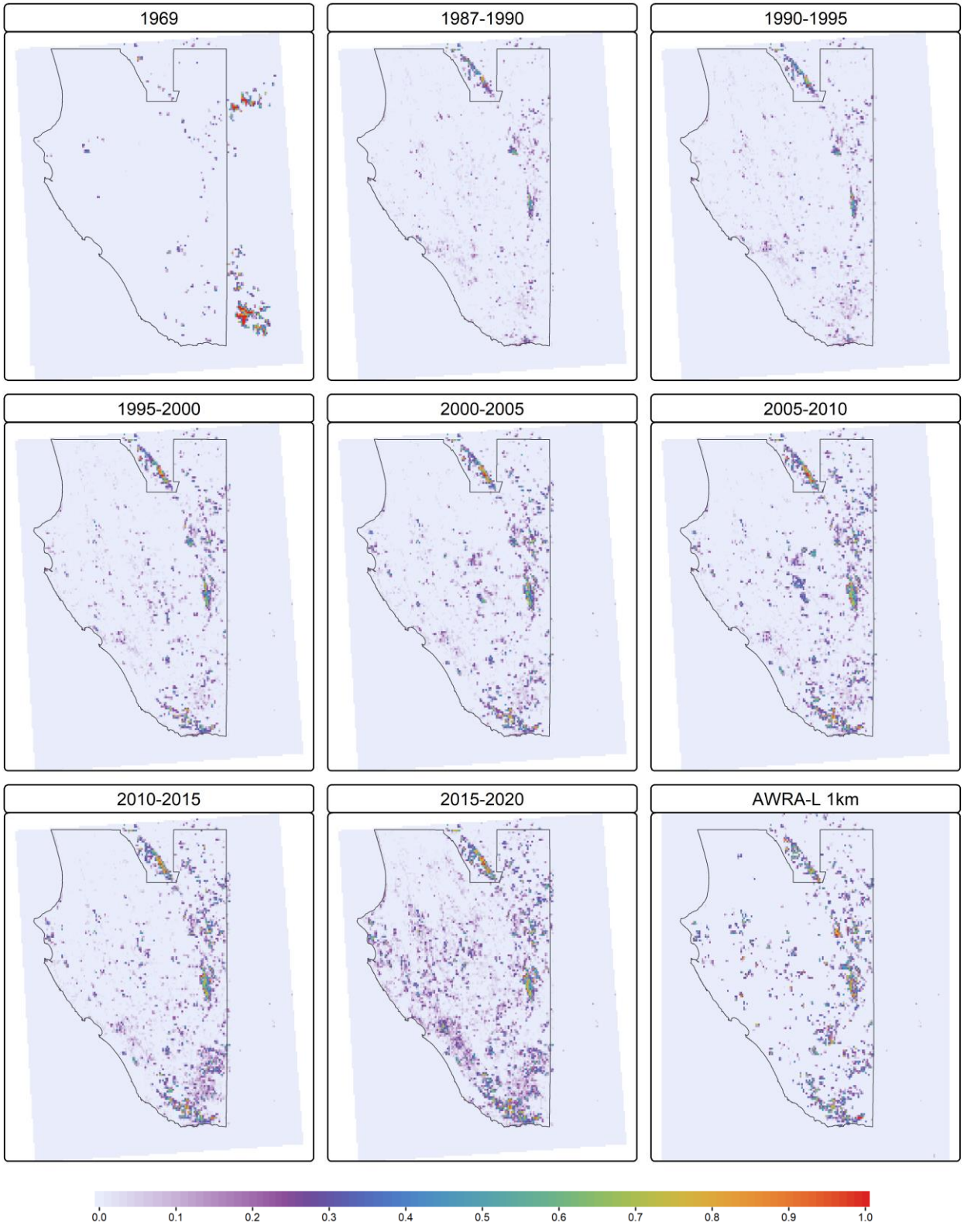

Figure 2-12 Proportion of irrigated area in each 1km grid cell over time, with boundary of the Lower Limestone Coast Prescribed Wells area for reference

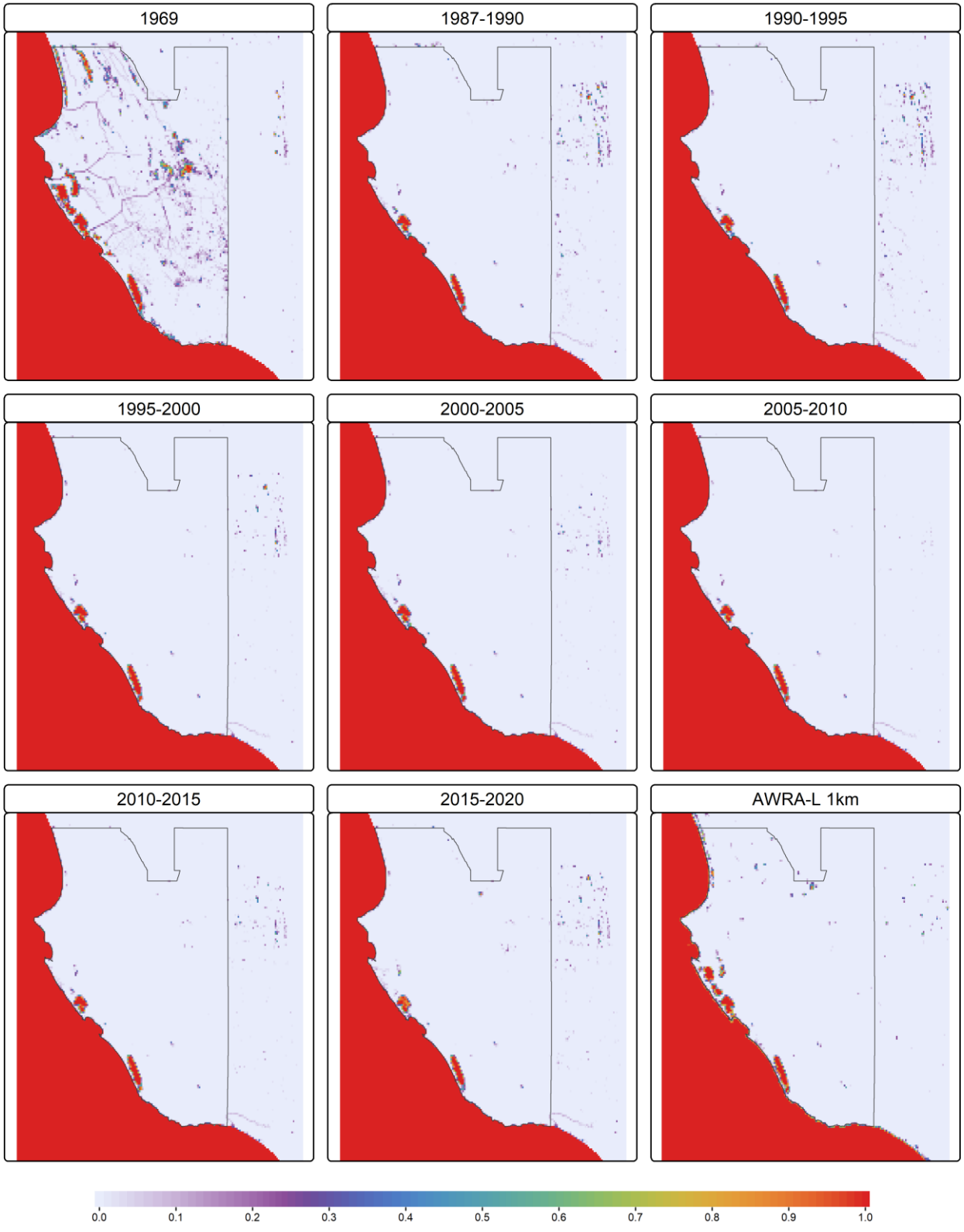

Figure 2-13 Proportion of water in each 1km grid cell over time, with boundary of the Lower Limestone Coast Prescribed Wells area for reference

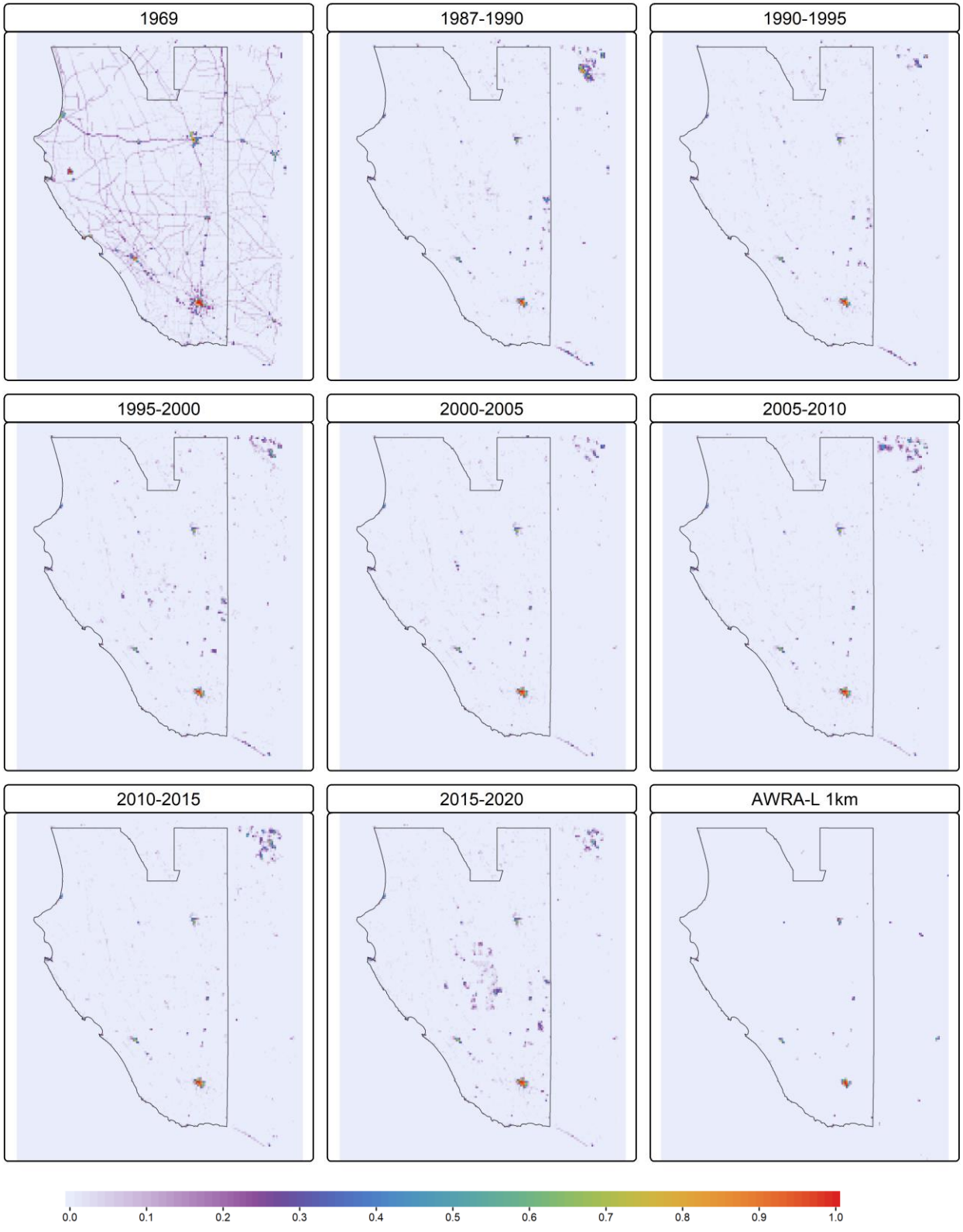

Figure 2-14 Proportion of impervious areas in each 1km grid cell over time, with boundary of the Lower Limestone Coast Prescribed Wells area for reference

2.3.3 SOIL PROPERTIES

AWRA-L requires input grids for saturated hydraulic conductivity and available water holding capacity in each of the three soil layers considered (0-10 cm, 10-100 cm and 100-600 cm), as well as the soil effective porosity and the hydraulic conductivity of the unconfined aquifer. The approach used in the existing AWRA-L inputs (Vaze et al., 2018) derived the soil parameters from clay content data available in the Australian Soil Resources Information System (ASRIS) database and pedotransfer functions (PTFs) to derive the parameter of interest (Dane and Puckett, 1994; Minasny et al., 1999). This approach was adopted to provide continuously varying soil properties in space and depth, as opposed to the approach of classifying regions of similar soil types, which results in the unrealistic case of homogeneous properties within a soil type and sharp discontinuities across soil type boundaries.

The national AWRA-L inputs for soil effective porosity and the hydraulic conductivity of unconfined aquifer are based on surface geology mapping and a lookup table from lithologies. While Morgan et al. (2015) noted that there is a surprisingly small amount of measured hydraulic parameter data available for the South East of South Australia, there have been several studies that have estimated these hydraulic properties that may provide more accurate regional scale estimates.

The 2015 South East Regional Water Balance Project (Harrington et al., 2015a) undertook modelling of the unsaturated zone to derive estimates of recharge, using models have similar data requirements compared to AWRA-L. The LEACHM modelling (Morgan et al., 2015) considered five soil textural classes based on existing mapping, in combination with different land use and climate variables. The WAVES modelling (Doble et al., 2015) used seven soil types based upon a classification of the clay content, with parameters adopted representative of the clay content (Carsel and Parrish, 1988). Similar to the LEACHM modelling, the different soil parameters were combined with different land use and climate variables. Both models considered the influence of depth to the water table on the recharge estimates.

Doble et al. (2017) used the WAVES recharge modelling as an input to MODFLOW groundwater model to undertake regional scale modelling of diffuse recharge, and as part of that modelling the hydraulic properties required for AWRA-L were compiled. The soil effective porosity and the hydraulic conductivity in AWRA-L have been updated based on the local scale work of Doble et al. (2017). The calibration process will scale the range of values across each grid to determine the final absolute values, and as such the magnitude of the values in each grid cell of each layer are of lesser concern than an accurate representation of the spatial patterns.

2.4 Calibration data

2.4.1 STREAMFLOW

An accurate representation of observed streamflow is a key objective of a rainfall-runoff model, and necessary to quantify water availability. Historic streamflow data is available for 48 gauging stations located in the study area (listed in Appendix B), however data from these sites are of varying quality and length. Available daily streamflow data was processed for all 48 gauging stations to assess and compare the quality of data and to help with identification of suitable sites for the purposes of model calibration.

Figure 2-15 shows the location of streamflow gauging stations using two classifications. The length of the recorded data at each station is represented by the size of the triangle symbols, while the proportion of the volume of recorded data that is less than the maximum gauged flow at each site is differentiated by symbol colour. A higher proportion indicates greater confidence in data quality as it means the majority of available data has been calculated based on the rating curves that have been developed using measurements of streamflow (gaugings), as opposed to theoretical or extrapolated relationships.

Since the AWRA-L model does not explicitly represent drain regulation, data from all stations that are affected by regulation need to be removed. These include many gauges in the Upper South East, as well as along Drain M downstream of Bool Lagoon. Other anthropogenic influences, such as discharge from Millicent

Wastewater Treatment Plant into the drain contributing to Drain 44 (A2390532) (SA Water, 2012), were also identified to remove measured streamflow stations that were influenced by human intervention, rather than the natural rainfall-runoff response. Station A2390523 was not used in calibration due to the difficulty in delineating the contributing catchment area. Due to the very flat terrain, the catchment area delineated using the approach of Wood and Way (2011) resulting in a catchment boundary that was implausibly large given the discharge recorded (see Section 3.4.1). Considering the two classifications presented in Figure 2-15 and these additional requirements for unregulated catchments with accurate catchment boundaries, seven stations (Table 2-3) were identified as high-quality unregulated stations suitable for model calibration, with the contributing catchment areas given in Figure 2-16.

Table 2-3 List of selected gauging stations for calibration purposes

Station number	Station name	Start	End	Catchment area (km^2)	Max. gauged flow (m^3/s)	Proportion of volume below max gauging (%)
A2390510	Drain L @ U/S Princes Highway	1971	2014	463	6.7	94.4
A2390513	Reedy Creek - Mt. Hope Drain @ 7.2km NE South End	1971	2022	538	26.2	98.9
A2390515	Bakers Range South Drain @ Robe-Penola Road	1971	2022	493	21.7	99.6
A2390519	Mosquito Creek @ Struan	1971	2022	1002	53.4	99.1
A2390527	Wilmot Drain @ 9.2km From Drain L	1973	2014	271	8.1	96.7
A2390531	Morambro Ck @ Bordertown-Naracoorte Road Bridge	1976	2022	567	8.6	95.0
A2390542	Naracoorte Creek @ Naracoorte	1985	2017	910	9.2	96.4

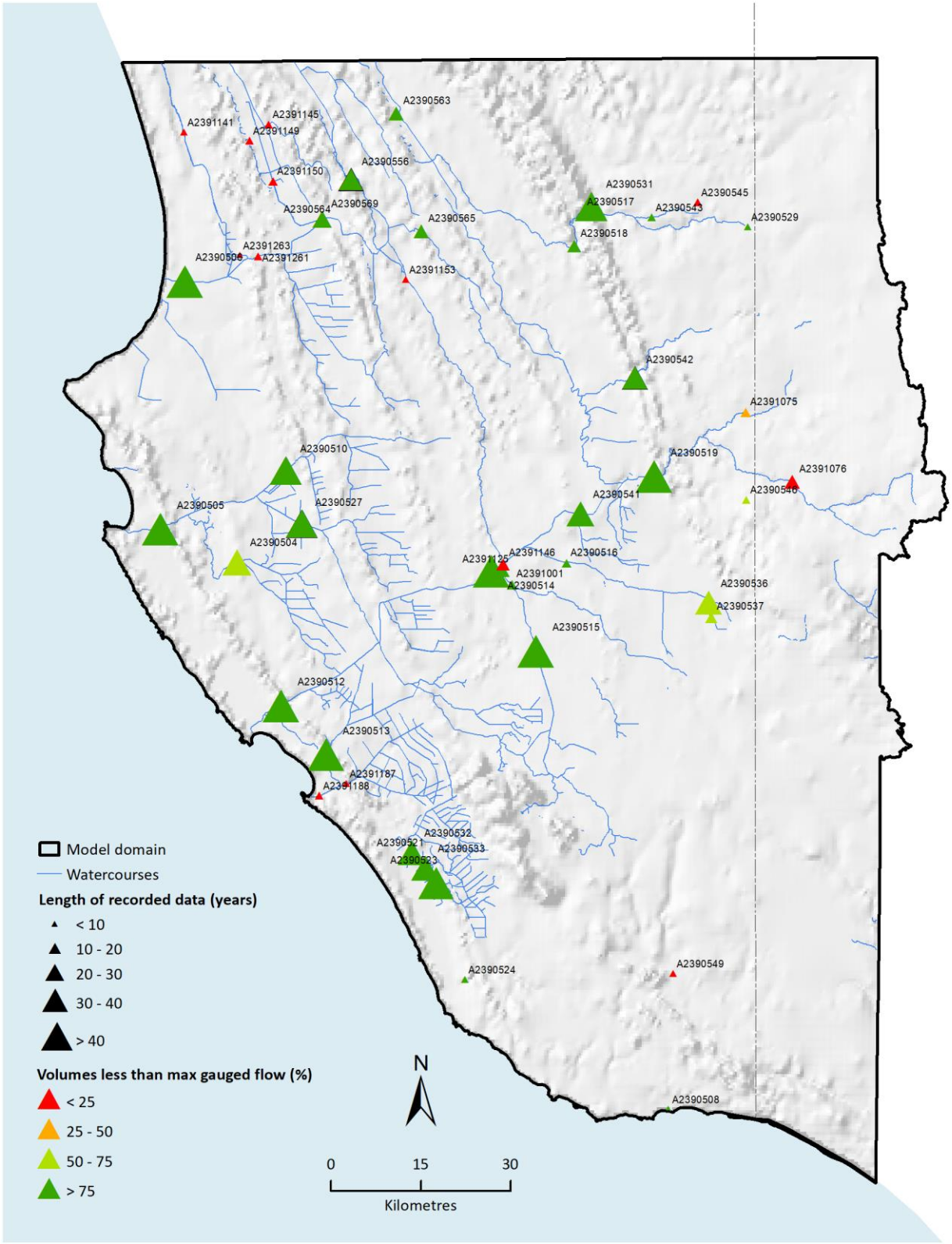

Figure 2-15 Available streamflow gauging stations, with data length and indication of rating curve quality, as the proportion of the recorded streamflow volume blow the maximum gauged flow

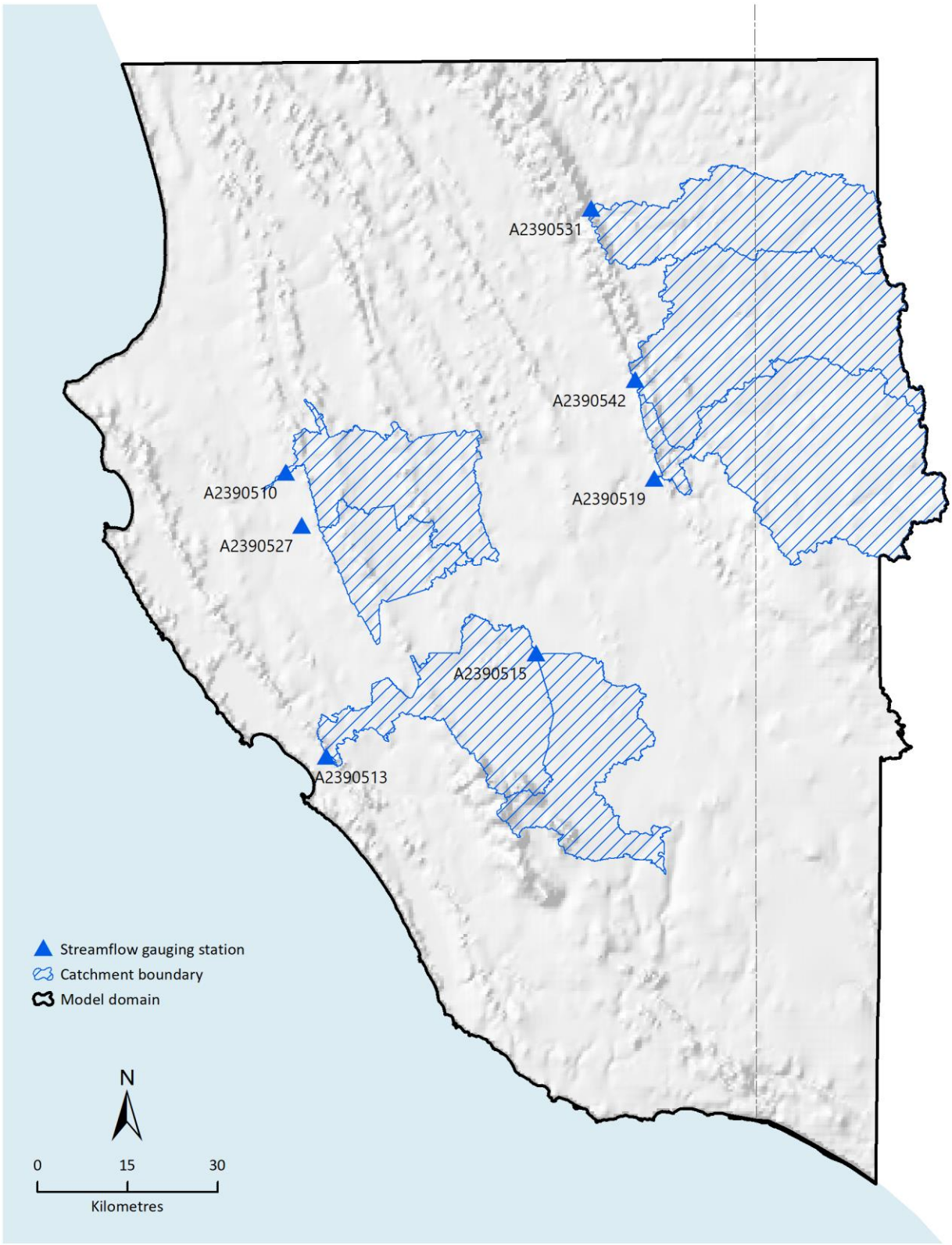

Figure 2-16 Catchment areas of streamflow gauging stations selected for calibration

Flow duration curves show the percentage of time for which a specified flow is equalled or exceeded over the period of the flow record. Flow duration curves are shown in Figure 2-17 to provide some information of the flow characteristics of the region, including data from each decade separately to indicate variability over time. For each of the streamflow gauges, the high-flow end of the flow duration curve is very steep, representing the component of runoff in these catchments that is highly responsive to rainfall, with the longer low-flow end of the flow duration curve indicative of the groundwater contribution to streamflow. Some of the flow duration curves in Figure 2-17 show a period of no-flow conditions, with the proportion of time with no-flow increasing in more recent decades.

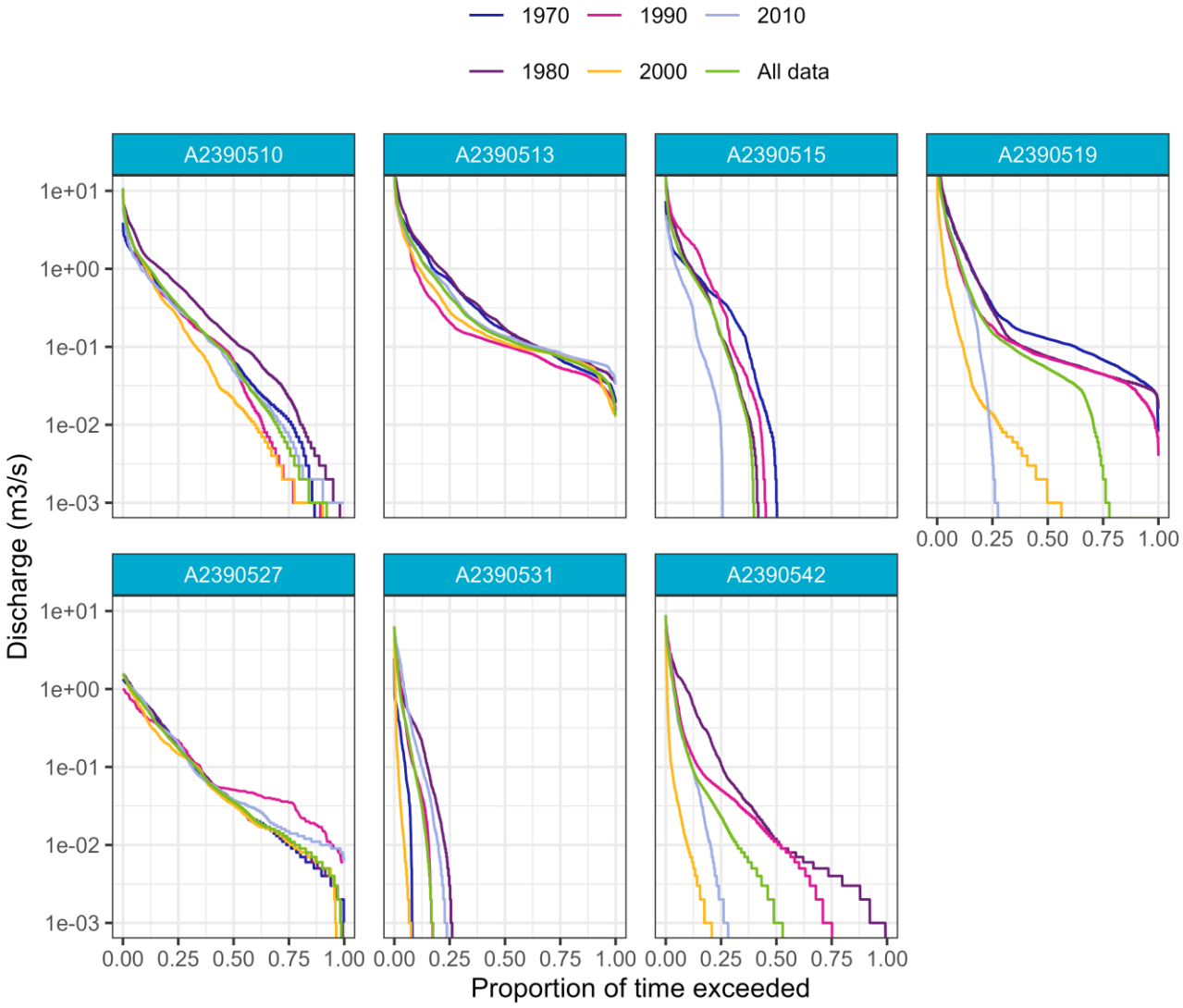

Figure 2-17 Flow duration curves for the high quality, unregulated, streamflow gauges

2.4.2 GROUNDWATER LEVEL

As the largest source of water for consumptive use in the region is groundwater, it is important to have a realistic representation of recharge and/or groundwater level in the water balance model. AWRA-L does not have a direct output of groundwater level that can be calibrated to observations. The model does have infiltration and drainage rates between the soil stores that could be calibrated to calculated recharge rates. However, it is difficult to determine a suitable recharge rate to use as a calibration target; for example, deciding if a gross recharge rate (e.g., from the water table fluctuation (WTF) method) or net recharge rate (e.g., chloride mass balance after extraction and evapotranspiration) is more appropriate, with up to an order of magnitude difference possible between these two estimates. Other issues with using recharge rates as calibration targets include the requirement to assume uncertain parameters, for example the specific yield in the case of the WTF method. Instead, it is proposed to correlate changes in the level of the storages in AWRA-L with changes in the observed groundwater level, to improve the model's representation of trends in the long-term stores. An objective function based on a correlation coefficient avoids the need to have values in the same units. Testing during the calibration process considered calibrating to different soil stores with different objective functions.

Water level data for the observation wells within the model domain were obtained from Bureau of Meteorology Groundwater Explorer (http://www.bom.gov.au/water/groundwater/explorer/map.shtml). Suitable wells were filtered to include those with sufficient data, defined as more than 20 years of records with more than 100 readings (Figure 2-18). For the purposes of model calibration, the groundwater levels were interpolated to a monthly time series using HydroSight (Peterson and Fulton, 2019), and spatially weighted (using Thiessen polygons) to calculate a catchment average water level time series.

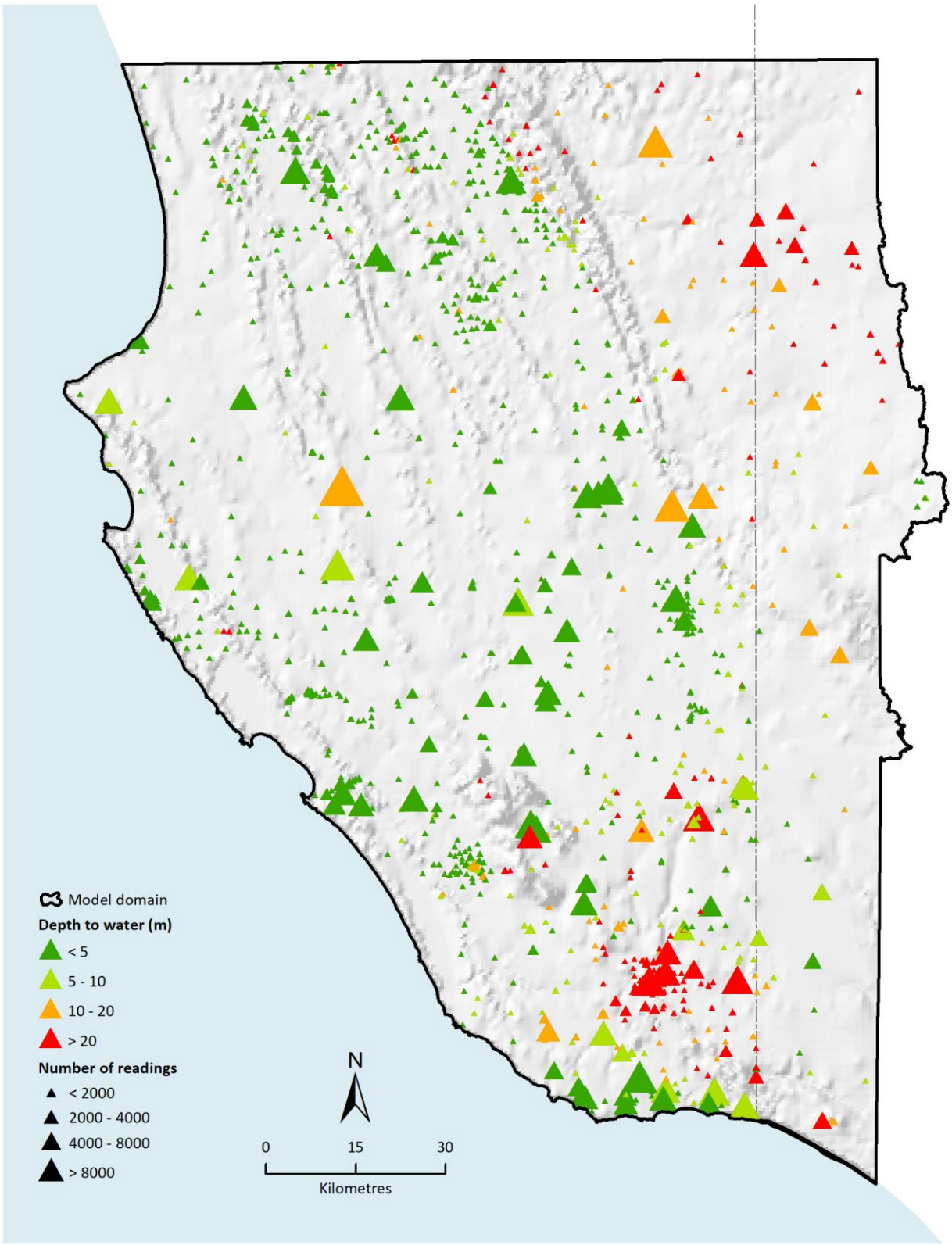

Figure 2-18 Groundwater observation wells with sufficient data for model calibration

2.4.3 SOIL MOISTURE

Soil moisture (SM) is widely recognized as a key parameter in land-atmosphere interactions (Ma et al., 2019; McColl et al., 2017). The intended purpose of the SM dataset is to provide a calibration target for the upper SM store in AWRA-L, representing the top 10 cm of soil. The water in this storage may not be in the same units as the SM data, and as such metrics like a correlation may need to be adopted to calibrate the model to patterns of high and low SM without necessarily producing the same values.

Ma et al. (2019) compared the accuracy of several remotely sensed SM datasets to 572 in situ measurements worldwide, including 46 sites in Australia across two sensor networks. The products assessed were the Soil Moisture Active/Passive mission (SMAP), two Soil Moisture and Ocean Salinity products, the Land Parameter Retrieval Model Advanced Microwave Scanning Radiometer 2 (LPRM AMSR2) product and the European Space Agency Climate Change Initiative (ESA CCI) product, which merges multiple single-sensor active and passive microwave SM products (Dorigo et al., 2017). The study found SMAP outperformed the other products in terms of representing temporal patterns according to the correlation value, with ESA CCI also producing very similar values for the two Australian networks. ESA CCI had the lowest Root Mean Square Error (RMSE) in the SM values, across the full comparison as well as for the two Australian networks. The ESA CCI data product was used by Humphrey et al. (2016) as an input for streamflow forecasting in the Drain M system.

The ESA CCI and SMAP data were compared to field soil moisture data to test the suitability of the remotely sensed data products in the region. Two SM sensors in Western Victoria were identified; the first site was the Cosmic-Ray Neutron Soil Moisture sensor at Hamilton maintained by the CosmOz network (Hawdon et al., 2014), and the second was at the Gatum Pasture flux station established by the Department of Environment, Land, Water in collaboration with Monash University and La Trobe University. The units for each dataset were different: SM content (%) at Hamilton over a variable depth using the Cosmic-Ray sensor; surface SM (mm) using SMAP; and the volume of water per unit volume of soil (m^3 water/m^3 soil) in the top 5 cm of soil at Gatum and from ESA CCI. To enable comparison across data sources, each dataset was normalised to have a mean value of zero and standard deviation of one. This is considered appropriate as a similar pattern matching will be used in the calibration of the AWRA-L model as the units will be different again (depth of water in a conceptual storage). An earlier SM dataset collected in forestry sites across the Green Triangle, as outlined in Benyon and Doody (2004), was also sourced for comparison. This data covers the period 2000-2008 and hence predate the SMAP satellite, with only a comparison to ESA CCI possible. The locations for each site can be seen in Figure 2-19.

The results indicate that the remotely sensed datasets provide a useful representation of SM when compared to field data for the sensors at Gatum and Hamilton (Figure 2-20 and Figure 2-21). From Figure 2-21 the SMAP dataset produced slightly higher R^2 values at Gatum compared to ESA CCI, possibly due to the higher spatial resolution (9 km compared to 25 km). However, the differences are relatively small, with similar low bias (lines of best fit are similar and along the 1:1 line) and variance (spread of points around this line is similar). The comparison between ESA CCI and the forestry field data sites is provided in Figure 2-22, with the field data available for different periods depending on the location. Again, the remotely sensed data product provides a good representation of the field data, particularly when short term variations are smoothed using a 14-day rolling average.

The SMAP dataset has a number of advantages, including a slightly higher correlation to field data in the study region and globally (Ma et al., 2019), comparatively higher spatial resolution, and near real time data is available. However, the major disadvantage of this dataset is the satellite was launched in 2016 and hence the data record for model calibration is relatively short. In comparison, the ESA CCI dataset draws on data sources commencing in 1978, including 5 active and 12 passive microwave sensors. Given this longer data

record and acceptable performance when compared to field soil moisture measurements in the study area, the ESA CCI data set has been used for model calibration and testing.

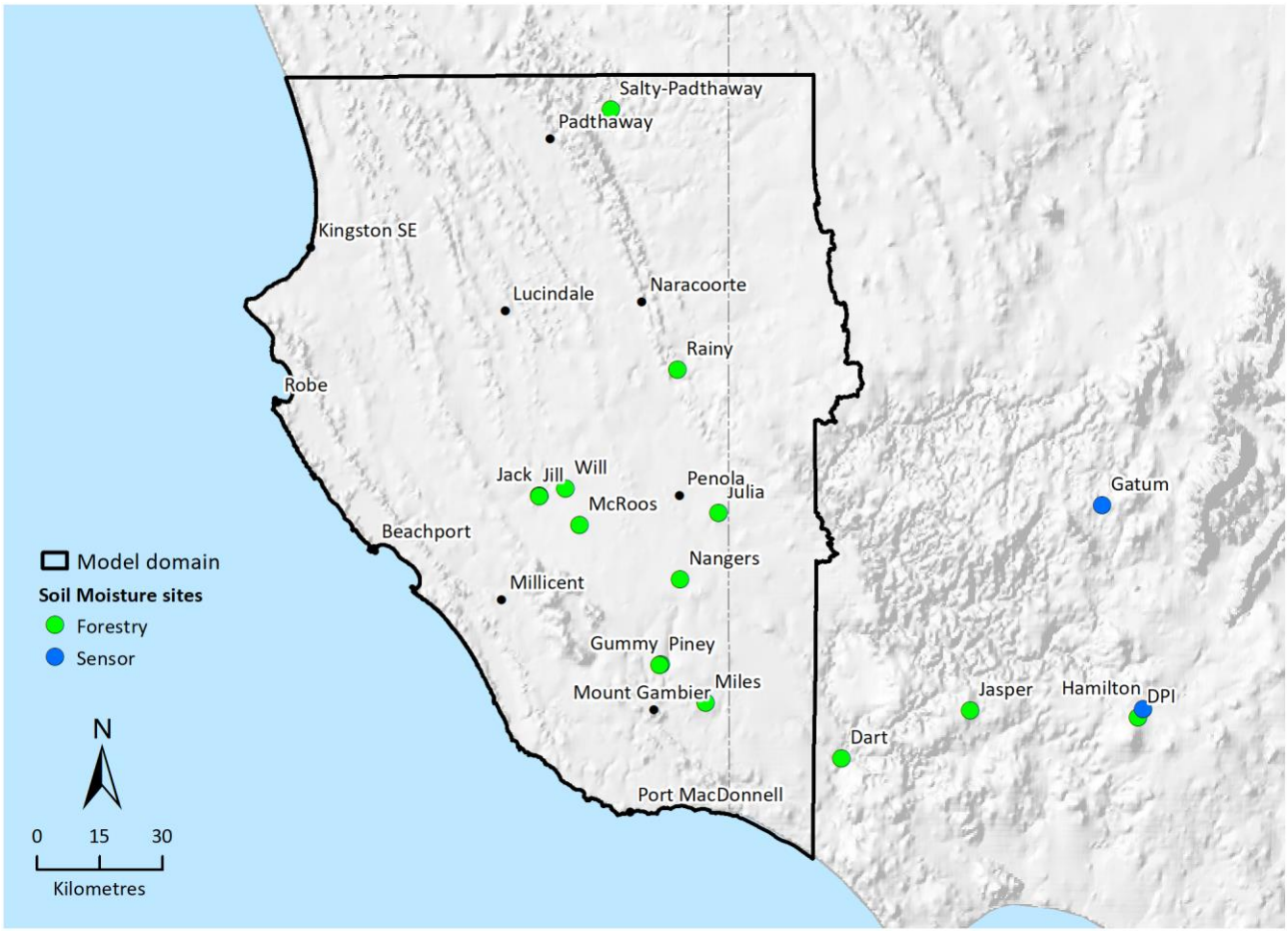

Figure 2-19 Locations of soil moisture and actual evapotranspiration field data

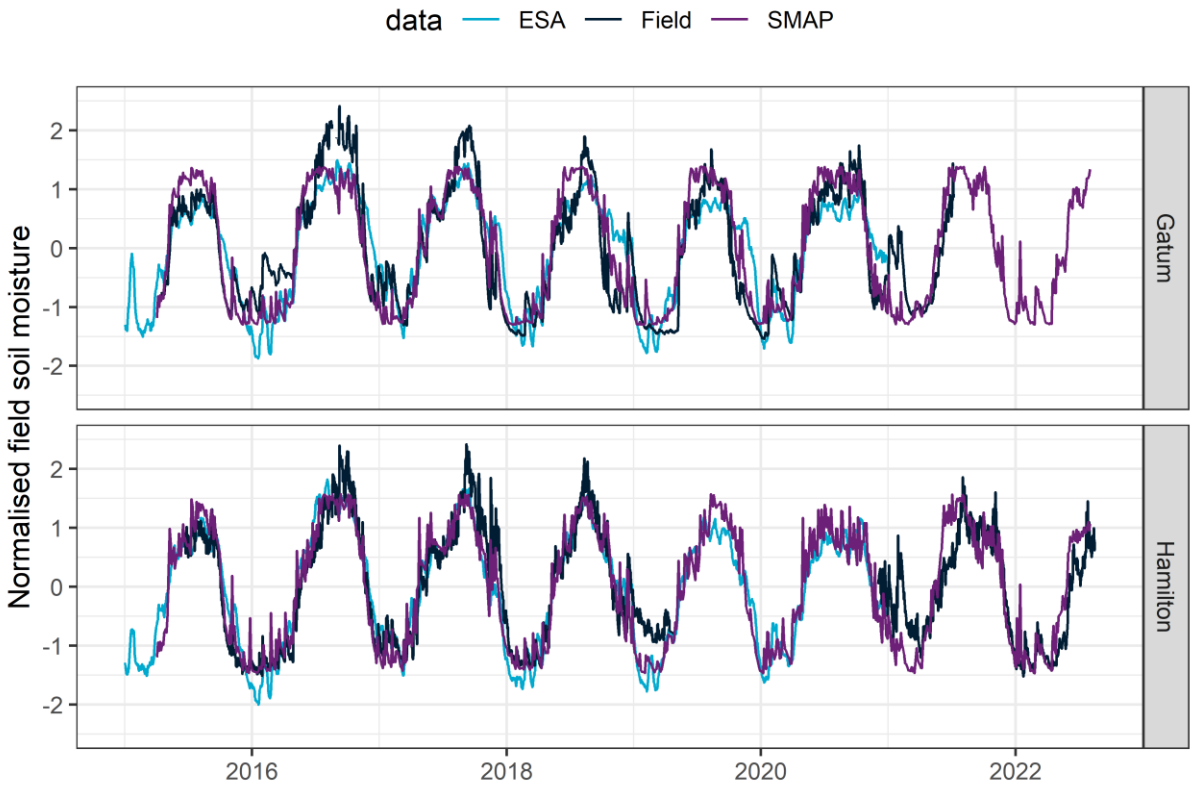

Figure 2-20 time series of soil moisture for in-situ sensors (field) and two remote sensing products

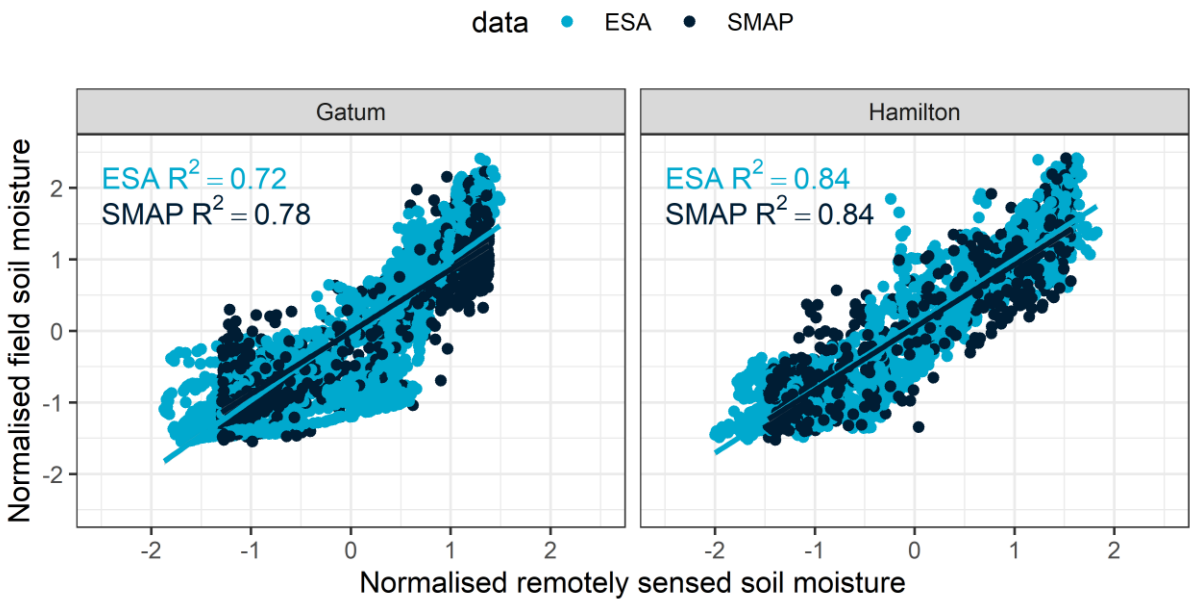

Figure 2-21 Scatter plot comparing field observed and remotely sensed soil moisture values

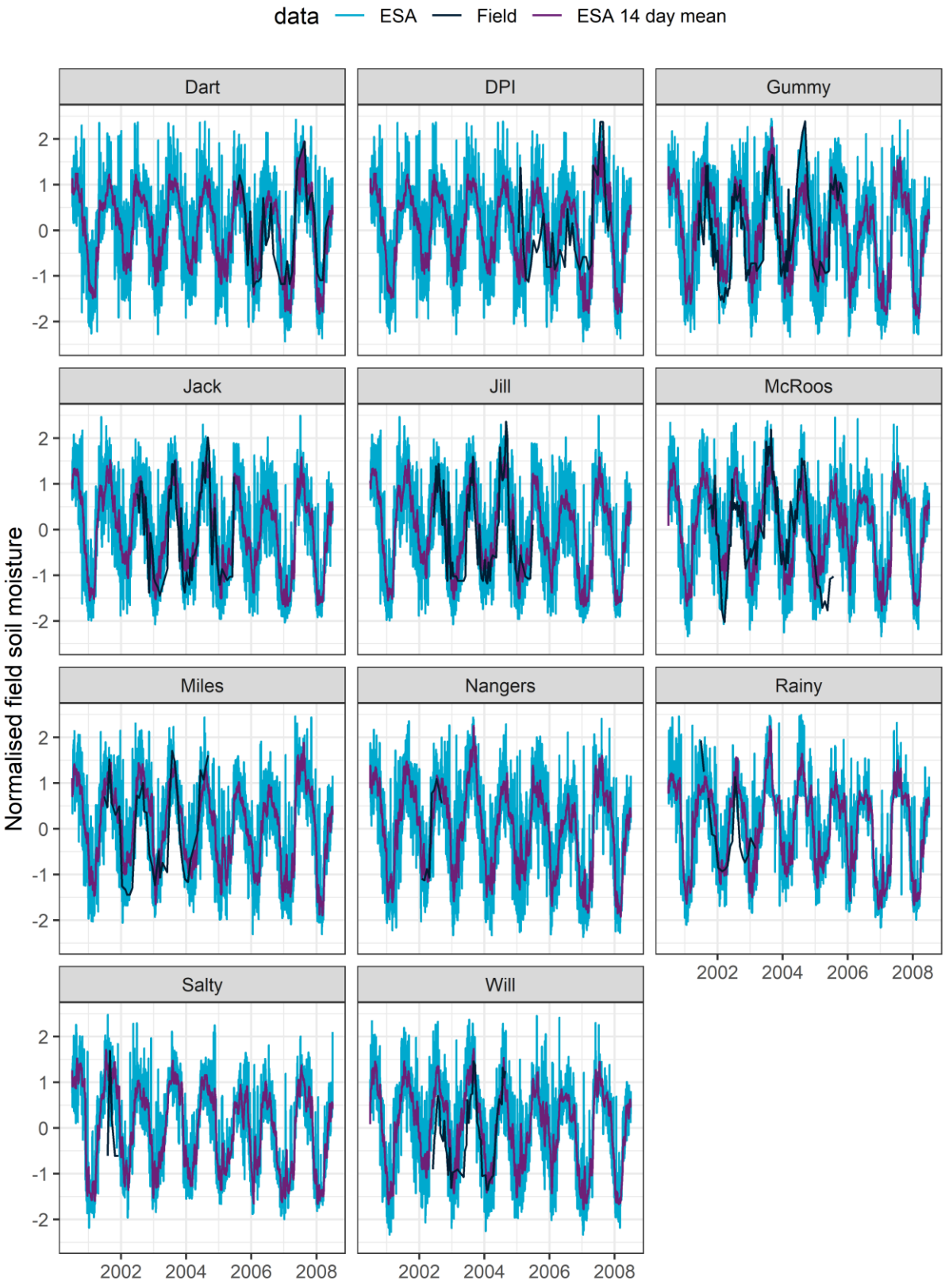

Figure 2-22 Time series of normalised soil moisture estimates from field sites (Benyon and Doody, 2004) and the remotely sensed European Space Agency (ESA) Climate Change Initiative product

2.4.4 ACTUAL EVAPOTRANSPIRATION

Evapotranspiration (ET) represents the largest water outflow from the region and approximately half the gross recharge is lost through ET from groundwater (Harrington et al., 2015a). Hence, accurate representation of actual ET (AET) (as opposed to potential ET, PET, defined as the ET that could occur with an infinite water supply) is important to represent in the water balance.

There are limited direct measurements of AET across Australia, with most of the monitoring stations and subsequent datasets coordinated by the OzFlux network. CMRSET (CSIRO MODIS ReScaled EvapoTranspiration) is a dataset that uses remote sensing indices to scale PET for estimating AET, calibrated to the observed data available from OzFlux. Version 2.2 of CMRSET includes a number of updates to the input data and methodology (Guerschman et al., 2022). The data is available via Google Earth Engine at a 30 m resolution and a monthly timestep commencing in 2000.

Doody et al. (2022) identified that tree water use was often overestimated by CMRSET based on field data from River Murray floodplains. The Australia-wide Machine Learning ET for Trees model (AMLETT) was developed as a residual error correction for CMRSET, using random forest machine learning algorithms to predict a monthly correction based on inputs of remotely sensed vegetation and water indices, as well as air temperature and solar radiation. Doody et al. (2023) developed AMLETT for plantation forestry in the South East, calibrated to field data collected during the same campaign as the soil moisture data used above (Benyon and Doody, 2004). The AMLETT corrected AET estimates improved the performance compared to the field ET data, from an RMSE of 34 mm/month (R^2=0.21) for CMRSET to a RMSE of 15 mm/month (R^2 = 0.86) with AMLETT. AMLETT has not been developed outside of the plantation forestry estates. Currently it is unclear if the machine learning residual error model developed is only applicable to the vegetation type on which the algorithm has been trained.

The Gatum site used for soil moisture (see Figure 2-19) also has an Eddy Covariance Flux Tower to measure evapotranspiration at a pasture site (i.e. non-forested). This site was not used in the calibration of CMRSET and hence provides an independent validation of that dataset. The observed data was aggregated to correspond to the monthly average values provided by CMRSET by summing the 30-minute data each day, then averaging the resulting daily values to produce the monthly averaged value of AET in mm/day. If a day was missing more than 1 hour of data it was considered missing, and if a month was missing more than 7 days of data the monthly average was considered missing data, hence there are some gaps in the flux data in Figure 2-23. The time series comparison indicates the CMRSET data generally agrees with the observed data, particularly the annual minima and maxima, and the winter-spring period between these extremes that are less likely to be water limited, and AET ≈ PET. The main differences occurred over the summer months, with CMRSET estimating more AET than recorded at the flux tower. The same data is compared as a scatter plot on Figure 2-24, with an R^2 value of 0.64 and the largest differences corresponding to these overestimated values over summer where the AET is likely to be water limited.

The uncertainty in remotely sensed ET products has been found to be higher than in gauged streamflow data (Vervoort et al., 2014). Rajib et al. (2018) found that MODIS ET, if used from the very beginning of the calibration process, inserts propagating errors that limit the accuracy of simulated streamflow that cannot be improved beyond a certain level. Huang et al. (2020) found ET data need to be bias corrected using a water balance approach for calibration, which the AET data is attempting to inform in the first place. Given these challenges in including AET data in calibration of hydrological models, the large differences between CMRSET AET and field data found by Doody et al. (2023), and initial model calibration testing undertaken in this work that found substantial degradation in streamflow performance when attempting to also calibrate to AET time series, AET data has not been used as a calibration target.

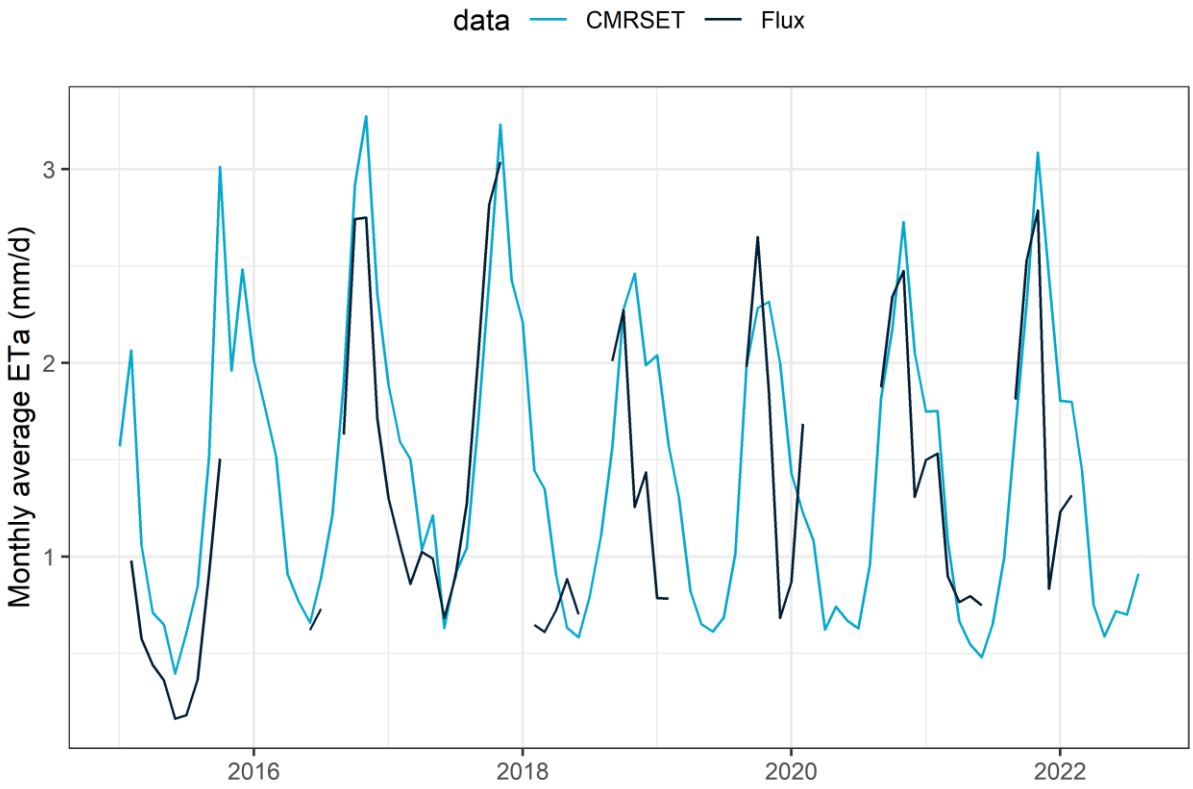

Figure 2-23 Time series of monthly averaged actual evapotranspiration recorded at the Gatum flux tower and calculated by CMRSET

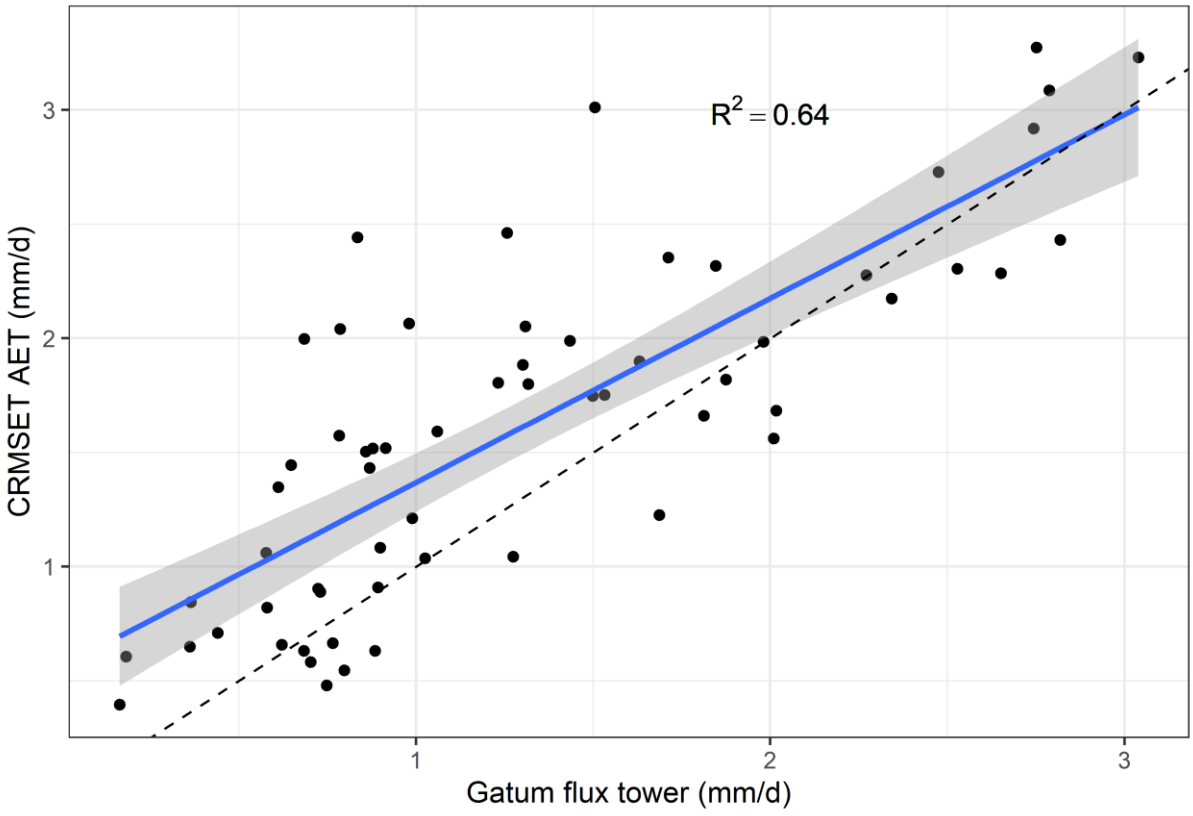

Figure 2-24 Scatter plot comparing the agreement between the monthly averaged actual evapotranspiration recorded at the Gatum flux tower and calculated by CMRSET

2.4.5 LEAF AREA INDEX

Seasonal vegetation dynamics in response to water availability are represented in the AWRA-L model. The vegetation dynamics have a direct influence on the evapotranspiration rate, and as such are a key component of the modelled water balance. The vegetation dynamics component of the model has been focused on to improve the ability of the different HRUs to represent the expected dynamics. The modelled leaf biomass for a HRU and grid cell is converted to Leaf Area Index (LAI) through a calibrated model parameter, and this LAI can be compared directly to remotely sensed observations.

MODIS LAI observations were used, as available through the OzWALD model-data fusion system, which provides additional data quality assurance, resulting in an internally-consistent dataset at 500-m and 8-day resolution (Van Dijk and Rahman, 2019). To provide a calibration dataset, the median value of OzWALD cells that were classified as over 95% of the HRU type (deep rooted or shallow rooted) over the model domain were adopted for the value in each time step (every 8 days). This approach was used to provide a representative value for the HRU while reducing the effect of errors in individual pixels, and benefits from using data across the model domain, as opposed to only the calibration catchments. The resulting time series is shown in Figure 2-25, where the LAI for shallow rooted vegetation peaks in winter-spring and reduces over the summer-autumn months, while the deep-rooted vegetation has a higher LAI and is much more consistent over time.

AWRA-L also has an input spatial grid of the maximum achievable Leaf Area Index in each model grid cell for both the deep and shallow rooted vegetation. These input grids were updated based on the longer time series of remotely sensed LAI data available since these inputs were last developed. The processing method to derive the input grids was as follows:

- Quality assuring the MODIS data by removing pixels affected by clouds and representing high-quality data only.
- Deriving the 99th percentile value for each MODIS LAI pixel over the record available (July 2002-June 2024). An extreme percentile was used as opposed to the absolute maximum value to exclude spurious values. This produced a grid of maximum observed LAI values at a 500 m resolution.
- The LAI maximum value for deep rooted vegetation was assumed to be the highest of the maximum LAI values within each model cell (with at least four 500m MODIS LAI pixels within a 1km model grid cell).
- The LAI maximum value for shallow rooted vegetation value was assumed to be the lowest of the maximum LAI pixel values within each model cell.

The updated grid was compared to the previously available model input grids and were found to be similar in pattern and magnitude, suggesting a suitable analysis.

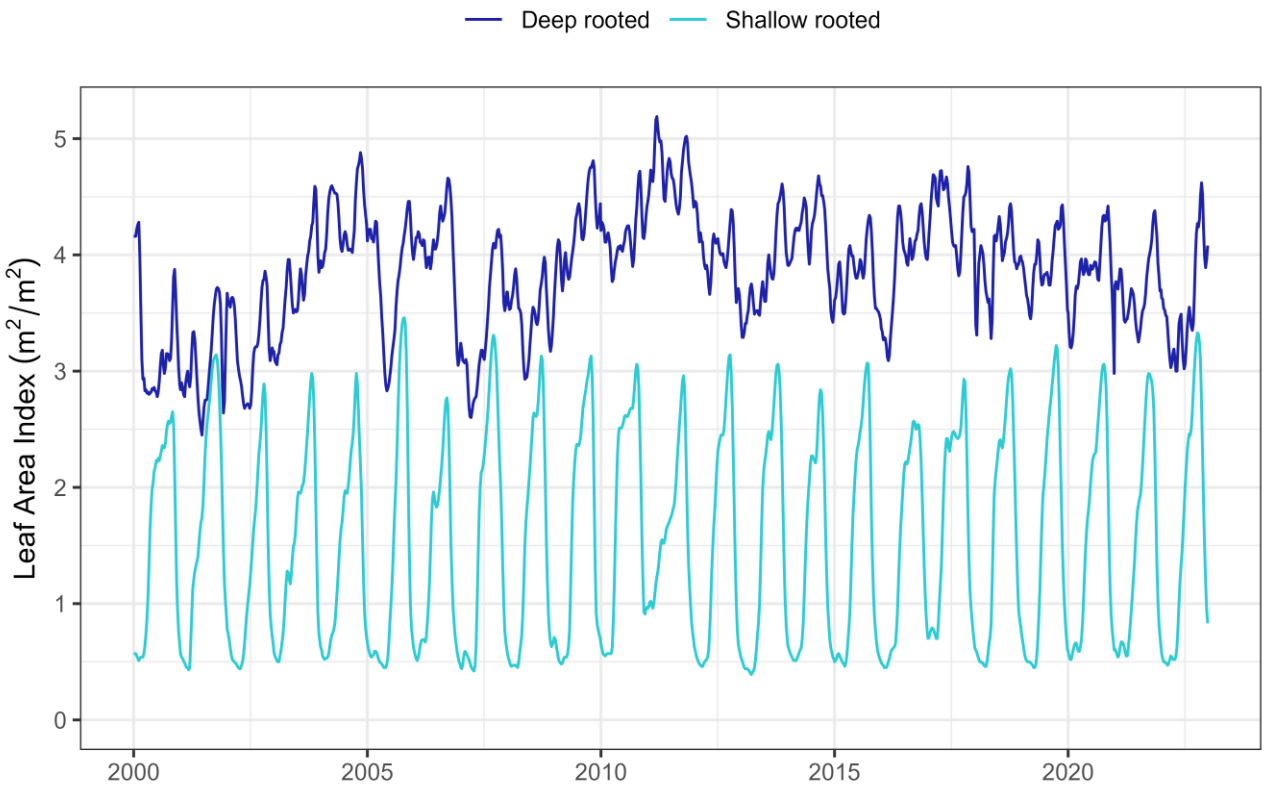

Figure 2-25 Median value over the model domain of remotely sensed Leaf Area Index for the deep (DR) and shallow rooted (SR) HRU areas

2.4.1 VEGETATION GREENNESS AND RATE OF CHANGE

Along with the leaf area index, the vegetation greenness also influences the modelled evapotranspiration rate. V_c is the Greenness index per unit canopy cover parameter, which Van Dijk (2010) suggests can be derived from remote sensing using the remotely sensed Enhanced Vegetation Index (EVI) per unit of canopy cover (fractional cover, FC). EVI was derived from MODIS Aqua on Google Earth Engine, available at a 1km resolution every 16 days since 4/7/2002. Digital Earth Australia's Fractional Cover 2.3.1 product was used for the canopy cover, derived from Landsat 5/7/8, available at a 30-m resolution most days commencing on 16/8/1986. Quality assurance and quality control bands available on Google Earth Engine were used to filter out poor quality pixels, while on GA Sandbox cloud and water masks were used to quality assure fractional cover data. A value of each remotely sensed variable for each image was derived for each of the shallow rooted and deep rooted vegetation HRUs in each calibration catchment by averaging the value for the coinciding pixels. EVI is plotted against FC in Figure 2-26, where the average slope across the calibration catchment for deep rooted HRU is Vc_hruDR = 0.92, and shallow rooted Vc_hruSR = 0.59. In comparison, Van Dijk (2010) reports values of 0.5-1.0 for inland grassland areas and forests.

The model has two more parameters controlling the vegetation dynamics: 1) the time scale for growth towards an equilibrium as water becomes more available in the wetter months, and 2) senescence towards an equilibrium during the drier months. These parameters influence the rate of change in leaf biomass and area index and are important to match the seasonal dynamics represented in the remotely sensed LAI data. While it may be possible to infer these rates from the LAI time series outlined in Section 2.4.5 they have been calibrated with the other model parameters in this work.

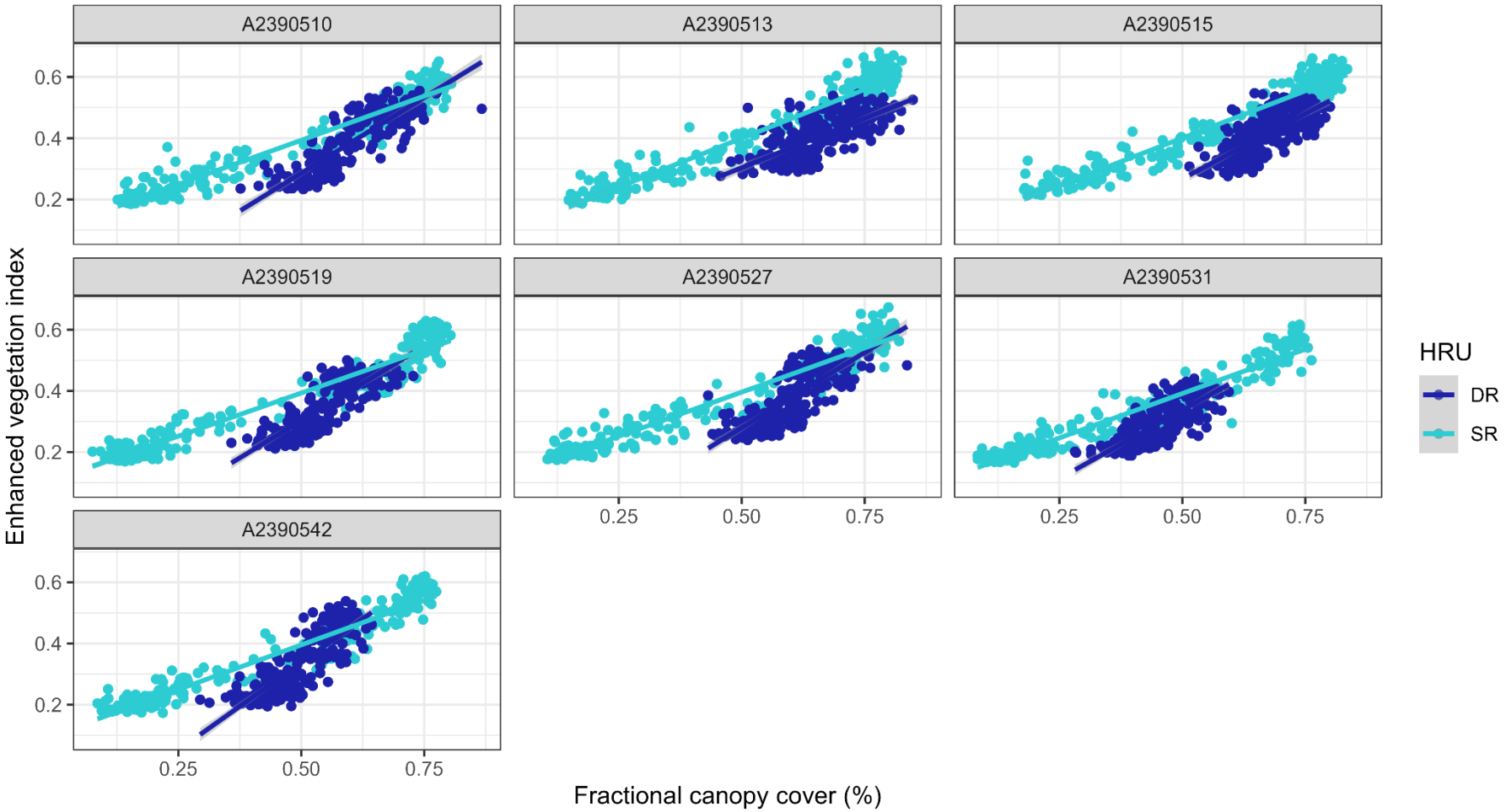

Figure 2-26 Monthly enhanced vegetation index to fractional canopy cover. The slope of the line represents the V_c parameter

3 AWRA-L model development

3.1 Model modifications

Three main changes were made to the AWRA-L version 6 model (Frost et al., 2018) for this project, outlined in more detail below. A model schematic is presented in Figure 3-1 to aid in the interpretation of the changes.

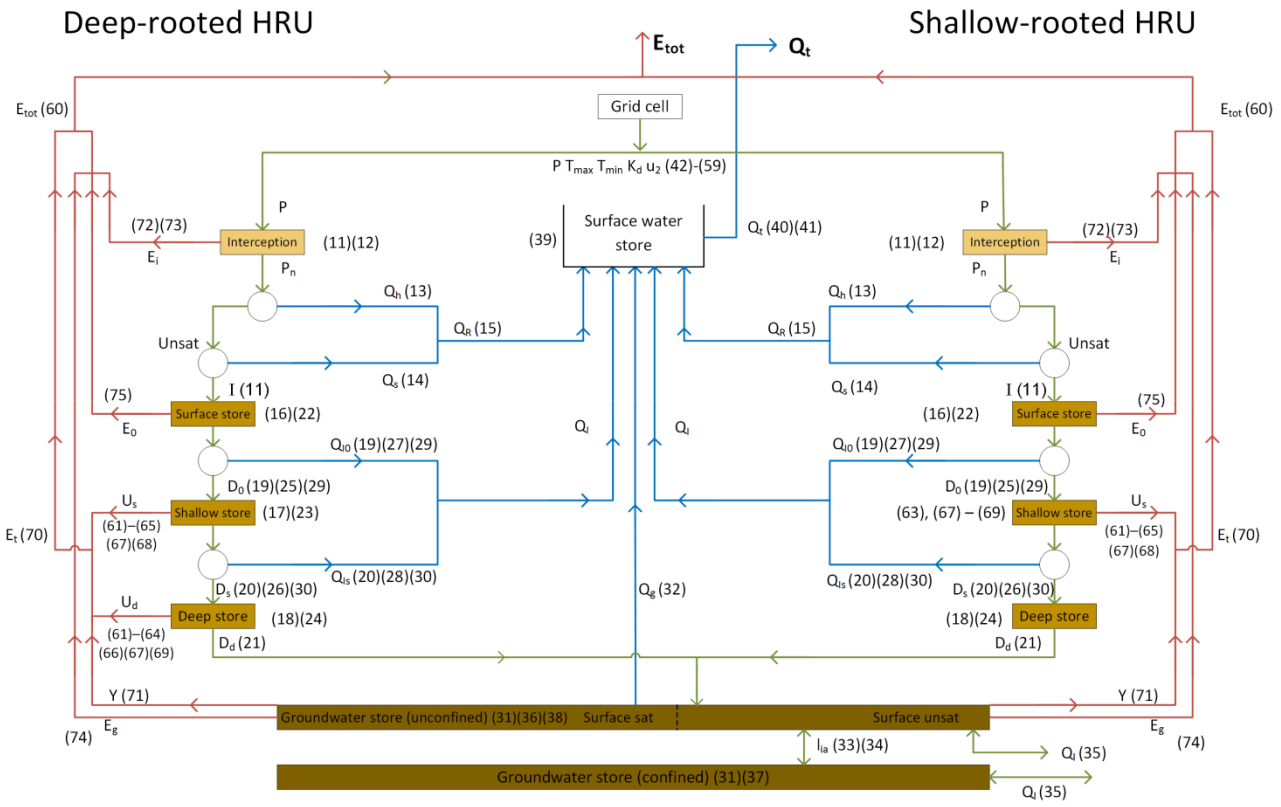

Figure 3-1 AWRA-L conceptual model for the two main HRUs, the deep and shallow rooted vegetation. The main difference is the deep-rooted vegetation has an evapotranspiration component from the deep soil store, U_d. Figure reproduced from Viney et al. (2015) with values in brackets corresponding to equations in that report

3.1.1 VARIABLE FUNCTIONAL UNIT PROPORTIONS

The main additional functionality added to the model was the ability to vary the proportion of the HRU in each grid cell over time to represent changes in land use. The 5 yearly datasets developed in Section 2.2.2 were interpolated to a daily time step to provide the HRU proportion for each grid cell in the model. The proportion of HRU each day for each calibration catchment is presented in Figure 3-2. For all catchments the shallow rooted HRU represents approximately 70-80% of the catchment, with the deep-rooted vegetation the next most common HRU. The proportion of the deep rooted HRU increases over 2000-2015 in some catchments, however, remains a relatively small proportion. The largest increase was in the Mt Hope catchment, A2390513, increasing from approximately 15 to 30% of the total catchment area, before reducing slightly in the most recent land use-land cover dataset.

At every time step in the model, each HRU has a level in each of the stores in the model (brown boxes in Figure 3-1), and if the proportion of HRUs changes then the level in each store must also be changed to ensure the water balance is conserved. All stores for the deep rooted and shallow rooted HRUs, and the irrigation HRU (which is effectively the shallow rooted HRU with irrigation applied based on the storage level in the surface and shallow stores) are modelled dynamically and conserve the water balance. However, for the permanent water HRU the surface, shallow, and deep stores are assumed to be full at all time steps, and they

were half full for the impervious HRU. To ensure the water stored within the model is conserved, the water and impervious HRUs were assumed to be at the weighted average of the shallow rooted, deep rooted, and irrigation HRUs, such that when the proportion of HRUs changed, the water stored in the model was the same before and after the change. To adjust the storage levels to maintain the water balance, if the proportion a given HRU reduces from one timestep to the next there is no need to adjust the storage levels. If the proportion of a given HRU increases into what was previously another HRU, then a weighted average of the storage levels is adopted, to represent the change in land use over a given water storage at that time step. This approach assumes instantaneous mixing of the soil and groundwater stores within a 1km grid cell, as the model does not account for lateral movement within or between cells. Implementing change in HRU proportions as a linear trend each day also smoothed transitions between the land cover layers each five years, minimising large changes in HRU proportions and water storage over time.

3.1.2 GROUNDWATER STORE DISCHARGE

Previous studies have identified that the AWRA-L model structure struggles to represent the zero flow period in ephemeral catchments (Azarnivand et al., 2022). In an attempt to allow the model to represent this behaviour, discharge from the groundwater store (Q_g in Figure 3-1) was redirected to contribute directly to the outflow of the catchment, Q_t, rather than into the surface water store. Both the groundwater and surface water stores have a routing constants to control the release of water at each time step, which may improve the ability of the model to represent faster and slow flowing components of the flow regime.

The model has a parameter that controls the rate of flow out of the groundwater store, k_g. This is calculated as the product of a grid of values, k_{gmap}, which is used to represent spatial variability in baseflow rates, derived based on effective porosity, hydraulic conductivity, drainage density and an assumed aquifer depth at the continental scale (Viney et al., 2015). This spatial value for each model grid cell is multiplied by a scaling factor, k_{gscale}, to improve the modelled representation of the calibration dataset. To enable potentially faster release of baseflow from the model, k_{gscale_c} was calibrated and related to the scaling parameter as an exponent, i.e. $k_{gscale} = 10^{kgscale\_c}$, and calibrated over a larger range of -1 to 6. This range was selected to provide values of K_{gscale} used in previous studies, but also resulting values of k_g that are in line with baseflow recession constants, typically approximately 0.925 (Nathan and McMahon, 1990).

3.1.3 WATER SOURCE FOR IRRIGATION HRU

In the AWRA-L 6.0 model, the irrigation HRU sources the irrigation water from an undefined source, assumed to be supplied from a river or irrigation district outside the grid cell, with a function to limit extraction to a maximum allocation. In the model region, almost all irrigation is supplied from groundwater rather than from a water source outside of the grid cell. To represent this process, the irrigation water was changed to be supplied from the groundwater store in the grid cell. This process represents irrigation from the unconfined aquifer only, with irrigation from the confined aquifer, typically around Kingston SE, not explicitly included.

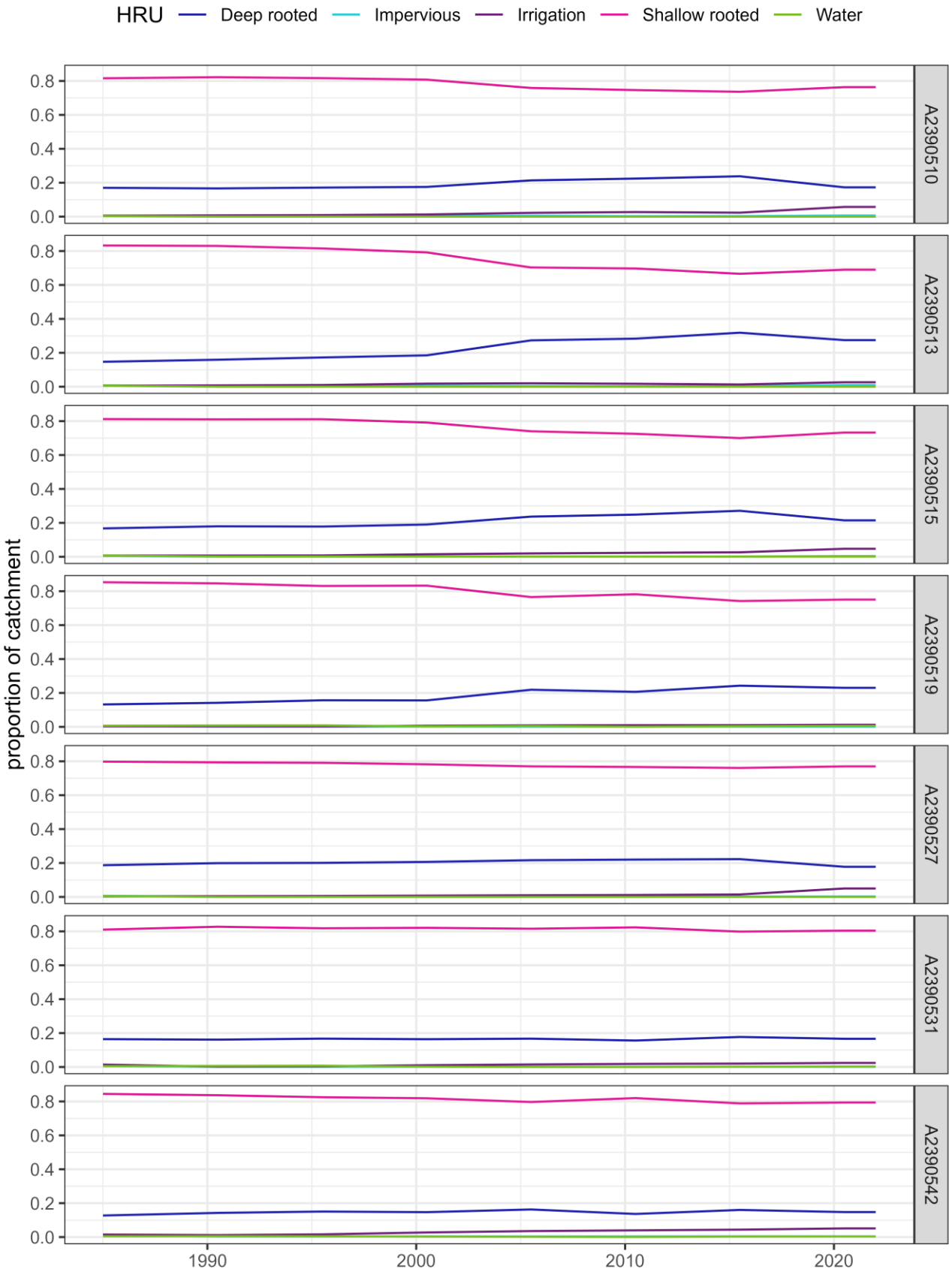

Figure 3-2 Changes in hydrological response unit (HRU) proportions over time for the calibration catchments

3.2 Parameterisation method

3.2.1 CALIBRATION PROCEDURE

As a semi-conceptual model, AWRA-L includes a large number of parameters, some of which are not easily prescribed and must be calibrated. This is done using a calibration algorithm based on comparing modelled and observed responses and seeking to minimise the differences between them. The datasets outlined in Section 2.3 are used as observed responses against which the model can be fit. Because of the number of parameters, and potentially different values for the same parameter for different HRUs, calibrating the values to multiple locations concurrently also constrains the parameter values and provides a mechanism to regionalise the model to where no observed data is available.

The performance of the model when calibrated to observed data, and evaluated on data for a period not used to calibrate the model (referred to as validation), has been tested for different combinations of the potential calibration datasets outlined in Section 2.3. The calibration period made use of the most recent data period where the remote sensing data is available to inform the model parameters, until the end of the climate data available from the 1km resolution product (see Section 2.3.1), spanning from 1/1/1985 to 31/12/2021. Streamflow and groundwater level data available before 1985 is used for model validation, testing the simulation on data not used to inform the parameter values. All calibration catchments, with the exception of Naracoorte Creek A2309542, have data in the validation period, with between 8 and 13 years of data held out for model validation. Mean annual rainfall and streamflow for the calibration and validation periods, and number of full years of data available, for each calibration catchment is summarised in Table 3-1. Mean annual rainfall varies from 500 mm/year in Morambro Creek (A2390531) in the northeast of the region, to just over 700 mm/year in Bakers Range South Drain (A2390515) in the south of the region. Highest mean annual runoff depth occurs in the western catchments of the Mount Hope-Reedy Creek Drain (A2390513) and Wilmot Drain (A2390527), followed by Drain L (A2390510). The calibration period is drier than the validation period, with a mean annual rainfall 8% lower in the calibration period resulting in 34% less runoff, when averaged across the calibration catchments.

Table 3-1 Mean annual rainfall and streamflow for the calibration and validation periods, and years of data available for each period

Catchment	Rainfall (mm/year)		Runoff (mm/year)		Years of data	
	Calibration	Validation	Calibration	Validation	Calibration	Validation
A2390510	599	633	27	25	29	12
A2390513	689	732	37	42	35	13
A2390515	702	747	21	29	34	13
A2390519	561	595	17	28	37	8
A2390527	620	648	37	43	29	11
A2390531	500	510	5	5	33	8
A2390542	523		5		28	

The optimisation method used for model calibration was the global search algorithm commonly used for hydrological applications, the Shuffled Complex Evolution (SCE), with SCE parameter values derived using relationships recommended by Duan et al. (1994). Several tests were undertaken to evaluate different calibration datasets and objective functions for model calibration. This included testing different combinations of the potential calibration datasets and the model with and without dynamic HRU proportions. Following the testing, a small number of model configurations were identified for final calibration runs. To account for the stochastic nature of the optimisation algorithm, the final runs included

three sequential runs of the calibration algorithm, initialised with the best solutions from the previous run to improve the sequential runs. The AWRA-L parameters to be calibrated, with the upper and lower limits considered, are outlined in Table 3-2. Table 3-3 provides the fixed values of other AWRA-L parameters that were not calibrated. These values are based on experience with the model in different catchments across Australia, see Viney et al. (2015).

The development of rainfall-runoff models incorporates a range of uncertainty ranging from measurement errors in spatial data (DEM and soil properties), input data (climate, streamflow data), and model structure limitations in representing the processes occurring within the catchment. The process complexities with flat topography, small proportion of rainfall observed as streamflow, and surface water-groundwater interactions make these uncertainties large in the South East of South Australia relative to other parts of Australia. Acknowledging and assessing uncertainty will increase transparency of the modelling process, identify areas for future improvements, and better quantify risks for decisions based on the model output.

To represent some of this uncertainty, a simplistic approach based on the Generalised Likelihood Uncertainty Estimation method (Bevan and Binley, 1992) has been used. Any set of model parameters that produced an objective function value within 5% of the best solution found was stored and treated as a 'behavioural' set of parameters, used to represent acceptable model performance and indicate the range in plausible sets of model parameter values and resulting outputs.

Table 3-2 Model parameters to be calibrated with the minimum and maximum bounds adopted. Values in red italics were modified from default ranges based on results from the initial testing, where the bound was found to be too tight during the testing calibration process

Parameter name	Short name	Minimum	Maximum
HRU:DR Conversion Coefficient From Vegetation Photosynthetic Capacity Index to Maximum Stomatal Conductance	cGsmax_hruDR	*0.01*	0.05
HRU:SR Conversion Coefficient From Vegetation Photosynthetic Capacity Index to Maximum Stomatal Conductance	cGsmax_hruSR	*0.01*	0.05
HRU:DR Ratio of Average Evaporation Rate Over Average Rainfall Intensity During Storms Per Unit Canopy Cover	ER_frac_ref_hruDR	0.04	*0.05*
Soil Evaporation Scaling Factor When Soil Water Supply is Not Limiting Evaporation (both DR and SR)	FsoilEmax	0.2	1
Scaling factor for groundwater drainage coefficient exponent	K_gw_scale	-1	6
Intercept coefficient for calculating rate coefficient controlling discharge to stream	K_rout_int	*0.01*	3
Scale coefficient for calculating rate coefficient controlling discharge to stream	K_rout_scale	*0.01*	3
Scale for saturated hydraulic conductivity surface layer	K0sat_scale	4	10
Scale for saturated hydraulic conductivity deep layer	Kdsat_scale	0.01	1
Scaling factor for ratio of saturated hydraulic conductivity	Kr_coeff	0.01	1
Scale for saturated hydraulic conductivity shallow layer	Kssat_scale	0.01	1
Scale for effective porosity	ne_scale	0.01	1
Scaling factor for reference precipitation	Pref_gridscale	0.1	8
HRU:DR Specific Canopy Rainfall Storage Capacity Per Unit Leaf Area	S_sls_hruDR	*0.04*	0.8
HRU:SR Specific Canopy Rainfall Storage Capacity Per Unit Leaf Area	S_sls_hruSR	*0.04*	0.8
Scale for Maximum water storage surface layer (Top)	S0max_scale	0.5	4
Scale for Maximum water storage deep layer (Deep)	Sdmax_scale	0.5	3
Scaling factor for slope	slope_coeff	0.1	1
Scale for Maximum water storage shallow layer (Shallow)	Ssmax_scale	0.5	5
HRU:DR Maximum Root Water Uptake Rates From Deep Soil	Ud0_hruDR	0.001	10
HRU:DR Specific Leaf Area	SLA_hruDR	0.7	70
HRU:SR Specific Leaf Area	SLA_hruSR	0.7	70
HRU:DR Characteristic Time Scale for Vegetation Growth Towards Equilibrium	Tgrow_hruDR	20	1000
HRU:SR Characteristic Time Scale for Vegetation Growth Towards Equilibrium	Tgrow_hruSR	20	300
HRU:DR Characteristic Time Scale for Vegetation Senescence Towards Equilibrium	Tsenc_hruDR	10	200
HRU:SR Characteristic Time Scale for Vegetation Senescence Towards Equilibrium	Tsenc_hruSR	10	200

Table 3-3 AWRA-L model parameters that were fixed to constant values based on alternate data or prior investigations, see Viney et al. (2015) for the basis of parameter values

Parameter name	Short name	Value
HRU:DR Dry Soil Albedo	alb_dry_hruDR	0.26
HRU:SR Dry Soil Albedo	alb_dry_hruSR	0.26
HRU:UR Dry Soil Albedo	alb_dry_hruUR	0.1
HRU:WR Dry Soil Albedo	alb_dry_hruWR	0.01
HRU:DR Wet Soil Albedo	alb_wet_hruDR	0.16
HRU:SR Wet Soil Albedo	alb_wet_hruSR	0.16
HRU:UR Wet Soil Albedo	alb_wet_hruUR	0.06
HRU:WR Wet Soil Albedo	alb_wet_hruWR	0.01
HRU:DR Reference Soil Cover Fraction That Determines The Rate of Decline in Soil Heat Flux With Increasing Canopy Cover	fvegref_G_hruDR	0.15
HRU:SR Reference Soil Cover Fraction That Determines The Rate of Decline in Soil Heat Flux With Increasing Canopy Cover	fvegref_G_hruSR	0.15
HRU:DR Fraction of Daytime Net Radiation Lost To Soil Heat Storage for an Unvegetated Surface	Gfrac_max_hruDR	0.3
HRU:SR Fraction of Daytime Net Radiation Lost To Soil Heat Storage for an Unvegetated Surface	Gfrac_max_hruSR	0.3
HRU:SR Height of Vegetation Canopy	hveg_hruSR	0.5
HRU:DR Reference Leaf Area Index (at which fveg = 0.63)	LAIref_hruDR	2.5
HRU:SR Reference Leaf Area Index (at which fveg = 0.63)	LAIref_hruSR	1.4
HRU:DR Rooting Depth	RD_hruDR	6
HRU:SR Rooting Depth	RD_hruSR	1
HRU:SR Maximum Root Water Uptake Rates From Deep Soil	Ud0_hruSR	0
HRU:DR Maximum Root Water Uptake Rates From Shallow Soil	Us0_hruDR	6
HRU:SR Maximum Root Water Uptake Rates From Shallow Soil	Us0_hruSR	6
HRU:DR Vegetation Photosynthetic Capacity Index Per Unit Canopy Cover	Vc_hruDR	0.92
HRU:SR Vegetation Photosynthetic Capacity Index Per Unit Canopy Cover	Vc_hruSR	0.59
HRU:DR Relative Top Soil Water Content at Which Evaporation is Reduced	w0limE_hruDR	0.85
HRU:SR Relative Top Soil Water Content at Which Evaporation is Reduced	w0limE_hruSR	0.85
HRU:DR Reference Value of w0 Determining the Rate of Albedo Decrease With Wetness	w0ref_alb_hruDR	0.3
HRU:SR Reference Value of w0 Determining the Rate of Albedo Decrease With Wetness	w0ref_alb_hruSR	0.3
HRU:DR Deep Water-Limiting Relative Water Content	wdlimU_hruDR	0.3
HRU:SR Deep Water-Limiting Relative Water Content	wdlimU_hruSR	0.3
HRU:DR Shallow Water-Limiting Relative Water Content	wslimU_hruDR	0.3
HRU:SR Shallow Water-Limiting Relative Water Content	wslimU_hruSR	0.3

3.2.2 OBJECTIVE FUNCTIONS

Surface water available in the drainage network is a key interest for the study, and as such the streamflow data was assigned the highest weight in the model calibration. Additionally, the monthly averaged groundwater level across the catchment, and the remotely sensed leaf area index and soil moisture, have been included in the objective function.

The objective function for streamflow data was based on the commonly used function developed by Viney et al. (2009). This function maximises a combination of daily and monthly flows, as well as minimise the overall volume error as:

$$f_{Q,s} = \frac{NSE\left(Q_{d,s}^{0.5}, Q_{d,o}^{0.5}\right) + NSE(Q_{m,s}, Q_{m,o})}{2} - 5|\log(1+B)|^{2.5}$$

$$B = \frac{\sum Q_{d,s} - \sum Q_{d,o}}{\sum Q_{d,o}}$$

where NSE() is the Nash Sutcliffe Efficiency, $Q_{d,s}$ and $Q_{d,o}$ are the daily simulated and observed time series, respectively, with $Q_{m,s}$ and $Q_{m,o}$ time series aggregated to a monthly time step and B is the total volume bias. The $f_{Q,s}$ values for each streamflow station were combined in a weighted average across all calibration sites, f_Q, using the length of the streamflow record at each station to derive the weightings.

The objective function attempts to weight the important components of the streamflow time series, with a square root transform applied to the daily flows allowing the full flow regime to influence the error calculated (Thirel et al., 2024; Wright et al., 2015). Without this, the NSE metric tends to focus on high flows, which are often the most uncertain. However, this transformation may not incorporate as large a focus on low flows as other transformations (a smaller power or a log transform, for example), however low flows are of less of a focus for this study primarily interested in water volumes. The NSE on a monthly time step incorporates factors of seasonal flow without an emphasis on the timing of the peaks, where the bias term is used to prioritise model parameter sets that accurately reflect the long-term water availability.

For LAI, the MODIS derived LAI time series for deep and shallow rooted vegetation was used as the calibration data (Section 2.4.5). The NSE values between the simulated and derived LAI values for each catchment were weighted in the same way as the streamflow objection function and then averaged across the deep rooted and shallow rooted HRUs to derive a value of f_{LAI} across the calibration catchments for a given parameter set.

For soil moisture and groundwater data, the units of the calibration datasets do not match the units of the stores in the model. For this case the NSE is not a suitable metric, and instead a Pearson correlation has been used to calibrate the model to match the pattern in the datasets. This does not control for the magnitude of the values; the same correlation could be derived from either very low or very high variability in the stores. Hence, using correlation alone is not likely to result in a suitable model, however including the streamflow and LAI components are expected to provide some control on the simulated water balance. The individual catchment objective functions for soil moisture, $f_{SM,s}$, were calculated as the correlation between the averaged soil moisture across the catchment each month and the average surface store level, S_0, across the HRUs and model cells in the catchment, before being weighted across the calibration catchments using the same factors as streamflow to derive f_{SM}. A similar approach was used for f_{GW} with the catchment-averaged monthly groundwater level correlated to the deep soil storage level, S_d.

To provide a single value to be maximised by the optimisation algorithm, OF, the different components were weighted as follows:

$$OF = 0.6f_Q + 0.2\frac{(f_{SM} + f_{GW})}{2} + 0.2f_{LAI}$$

This objective function is referred to as the 'combined' objective function. The AWRA-L model has also been calibrated to only f_Q, referred to as Q-only, to investigate the benefit or trade-offs from including the groundwater and remotely sensed data in the objective function. One model simulation of the calibration catchments from 1/1/1930 - 31/12/2021 on one CPU took approximately 40 minutes. The earlier start date

used to ensure groundwater stores were 'warmed up' before influencing the calibration results. Running one SCE calibration in parallel on 64 CPUs took approximately 8 days for convergence, after approximately 20,000 simulations.

3.3 Results

Performance metrics for both the Q-only and combined objective functions over the calibration period are provided in Figure 3-3. NSE values range from -∞ to 1, with a value of 1 indicating no difference between modelled and observed, NSE values of approximately 0.6 typically considered acceptable for streamflow simulations and values less than 0 indicating worse performance than a constant value of the average. It would be expected that the f_Q (Q-only) objective function performs the best on the streamflow metrics during the calibration period, as other components of the model output do not influence the objective function value. This is the case for four driest catchments, with the catchments plotted in order from wettest to driest in Figure 3-3. However, in general the combined objective function performed as well or better on the three wetter catchments. The f_Q (Q-only) objective function achieved a better volume bias (closer to zero) than the combined objective function, however this came at the expense of the other components not included in the Q-only objective function. The combined function performed better for LAI, soil moisture and all but the two driest catchments for the correlation to groundwater level.

Over the earlier independent validation period (Figure 3-4), the NSE metrics follow similar patterns with the f_Q calibration performing better on the drier catchments. However, on the validation period the combined model produces a better volume bias for four of the six catchments and is very similar to f_Q calibration on the other two. The correlation between the deep soil store and groundwater level is higher for all but one catchment. Note that there is no streamflow data for Naracoorte Creek, A2390542, over the validation period, and this period predates the remotely sensed soil moisture and leaf area index datasets.

The streamflow results for catchment A2390510 are summarised in Figure 3-5, with other catchments presented in Appendix C. The two exceedance curves in the left panel provide an indication of the flow regime; the top left figure has a log y-axis scale to focus on low flows, and the bottom left figure has a linear scale for focusing on high flows. Overall, the model provides a suitable representation of the flow regime, considering the application of the model to quantify overall water availability as opposed to flood risk or ecohydrological metrics, for example, which have more focus on high flow or low flows, respectively. The AWRA-L model tends overestimate very low flows, and the ability for the model to completely cease to flow is a known limitation with this model and some other conceptual rainfall runoff models (Azarnivand et al., 2022). Changes were made to the model structure in an attempt to improve this behaviour (Section 3.1.2), however it appears the changes made little improvement. High flows can also tend to be underestimated by the calibrated model. This is expected to be due to a combination of factors including 1) the objective functions used, focusing on the overall water balance rather than targeting peak flows, and 2) the gridded rainfall input product "smoothing out" the most extreme rainfall events (e.g. Bárdossy and Anwar, 2023).

The top plot on the right-side of Figure 3-5 compares observed and simulated annual volumes, with the dots indicating the proportion of each year with good quality data, and the red shaded area indicating the validation period. The middle right figure in Figure 3-5 presents the residual mass curve, or the cumulative sum of the difference between the daily streamflow and the observed average daily streamflow. Periods with above average streamflow result in a positive slope, and below average periods a negative slope. When the observed and modelled lines are parallel the model is representing the observed streamflow accurately, with steps introduced when there are differences in the volumes simulated. Finally, the bottom right figure in Figure 3-5 presents the monthly streamflow, to provide an indication of the seasonal variability in flows from month to month and across years. This figure also suggests the highest flows are underestimated; however, this is less of the case for the combined objective function model. These results indicate the model output may not be suitable for assessing flooding impacts, which is of little concern for this study.

Figure 3-6 presents the monthly streamflow on a log scale, as well as LAI for the deep and shallow rooted HRUs, and monthly soil moisture and groundwater data compared to the relevant model storage levels. Figure 3-6 presents the results for catchment A2390510, with results from other catchments provided in

Appendix D. The S_0 and S_d model stores that are correlated to the catchment average groundwater level and remotely sensed soil moisture data is in different units, and as such are presented on a normalised scale. On a log scale the combined objective function model tends to simulate lower flows slightly better than the Q-only model. There is very little difference between the models for the soil moisture data (SM), indicating the model tends to accurately represent the surface store dynamics even without calibrating to the remotely sensed data. With the combined model calibrating S_d to the groundwater level data, and the LAI to the MODIS derived time series, this does result in a substantial improvement in the representation of these time series, as would be expected. While the magnitude is greatly improved by including LAI data in the model calibration, the dynamics for the deep-rooted vegetation do not match as well, which is an acknowledged limitation of the simple vegetation module within AWRA-L (Van Dijk, 2010).

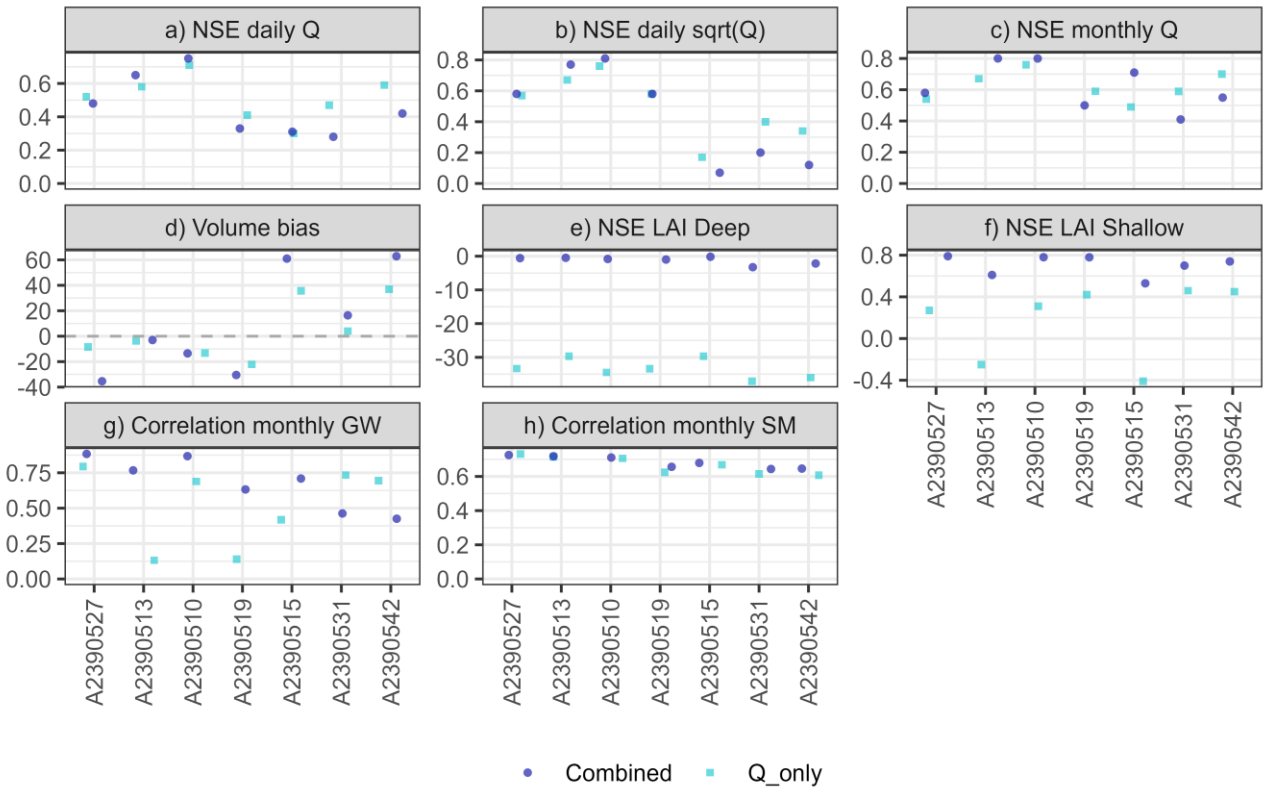

Figure 3-3 Calibration period results comparing objective functions for streamflow (Q) only, and the combined objective function including streamflow, soil moisture (SM), groundwater level GW) and leaf area index (LAI)

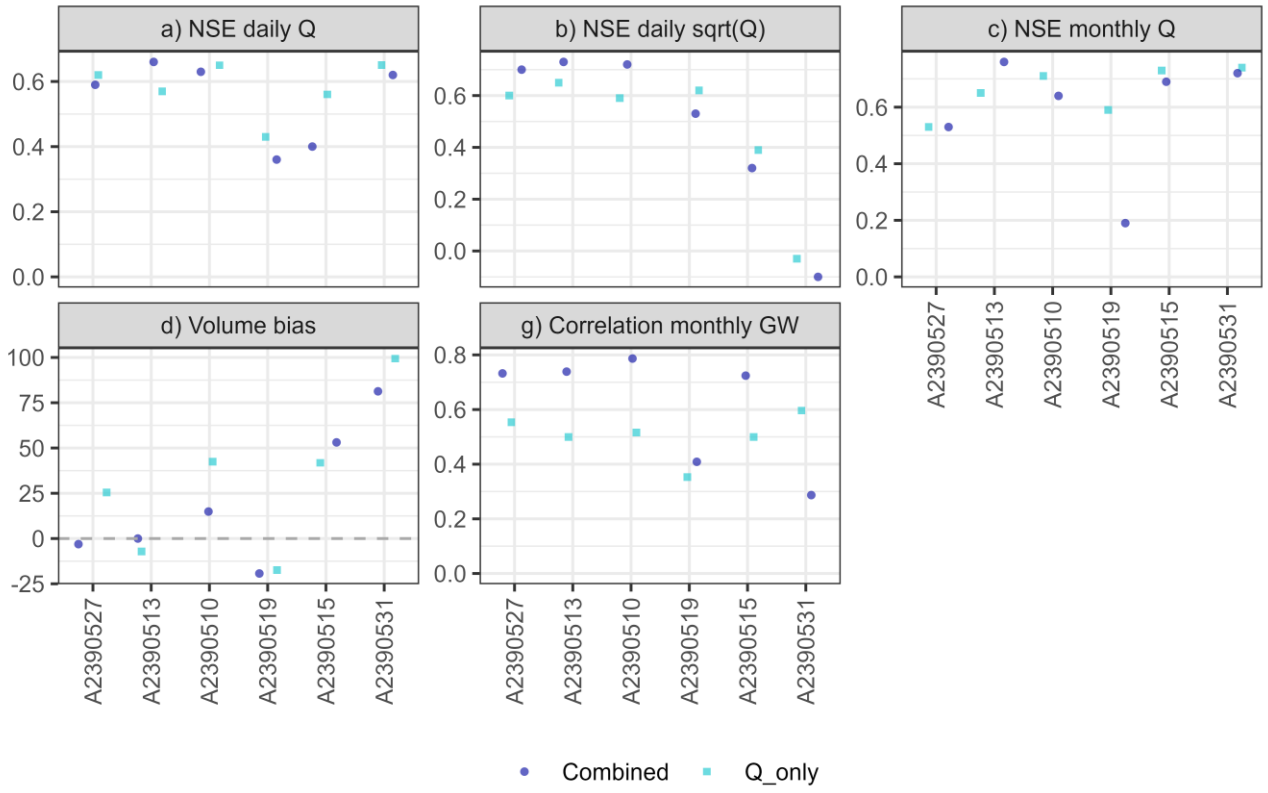

Figure 3-4 Validation period results comparing objective functions for streamflow (Q) only, and the combined objective function including streamflow, soil moisture (SM), groundwater level GW) and leaf area index (LAI)

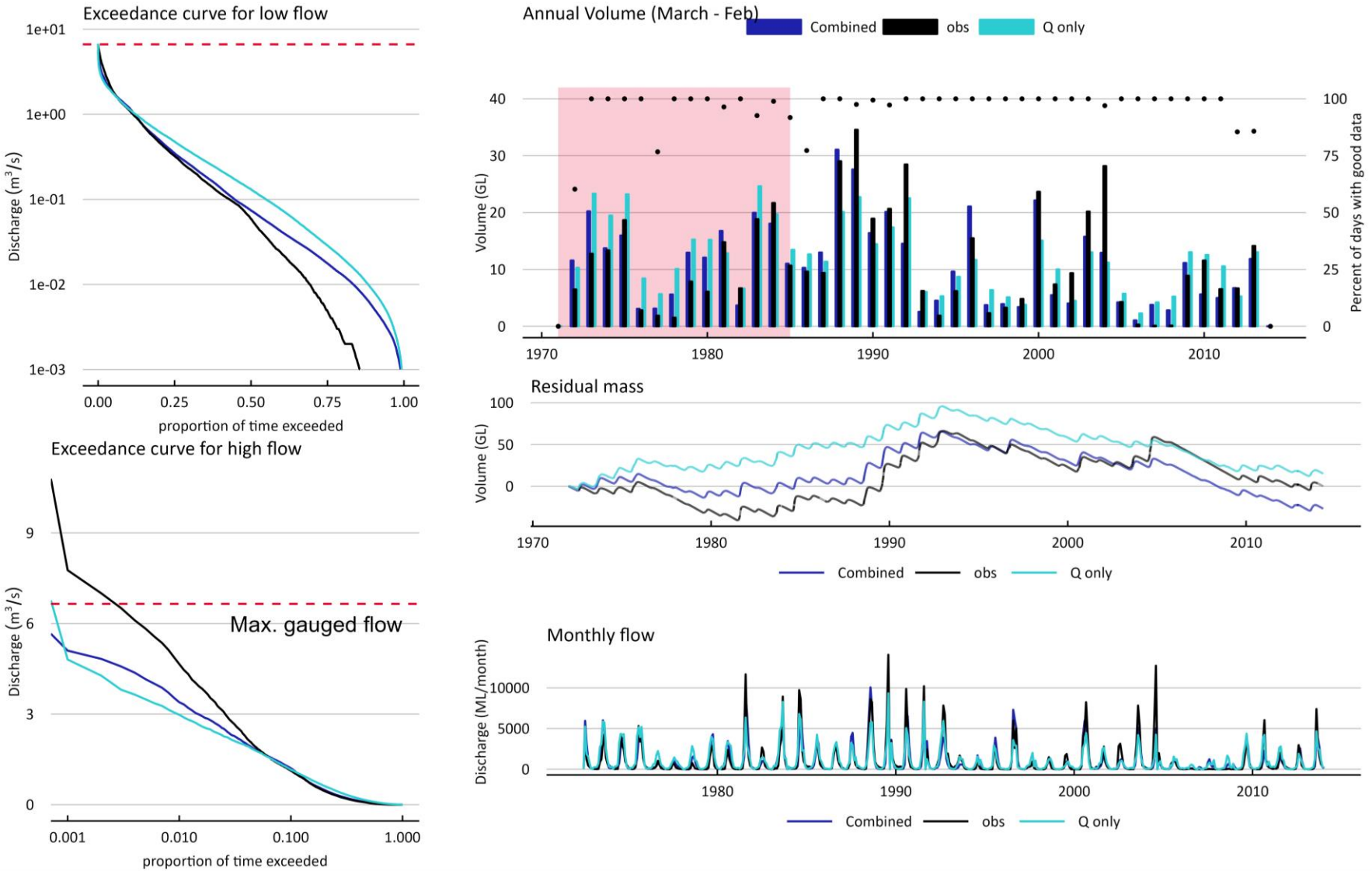

Figure 3-5 Streamflow results for an example catchment, Drain L upstream of the Princess Highway (A2390510). The two left panel plots are flow duration curve on log and linear y-axis scales, to focus on the low and high flows, respectively. Performance metrics on the calibration and validation periods are included in the two tables. The two highest flow events in the record are showing in the two top right plots. Middle right presents annual streamflow volumes, with bottom right the cumulative deviation from the mean streamflow, showing periods of wetter (positive slope) and drier (negative slope) streamflow. Other stations are presented in Appendix C

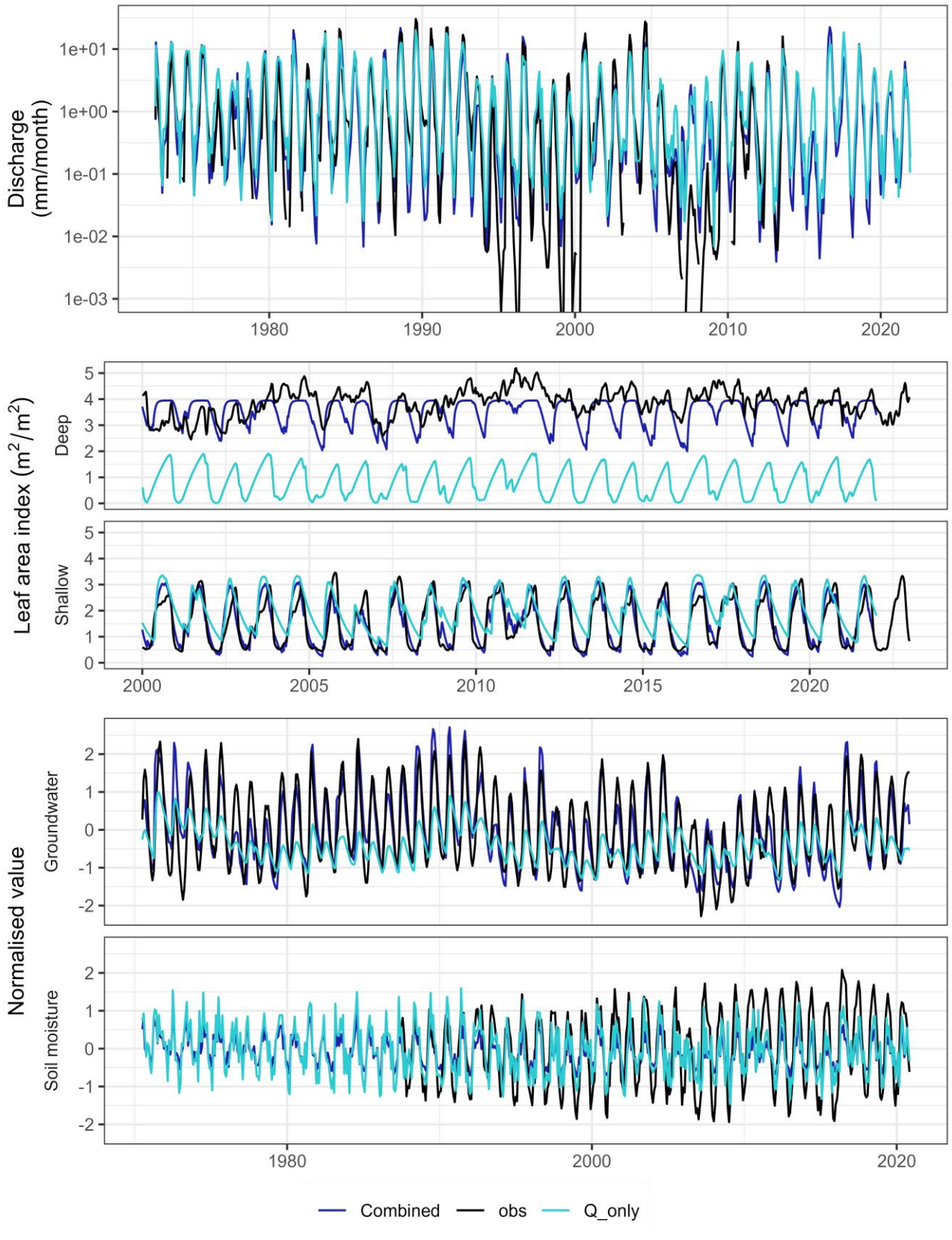

Figure 3-6 Catchment average model states used in the combined objective function for A2390510, streamflow at the daily and monthly time scale, and the capacity of the S_d store compared to groundwater levels, and remotely sensed soil moisture compared to the capacity of the S_0 store. The bottom two plots are on a normalised scale, as the observed (Obs) and modelled terms are on different scales. Other stations are presented in Appendix D

The modelled deep drainage, D_d, was compared to annual groundwater recharge values, with the observed recharge rates derived using the water table fluctuation method, as outlined in Crosbie et al. (2015). The results of Crosbie et al. (2015) were extended from 2012 to 2021 using the same method. A catchment average recharge rate was calculated by area-weighting the recharge rates calculated at individual wells using Thiessen polygons, with modelled and observed annual time series seen as the thin lines in Figure 3-7. The thicker lines in Figure 3-7 are locally estimated scatterplot smoothing (loess) second order polynomial regression lines to compare longer term trends, with the shaded grey area representing the standard error of each regression line.

By including the groundwater level in the model calibration, the combined model produces recharge rates much closer to the water table fluctuation derived recharge rates, albeit with slightly reduced variability. NSE values are zero or greater, indicating the annual variability is a better representation of the data than the long-term average, which is not the case for the Q-only model. Biases vary from catchment to catchment but are closer to the observed recharge rates than the Q-only model, which underestimates recharge rates by over 50% in each catchment (Table 3-4). The improvement in the modelled annual recharge from the combined objective function, along with the representation of LAI influencing the calculated evapotranspiration rate, represents a significant improvement these two important components of the water balance for the region.

Table 3-4 Recharge (mm/year), calculated as mean annual deep drainage, D_d, compared to water table fluctuation (WTF) recharge

Catchment	Average recharge (mm/y)			NSE		Bias (%)	
	Observed	Combined	Q-only	Combined	Q-only	Combined	Q-only
A2390510	89	94	36	0.41	-2.24	5.7	-59.1
A2390513	138	108	41	0.08	-3.58	-21.5	-70.3
A2390515	131	112	42	0.26	-2.59	-15	-67.9
A2390519	69	62	17	0	-2.13	-9	-74.6
A2390527	91	87	30	0.45	-3.36	-4.9	-67.6
A2390531	40	53	18	0.25	-0.72	34.2	-53.8
A2390542	41	51	14	0.3	-0.7	23.2	-66.9

Distributions of parameter values that resulted in a combined objective function value within 5% of the best value found are shown in Figure 3-8. These parameter sets were derived from the solutions found by the final SCE calibration run, and as such may not represent a complete sampling of the parameter space. For many parameters the combined objective function has a narrower distribution, indicating that the parameters were better identified than the Q-only model, where a wide range in parameter values produced similar model performance (as evaluated by the streamflow only metrics). The parameters involved in LAI dynamics, t_{scen} and t_{grow}, are different for both shallow and deep rooted HRUs, along with a number of other parameters at alternate ends of the parameter ranges.

Given these results, the model parameters derived based on calibration to the combined objective function have been selected for scenarios analysis in the reminder of this work.

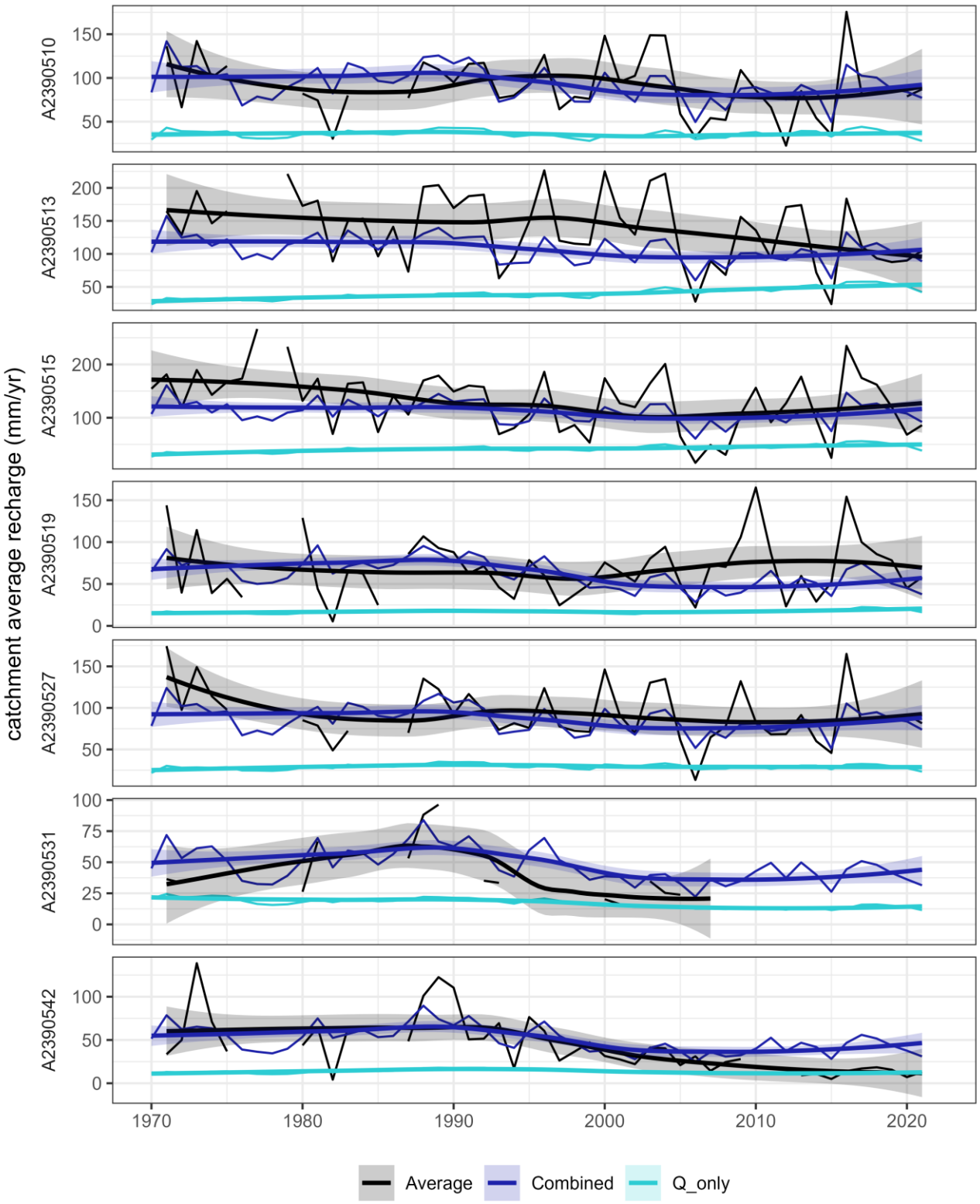

Figure 3-7 Annual recharge averaged across the calibration catchments based on the water table fluctuation method (Average) and from the model for the two objective functions. Thin lines represent the annual results, with the thicker line a locally estimated scatterplot smoothing (loess) second order polynomial regression applied to the annual results to compare longer term trends. Shaded grey area corresponds to the standard error of the regression line

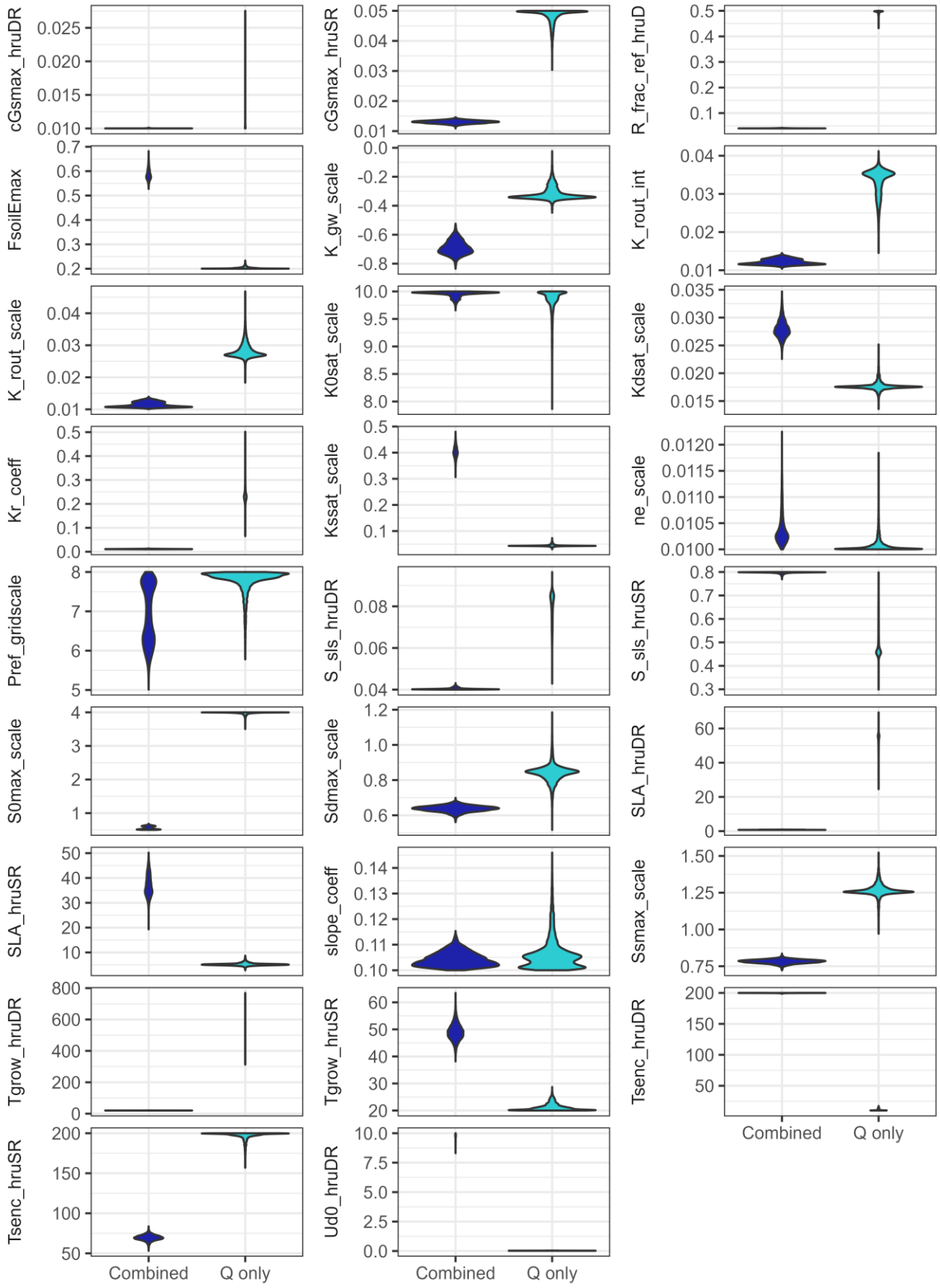

Figure 3-8 Distributions of parameter values for the best 5% of solutions for each objective function. Parameter descriptions are outlined in Table 3-2

3.4 Comparison to other datasets

3.4.1 SURFACE WATER

The full domain model outputs have been compared to all flow data available, beyond the seven calibration catchments with unregulated, long term, and high-quality records. Data for complete water years (March – February, defined as at least 335 days in the year with data coded with good quality) were averaged to determine the mean annual streamflow volume at each gauge. Two locations were identified where the simulated mean annual streamflow overestimated the observed records substantially. The first are the two catchments contributing to Lake Bonney (pink dots in Figure 3-9). The total modelled streamflow was derived by summing the output from the model cells that are within a catchment boundary—derived from the 2m LiDAR as outlined by Wood and Way (2011)—Figure 3-10 for these two gauges. It is expected that the very flat terrain in this area has resulted in larger catchments being calculated than contributes to these points in reality. The assumed contributing catchment area was reduced to the solid yellow area in Figure 3-10 delineated by the Kongorong-Tantanoola Road for the Stoney Creek station (A2390523), and assuming Drain 37B does not contribute to Drain 44 (A2390532), noting that Millicent wastewater treatment plant has discharged into Drain 44 historically.

The second location that the model overestimates mean annual streamflow is along Drain M downstream of Bool Lagoon and the catchments that contribute to this drain from the southeast (purple dots in Figure 3-9). This is in part due to the approach of aggregating upstream model cells not accounting for large storages, in particular Bool Lagoon (A2390541). This does not fully explain the overestimation though, with more modelled flow along Drain C (A2390516, A2390536 and A2390537, noting these flow records are very short), Bakers Range South Drain (A2390515 and A2391001), and where these sites contribute to Drain M at Callendale (A2390414). The source of the overestimation is unclear; there are possibly errors in the soil spatial layers used as input to the model, underestimation of evapotranspiration, challenges representing surface water – groundwater interactions, or the 1D assumptions in the model may not adequately represent 2D effects in this area, resulting in runoff in upstream parts of the catchment not reaching the gauge in reality. A piecewise linear loss model was calibrated for each gauge to improve the representation of the flow duration curve at each of the stations outlined above, using the Drain M Source Model developed in a past Goyder Institute project (Gibbs et al., 2015). The resulting losses were applied to the AWRA-L grid cell output for these contributing catchments by scaling the daily flow in each cell by the same fraction as the resulting reduction caused by the loss node in the Source model and adding the removed streamflow to the total evapotranspiration output.

The resulting modelled mean and median annual streamflow was compared to the observed data, based on the corresponding years with data available at each gauge (Figure 3-9). Good agreement was achieved at this scale of mean and median volumes, with the slope of the line of best fit between the observed and simulated volumes close to 1 (0.99 and 1.04 for mean and median, respectively) and coefficients of determination of R^2=0.91 and R^2=0.87 for mean and median, respectively.

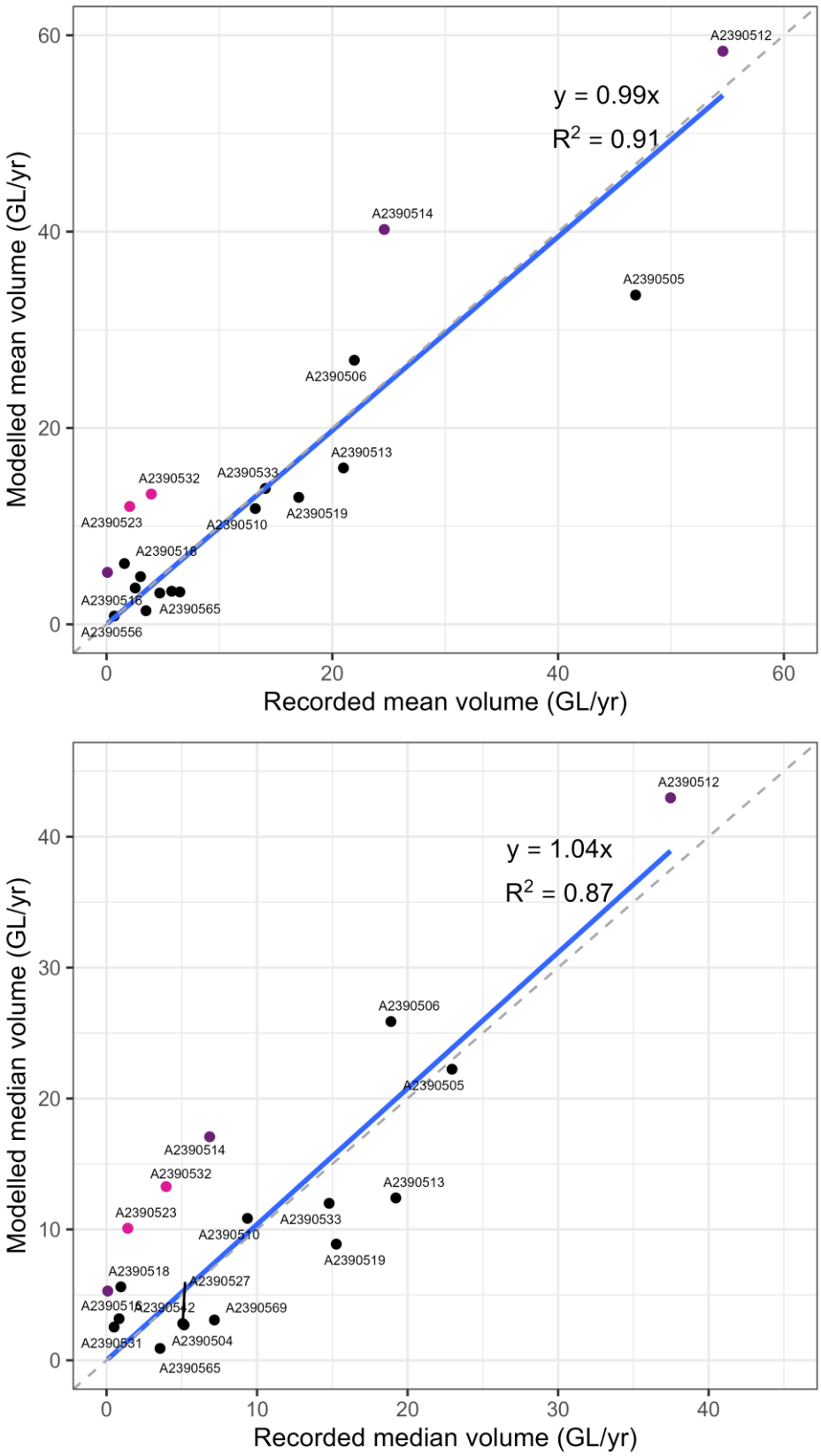

Figure 3-9 Mean (top) and median (bottom) annual streamflow for all stations with data available in the region. Drain M gauges downstream of Bool Lagoon (including contributing catchments) shown in purple, and two gauges contributing to Lake Bonney in pink

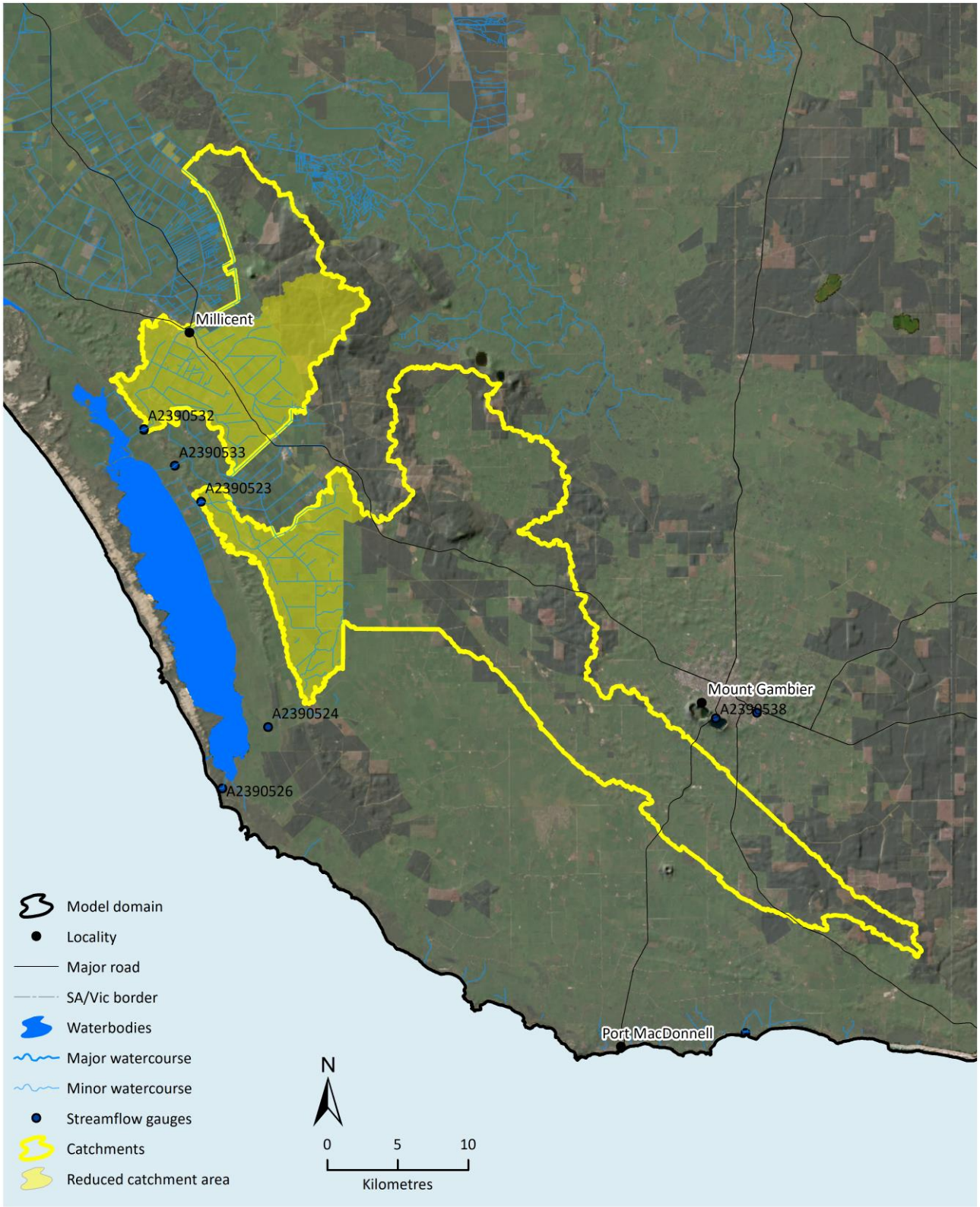

Figure 3-10 Catchments delineated contributing to Lake Bonney, as defined in Wood and Way (2011), with reduced catchment areas considered in solid yellow

3.4.2 RECHARGE

The modelled recharge has also been compared to the assumed values in the Appendices for the Lower Limestone Coast Water Allocation Plan. Any model cells with negative deep drainage, representing irrigation occurring, were excluded from the calculation of the average recharge rate across an unconfined management zone. A large proportion of the variability is explained by the modelled values (R^2 = 0.87), however the modelled result tends to slightly underestimate the WAP-assumed recharge rates (slope of 0.86). These results are also shown as a map in Figure 4-5.

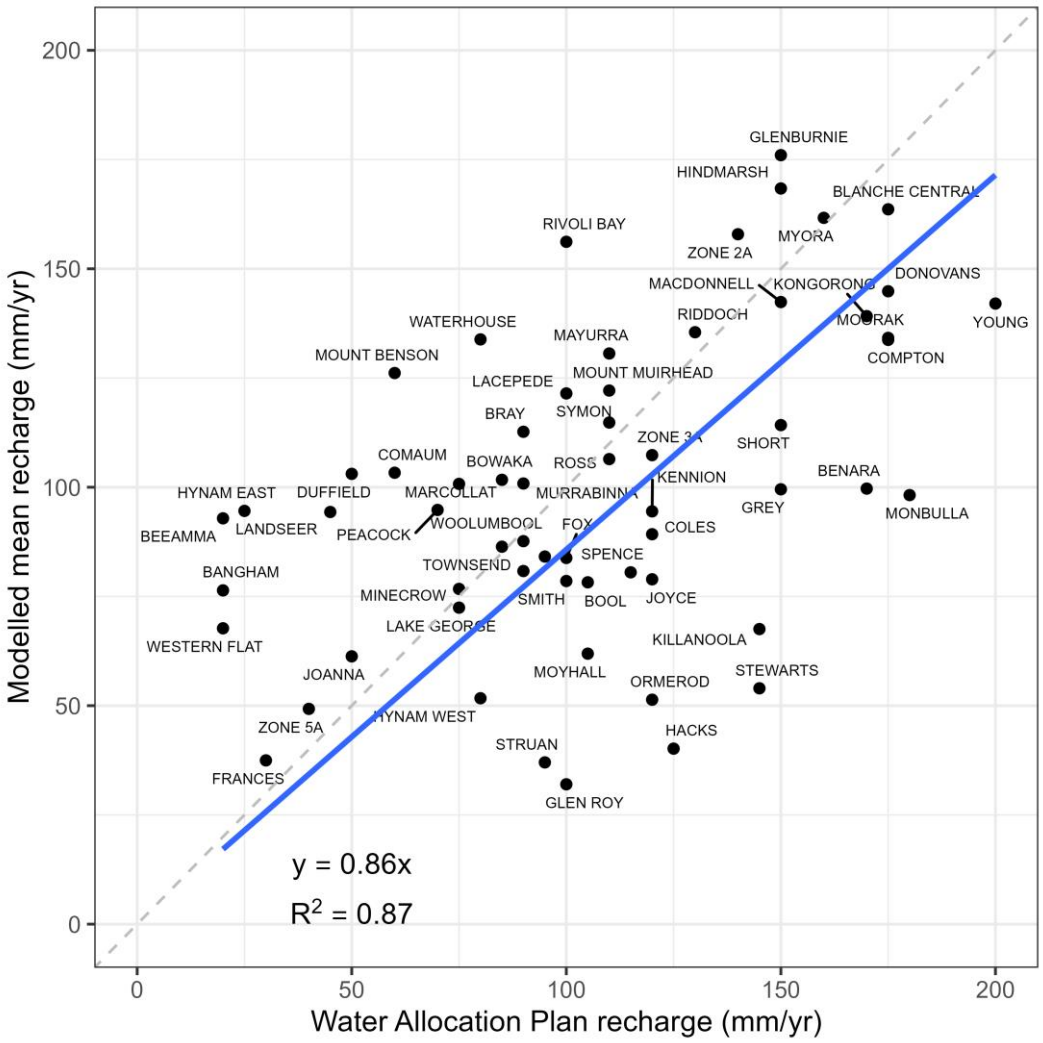

Figure 3-11 Modelled vs assumed recharge for each unconfined management area in the Lower Limestone Coast Water Allocation Plan

4 Historical water availability

The results from the calibrated model across the region from the full model domain have been summarised to answer of the key questions of this work: how do components of the water balance (runoff, recharge and actual evapotranspiration) vary over time and across the region?

One measure of water availability is rainfall minus AET i.e., how much of the rainfall that fell in a location is expected to have been lost to evapotranspiration. This is presented on a pixel by pixel basis over the period of record with AET data available (see Section 2.4.4) in Figure 4-1 and in five-year periods in Figure 4-2. The permanent and intermittent water bodies, such as the coastal lakes and Bool Lagoon, are evident in the figures with negative water available, indicating more evapotranspiration than rainfall occurred in that location due to the accumulation of water from upstream. Areas of plantation forestry and irrigation in the Coonawarra and south of the region are also evident from negative water available and more evapotranspiration than rainfall at these locations, most likely due to accessing local groundwater. The reduction in evapotranspiration, and hence increase in water available, seen in the 2016-2021 map, coincide with reductions in the forestry footprint Figure 4-2. These maps provide an indication of where water may be available in the region to be redirected to support wetlands and subsequent recharge to groundwater.

An indication of the water availability in the drainage network is shown in Figure 3-9 as the mean and median volumes observed and simulated across the system. To represent the streamflow along drains throughout the domain, as opposed to only at specific flow gauges, the DEM was processed to determine the downstream flow direction for each model cell, with the flow at each grid cell accumulated from the runoff from upstream cells to that location. The resulting median annual flow across the model domain is presented in Figure 4-3. To provide an indication of the variability in flow from year to year, the 20th and 80th percentile exceedance volumes—which a dry year exceeded 4 years in 5 on average, and a wet year exceeded 1 year in 5, respectively—is shown in Figure 4-4. The differences between the 20th and 80th percentile maps indicate the high inter annual variability in flow in the region. The hydrological reference stations on Mosquito Creek (A2390519), Morambro Creek (A2390513) and Stoney Creek (A2390523) have annual coefficients of variability of 1.04, 1.31 and 0.97, respectively, which represent very high variability in the context of Australian rivers for catchments with a mean annual rainfall in the range of 500-700 mm (Petheram et al., 2008). This variability represents a challenge for infrastructure designed to optimise the use of excess flows, as these conditions can be unreliable.

The recharge rates presented in Figure 3-11 are presented spatially in Figure 4-5, for both the assumed WAP and modelled rates. The results show that the spatial patterns are relatively consistent, with more recharge in the south of the region and less recharge to the north, in line with the rainfall gradient. Further analysis of the water balance and availability for the historical climate is provided in Section 5, as part of the comparison to future climate scenarios.

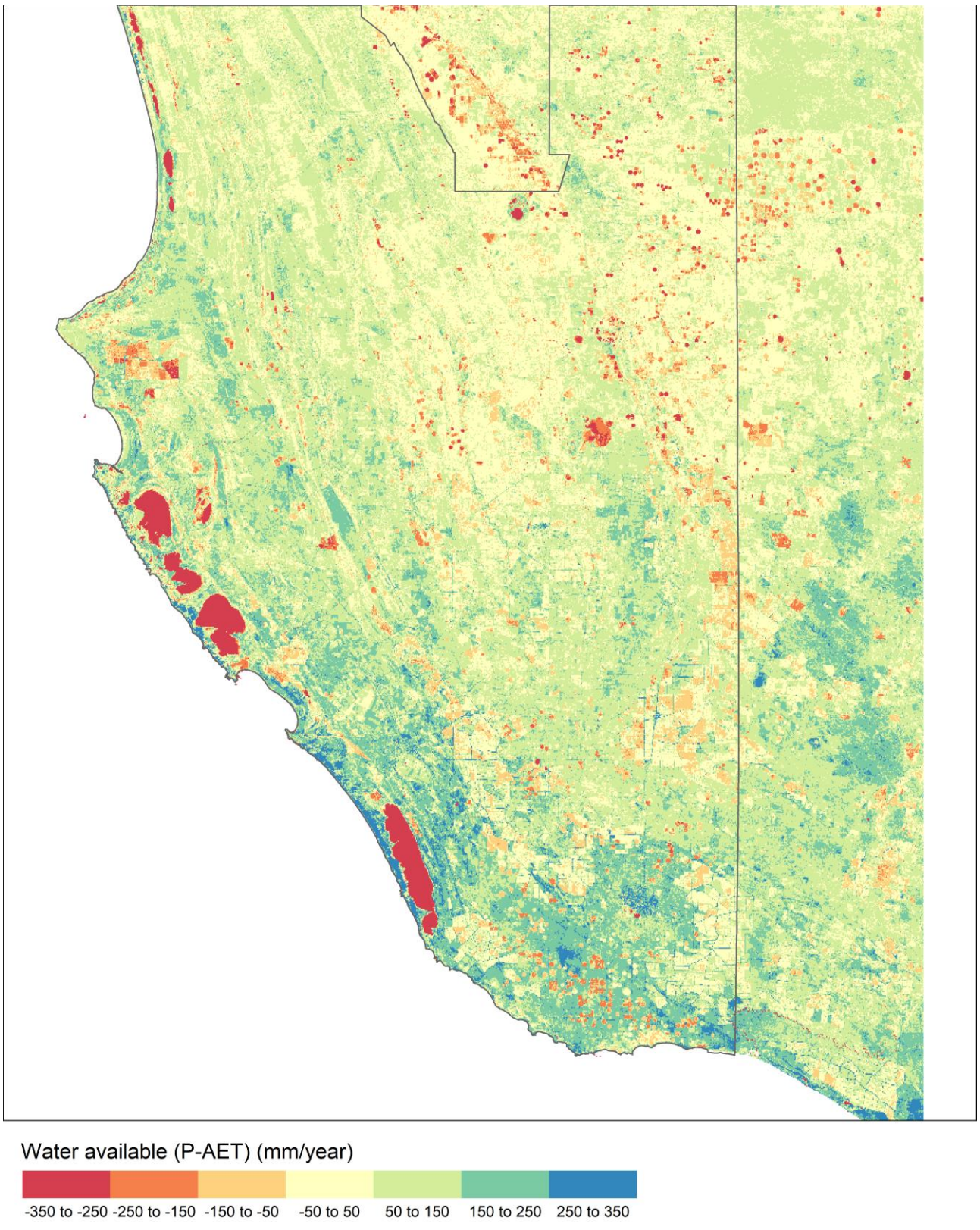

Figure 4-1 Water available across the region, as defined as precipitation (P) minus actual evapotranspiration (AET). Precipitation data sourced from Australian Water Availability Product and AET from CMRSET. The period shown is based on the water year (March-Feb) and availability of CMRSET data, from March 2000 to February 2022

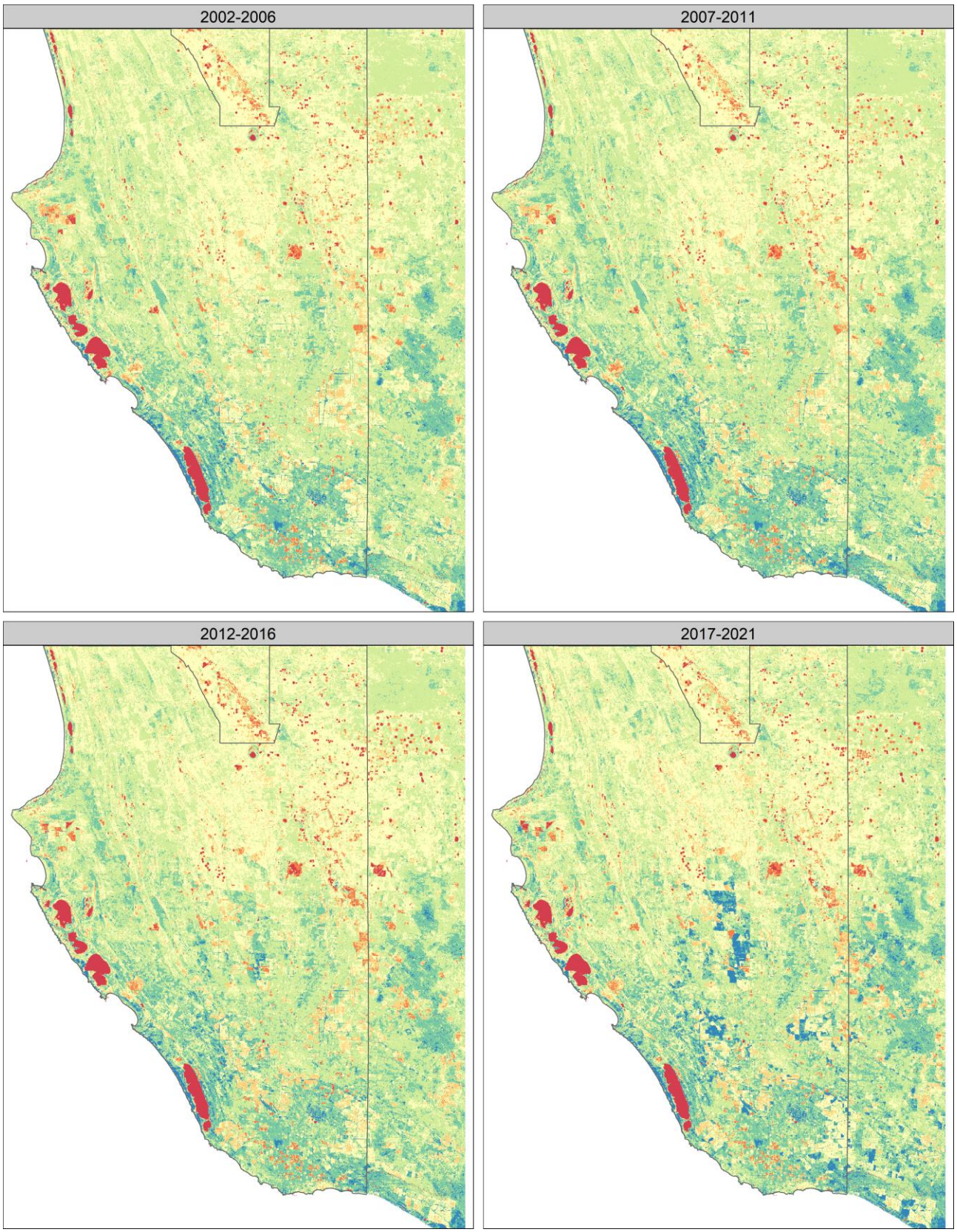

Figure 4-2 Water available across the region for five-year periods, as defined as precipitation (P) minus actual evapotranspiration (AET). Precipitation data sourced from Australian Water Availability Product and AET from CMRSET. See Figure 4-1 for the colour scale

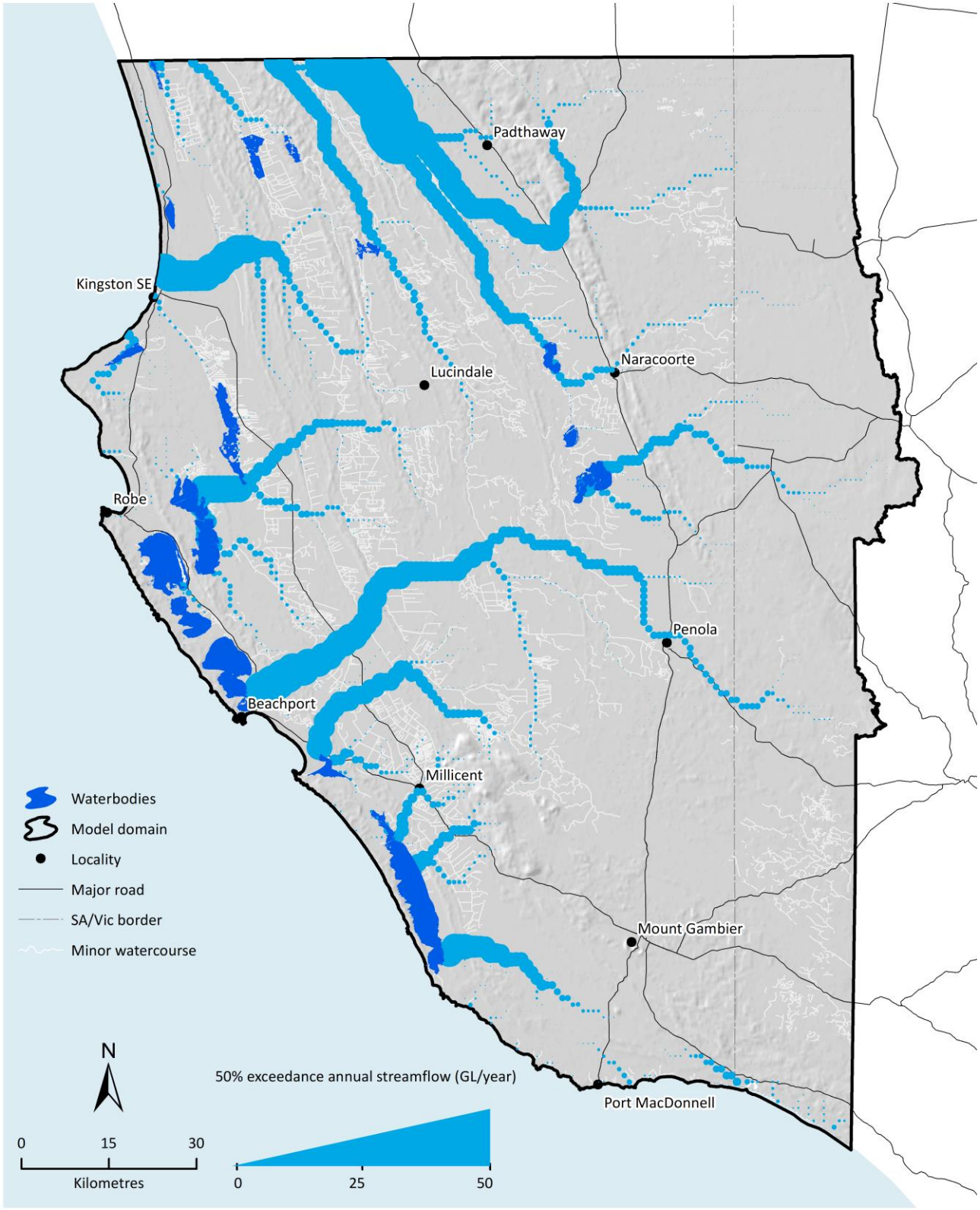

Figure 4-3 Modelled median annual streamflow in the model domain over 1970-2020

Storage in wetlands is only explicitly represented in Bool Lagoon (waterbody between Naracoorte and Penola), other water courses are not accounted for in the flow accumulation. Hence, streamflow volumes downstream of coastal lakes and Lake Hawdon not shown, as these lakes are not represented. Loss relationships have only been applied to Drain M and contributing catchments, seen flowing from Penola to Beachport. Flow accumulation for the Glenelg River, with the contributing catchment predominately in Victoria, is not shown

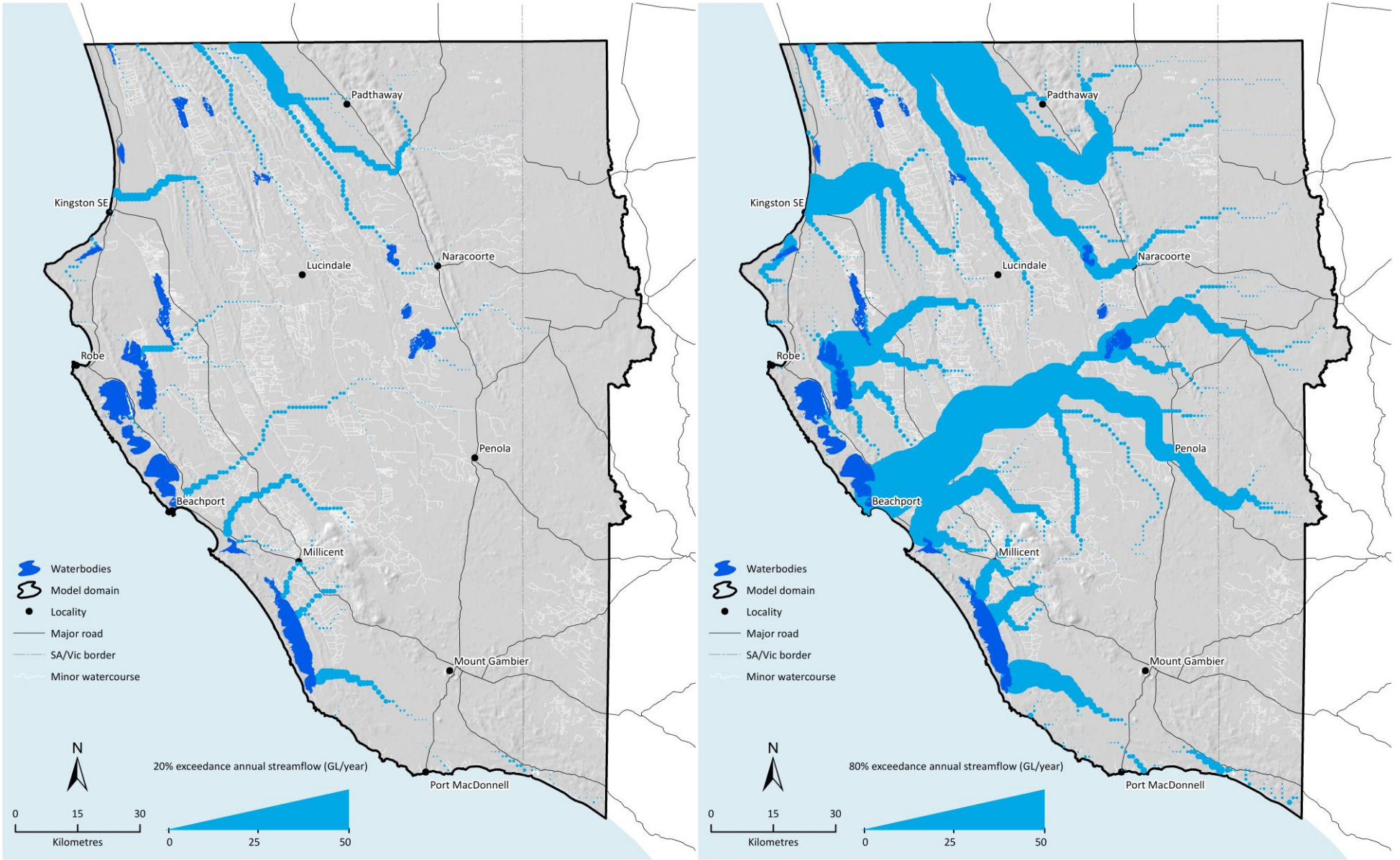

Figure 4-4 20th (left) and 80th (right) percentile exceedance annual streamflow across the model domain. The same caveats as Figure 4-3 apply

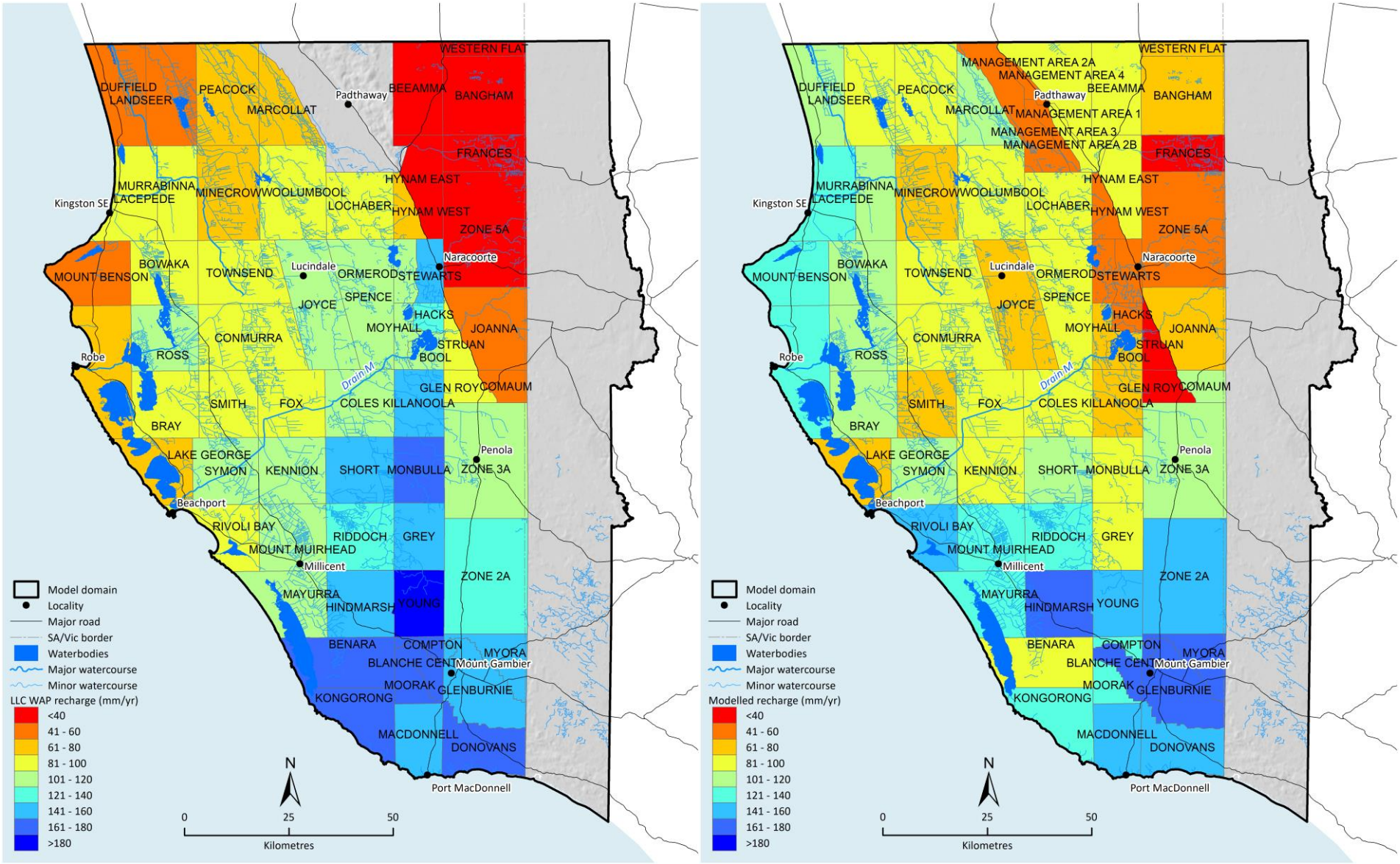

Figure 4-5 Lower Limestone Coast Water Allocation Plan recharge (left) compared to mean annual deep drainage from AWRA-L, spatially averaged for each unconfined management area (1970-2021)

4.1 Historical hydroclimate trends

As a further summary of historical water availability, with a view toward future water availability, trends in relevant datasets have been investigated. State of the Climate 2024 (CSIRO and Bureau of Meteorology, 2024) (CSIRO and Bureau of Meteorology, 2024) provides an overview of observed changes in Australia's climate. Key points from that report include:

- Australia's climate has warmed by an average of 1.51 ± 0.23 °C since national records began in 1910.
- In the south-east of Australia, there has been a decrease of around 9% in April to October rainfall since 1994.
- Cool season rainfall in southern Australia has been above the 1961–1990 average in only 6 of the 30 years from 1994−2023.
- There has been a decrease in streamflow at most gauges across Australia since 1970 (see also Wasko et al., 2024). All six hydrological reference stations assessed in the Millicent Coast and Glenelg River regions showed statistically significant declining trends in streamflow.
- Sea levels are rising around Australia, including more frequent extreme high levels that increase the risk of inundation and damage to coastal infrastructure and communities.

The remainder of this section reviews trends observed within the study region, and the model's ability to capture them.

4.1.1 Temperature

The Bureau of Meteorology maintains a number of observational datasets to identify, monitor and attribute variations and changes in the Australian climate. For air temperature this is the Australian Climate Observations Reference Network – Surface Air Temperature (ACORN-SAT) network, which has two stations in the study area, Mount Gambier and Robe. At Mount Gambier, 1.1 degrees of warming has been experienced since 1911, with a larger increase in the minimum daily temperature than the maximum (Figure 4-6). The frequency of hot days, here defined as the temperature exceeding the 2.5th percentile (or on average 10 days/year), has increased by approximately 50% at Mt Gambier over the past 113 years (1911 to 2023), with half the number of days below the cold days threshold, defined using the same percentile at zero degrees (Figure 4-7). At Robe, the other high quality temperature station in the region, the changes are smaller due to the mitigating effect of the heat capacity of the ocean on the coast. Nonetheless, the same trends are observed.

4.1.2 Rainfall

Rainfall trends for all stations available in the study region are outlined in Section 2.3.1. Four of these stations are included in the BoM high quality monthly rainfall station network, with annual rainfall presented in Figure 4-8. The slope of the line of best fit between annual rainfall and time suggests a decline in rainfall between 1.1 and 6.6 mm per decade, however only the trend in annual rainfall at Keilira Station is statistically significant. Due to the high variability from year to year, it is difficult to observe a statistically significant trend in annual rainfall at these stations. The rainfall change represents a 2-6% reduction in annual rainfall over the length of record for three of the sites, and a 13% reduction at Keilira station. Similar trends are observed over the cool season months, April-October inclusive. Changes in catchment-averaged rainfall for the calibration catchments are considered further in Section 4.1.4.

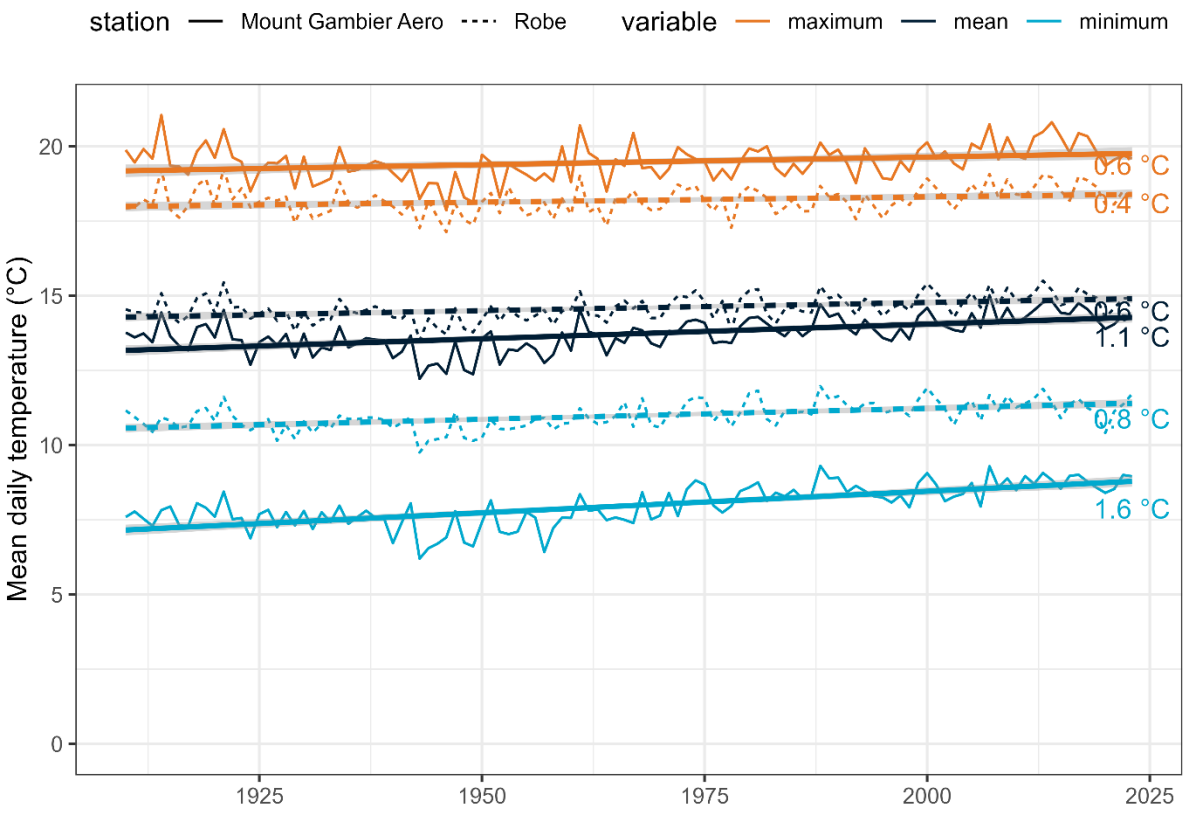

Figure 4-6 Observed annual temperatures and trends at Mt Gamber and Robe, stations that are part of the Australian Climate Observations Reference Network – Surface Air Temperature (ACORN-SAT) network

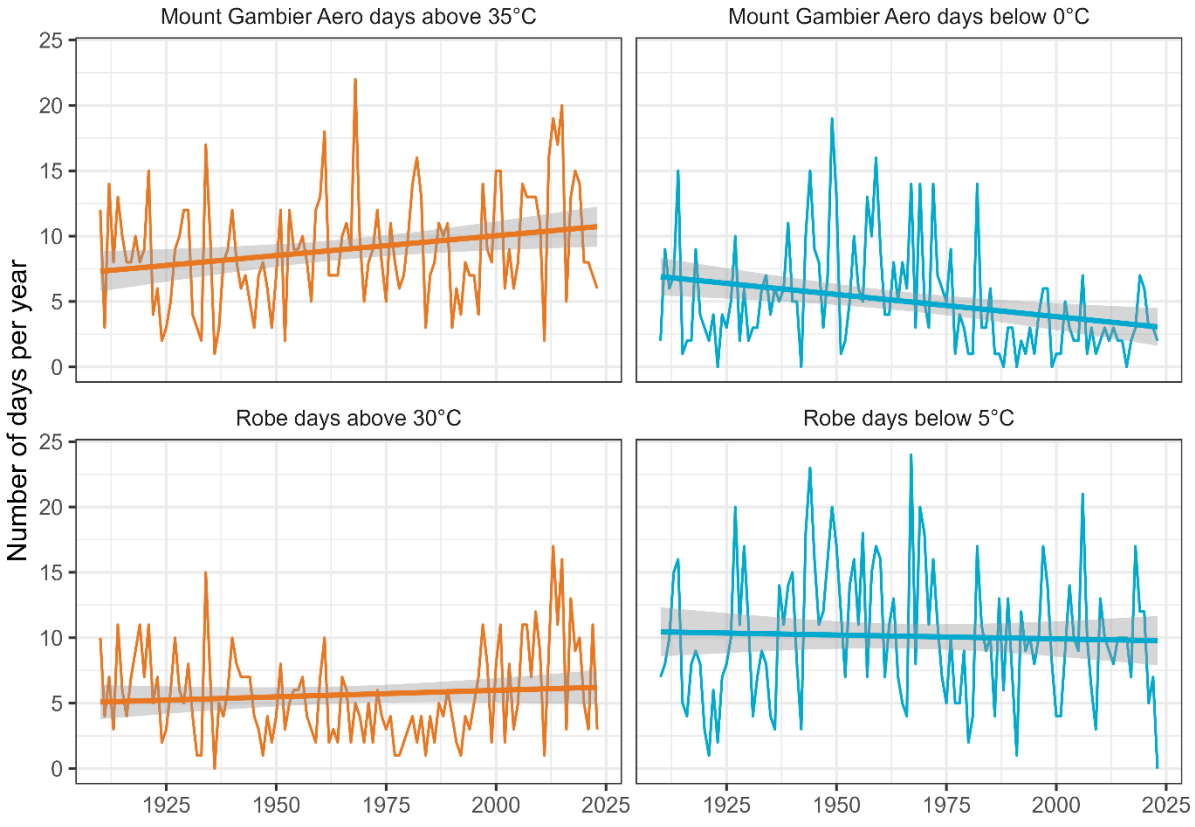

Figure 4-7 Observed changes in extreme temperatures. The temperature thresholds used to identify extreme days used are based on a 2.5% exceedance over the data record at each site.

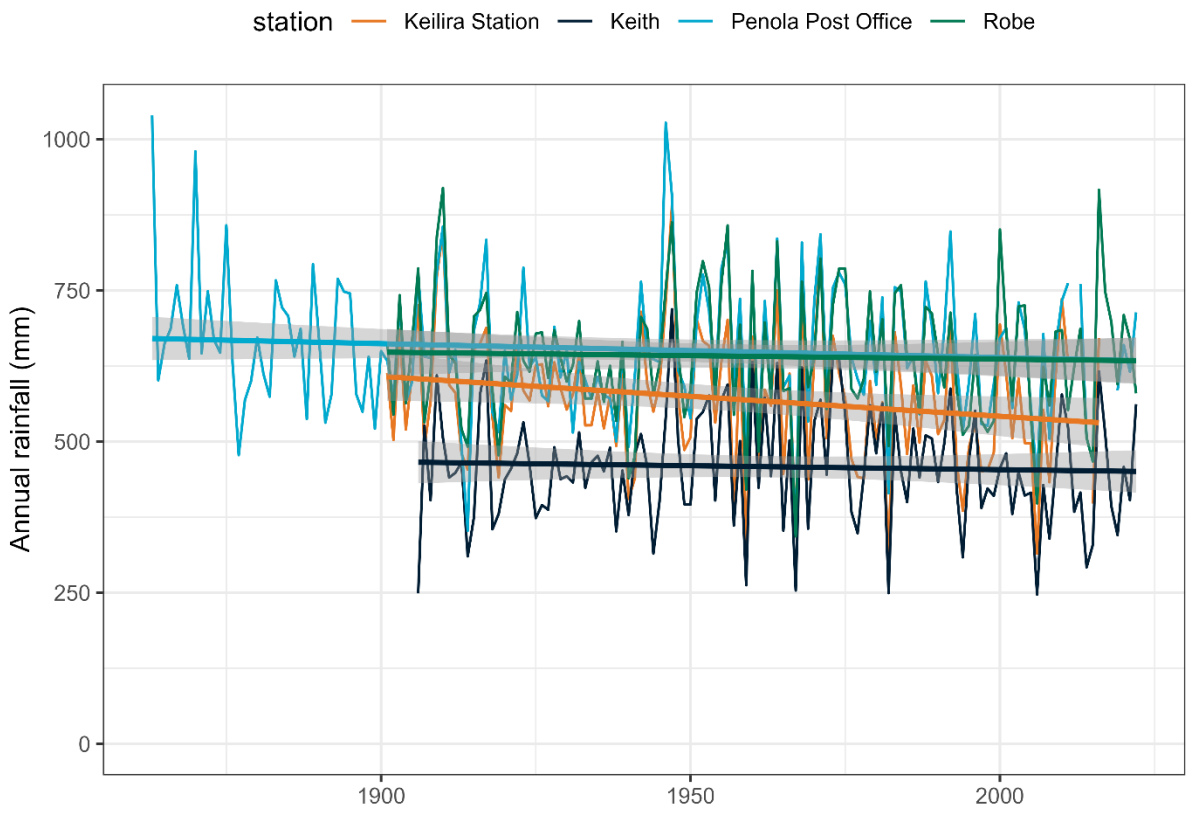

Figure 4-8 Annual rainfall trends at high quality sites in the region. Data source: http://www.bom.gov.au/climate/change/hqsites/

4.1.3 STREAMFLOW

Declining trends were observed at all streamflow stations identified as suitable for model calibration. Table 4-1 presents the slope of the linear trend in annual streamflow, and the corresponding p-value, the probability that the slope calculated could be derived with no trend between the annual streamflow volume and the year that it occurred. The Mann Kendall test for a monotonic trend in a dataset (not necessarily linear) is also presented in Table 4-1, where the statistic represents the direction of the trend (negative value indicating a decreasing trend), and the p value indicating the probability that the null hypothesis (i.e., there is no trend) can be rejected. P values less than 0.05 for both statistics are shaded red, representing the threshold typically used to represent statistical significance. Both statistics have been applied to annual streamflow volumes derived from the observed data as well as the modelled output.

Statistically significant declines in streamflow were derived from both the model output and observed data, and using both statistics, for the cross-border catchments of Naracoorte Creek (A2390542) and Mosquito Creek (A2390519). The model output also identified statistically significant declines in the remaining cross border catchment of Morambro Creek (A2390531), however the declining trend in observed data was not deemed significant, likely due to difficulty in identifying a trend in the context of the high variability at this station (see Section 3.4.1). In the observed data commencing in 1976, 10 of the 14 years with no flow have occurred since 1997.

A statistically significant declining trend based on observed data was also identified in the Bakers Range South Drain (A2390515). The declining trend was not significant in the model output, however the catchments contributing to Drain M were found to overestimate the observed data (see Section 3.4.1). Smaller declining trends were derived for the stations closer to the coast, in the Drain L catchment (A2390510 and A2390527) and the Reedy-Creek Mt Hope Drain (A2390513).

Table 4-1 Trends in annual streamflow data, based on linear regression and the Mann-Kendall test for a monotonic relationship. P values represent the probability that the trend could be obtained by chance, with values less than 0.05 shaded red

	Observed data				Modelled			
station	linear trend (mm/yr)	p value	Mann-Kendall statistic	p value	linear trend (mm/yr)	p value	Mann-Kendall statistic	p value
A2390510	-0.06	0.58	-0.05	0.61	-0.16	0.08	-0.16	0.14
A2390513	-0.16	0.27	-0.08	0.41	-0.10	0.40	-0.08	0.43
A2390515	-0.21	0.02	-0.22	0.03	-0.12	0.28	-0.11	0.28
A2390519	-0.45	0.01	-0.30	0.00	-0.36	0.00	-0.37	0.00
A2390527	-0.03	0.32	-0.05	0.65	-0.07	0.01	-0.24	0.03
A2390531	-0.02	0.50	-0.09	0.38	-0.09	0.02	-0.36	0.00
A2390542	-0.22	0.01	-0.44	0.00	-0.31	0.00	-0.47	0.00

4.1.4 RAINFALL-RUNOFF

Declining trends in rainfall and runoff have been observed in the study area. This section investigates if the rainfall-runoff relationship has also changed, i.e., given a certain rainfall, has the runoff generated also changed? One way to test for changes in a relationship is a double mass curve (Figure 4-9) plotting cumulative runoff against cumulative rainfall, where changes in the relationship are indicated by changes in the slope of the resulting line. A calibrated GR6J rainfall-runoff model was used to infill any gaps in the observed streamflow record. Changes in slope along the double mass plots were identified using the *segmented* R package (Muggeo, 2008). The method identifies the location of a breakpoint in a dataset compared to linear regression (see Muggeo, 2003), and a bootstrap method is used to represent the uncertainty in the location of any breakpoint (Wood, 2001). All streamflow stations had a breakpoint for a change in the relationship between rainfall and runoff identified (Figure 4-9), with the 95% confidence interval of the location of the breakpoint given in brackets. The change typically occurs in the early to mid-1990s but occurred later for the Drain L catchment (2003 for A2390510).

Table 4-2 presents the mean annual rainfall and rainfall-runoff ratios (mean annual runoff divided by mean annual rainfall) before and after the breakpoint identified in Figure 4-9. rainfall-runoff ratios, the proportion of annual rainfall that is observed as runoff on average, are low in the region, between 1 and 7% (Table 4-2). In contrast, upper catchments of the Mount Lofty Ranges typically have rainfall-runoff ratios of 30-40%. Rainfall reductions for all catchments were between 4 and 13%, with reductions in rainfall-runoff ratios substantially higher, typically between 20 and 40%, but up to 70% at A2390542 on Naracoorte Creek.

The rainfall-runoff relationship can also be investigated by plotting the annual rainfall and observed streamflow each year if the streamflow is transformed to a normal distribution (using a Box-Cox transformation with the lambda scale factor calibrated for each station) the relationship is typically linear. Relationships before and after 1995 are presented in Figure 4-10, with 1995 used as it generally coincides with the breakpoints in Figure 4-9, and results in an even number of years each side of 1995. A shift in the resulting linear relationship in the more recent period is evident for all stations, particularly in lower rainfall years.

Hence, the data available for the region indicates that rainfall and runoff has declined across the catchments considered, and the proportion of the rainfall that is observed as runoff in the drainage network has also reduced.

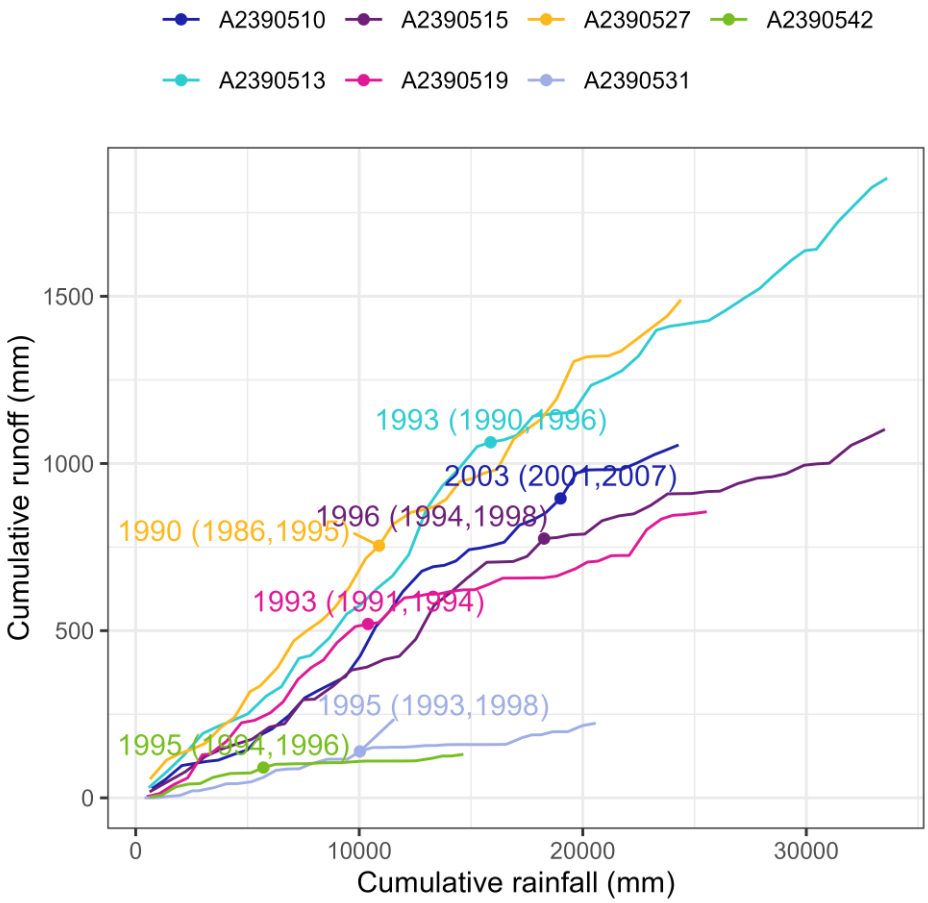

Figure 4-9 Double mass plot of rainfall against runoff (streamflow). Dots represent the breakpoint suggesting a change in the rainfall-runoff relationship, defined as a statistically significant changes in slope. The year the change in slope occurred is presented, with the 95% confidence interval of the time of the change in brackets

Table 4-2 Summary of mean annual rainfall and runoff/rainfall ratio before and after the breakpoint identified in Figure 4-9

Station number	Breakpoint year	Before breakpoint		After breakpoint		Percent change	
		Rainfall (mm/year)	Runoff/Rainfall ratio	Rainfall (mm/year)	Runoff/Rainfall ratio	Rainfall (%)	Runoff/Rainfall ratio (%)
A2390510	2003	611	0.046	587	0.03	-4	-34.8
A2390513	1993	727	0.069	682	0.045	-6.2	-35.2
A2390515	1996	729	0.039	693	0.015	-5	-62.5
A2390519	1995	614	0.048	548	0.024	-10.7	-50.6
A2390527	1990	643	0.067	614	0.052	-4.6	-23
A2390531	1995	526	0.012	480	0.008	-8.9	-33.5
A2390542	1995	573	0.015	497	0.005	-13.2	-70.3

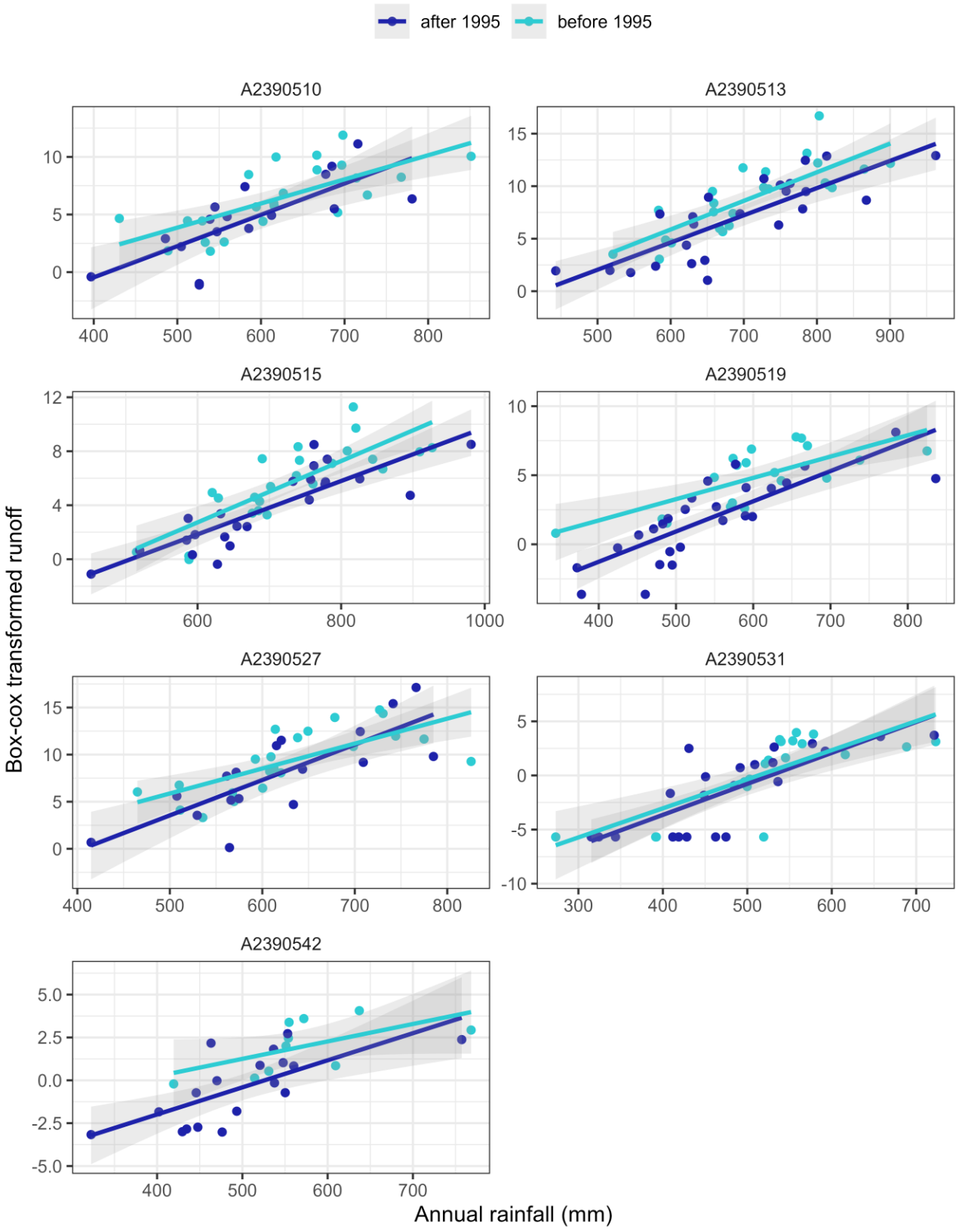

Figure 4-10 Annual rainfall and observed annual streamflow (mm/yr), with the streamflow transformed to represent a normal distribution, resulting in a more linear relationship between rainfall and runoff. Shaded bounds represent 95th confidence interval around the linear trend

4.1.5 RECHARGE

A similar trend analysis to that outlined in Section 4.1.3 for streamflow has also been applied to recharge for each unconfined aquifer management zone. In total 66 zones are considered, the 61 in the Lower Limestone Coast, along with five management areas in Padthaway (seen in Figure 4-5, noting this is now two zones in the Water Allocation Plan). For the observed data one zone did not have sufficient groundwater data to derive a trend (Western Flat), hence there are 65 zones considered. The recharge at individual groundwater wells, derived based on the method outlined in Section 3.3, was area weighted to produce an annual recharge time series for each zone based on observed groundwater levels and the modelled deep drainage.

The results for each zone are provided in Appendix E and summarised in Table 4-3. Over the full data record available most zones (57 of 65) had a declining trend in recharge rate based on observed data and the Mann Kendall test, with 31 of these trends statistically significant. Based on the model output 60 of the 66 zones had a declining trend in annual deep drainage, with 24 zones a statistically significant trend. While there are some differences between zones (Appendix E), this result indicates the model was able to represent the broader pattern of declining trends in recharge rate represented by the observed data.

Eight zones had a non-significant increasing trend in recharge rate based on observed data, while no zones had statistically significant positive trends based on the recharge data derived from observed groundwater levels. Four significant positive trends were calculated from the model output, however these are all associated with zones that have large proportions of the permanent water HRU, Bool and management zones around Lake George and Lake Hawdon. Hence, these results are likely to be a factor of the assumptions involved in this HRU, namely that the proportion of the cell identified as permanent water is always full and available to recharge. This result of declining trends in recharge across the region is in line with other assessments of groundwater levels in the region, for example Department for Environment and Water (2023) found 82% of wells in the unconfined aquifer had a declining trend, with 12% stable and 6% rising.

Table 4-3 Number of unconfined groundwater management areas with trends in recharge in different categories. See Appendix E for the results for individual management zones

	Groundwater data		Modelled	
	Linear regression	Mann Kendall	Linear regression	Mann Kendall
Negative trend (significant)	33	31	31	24
Negative trend (not significant)	25	26	31	36
Positive trend (not significant)	7	8	0	2
Positive trend (significant)	0	0	4	4

4.2 Summary

The historical water available across the region has been quantified through the development of a fully integrated water balance. A more complete water balance, and changes with future climate projections, are presented in the next section. Trends of reducing rainfall and increased temperature have been observed in high quality datasets in the region and are in line with observations across the nation (CSIRO and Bureau of Meteorology, 2024). 57 of 65 unconfined groundwater management zones had declining trends in recharge over time, with 31 of these statistically significant. All streamflow stations considered had declining trends identified, with 3 of 7 catchments exhibiting statistically significant trends. This was not only driven by reduced rainfall, but the proportion of rainfall resulting in runoff was also observed to have reduced since the 1990s. These trends set the context for the following section, where future climate projections have been selected and applied to the AWRA-L model.

5 Future water availability

IPCC's Sixth Assessment Report (IPCC, 2022) enhances understanding of the state of Australia's future climate. The changes are projected to include continued warming, with more extremely hot days and fewer extremely cool days, further decreases in cool season rainfall across many regions of the south and east, and likely increases in the average duration of drought and aridity in regions within the south and east (CSIRO and Bureau of Meteorology, 2024).

5.1 Climate scenarios

The Intergovernmental Panel on Climate Change (IPCC) considered five different climate scenarios in its Sixth Assessment Report (IPCC, 2022). These scenarios are called Shared Socioeconomic Pathways, or SSPs, and are defined as follows:

- SSP1-1.9: emissions rapidly decline to net zero by about 2050, and become negative after that
- SSP1-2.6: emissions decline to net zero by about 2075, and become negative after that
- SSP2-4.5: emissions rise slightly, before declining after 2050, but not reaching net zero by 2100
- SSP3-7.0: emissions rise steadily to become double their current amount by 2100
- SSP5-8.5: emissions rise steadily, doubling by 2050 and more than tripling by the end of the century.

Each of these scenarios has associated global temperature changes, which are summarised in Figure 5-1 and Table 5-1. The IPCC does not make statements about which of these scenarios is more likely. Hausfather and Peters (2020) provide a qualitative estimate of likelihood for a range of SSPs (Table 5-1). SSP SSP2-4.5 has been adopted in this work as a midway projection, and considered likely by Hausfather and Peters (2020). A 2060 time horizon has also been assumed to be of interest, within three iterations of water allocation plan reviews and not so distant that the assumptions represented by different SSPs have a substantial influence on the climate changes projected (Figure 5-1). At 2060 SSP2-4.5 is representative of a ~1.6 °C temperature rise relative to a time slice centred around 1990.

5.1.1 Available Global Climate Models

Global climate models (GCMs) are an important tool for simulating global and regional climate for a given SSP. Future climate projections from a large range of archived GCM simulations have been interrogated for use in this work, available as part of the Coupled Model Intercomparison Project (CMIP6, https://pcmdi.llnl.gov/CMIP6/). Of the 92 available GCMs, 32 included the rainfall, temperature data, solar radiation and humidity data required for the AWRA-L model.

GCM evaluation based on representation of past climate for a region and climate variables of interest has been used to inform selection of CMIP6 models. Grose et al. (2023) assessed the CMIP6 models using multiple criteria including performance over a large Indo-Pacific and Australian domain, atmospheric circulation, teleconnection to large scale drivers, and existing literature to select models for application in Australia. Models identified as performing poorly against these criteria were excluded from consideration in this work (identified in Table 1 of Grose et al. (2023)). This resulted in 21 models available to be used.

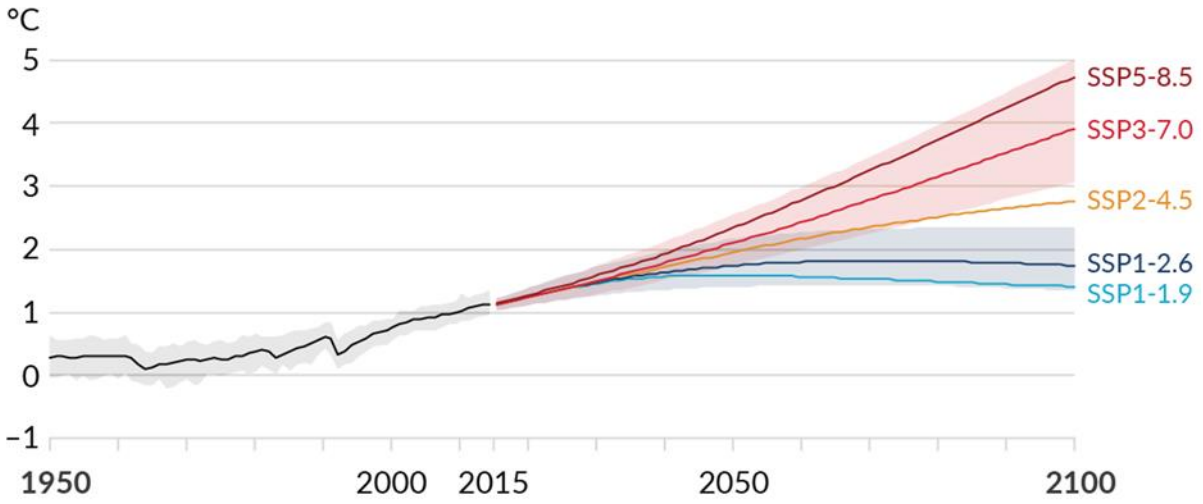

Figure 5-1 Global surface temperature changes in °C relative to 1850–1900. These changes were obtained by combining Coupled Model Intercomparison Project Phase 6 (CMIP6) model simulations with observational constraints based on past simulated warming, as well as an updated assessment of equilibrium climate sensitivity. Changes relative to 1850–1900 based on 20-year averaging periods are calculated by adding 0.85°C (the observed global surface temperature increase from 1850–1900 to 1995–2014) to simulated changes relative to 1995–2014. Very likely ranges are shown for SSP1-2.6 and SSP3-7.0. Source: IPCC 2021

Table 5-1 Changes in global surface temperature relative to a 1990 baseline for selected 20-year time periods across the five emissions scenarios presented by the IPCC Sixth Assessment Report. Likelihood based on Hausfather and Peters (2020)

Scenario	MID TERM, 2041–2060	Likelihood
SSP1-1.9	1.0 °C (0.6 to 1.4 °C)	Unlikely
SSP1-2.6	1.2 °C (0.6 to 1.5 °C)	Likely
SSP2-4.5	1.6 °C (1.2 to 1.9 °C)	Likely
SSP3-7.0	1.8 °C (1.4 to 2.3 °C)	Unlikely
SSP5-8.5	2.2 °C (1.7 to 2.8 °C)	Highly unlikely

5.1.2 SEASONAL PATTERN SCALING METHOD

The GCM outputs are at a resolution that is too coarse to be used directly in the model. Dynamic downscaling for the region has recently been undertaken through the NSW and Australian Regional Climate Modelling (NARCliM 2.0) project. While maps of projections from this project for NSW were released in 2024, the daily downscaled outputs for the region were not released at the time of writing (April 2025). To make use of the most recent CMIP6 GCMs a simpler downscaling approach has been adopted, the seasonal pattern scaling (PS) method. The approach is summarised here with more details provided in Chiew et al. (2009). The first step involved estimating the seasonal scaling factors for four 3-month blocks (December to February, March to May, June to August and September to November) for the changes between two time slices centred around 1990 (1975 to 2005) and 2060 (2046 to 2075). For each season and over each time slice, the total rainfall was calculated. Seasonal scaling factors were then calculated as the ratio of the total season's rainfall over the 2060 time slice divided by the total rainfall over the 1990 time slice. The historical climate sequence was scaled using these seasonal scaling factors. The second step involved rescaling the entire series so that it matches the annual scaling factors, to maintain consistency with annual projected changes in the GCMs (Chiew et al., 2009).

This process was repeated for each GCM, for each season, and for each GCM grid cell, and applied to each model input grid cell, based on the ANU Climate (GH70) v2 product. The method was then repeated for each climate parameter, except for temperature where the difference rather than ratio between the two periods was used to scale the historical sequence.

5.1.1 SELECTION OF GLOBAL CLIMATE MODELS

The changes in annual and seasonal rainfall and PET following the pattern scaling processes, averaged across the model domain, are presented in Figure 5-2. GCMs are ranked from largest to smallest reduction in mean annual rainfall in Figure 5-2. After reducing the number of GCMs considered based on the review by Grose et al. (2023), all GCMs project a reduction in mean annual rainfall. While there is variability in the changes in rainfall from season to season across the GCMs, in general seasonal rainfall is also projected to reduce, with two of 21 models having an increase in spring rainfall, and 4 models projecting increases in rainfall for the other seasons. Projections in the change in PET are more consistent, with an average increase of approximately 5% (range 3-9% depending on the season).

Projections from three GCMs were selected to apply to the AWRA-L model to represent the range in future projections from the selected GCMs. Dry and wet scenarios were identified based on the 10th and 90th percentile (i.e. second highest and lowest) exceedance ranking by annual rainfall, based on the EC-Earth3-Veg and EC-Earth3 GCMs, respectively. For a middle projection the GFDL-CM4 model is the median of the 21 GCMs, however this model has the largest reduction in summer rainfall which may not be representative of a mid-point scenario. The CanESM5 model has a very similar projected reduction in mean annual rainfall as GFDL-CM4 and has been selected to represent a median case. This median case has a similar seasonal pattern to the average of GCM projections adopted for the SA climate projections for risk assessment (Department for Environment and Water, 2022), albeit with a slightly smaller reduction in rainfall (Table 5-2).

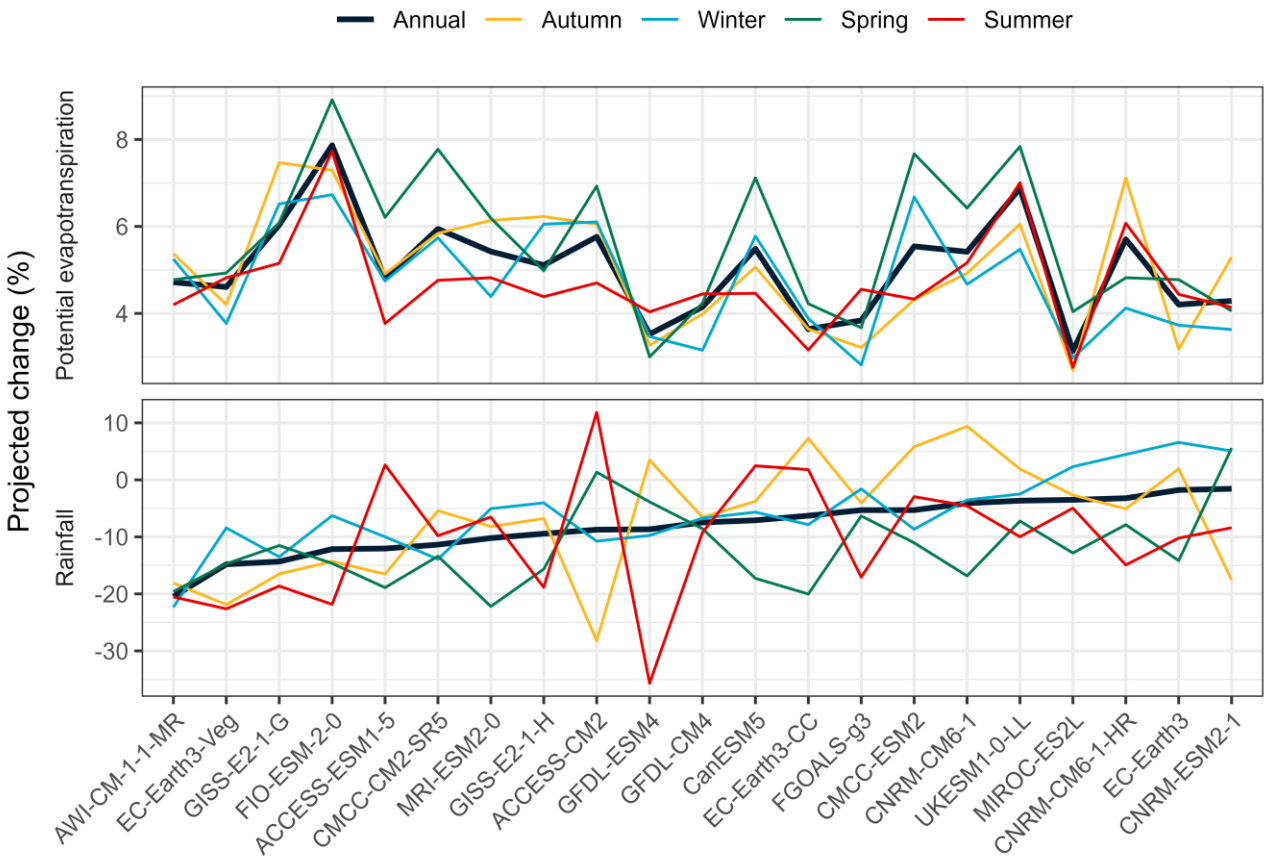

Figure 5-2 Percentage change in mean annual rainfall and potential evaporation across the AWRAL model domain for 2060 under SSP2-4.5

Table 5-2 Percent change in average rainfall for the three GCMs selected (bold) for a 2060 time horizon, compared to SA future climate scenarios for Limestone Coast Landscape SA region and medium emission scenario RCP4.5

Season	Baseline (mm) 1986-2005	2020-2039	2040-2059	**EC-Earth3 GCM-PS (Wet)**	**CanESM5 GCM-PS (Mid)**	**EC-Earth3-Veg GCM-PS (Dry)**	2060-2079	2080-2099
Annual	525	-7	-10	**-2**	**-7**	**-15**	-14	-8
Summer	76	-5	2	**-10**	**2**	**-23**	-9	-13
Autumn	122	-7	-6	**2**	**-4**	**-22**	-13	-2
Winter	185	-2	-8	**7**	**-6**	**-8**	-5	0
Spring	139	-15	-22	**-14**	**-17**	**-15**	-26	-22

5.2 Change in mean annual recharge and runoff

The pattern-scaled climate data from each of the Dry, Mid and Wet GCMs was applied to the AWRA-L model to simulate the implications on the total water balance. For the future climate scenarios the HRUs have been fixed at the most recent fractions used, from the 2020 land cover estimates (see Section 2.3.2), and the historical climate was simulated with these fixed HRUs for comparison. A range of different reporting areas have been considered, based on surface water catchments and the unconfined aquifer management zones (Figure 5-3). Surface water catchments have been aggregated to represent the main drainage networks of the Blackford Drain, Drain L, Drain M and Lake Frome – Mount Hope drain. Catchments to the north and south of these systems were lumped into the northern and southern catchments, with each aggregated area representing a similar zone of mean annual rainfall (Figure 5-3). The unconfined groundwater management zones have also been used to aggregate the 1km model outputs for the Lower Limestone Coast and Padthaway management areas.

The projected change in runoff for the aggregated surface water catchments can be seen in Figure 5-4. The wet scenario resulted in similar or increased runoff, due to the projected increase in winter rainfall from this GCM, even though there was a reduction in annual rainfall. The Mid and Dry GCMs resulted in relatively large reductions in runoff compared to the reduction in rainfall, with the slope of the relationship (or 'elasticity') 4.2; that is, for a 1% reduction in rainfall, a 4.2% reduction in runoff was modelled (Figure 5-4A). Based on the Mid GCM results, the reduction tended to be slightly less in the two wetter catchments with a projected mean annual rainfall greater than 700 mm/year. The additional transmission losses and explicit representation of Bool Lagoon in the Drain M catchment resulted in larger reductions in this catchment than the others (Figure 5-4B). Reductions in recharge over the same catchment areas were smaller than runoff, but still larger than the corresponding reduction in rainfall, with an elasticity of 1.9. The relationship between rainfall and runoff tended to remain relatively consistent given the variability across catchments (Figure 5-4D), however there is some indication of less runoff for a given amount of rainfall for the drier scenarios (smaller intercept values for the trend lines in Figure 5-4D).

The same format of plot based on the model output aggregated to the unconfined aquifer management zones is shown in Figure 5-5. A similar recharge elasticity was derived from the management zones of a 2.1% change in recharge for a 1% change in rainfall. There is relatively large variability in this result though, with a range from around 5-30% change in recharge for the Mid GCM rainfall reduction of 7% (Figure 5-5A). This variability can be explained in part by the mean annual rainfall, with the wettest zones, above approximately 750 mm/year, reducing by a similar amount as the rainfall reduction, and then as the mean annual rainfall reduces the change in recharge increases (Figure 5-5B). The variability that remains in this relationship is driven by the other factors included in the model, including soil characteristics, vegetation type and topography.

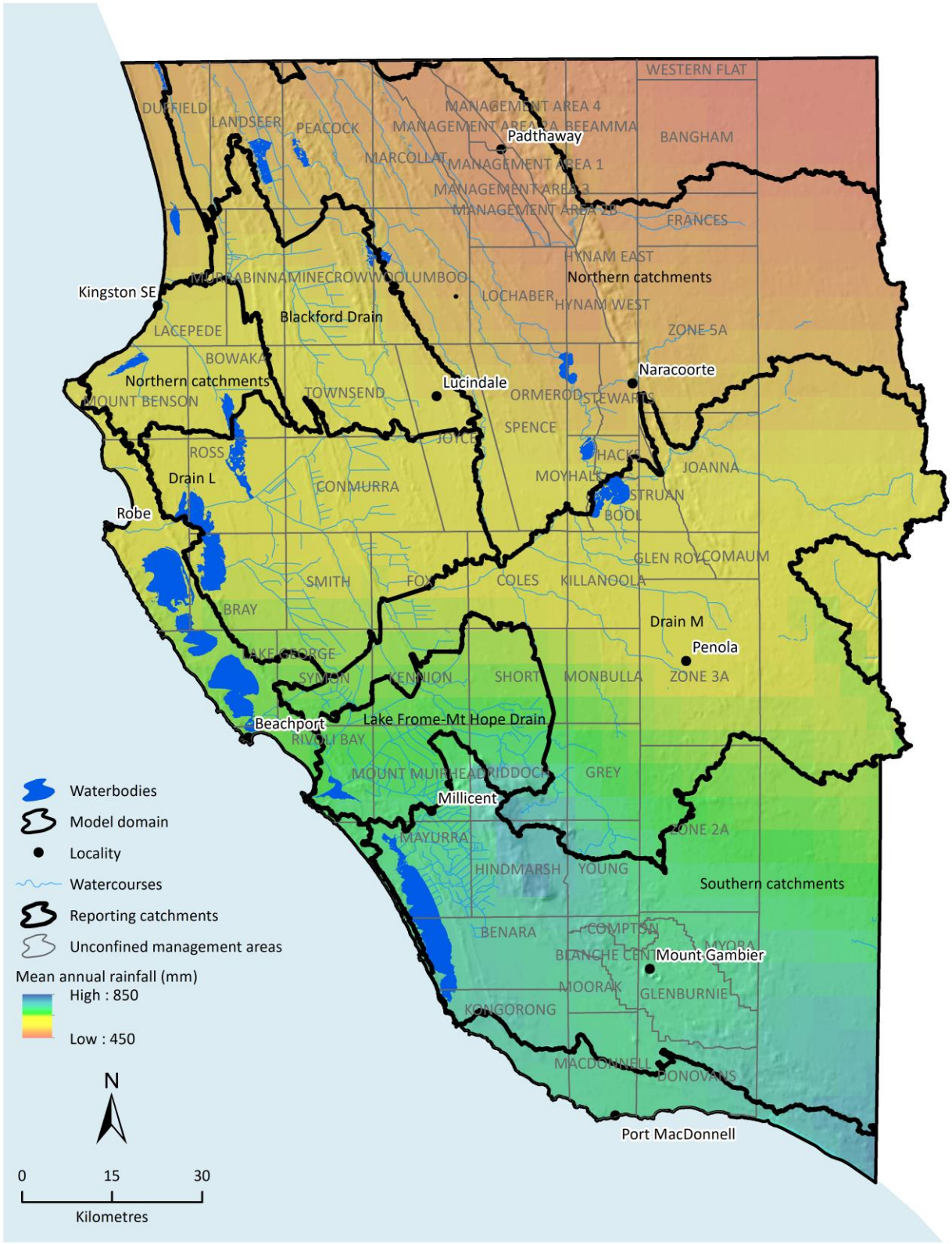

Figure 5-3 Catchment areas used for reporting of changes to future water availability for runoff, and unconfined aquifer management zones used for reporting of changes to recharge

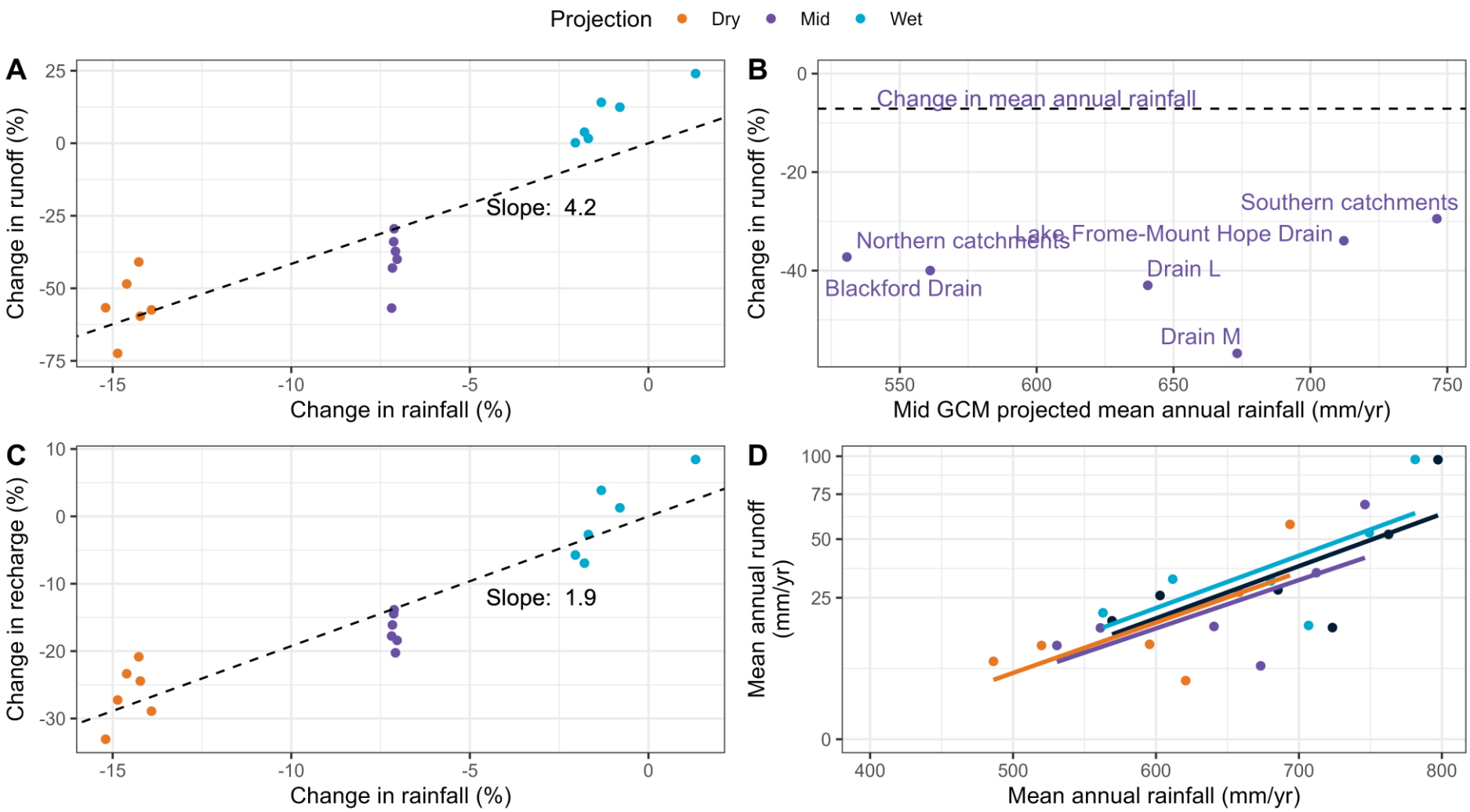

Figure 5-4 Changes in water available for the surface water reporting areas, with the colours representing the different climate projection scenarios considered. The percentage change in mean annual runoff for a given change in mean annual rainfall (A) and plotted against mean annual rainfall for the Mid scenario (B). Change in recharge for the same reporting zones against the change in rainfall is shown in (C), with the relationship between rainfall and runoff for each scenario and catchment in (D), noting a square root transform is used on the y axis of (D) to produce a more linear relationship

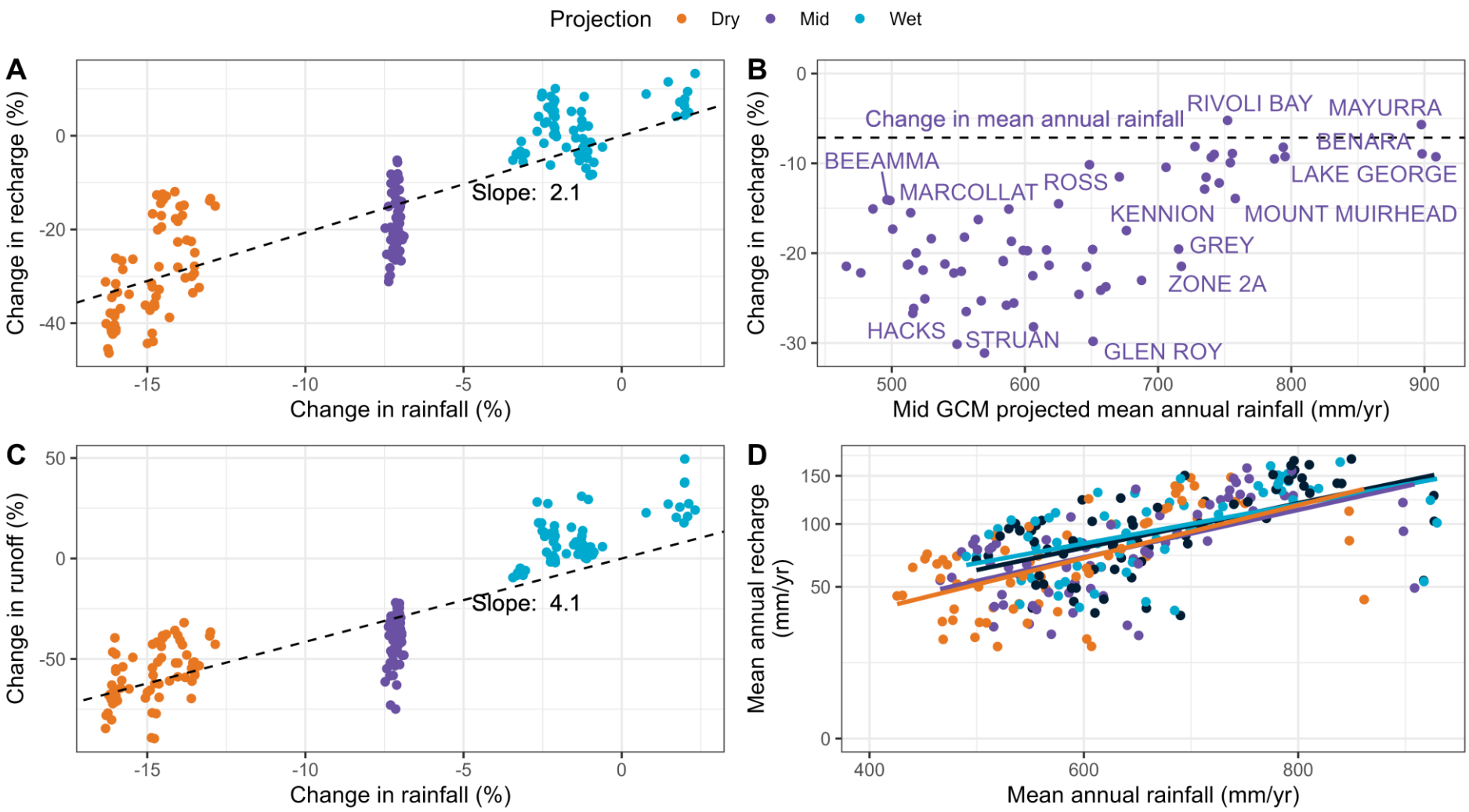

Figure 5-5 Changes in water available for the groundwater water reporting areas, with the colours representing the different climate projection scenarios considered. The percentage change in mean annual recharge for a given change in mean annual rainfall (A) and plotted against mean annual rainfall for the Mid scenario (B). Change in runoff for the same reporting zones against the change in rainfall is shown in (C), with the relationship between rainfall and recharge for each scenario and catchment in (D) , noting a square root transform is used on the y axis of (D) to produce a more linear relationship

5.3 Historical and future water balance

The combined water balance for each of the reporting zones considered above is presented in Figure 5-6 for the aggregated surface water catchments and Figure 5-7 for a selection of unconfined aquifer management zones, with results for all zones in Appendix F. The total height of the bar in each case is representative of the input mean annual rainfall, but there can be some differences due to changes in storage in the soil and groundwater storages in the model. The amount of the input water available that resulted in different components of the water balance are shown in different colours. Recharge has been split into two components: 1) gross recharge as presented in Section 5.2 and total recharge reaching the groundwater store in the model in line with the values reported above; and 2) net recharge, the recharge that is not evaporated or transpired from the groundwater store. The net recharge shown in brackets is included in the values presented for gross recharge value above in Figure 5-6 and Figure 5-7, where the other evapotranspiration and runoff components are additional values.

Evapotranspiration is by far the most dominant component of the water balance. The amount of AET generally reduces in the drier Mid and Dry scenarios even though the air temperature inputs to the AWRA-L model that drive the modelled AET increased, as the amount of water available from rainfall has reduced. The reduction in AET tends to be less than the reduction in rainfall for the future scenarios, meaning that there is a further reduction in water available to become runoff or recharge.

Runoff is a small proportion of the overall water balance, as indicated in Section 4.1.4, with runoff to rainfall ratios of 1 – 7%. This proportion of the water balance that results in streamflow was projected to only reduce further, as outlined in Section 5.2, with an elasticity of approximately 4.2, and has been observed to have reduced since the mid-1990s (Section 4.1.4).

Examples of water balances for unconfined aquifer management areas across a range of rainfall amounts are given in Figure 5-7, with all zones presented in Appendix F. The patterns of change are similar to the results aggregated across streamflow catchments in Figure 5-6, with AET the largest component and streamflow less than gross recharge. Net recharge rates can be small, and in some areas negative, occurring when the mean evapotranspiration from the groundwater store is greater than the deep drainage, resulting in a declining storage level in the model. Net recharge rates are generally in line with published chloride mass balance (CMB) net recharge estimates (Crosbie and Davies, 2013). The median net recharge across the management zones is very similar at 15 mm/year between the results from the AWRA-L model and that reported by Crosbie and Davies (2013), however the model tends to underestimate the zones with higher CMB net recharge rate (above 50 mm/year) noting these higher CMB estimates have larger ranges between the confidence intervals.

The median annual surface water availability for the future climate scenarios across the drainage network is presented in Figure 5-8. The width of the watercourse represents the median annual runoff, based on the annual runoff volume accumulated from the upstream catchment. It should be noted that this plot does not include any operation of the drainage network (e.g. diversions using regulators) or losses in wetlands or watercourses outside the Drain M catchment. The main watercourses flowing to the ocean can be seen, Blackford Drain, Drain L, Drain M, the Mount Hope – Lake Frome system and the drains contributing to Lake Bonney. The Mid and Dry scenarios have much reduced median annual runoff, in line with that presented in Section 5.2 (noting Figure 5-8 presents the median runoff, as opposed to mean). There is some variability across the region for the Wet scenario compared to the Historical climate scenario, where in some catchments there is an increase in median annual runoff from the Wet scenario (e.g. the Blackford Drain terminating near Kingston), where in other catchments the difference is minimal, or represents a slight reduction compared to the historical climate.

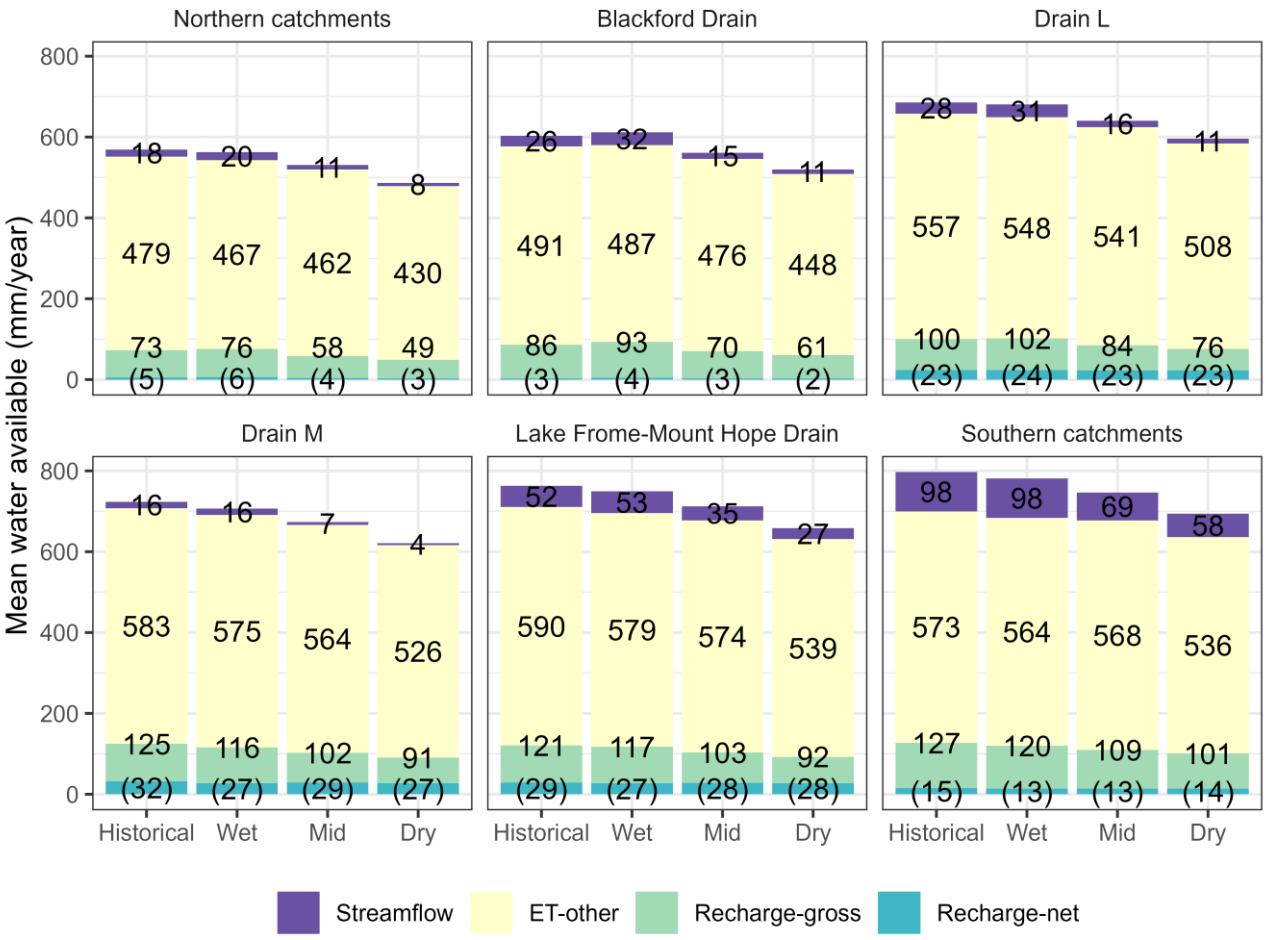

Figure 5-6 Water balance for aggregated surface water catchments. Recharge-net is in brackets as it is included in Recharge-gross, with the difference modelled to evapotranspire from the groundwater store

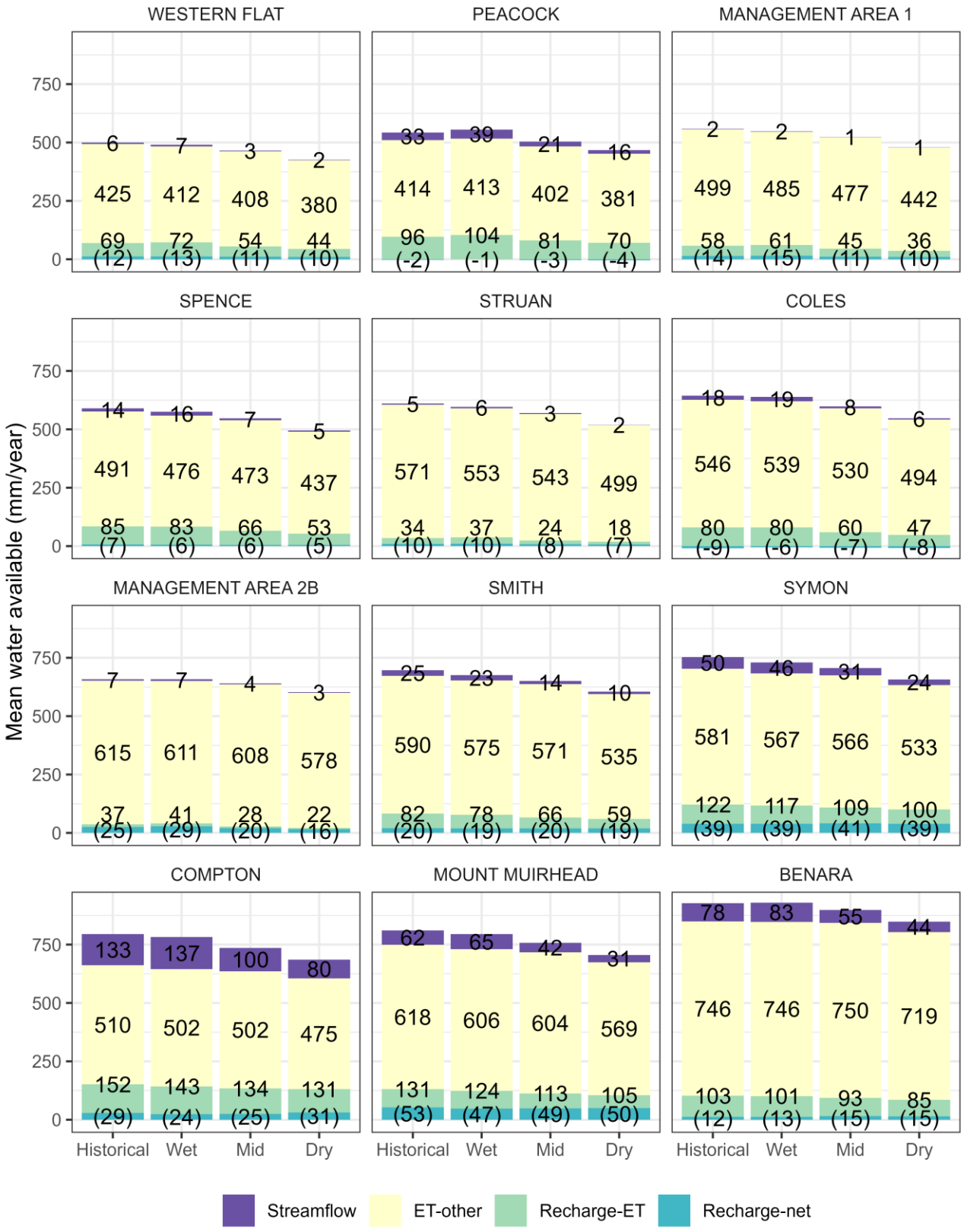

Figure 5-7 Water balance for aggregated groundwater reporting areas. Recharge-net is in brackets as it is included in Recharge-gross, with the difference modelled to evapotranspire from the groundwater store

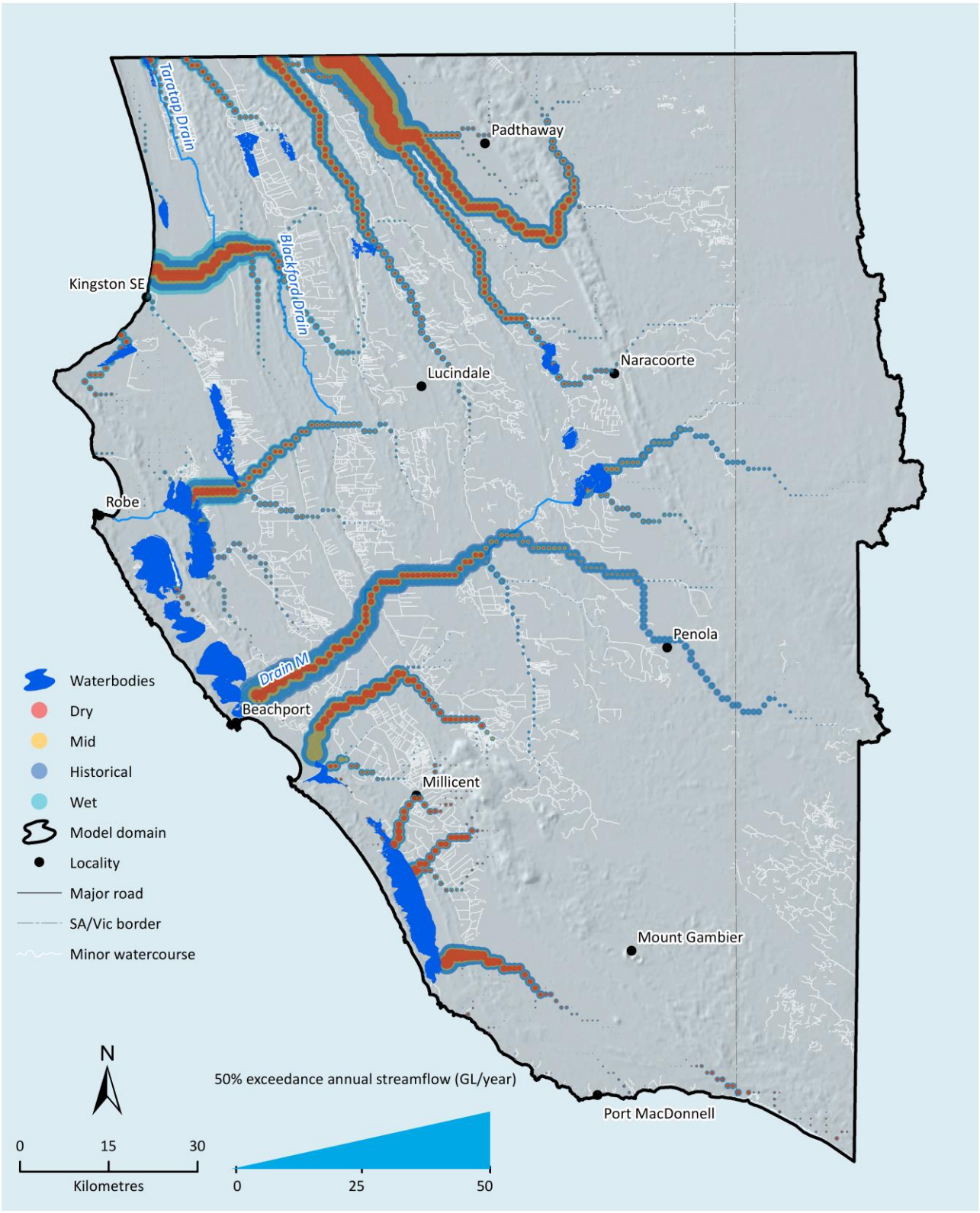

Figure 5-8 Modelled median annual streamflow in the model domain for the climate projection scenarios. Hydrological response units were held constant at 2020 proportions for all scenarios. The same caveats as Figure 4-3 apply

5.4 Periods of drought

The above analyses have presented changes in mean or median annual volumes or totals to represent the overall water balance. However, changes in water availability over time are also of interest, particularly at times of low water availability. A standardised drought index has been used to investigate this question and quantify the historical and projected future periods in drought conditions. The implementation of the Standardised Precipitation-Evapotranspiration Index (SPEI) of Beguería et al. (2014) has been used with a Gamma distribution and a time scale of 12 months. The index has been applied to the input rainfall data, representing climatological drought, as well as the modelled runoff, representing hydrological drought, and soil moisture from the shallow soil store (0.1 – 1 m of soil depth), representing agricultural drought. Historical and future climate scenarios were considered for each of the six surface water reporting catchments. The SPEI parameters were fitted to the outputs from the historical period, and those same parameters used for the climate projection scenarios, to ensure the same baseline conditions were maintained for a given analysis of catchment and drought variable.

An example of the resulting drought index for the Drain M catchment based on the shallow soil storage level for the historical and future climate scenarios is shown in Figure 5-9. The more negative the drought index value the stronger the drought, and drought conditions have been assumed for an index value below -0.8, corresponding to D1 drought from the U.S. Drought Monitor (Hao et al., 2017; Svoboda et al., 2002). The peak of the Millenium Drought over 2006-2010 is evident as the strongest drought in the period, with a period around 2015 another recent high intensity drought period. Periods of drought, i.e., the percentage of months with a drought index value less than -0.8, for the different catchments and hydrological variables is presented in Figure 5-10. By this definition, drought conditions have occurred approximately 20% of the time historically across the catchments and drought variables, and the Wet scenario remained relatively consistent with historical conditions. Drought conditions were projected to double to approximately 40% of the time for the Mid scenario, and over 50% of the time for the Dry scenario. Typically, hydrological (runoff) and agricultural (soil moisture) drought occur more frequently than climatological drought (rainfall) for the Mid and Dry future climate scenarios.

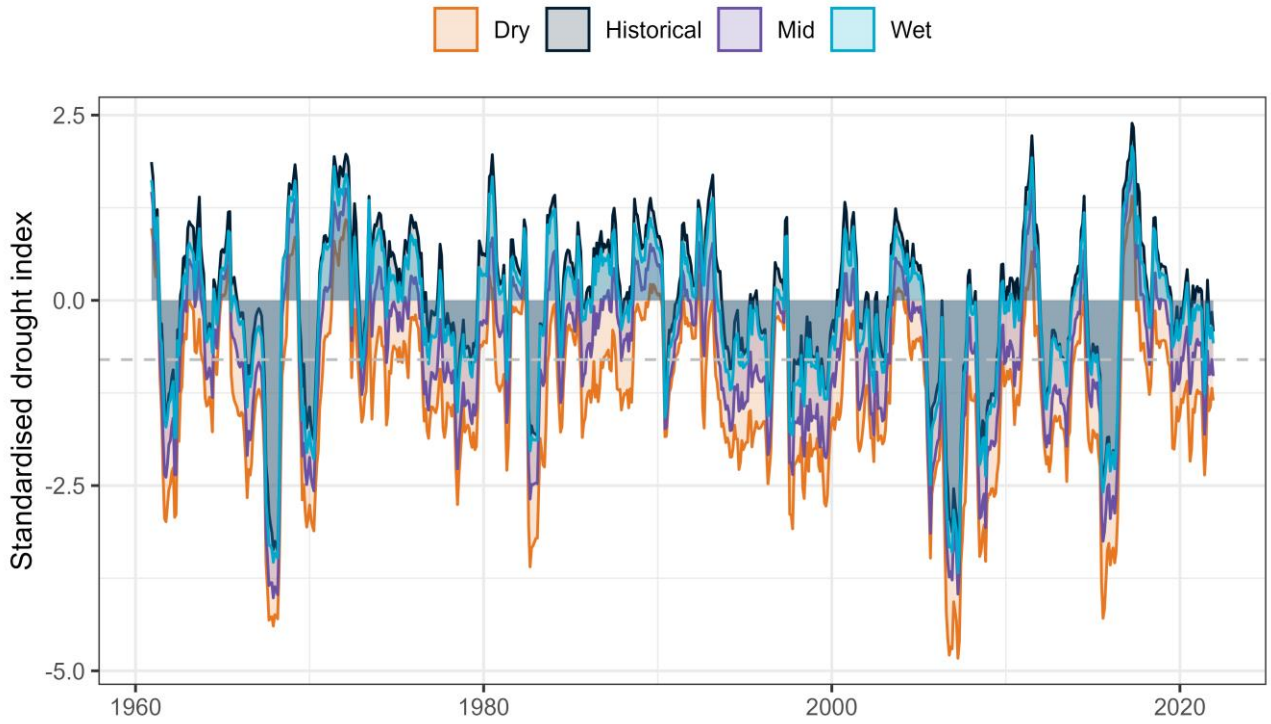

Figure 5-9 Example standardised drought index time series for the Drain M catchment based on the shallow soil store (0.1-1m). An index value less than -0.8 (dashed grey line) is considered to represent drought conditions

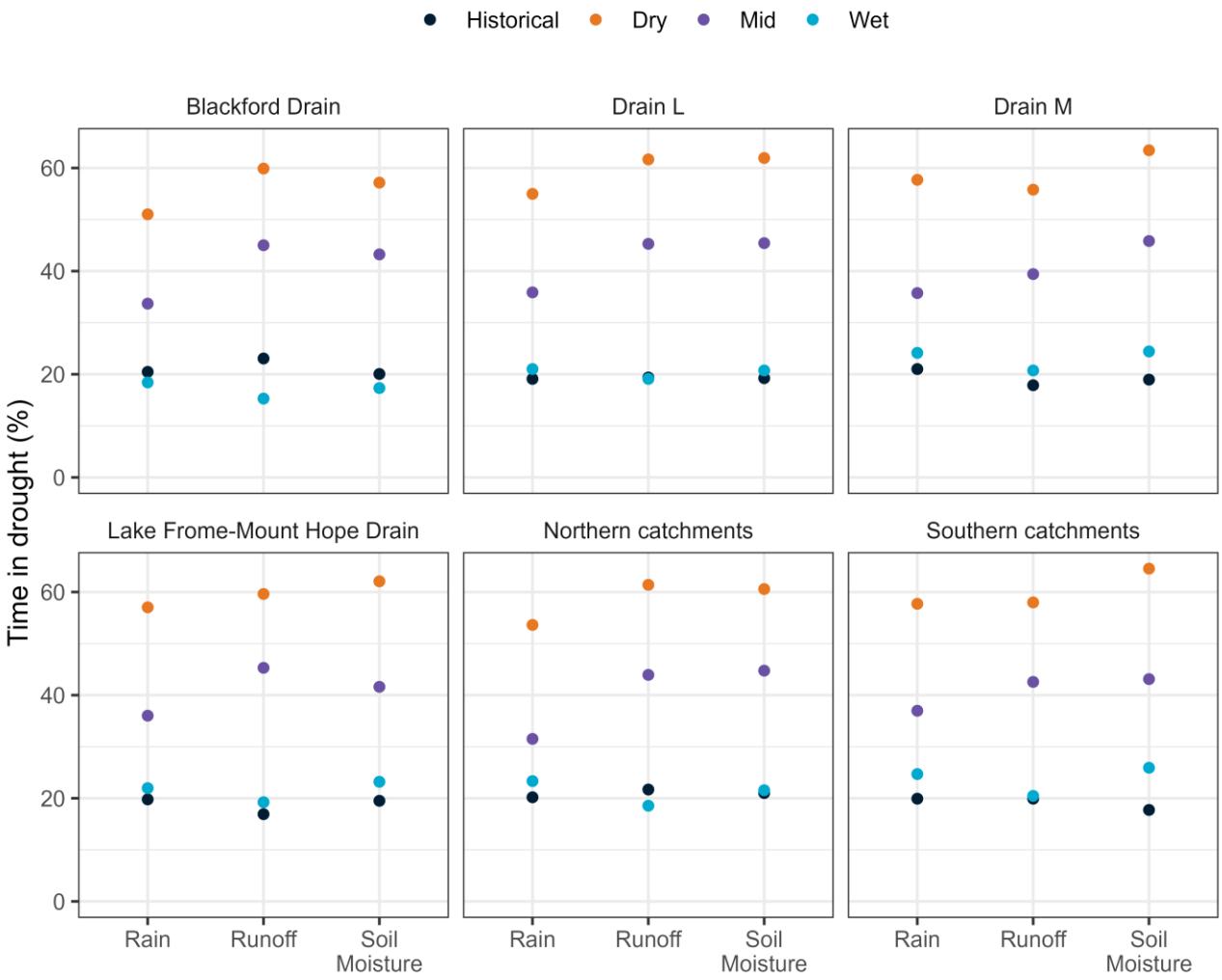

Figure 5-10 Time in drought for different projections, based on different modelled variables

6 Discussion

6.1 Changes to the Lower Limestone Coast Water Availability

A detailed analysis of trends in datasets representing different components of water availability in the region was undertaken in Section 4. Trends of reducing rainfall and increased temperature were identified, resulting in declining trends in recharge (57 of 65 unconfined groundwater management zones), and in streamflow (all stations considered). This was not only driven by reduced rainfall, but the proportion of rainfall resulting in runoff was also observed to have reduced since the 1990s. This indicates the proportion of rainfall becoming AET has increased, also indicated by the streamflow and recharge elasticity relationships (Section 5.2). A runoff elasticity of 4.2 (4.2% reduction in runoff for a 1% reduction in rainfall) is high in the context of Australian catchments, but in line with previous estimates for the region, and catchments with similar rainfall runoff coefficients and mean annual rainfall (Chiew, 2006). Much higher values have been derived globally (Berghuijs et al., 2017). Recharge changes were modelled to be less sensitive to changes in rainfall than runoff, however an elasticity of approximately 2 times rainfall still represents a substantial reduction in average water availability projected into the future. Other studies on projected future changes in recharge in the region, using different climate projections and a specific recharge model WAVES, have found a similar recharge elasticity of 1.5 – 2.5 times the rainfall change (Doble et al., 2022). Hence, while the median projection considered for a 2060 time horizon with a medium emissions scenario was for a relatively small reduction in future rainfall (7%), this is expected to result in a much larger reduction in runoff and recharge, which was only magnified further for the Dry scenario considered (Figure 5-2, Figure 5-4).

Evaporative demand has been observed to have increased across much of Australia (Stephens et al., 2018), in part associated with warming-related increases in vapor pressure deficit (Denson et al., 2021), and increases in PET are projected to continue in the future (Section 5.1.1). The relationship between PET and AET is not straightforward, since AET is also dependent on water availability (Wasko et al., 2024). This work has found AET may reduce due to reduced rainfall, even though PET was assumed to increase by approximately 5% for a 2060 scenario compared to a 1990 baseline. However, the partitioning between AET and available water (runoff/recharge) is not constant, and a larger proportion of the rainfall was modelled to be partitioned into AET than available water, further reducing water availability. Other studies have also found this change in partitioning, and in some cases AET increases despite less rainfall available to evapotranspire (Stephens et al., 2023).

The analysis of drought periods found hydrological or agricultural droughts (based on modelled streamflow and soil moisture, respectively), would be 2 and 3 times more common for the Mid and Dry scenarios, respectively, relative to the historical climate baseline. For the Dry scenario this increase was to more than 50% of the time. This suggests that periods of additional water for storage in the landscape, above and beyond the existing environmental water requirements and capacity of the drainage network to divert water out into wetlands, are projected to become even less frequent.

The climate downscaling approach used incorporates the projected changes in different seasons, increased summer rainfall and reduced autumn rainfall for example. But the approach is based on scaling the historical record and as such does not account for changes in rainfall intensity or longer-term changes such as longer drought periods. Stochastic or dynamic downscaling approaches account for these changes more explicitly but introduce a new problem; modelled climate data tends to introduce biases or errors, and the generated data no longer accurately represents the historical rainfall intensity or spatial distribution, which can then be propagated through to the projections of future climate. Scenario neutral stress testing, or 'bottom up' approaches, may be beneficial to identify the degree of change required before an identified system failure occurs, to guide options and timeframes for climate adaptation (see Fowler et al., 2024).

6.2 Qualitative assessment of water management measures in the region

Management options to modify the drainage network to increase water storage in the region have not been explicitly considered in the modelling framework, but the results provide a guide to potential options. Options are discussed in this section qualitatively, which may provide direction for future analysis.

The flow accumulation maps (Figure 4-3, Figure 4-4 and Figure 5-8), along with the flow monitoring network (Figure 2-15) indicate the water that is available in the drainage network is concentrated in the downstream section of the main drainage catchments closer to the west coast of the region, with little surface water available in the eastern and southern parts where demand may be higher (IGS, 2023). This suggests that to capture larger volumes of water in the drainage network for use further upstream, active management would be required, e.g., pumping to upstream storages. This would be a significant undertaking, with limited opportunities for storage at downstream or upstream locations, and large upfront construction and ongoing operation and maintenance costs. Notwithstanding this challenge, most of the drainage networks have already been modified to support retaining water in the landscape (see Section 1.3), and are expected to offer limited additional water in all but the wettest years (when there is unlikely to be storage available in any case), and these wet years are projected to be less frequent in the future. This suggests the main drainage networks already has the functionality to divert water into wetlands to support more environmental water requirements that there is water to meet these requirements.

At a smaller scale, holding water in wetlands in the landscape may have localised recharge benefits. However, using water from wetland recharge to support consumptive use is likely to require detailed monitoring. If extraction is close enough to a wetland to benefit from recharge, it is likely also close enough to impact on water available to groundwater dependent ecosystems. Setback distances for priority wetland complexes in the Lower Limestone Coast Water Allocation Plan (SENRMB, 2019) provide an indication of the scale of recharge from wetlands, in the order 1 – 2.4 km. For recharge to support extractive use directly, specifically designed systems such as active managed aquifer recharge (MAR) (Innovative Groundwater Solutions, 2023; Page et al., 2021) or water banking (e.g. Kiparsky et al., 2021) are more likely to avoid trade-offs with environmental assets, but would be more costly to implement and require a mechanism to account for the volume intercepted or extracted, and the credits and debits from a water banking system.

Innovative Groundwater Solutions (2023) investigated opportunities for managed aquifer recharge from the drainage network. A 2 km buffer from the network as a maximum extent for recharge from drain or a viable distance to pump water for MAR was adopted. There is a relatively limited understanding of surface water – groundwater interactions from the drainage network to quantify where and when recharge from the drainage network may occur. Monitoring undertaken by Harrington et al. (2012) found predominantly gaining conditions across the drains sampled. Similarly, Cranswick and Herpich (2018) found the longest length of drains could be classified as ‘very high’ and ‘high’ likelihood of gaining conditions, with variable proportions over time. The slow recession observed in streamflow data (e.g. Figure 2-17), very flat terrain and shallow groundwater also implies flow in the drains has a large baseflow component. These gaining conditions suggest recharge from the drains to groundwater would be limited, as the direction of flow tends to be from groundwater to the drain. Once groundwater levels fall in late spring and summer due to evapotranspiration some recharge may occur, but the duration of recharge would be expected to be short before the drain ceases to flow. Additionally, clogging layers that form in drains would be expected to have a low permeability and limit recharge rates (Noorduijn et al., 2014), retaining water in the drains that may lead to a water logging risk (IGS, 2023), as well as reduce or remove the drainage function provided by the network. Doble et al. (2022) modelled the infilling drains to retain water in the landscape to supplement groundwater extraction but found that groundwater recovery was localised and the volume of water retained is likely to be reduced under drier climates. Hence, the spatial extent, duration and, in turn, volume of recharge to the unconfined aquifer from water stored within, or discharged to, the drainage network is likely to be limited.

6.3 Assumptions, limitations and implications

Run time of over a week to undertake a model calibration, even when highly parallelised, prevented systematic testing of many of the assumptions made in the model configuration and calibration. In the absence of a more formal sensitivity or uncertainty analysis, these assumptions are qualitatively discussed in this section.

The partitioning of data into sets for model calibration and validation is a recognised factor influencing perceived model performance and ultimately generalisability (Ji et al., 2025; Maier et al., 2023). Maier et al. (2023) outlines principles for selecting data splitting periods, that 1) datasets used for model development (calibration) and evaluation (validation) are different, that all types of events are included in the model development subset, and ideally all types of patterns are also represented in the evaluation set. The first two criteria are satisfied in this work, with different periods used for calibration and validation, and the calibration period containing the driest periods in the late 2000s and the wettest period in the early 1990s. Given the need to split the data into two consecutive parts, such that the influence of the 'memory' in the catchment is captured correctly, it can be difficult to meet criteria three, that the validation period also includes all types of events. The validation period was wetter than the calibration period on average (Table 3-1) but ultimately it was decided to capture the most recent, and drier period, in the calibration dataset and ensure the current state of the catchments and drier conditions relevant to the climate projection scenarios informed the model development. Additional confidence in the ability of the model to predict in out of sample (data not used in calibration) is provided by the evaluation in Section 3.4, where model output was compared to data in regions not used in calibration, outside of the catchments that had the highest quality streamflow data.

The objective function used to summarise the model performance into one number to be optimised can also influence the selection of the best model parameters. For streamflow the combined objective function of Viney et al. (2009) was used and has been commonly used to calibrate models for previous climate change impact assessments (e.g. Chiew et al., 2018; Robertson et al., 2023). A number of optimisation trials were undertaken to test and refine the form of the objective function for the other datasets used in the Combined objective function. Initially actual evapotranspiration datasets were trialled, however as outlined in Section 2.4.4 was ultimately found to degrade the performance of the model for other components of the water balance, and LAI was used to improve the modelled vegetation dynamics. No additional testing of the remotely sensed LAI data was undertaken. A number of approaches for how to inform the model parameters using groundwater data were trialled, including calibration the deep drainage to a water table fluctuation derived recharge, and correlating changes in the groundwater store (S_g in Figure 3-1) instead of the deep soil store ultimately used, S_d. These trials indicated that uncertainty in the derived recharge (e.g. an assumed specific yield) influenced the model results, and that changes in the S_g store of the model tended to be much slower than changes observed in the groundwater data, and ultimately the S_d storage level, representing the soil profile 1 – 6 m (typically the depth to the unconfined aquifer) was selected as conceptually the most logical, and also best performing, option to include groundwater data in the calibration of the model. Ultimately these decisions influence the calibration of the model and the resulting water balance derived, and this initial testing of the objective function was undertaken to attempt to result in a model that is best suited to the application in this work, estimate the long term water balance across the dominant terms (runoff, recharge and evapotranspiration) under the historical and a projected future warmer and drier climate.

Resulting parameter values, including ranges from parameter sets that produces similarly, was presented in Figure 3-8. It was found that for some parameters the Combined objective function has a narrower distribution, indicating that the parameters were better identified than the Q-only model, potentially due to the additional datasets used in the Combined objective function providing more information to inform the 'better' parameter values. For some parameters this may indicate the parameter value does not have a strong influence on the resulting objective function value. As noted above, simulation time prevented more rigorous sensitivity or uncertainty analysis being undertaken.

In some cases where only the Combined object function would be expected to influence directly, for example the t_{scen} and t_{grow} parameters controlling the rate of change in leaf biomass, it is expected the Combined objective function has resulted in more realistic values, rather than relying on the influence of this

component of the model on streamflow to identify the most suitable values. Given the large number of parameters to calibrate (21 decision variables) and the potentially limited information in the streamflow time series (zero or low flow for large parts of the year), relying on streamflow only for this calibration is expected to have resulted in a wider range of parameter values resulting in similar streamflow performance (termed model equifinality). Some of the parameters representing scaling factors of derived spatial data calibrated to very low values, e.g. ne_scale. Some of these parameters, e.g. kd_scale, are not well known and a suitable scaling could take on a wide range of values. However, for other parameters that scale spatial grids of relatively well quantified variables, such as effective porosity, the magnitude of the scaling factor is not expected, and suggests the input grid is overestimated by two orders of magnitude. The reason for these calibrated values is unclear and may indicate that structure changes to the model or other interactions could result in more physically plausible parameter values adopted.

Only the storage effects of Bool Lagoon and losses in the Drain M catchment downstream were represented in the modelled results, through application of an explicit routing model for these catchments (Section 3.4.1). This additional analysis was included for this catchment as it represents the largest area and volume of water available in the eastern side of the region, where water demand is expected to be highest. Including these extra components in the Drain M catchment resulted in larger reductions in runoff compared to those in the other catchments considered (Figure 5-4). The need to apply losses to the Drain M results suggests that runoff may be overestimated in the most southern areas in the model, while model biases were reasonably accurate in the catchments with calibration data (Figure 3-3 and Figure 3-4). Results for areas outside of Drain M represent runoff from each model grid which is then aggregated to the reporting zone without any additional losses included, and as such may provide an underestimate of streamflow, and change in streamflow at downstream locations.

The karst volcanics catchment along the southern coast of the region has been included in the model for completeness. However, the process represented by the AWRA-L model, driven by the rainfall-runoff relationship, does not represent the processes producing surface water in this catchment. The hydrology there is driven by groundwater close to the surface, in many cases expressing as springs and soaks, and this groundwater hydraulic process (i.e. lateral movement between cells) is not represented by AWRA-L. In this area the groundwater discharge, adaption of the drainage network that runs from karst springs, and other considerations such as seawater intrusion, are better represented by a 3D groundwater model, such as that currently under development by the Department for Environment and Water.

7 Summary

Previous water balances for the Lower Limestone Coast region have reported lumped annual averages for the region as a whole (e.g. Harrington et al., 2015a), or focused on specific components of the water balance, such as runoff (Humphrey et al., 2016; Wood and Way, 2011) or recharge (Doble et al., 2015; Harrington et al., 2015a). This work has developed an integrated water balance that concurrently captures actual evapotranspiration, runoff and recharge, including seasonal dynamics and the variability across the region. The model was calibrated to the high-quality streamflow gauges in the region that are not influenced by regulation, remotely sensed leaf area index to provide an indication of actual evapotranspiration, remotely sensed soil moisture, as well as representing the patterns in water storage recorded by groundwater levels. The range in climate projections for a 2060 time horizon and medium emissions scenario (SSP 2-4.5) were reviewed and applied to simulate projected future water availability. The management questions that this task set out to answer are summarised below.

7.1 How do components of the water balance vary over time and across the region?

The AWRA-L model developed was at a 1 km spatial resolution and daily temporal resolution, to provide high resolution detail on variability in space and time. Mean annual water balances were calculated for different surface water catchments and unconfined aquifer management zones and indicated that actual evapotranspiration was the dominant component of the water balance; runoff was typically less than 5% of rainfall; and the median gross recharge (before evapotranspiration from groundwater) across the management zones was approximately 15% of rainfall. The spatial variability in the water balance follows the rainfall gradient from drier in the north to wetter in the south, with the general direction of drain flow from east to west accumulating more surface water toward the western sides of the region and the coast (Figure 4-3).

Temporal variability in annual recharge and runoff was represented relatively well by the model (e.g. Figure 3-5 and Figure 3-7), to quantify variability over time. Runoff can vary substantially from year to year, with high coefficients of variability in the context of Australian catchments and indicated by the 20th and 80th percentile water availability maps (Figure 4-4). Drought conditions were estimated to occur approximately 20% of the time over the historical climate, depending on the catchment and drought definition, climatological, hydrological or agricultural (Figure 5-10), increasing to 2 to 3 times this frequency for the Mid and Dry climate projections, respectively.

A dashboard has been developed to allow for further interrogation of the water balance and at specific wetlands across the region and throughout time.

7.2 How might the water availability change with future climate projections?

The observational record was reviewed to find declining trends in rainfall, runoff and recharge, with approximately half of the declining trends in runoff and recharge statistically significant. The relationship between rainfall and runoff was also observed to have reduced; that is, the same amount of rainfall lead to less runoff in the latter half of the data. Hence, water availability has been observed to have reduced across the region, in part due to the 1.1 degrees of warming that has been observed at Mount Gambier since 1910.

Future projections are represented by GCMs. A total of 21 GCMs that provide the outputs necessary for hydrological modelling and deemed as a suitable representation of the climate systems that influence Australia (Grose et al., 2023) were considered. All GCMs project a reduction in annual rainfall for a 2060 time horizon and a medium emission scenario (SSP2-4.5). While the Wet scenario GCM projected a modest reduction in annual rainfall, it did project an increase in winter rainfall, which resulted in no change, or slight

increases, in modelled water availability. However, the overwhelming majority of models considered project a reduction in annual and winter rainfall, with the median case a 7% reduction in annual rainfall, and in the most extreme case a 20% reduction in rainfall.

Runoff and recharge elasticities were modelled to be approximately 2 for recharge and 4.2 for runoff; that is, a 7% reduction in rainfall translates to a 14% reduction in recharge and a 29% reduction in runoff. There was some variability to these average elasticity estimates depending on the annual rainfall, with higher rainfall zones having a smaller projected change closer to the change in rainfall (particularly for recharge), and larger proportions of change in the lower rainfall zones. Hence, future climate projections indicate that average water availability will continue to reduce over the coming decades, and periods of drought were estimated to approximately double for the median climate scenario.

7.3 Which locations, and under which conditions, is there water available in the landscape to support further water uses?

Reductions in recharge were modelled to be more similar to reductions in rainfall in the higher rainfall areas (as opposed to two times the rainfall change), and reductions in runoff were also slightly less in these areas compared to lower rainfall zones. These areas represent locations where there is projected to be the highest amounts of water available, due to the higher rainfall, as well as the proportion of rainfall projected to be available as runoff or recharge.

However, in the context of a drying climate for the region, locations and conditions with water available to support further water uses appear limited. The drainage network, particularly north of and including Drain M, has been modified extensively to have multiple options to divert water from the drains into wetlands and watercourses. Some of these drains have been used rarely due to low water availability over the past 15 years (e.g. REFLOWS Western Floodway out of Drain M). Diverting flow from the next catchment south, the Reedy Creek – Mount Hope Drain, into Drain M to increase the water available to meet volume commitments to Lake George has been proposed (South East Natural Resources Management Board and South Eastern Water Conservation and Drainage Board, 2019). Hence, it appears there is limited water available in the main drainage network that does not already have the ability to be diverted to multiple wetlands or watercourses where there is an environmental water requirement not currently being met. These locations tend to be near the coast or to the north of the region, which potentially do not align with the highest consumptive demand for water.

At a more local scale there are examples of restoration where wetland sills have been restored to remove historical drainage, for example Mt Burr Swamp and Pick Swamp, as well as the regulator under construction at the outlet of Lake Hawdon. No analysis of the changes to recharge from past wetland restoration efforts is known to have been undertaken to date. Also, extraction of any recharge created by wetland restoration will require targeted monitoring, as if an extraction well is close enough to the wetland to benefit from additional recharge, is it likely also close enough to create drawdown near the wetland, potentially impacting on the ability to meet environmental water requirements. These wetlands were originally drained for a purpose, and as such reinstating a more natural wetland sill may result in land currently in productive use being inundated. The same logic can be applied to a drain, where drains could be managed or infilled to create additional inundation and hence recharge (or reduce groundwater discharge as baseflow), however the original function of the drain—to remove water logging or periods of inundation—is removed.

References

Azarnivand, A., Sharples, W., Bende-Michl, U., Shokri, A., Srikanthan, S., Frost, A. and Baron-Hay, S. 2022 Analysing the uncertainty of modelling hydrologic states of AWRA-L – understanding impacts from parameter uncertainty for the National Hydrological Projections, Bureau of Meteorology, Melbourne.

Bárdossy, A. and Anwar, F. 2023. Why do our rainfall–runoff models keep underestimating the peak flows? Hydrol. Earth Syst. Sci. 27(10), 1987-2000.

Beguería, S., Vicente-Serrano, S.M., Reig, F. and Latorre, B. 2014. Standardized precipitation evapotranspiration index (SPEI) revisited: parameter fitting, evapotranspiration models, tools, datasets and drought monitoring. International Journal of Climatology 34(10), 3001-3023.

Benyon, R. and Doody, T. 2004 Water Use by Tree Plantations in South East South Australia, CSIRO, Mt Gambier.

Berghuijs, W.R., Larsen, J.R., van Emmerik, T.H.M. and Woods, R.A. 2017. A Global Assessment of Runoff Sensitivity to Changes in Precipitation, Potential Evaporation, and Other Factors. Water Resources Research 53(10), 8475-8486.

Brookes, J.D., Aldridge, K., Dalby, P., Oemcke, D., Cooling, M., Daniell, T., Deane, D., Johnson, A., Harding, C., Gibbs, M., Ganf, G., Simonic, M. and Wood, C. 2017. Integrated science informs forest and water allocation policies in the South East of Australia. Inland Waters 7(3), 358-371.

Carsel, R.F. and Parrish, R.S. 1988. Developing joint probability distributions of soil water retention characteristics. Water Resources Research 24(5), 755-769.

Chiew, F.H.S. 2006. Estimation of rainfall elasticity of streamflow in Australia. Hydrological Sciences Journal 51(4), 613-625.

Chiew, F.H.S., Teng, J., Vaze, J., Post, D.A., Perraud, J.M., Kirono, D.G.C. and Viney, N.R. 2009. Estimating climate change impact on runoff across southeast Australia: Method, results, and implications of the modeling method. Water Resources Research 45(10).

Chiew, F.H.S., Zheng, H. and Potter, N.J. 2018. Rainfall-Runoff Modelling Considerations to Predict Streamflow Characteristics in Ungauged Catchments and under Climate Change. Water 10(10), 1319.

Cranswick, R. and Herpich, D. 2018 Groundwater–surface water exchange in the South East: 30 years of change, Government of South Australia, Department for Environment and Water, Adelaide.

Crosbie, R. and Davies, P. (2013) Framework for a Regional Water Balance Model for the South Australian Limestone Coast Region. Harrington, N. and Lamontagne, S. (eds), Goyder Institute for Water Research, Adelaide, South Australia.

Crosbie, R.S., Davies, P., Harrington, N. and Lamontagne, S. 2015. Ground truthing groundwater-recharge estimates derived from remotely sensed evapotranspiration: a case in South Australia. Hydrogeology Journal 23(2), 335-350.

Crosbie, R.S., Pickett, T., Mpelasoka, F.S., Hodgson, G., Charles, S.P. and Barron, O.V. 2013. An assessment of the climate change impacts on groundwater recharge at a continental scale using a probabilistic approach with an ensemble of GCMs. Climatic Change 117(1), 41-53.

CSIRO and Bureau of Meteorology 2024 State of the Climate 2024, Government of Australia.

Dane, J. and Puckett, W. 1994 Field soil hydraulic properties based on physical and mineralogical information. al., M.v.G.e. (ed), pp. 389–403, University of California: Riverside, CA.

Denny, M., Herpich, D., Cetin, L. and Green, G. 2015 South East wetlands: climate change risks and opportunities for mitigation, Adelaide.

Denson, E., Wasko, C. and Peel, M.C. 2021. Decreases in relative humidity across Australia. Environmental Research Letters 16(7), 074023.

Department for Environment and Water 2022 Guide to Climate Projections for Risk Assessment and Planning in South Australia 2022, Government of South Australia, through the Department for Environment and Water, Adelaide.

Department for Environment and Water 2023 Limestone Coast Prescribed Areas, 2020–21 water resources assessment, Government of South Australia, Department for Environment and Water, Adelaide.

Doble, R., Janardhanan, S., Foran, T. and Pickett, T. 2022 Groundwater in the South East SA under climate change: scenario modelling and stakeholder perspectives of impacts, adaptation and management, CSIRO, Adelaide, Australia.

Doble, R.C., Pickett, T., Crosbie, R.S. and Morgan, L. 2015 A new approach for modelling groundwater recharge in the South East of South Australia using MODFLOW, Goyder Institute for Water Research, Adelaide.

Doble, R.C., Pickett, T., Crosbie, R.S., Morgan, L.K., Turnadge, C. and Davies, P.J. 2017. Emulation of recharge and evapotranspiration processes in shallow groundwater systems. Journal of Hydrology 555, 894-908.

Doody, T., Benyon, R. and Gao, S. 2023. Fine scale 20-year timeseries of plantation forest evapotranspiration for the Lower Limestone Coast. Hydrological Processes 37(3), e14836.

Doody, T., Gao, S., Vervoort, W., Pritchard, J., Davies, M. and Nolan, M. 2022. A river basin scale spatial model to advance understanding of riverine tree response to hydrological management. Journal of Environmental Management accepted.

Dorigo, W., Wagner, W., Albergel, C., Albrecht, F., Balsamo, G., Brocca, L., Chung, D., Ertl, M., Forkel, M., Gruber, A., Haas, E., Hamer, P.D., Hirschi, M., Ikonen, J., de Jeu, R., Kidd, R., Lahoz, W., Liu, Y.Y., Miralles, D., Mistelbauer, T., Nicolai-Shaw, N., Parinussa, R., Pratola, C., Reimer, C., van der Schalie, R., Seneviratne, S.I., Smolander, T. and Lecomte, P. 2017. ESA CCI Soil Moisture for improved Earth system understanding: State-of-the art and future directions. Remote Sensing of Environment 203, 185-215.

Duan, Q., Sorooshian, S. and Gupta, V.K. 1994. Optimal use of the SCE-UA global optimization method for calibrating watershed models. Journal of Hydrology 158(3), 265-284.

Fowler, K.J.A., McMahon, T.A., Westra, S., Horne, A., Guillaume, J.H.A., Guo, D., Nathan, R., Maier, H.R. and John, A. 2024. Climate stress testing for water systems: Review and guide for applications. WIREs Water 11(6), e1747.

Frost, A., Ramchurn, A. and Smith, A. 2018 The Australian Landscape Water Balance model (AWRA-L v6). Technical Description of the Australian Water Resources Assessment Landscape model version 6. , Bureau of Meteorology.

Fu, G., Crosbie, R.S., Barron, O., Charles, S.P., Dawes, W., Shi, X., Van Niel, T. and Li, C. 2019. Attributing variations of temporal and spatial groundwater recharge: A statistical analysis of climatic and non-climatic factors. Journal of Hydrology 568, 816-834.

Gibbs, M., Alcorn, M. and Vaze, J. 2024. The SWTools R package for SILO data acquisition, homogeneity testing and correction. Australasian Journal of Water Resources 28(1), 123-135.

Grose, M.R., Narsey, S., Trancoso, R., Mackallah, C., Delage, F., Dowdy, A., Di Virgilio, G., Watterson, I., Dobrohotoff, P., Rashid, H.A., Rauniyar, S., Henley, B., Thatcher, M., Syktus, J., Abramowitz, G., Evans, J.P., Su, C.-H. and Takbash, A. 2023. A CMIP6-based multi-model downscaling ensemble to underpin climate change services in Australia. Climate Services 30, 100368.

Guerschman, J.P., McVicar, T.R., Vleeshower, J., Van Niel, T.G., Peña-Arancibia, J.L. and Chen, Y. 2022. Estimating actual evapotranspiration at field-to-continent scales by calibrating the CMRSET algorithm with MODIS, VIIRS, Landsat and Sentinel-2 data. Journal of Hydrology 605, 127318.

Hao, Z., Hao, F., Singh, V.P., Ouyang, W. and Cheng, H. 2017. An integrated package for drought monitoring, prediction and analysis to aid drought modeling and assessment. Environmental Modelling & Software 91, 199-209.

Harrington, N., Lamontagne, S., Crosbie, R.S., Morgan, L., Doble, R.C. and Werner, A. 2015a South East Regional Water Balance Project – Phase 2. Project Summary Report, Goyder Institute for Water Research Adelaide.

Harrington, N., Millington, A., Sodahlan, M. and Phillips, D. 2015b Development of Preliminary 1969 and 1983 Land Use Maps for the South East of SA, Goyder Institute for Water Research, Adelaide.

Harrington, N., Noordijn, S. and Cook, P. 2012 Evaluation of approaches to modelling surface water groundwater-interactions around drains in the South East of South Australia. Phase 1., Goyder Institute for Water Research.

Hausfather, Z. and Peters, G. 2020. Emissions – the 'business as usual' story is misleading. Nature 577(7792), 618-620.

Hawdon, A., McJannet, D. and Wallace, J. 2014. Calibration and correction procedures for cosmic-ray neutron soil moisture probes located across Australia. Water Resources Research 50(6), 5029-5043.

Huang, Q., Qin, G., Zhang, Y., Tang, Q., Liu, C., Xia, J., Chiew, F.H.S. and Post, D. 2020. Using Remote Sensing Data-Based Hydrological Model Calibrations for Predicting Runoff in Ungauged or Poorly Gauged Catchments. Water Resources Research 56(8), e2020WR028205.

Humphrey, G.B., Gibbs, M.S., Dandy, G.C. and Maier, H.R. 2016. A hybrid approach to monthly streamflow forecasting: Integrating hydrological model outputs into a Bayesian artificial neural network. Journal of Hydrology 540, 623-640.

Innovative Groundwater Solutions 2023 South East Drainage Network Assessment and Managed Aquifer Recharge Feasibility Study, Prepared for the Limestone Coast Landscape Board.

IPCC 2022 Climate Change 2022: Impacts, Adaptation, and Vulnerability. Contribution of Working Group II to the Sixth Assessment Report of the Intergovernmental Panel on Climate Change, Cambridge University Press, Cambridge, UK and New York, NY, USA.

Jeffery, S.J., Carter, J.O., Moodie, K.B. and Beswick, A.R. 2001. Using spatial interpolation to construct a comprehensive archive of Australian climatic data. Environmental Modelling & Software 16, 309-330.

Jeffrey, S.J., Carter, J.O., Moodie, K.B. and Beswick, A.R. 2001. Using spatial interpolation to construct a comprehensive archive of Australian climate data. Environ Modell Softw 16(4), 309-330.

Ji, Y., Zheng, F., Wen, J., Li, Q., Chen, J., Maier, H.R. and Gupta, H.V. 2025. An R package to partition observation data used for model development and evaluation to achieve model generalizability. Environmental Modelling & Software 183, 106238.

Jones, D.A., Wang, W. and Fawcett, R. 2009. High-quality spatial climate data-sets for Australia. Aust Meteorol Ocean 58(4), 233-248.

Kiparsky, M., Miller, K., Goulden, P., Milman, A. and Owen, D. 2021. Groundwater Recharge for a Regional Water Bank: Kern Water Bank, Kern County, California. Case Studies in the Environment 5(1).

Lucas, R., Mueller, N., Siggins, A., Owers, C., Clewley, D., Bunting, P., Kooymans, C., Tissott, B., Lewis, B., Lymburner, L. and Metternicht, G. 2019. Land Cover Mapping using Digital Earth Australia. Data 4(4), 143.

Ma, H., Zeng, J., Chen, N., Zhang, X., Cosh, M.H. and Wang, W. 2019. Satellite surface soil moisture from SMAP, SMOS, AMSR2 and ESA CCI: A comprehensive assessment using global ground-based observations. Remote Sensing of Environment 231, 111215.

Maier, H.R., Zheng, F., Gupta, H., Chen, J., Mai, J., Savic, D., Loritz, R., Wu, W., Guo, D., Bennett, A., Jakeman, A., Razavi, S. and Zhao, J. 2023. On how data are partitioned in model development and evaluation: Confronting the elephant in the room to enhance model generalization. Environmental Modelling & Software 167, 105779.

McColl, K.A., Alemohammad, S.H., Akbar, R., Konings, A.G., Yueh, S. and Entekhabi, D. 2017. The global distribution and dynamics of surface soil moisture. Nature Geoscience 10(2), 100-104.

Minasny, B., McBratney, A.B. and Bristow, K.L. 1999. Comparison of different approaches to the development of pedotransfer functions for water-retention curves. Geoderma 93(3), 225-253.

Morgan, L., Harrington, N., Werner, A., Hutson, J., Woods, J. and Knowling, M. 2015 South East Regional Water Balance Project – Phase 2. Development of a Regional Groundwater Flow Model, Goyder Institute for Water Research, Adelaide.

Muggeo, V. 2008. Segmented: An R Package to Fit Regression Models With Broken-Line Relationships. R News 8, 20-25.

Muggeo, V.M.R. 2003. Estimating regression models with unknown break-points. Stat Med 22(19), 3055-3071.

Nathan, R.J. and McMahon, T.A. 1990. Evaluation of automated techniques for base flow and recession analyses. Water Resources Research 26(7), 1465-1473.

Noorduijn, S.L., Shanafield, M., Trigg, M.A., Harrington, G.A., Cook, P.G. and Peeters, L. 2014. Estimating seepage flux from ephemeral stream channels using surface water and groundwater level data. Water Resources Research 50(2), 1474-1489.

Page, D., Vanderzalm, J., Gonzalez, D., Castellazzi, P., Bennett, J., Barron, O. and Peake, A. 2021 Rapid appraisal of Managed Aquifer Recharge (MAR) opportunities for agriculture, CSIRO.

Peeters, L.J.M., Crosbie, R.S., Doble, R.C. and Van Dijk, A.I.J.M. 2013. Conceptual evaluation of continental land-surface model behaviour. Environmental Modelling & Software 43, 49-59.

Peterson, T.J. and Fulton, S. 2019. Joint Estimation of Gross Recharge, Groundwater Usage, and Hydraulic Properties within HydroSight. Groundwater 57(6), 860-876.
Petheram, C., McMahon, T.A. and Peel, M.C. 2008. Flow characteristics of rivers in northern Australia: Implications for development. Journal of Hydrology 357(1), 93-111.
Rajib, A., Evenson, G.R., Golden, H.E. and Lane, C.R. 2018. Hydrologic model predictability improves with spatially explicit calibration using remotely sensed evapotranspiration and biophysical parameters. Journal of Hydrology 567, 668-683.
Robertson, D.E., Zheng, H., Peña-Arancibia, J.L., Chiew, F.H.S., Aryal, S., Malerba, M. and Wright, N. 2023. How sensitive are catchment runoff estimates to on-farm storages under current and future climates? Journal of Hydrology 626, 130185.
SA Water 2012 SA Water Wastewater Treatment Plants and Catchments, SA Water, Government of South Australia, Adelaide.
SENRMB 2019 Water Allocation Plan for the Lower Limestone Coast Prescribed Wells Area, South East Natural Resources Management Board, Government of South Australia.
South East Natural Resources Management Board and South Eastern Water Conservation and Drainage Board 2019 South East Drainage and Wetland Strategy, Government of South Australia.
Stephens, C.M., Band, L.E., Johnson, F.M., Marshall, L.A., Medlyn, B.E., De Kauwe, M.G. and Ukkola, A.M. 2023. Changes in Blue/Green Water Partitioning Under Severe Drought. Water Resources Research 59(11), e2022WR033449.
Stephens, C.M., McVicar, T.R., Johnson, F.M. and Marshall, L.A. 2018. Revisiting Pan Evaporation Trends in Australia a Decade on. Geophysical Research Letters 45(20), 11,164-111,172.
Svoboda, M., LeComte, D., Hayes, M., Heim, R., Gleason, K., Angel, J., Rippey, B., Tinker, R., Palecki, M., Stooksbury, D., Miskus, D. and Stephens, S. 2002. The Drought Monitor. Bulletin of the American Meteorological Society 83(8), 1181-1190.
Thirel, G., Santos, L., Delaigue, O. and Perrin, C. 2024. On the use of streamflow transformations for hydrological model calibration. Hydrol. Earth Syst. Sci. 28(21), 4837-4860.
Tonkin 2020 Coorong Infrastructure Investigations Technical Review, Department for Environment and Water, Adelaide
Van Dijk, A. 2010 The Australian Water Resources Assessment System Technical Report 3. Landscape Model (version 0.5) Technical Description, CSIRO.
Van Dijk, A. and Rahman, J. 2019 Synthesising multiple observations into annual environmental condition reports: the OzWALD system and Australia's Environment Explorer. Elsawah, S. (ed), pp. 884-890, Modelling and Simulation Society of Australia and New Zealand, Canberra, ACT, Australia.
Vaze, J., Mateo, C. and Wang, B. 2017 AWRA-L implementation with 2 and 5 HRUs at 5km and 5 HRUs at 1km spatial resolution – inter-comparison and comparison with observations, CSIRO, Australia.
Vaze, J., Mateo, C., Wang, B., Teng, J. and Marvanek, S. 2018 AWRA-L input spatial layers at 1 km and 5 km resolutions for the Australian continent - Source data and comparison between 1 km and 5 km resolutions. , CSIRO, Australia.
Vaze, J., Wang, B., Mateo, C. and Hughes, J. 2016 Methodology for incorporation of extra hydrological response units (HRU's) in AWRA-L structure, CSIRO, Australia.
Vervoort, R., Miechels, S.F., van Ogtrop, F.F. and Guillaume, J.H.A. 2014. Remotely sensed evapotranspiration to calibrate a lumped conceptual model: Pitfalls and opportunities. Journal of Hydrology 519, 3223-3236.
Viney, N., Perraud, J., Vaze, J., Chiew, F., Post, D. and Yang, A. 2009 The usefulness of bias constraints in model calibration for regionalisation to ungauged catchments, Cairns, Australia.
Viney, N., Vaze, J., Crosbie, R., Wang, B., Dawes, W. and Frost, A. 2015 AWRA-L v5.0: technical description of model algorithms and inputs, CSIRO, Australia.
Wasko, C., Stephens, C., Peterson, T.J., Nathan, R., Pepler, A., Hettiarachchi, S., Vogel, E., Johnson, F. and Westra, S. 2024. Understanding the implications of climate change for Australia's surface water resources: Challenges and future directions. Journal of Hydrology 645, 132221.
Willoughby, N., Thompson, D., Royal, M. and Miles, M. 2018 South Australian Land Cover Layers: an Introduction and Summary Statistics, Government of South Australia, Department for Environment and Water, Adelaide.
Wood, G. and Way, D. 2011 Basis for a regional flow management strategy for the South East of South Australia, Government of South Australia, through Department for Water, Adelaide.
Wood, S. 2001. Minimizing Model Fitting Objectives That Contain Spurious Local Minima by Bootstrap Restarting. Biometrics 57, 240-244.
Wright, D.P., Thyer, M. and Westra, S. 2015. Influential point detection diagnostics in the context of hydrological model calibration. Journal of Hydrology 527, 1161-1172.

Appendix A – AWRA-L spatial inputs

Table A-1 AWRA-L spatial and spatiotemporal input data layers at 0.01^0 and 0.05^0 across the Australian continent

AWRA-L SPATIAL LAYER (NAME AS IN AWRA-L MODEL SOURCE CODE)	UNITS	DESCRIPTION	SOURCE DATA USED TO DERIVE THE LAYER	PROCESSING TECHNIQUE
K_{0sat}	mm d^{-1}	Saturated hydraulic conductivity for the top soil layer (0 – 1 cm)	Soil physical properties from TERN	Derived using Dane and Puckett 1994 pedotransfer function (as described in Appendix A)
K_{ssat}	mm d^{-1}	Saturated hydraulic conductivity for the shallow soil layer (10 – 100 cm)	Same as above	Same as above
K_{dsat}	mm d^{-1}	Saturated hydraulic conductivity for the deep soil layer (100 – 600 cm)	Same as above	Same as above
S_{0AWC}	dimensionless	Available water holding capacity for the top soil layer (0 – 10 cm)	Soil physical properties from TERN	Derived using Minasny et al 1999 pedotransfer function (as described in Appendix A)
S_{sAWC}	dimensionless	Available water holding capacity for the shallow soil layer (10 – 100 cm)	Same as above	Same as above
S_{dAWC}	dimensionless	Available water holding capacity for the deep soil layer (100 – 600 cm)	Same as above	Same as above
ne	dimensionless	Soil effective porosity	Surface geology mapping and a lookup table from lithologies used to derive effective porosity which is used as a surrogate for specific yield	Derived using the "Polygon to Raster" tool in the "Conversion Tools" of the ArcGIS ArcToolbox
K-gw	d^{-1}	Groundwater drainage coefficient	Derived from effective porosity, hydraulic conductivity, drainage density, and assumed aquifer depth	Derived using eq. 10 in Viney et al., 2015
K	md^{-1}	Hydraulic conductivity of unconfined aquifer	Surface geology mapping and a lookup table from lithologies used to derive hydraulic conductivity of unconfined aquifer	Derived using the "Polygon to Raster" tool in the "Conversion Tools" of the ArcGIS ArcToolbox

Slope (β)	radians	Average slope within a grid cell	Derived from SRTM DEM	Derived by reprojecting the input (using bi-linear resampling) using the "Project Raster" tool then aggregating the finer resolution input to 1k and 5k resolution using the "Aggregate" tool (mean) in ArcGIS
f_grass (2 HRU)	dimensionless	Fraction of shallow rooted vegetation cover within each grid cell (calculated using fPar)	Derived from Advanced Very High Resolution radiometer (AVHRR) satellite derived fractions of recurrent photosynthetically active absorbed radiation (fPAR) (Donohue et al., 2008).	Adjusted such that the total of f_grass and f_tree is equal to 1.
f_grass (5 HRU)	dimensionless	Fraction of shallow rooted vegetation cover within each grid cell (calculated using fPar)	Derived from Advanced Very High Resolution radiometer (AVHRR) satellite derived fractions of recurrent photosynthetically active absorbed radiation (fPAR) (Donohue et al., 2008)	Adjusted such that the total of f_grass, f_tree, f_impervious, f_irrgated, and f_waterbody is equal to 1
f_tree	dimensionless	Fraction of tree cover within each grid cell (calculated using fPar)	Derived from Advanced Very High Resolution radiometer (AVHRR) satellite derived fractions of persistent photosynthetically active absorbed radiation (fPAR) (Donohue et al., 2008)	Derived by reprojecting the input to GCS_GDA_94 (using bi-linear resampling) at 1k resolution using the "Project Raster" tool in ArcGIS.
f_impervious	dimensionless	Fraction of impervious area within each grid cell (calculated using RS)	Derived by combining impervious area mapping from Geoscience Australia (GA) and rock outcrop and urban mapping from Juan Guerschman (work undertaken as part of AWRA in 2011-2012)	Derived by aggregating the finer resolution input to 1k and 5k resolution using the "Aggregate" tool in "Generalization" (mean) tool of the "Spatial Analyst Tools" in ArcGIS ArcToolbox.
f_irrigated	dimensionless	Fraction of permanent irrigated area within each grid cell (calculated using CLUM)	Derived by combining irrigated area mapping from Geoscience Australia (GA) and the CLUM data for MDB from Justin Hughes (work done as part of AWRA-R irrigation modelling in 2014-2015)	Same as above
f_waterbody	dimensionless	Fraction of large water bodies within each grid cell (calculated using RS)	Derived from Water Observation from Space (WOfS) data from Geoscience Australia which is better in eastern Australia and water bodies mapping undertaken by CSIRO which is better in western Australia	Same as above
meanP	mm	Long term mean daily precipitation	Derived from 1970 – 2012 ANUClimate data	Calculated the arithmetic mean of the daily precipitation from 19702012 at 1k resolution, then aggregated to 5k resolution using the "Aggregate" (mean) tool in ArcGIS.
meanPET	mm d_{-1}	Long term mean daily potential evaporation	Derived from 1970 – 2012 AWAP data	Calculated the arithmetic mean of the daily potential evapotranspiration from 1970-2012 at 5k resolution, then resampled to 1k resolution using the "Resample" tool in "Raster Processing" in ArcGIS

Latitude (*φ*)	radians	Latitude (negative in the southern hemisphere)	Latitude (negative in the southern hemisphere)	Derived from the latitude of the centroid of each 5k and 1k grid in continental Australia
Windspeed (u_2)	m s^{-1}	Wind speed at 2 m supplied by McVicar et al. (2008)	Wind speed derived from data aggregating the 1k data using the Bureau "Aggregate" (mean) tool in ArcGIS	Derived the 5k data by updated to 2016 using station data
Hveg_hruDR	m	Vegetation height for deep rooted HRU	Derived from the global 1 km lidar estimates of Simard et al. (2011)	Derived by reclassing all grid values greater than 1000 in 1k resolution as NoData, then aggregating to 5k using the "Aggregate" (mean) tool in ArcGIS
Pref		mm d_{-1} Reference precipitation Viney et al.,	Derived as a function of hydraulic conductivity of the topsoil and	Derived using eq. 1 in 2015 slope
HypPerc000	dimensionless	Hypsometric curve value at this percentage for each AWRA grid	The hypsometric curve is the cumulative distribution of 2013 elevation within an AWRA grid cell, based on the 3 sec SRTM DEM	Calculated using Peeters et al.,
HypPerc001	dimensionless	Hypsometric curve value at this percentage for each AWRA grid	Same as above	Same as above
HypPerc002	dimensionless	Hypsometric curve value at this percentage for each AWRA grid	Same as above	Same as above
HypPerc003	dimensionless	Hypsometric curve value at this percentage for each AWRA grid	Same as above	Same as above
HypPerc004	dimensionless	Hypsometric curve value at this percentage for each AWRA grid	Same as above	Same as above
HypPerc005	dimensionless	Hypsometric curve value at this percentage for each AWRA grid	Same as above	Same as above
HypPerc006	dimensionless	Hypsometric curve value at this percentage for each AWRA grid	Same as above	Same as above
HypPerc007	dimensionless	Hypsometric curve value at this percentage for each AWRA grid	Same as above	Same as above
HypPerc008	dimensionless	Hypsometric curve value at this percentage for each AWRA grid	Same as above	Same as above
HypPerc009	dimensionless	Hypsometric curve value at this percentage for each AWRA grid	Same as above	Same as above

HypPerc010	dimensionless	Hypsometric curve value at this percentage for each AWRA grid	Same as above	Same as above
HypPerc015	dimensionless	Hypsometric curve value at this percentage for each AWRA grid	Same as above	Same as above
HypPerc020	dimensionless	Hypsometric curve value at this percentage for each AWRA grid	Same as above	Same as above
HypPerc030	dimensionless	Hypsometric curve value at this percentage for each AWRA grid	Same as above	Same as above
HypPerc040	dimensionless	Hypsometric curve value at this percentage for each AWRA grid	Same as above	Same as above
HypPerc050	dimensionless	Hypsometric curve value at this percentage for each AWRA grid	Same as above	Same as above
HypPerc060	dimensionless	Hypsometric curve value at this percentage for each AWRA grid	Same as above	Same as above
HypPerc075	dimensionless	Hypsometric curve value at this percentage for each AWRA grid	Same as above	Same as above
HypPerc090	dimensionless	Hypsometric curve value at this percentage for each AWRA grid	Same as above	Same as above
HypPerc100	dimensionless	Hypsometric curve value at this percentage for each AWRA grid	Same as above	Same as above
LAImax_hruSR	dimensionless	Maximum achievable LAI for shallow rooted HRU (calculated using MODIS)	Derived from a time series of LAI from the Moderate Resolution Imaging Spectroradiometer (MODIS) satellite	Derived by (1) re-projecting and resampling (nearest) the source data to ~200m resolution using the "Project Raster" tool in ArcGIS, and (2) aggregating the output of 1 to 1km and 5km using the "Aggregate" (mean aggregation technique) tool in ArcGIS. Maximum LAI is capped at 4.
LAImax_hruDR	dimensionless	Maximum achievable LAI for deep rooted HRU (calculated using MODIS)	Derived from a time series of LAI from the Moderate Resolution Imaging Spectroradiometer (MODIS) satellite	Same as above, but maximum LAI is not capped.

LAImax_hruIRR	dimensionless	Maximum achievable LAI for irrigated crop HRU (calculated using MODIS – same values as shallow rooted HRU)	Derived from a time series of LAI from the Moderate Resolution Imaging Spectroradiometer (MODIS) satellite	Same as LAImax_hruSR but calculation was done for irrigated areas only.
Irr_start	day of the year	Start of irrigation period	Field knowledge and discussions with field experts	Irrigated summer crops are assigned a value of 244 (start of September), year-round crops are assigned a value of 1 (start of January)
Irrd	day of the year	End of irrigation period	Field knowledge and discussions with field experts	Irrigated summer crops are assigned a value of 151 (end of May), year-round crops are assigned a value of 365 (end of December)
Irr_allocation	mm y^{-1}	Water allocation for irrigation	Field knowledge and discussions with field experts	Irrigated sugarcane are assigned a value of 2100, the rest are assigned a value of 800
AWRA-L SPATIOTEMPORAL LAYER	UNITS	DESCRIPTION	SOURCE DATA USED TO DERIVE THE LAYER	**PROCESSING TECHNIQUE**
K_D	MJ M^{-2} D^{-1}	Incoming shortwave radiation	AWAP at 0.05° and resampled uniformly to 0.01°	Derived using Python scripts.
P	mm	Precipitation (daily)	ANUClimate from TERN (Michael Hutchinson)	Derived using Python scripts.
T_{max}	°C	Maximum temperature (daily)	ANUClimate from TERN (Michael Hutchinson)	Derived using Python scripts.
T_{min}	°C	Minimum temperature (daily)	ANUClimate from TERN (Michael Hutchinson)	Derived using Python scripts.

Appendix B – Streamflow data

Station number	station name	start	end	% of good data	max gauged flow, m3/s	% of volume below max gauging	Use for calibration?
A2390504	BRAY DRAIN @ Site B (0.3km D/S Site A)	4/09/1975	6/05/2014	90.4	7.2	65.1	No – big gap 1990-2010 and backwater effects from Lake Hawdon
A2390505	DRAIN L @ Boomaroo Park Amtd 7.3 km	16/04/1971	27/11/2022	61.6	18.0	80.9	No –DS of Lake Hawdon, possible rating curve issues
A2390506	BLACKFORD DRAIN @ Amtd 4.0km	16/07/1971	27/11/2022	86.8	17.5	100.0	No - regulated
A2390508	EIGHT MILE CREEK @ AMTD 0.3KM	19/05/2009	16/05/2014	53.1	2.6	100.0	No – very limited data
A2390510	DRAIN L @ U/S Princes Highway	16/07/1971	30/04/2014	90.9	6.7	94.4	Yes
A2390512	DRAIN M @ Woakwine Amtd 5.1km	14/07/1971	27/11/2022	70.1	48.4	99.3	No – regulated by Bool Lagoon
A2390513	REEDY CREEK - MT. HOPE DRAIN @ 7.2km NE South End	14/07/1971	27/11/2022	91.4	26.2	98.9	Yes
A2390514	DRAIN M @ D/S Callendale Regulator	13/07/1971	27/11/2022	82.0	32.6	92.0	No – regulated by Bool Lagoon
A2390515	BAKERS RANGE SOUTH DRAIN @ Robe-Penola Road	13/07/1971	27/11/2022	54.7	21.7	99.6	Yes
A2390516	DRAIN C @ Balma Carra	20/06/1973	1/08/1979	69.2	2.8	100.0	No – short record
A2390517	MORAMBRO CREEK @ The Gap	27/06/1973	5/09/1975	0.2	1.4	52.8	No – Short record
A2390518	MORAMBRO CREEK @ Rangeview	14/07/1971	26/02/1985	95.5	11.3	100.0	No – limited events in data
A2390519	MOSQUITO CREEK @ Struan	3/06/1971	27/11/2022	80.1	53.4	99.1	Yes

A2390521	DRAIN 44 @ Milne Gap	31/05/1973	17/01/1979	11.7	1.2	71.2	No – short record, use US bridge site instead
A2390523	STONY CREEK @ Woakwine Range	31/05/1973	27/11/2022	73.4	3.6	97.6	Yes
A2390524	BENARA CREEK @ Woakwine Range	18/12/1973	22/01/1976	0.3	0.2	79.3	No – short record
A2390527	WILMOT DRAIN @ 9.2km From Drain L	14/03/1973	30/04/2014	87.8	8.1	96.7	Yes
A2390529	MORAMBRO CK @ Frances (Rly Bridge)	18/06/1987	2/02/1990	61.3	11.4	87.8	No - short record
A2390531	MORAMBRO CK @ Bordertown-Naracoorte Road Bridge	10/08/1976	31/03/2022	89.3	8.6	95.0	Yes
A2390532	DRAIN 44 @ 100m U/S Lake Bonney Rd Bdge	22/07/1976	18/03/2014	60.6	3.0	92.9	Yes
A2390533	DRAIN 48 @ 200m U/S Lake Bonney Rd Bdge	22/07/1976	18/03/2014	82.0	1.3	98.2	No – paper mill discharge
A2390536	DRAIN C @ U/S Coonawarra	2/05/1978	5/05/2014	92.2	1.0	63.1	No –short effective record (closed in late 1980s)
A2390537	DRAIN C2 @ U/S Rocky Point	10/05/1978	14/01/1988	84.2	0.2	52.5	No – short record
A2390541	DRAIN M @ D/S Bool Lagoon Outlet	24/04/1985	27/11/2022	46.1	13.9	77.6	No – regulated by Bool Lagoon
A2390542	NARACOORTE CREEK @ Naracoorte	24/04/1985	7/11/2017	93.9	9.2	96.4	Yes
A2390543	PRETTY GULLY CREEK @ U/S of Runaway Hole	21/06/1987	10/02/1992	76.9	0.6	85.6	No – short record
A2390545	CRINOGLE BORE @ near Woolshed	2/07/1987	10/02/1992	82.8	-	-	No – short record
A2390546	ATTADALE CREEK @ Upstream of Attadale Runaway Hole	26/06/1987	10/02/1992	67.3	0.0	60.6	No – short record
A2390549	SINKHOLE @ Woods & Forests Dept	16/10/1989	24/01/1992	100.0	-	-	No – short record

A2390556	BAKERS RANGE WATERCOURSE @ G Cutting	10/04/1992	15/11/2022	76.6	4.8	100.0	No – regulated by Bool Lagoon
A2390563	MARCOLLAT WATERCOURSE @ Rowney Road	22/10/1997	11/07/2013	84.8	10.1	100.0	No – limited events
A2390564	FAIRVIEW DRAIN @ Upstream Keilira Road (original site)	23/04/1998	20/04/2000	66.8	0.9	95.8	No – short record
A2390565	FAIRVIEW DRAIN @ Pitts	18/06/1998	13/05/2014	62.9	0.4	96.1	No – minimal events in record
A2390569	FAIRVIEW DRAIN @ Downstream of Keilira Road	20/04/2000	20/10/2022	50.4	2.0	95.6	No - regulated
A2391001	BAKERS RANGE SOUTH DRAIN @ Phillips Road	2/12/2002	2/12/2009	76.8	13.9	100.0	No – short record
A2391075	Yelloch Creek @ Laurie Park	25/08/2006	21/04/2014	51.0	1.2	44.2	No – short record
A2391076	Mosquito Creek at Langkoop Hall	12/09/2006	27/11/2022	26.3	0.1	3.9	No – use Struan site
A2391125	Bakers Range South Drain at 0.85km u/s Callendale Reg	24/03/2010	27/11/2022	1.6	2.8	78.6	No – poor data quality
A2391141	Taratap Drain at Englands Crossing	28/07/2010	8/07/2013	4.5	-	-	No – short record
A2391145	Wimpinmerit Drain at Bald Hill Road	2/03/2011	23/07/2015	21.8	-	-	No – short record
A2391146	Baker Range Watercourse at Callendale	16/05/2011	27/11/2022	12.8	-	-	No – short record
A2391149	West Avenue Watercourse at Robertson Road	28/02/2011	29/07/2014	60.9	-	-	No – short record
A2391150	Bald Hill Drain at Ratcliffe Boundary	7/04/2011	9/04/2017	22.2	-	-	No – short record
A2391153	Baker Range Watercourse at Tatiara Swamp	28/03/2013	11/09/2014	89.1	-	-	No – short record
A2391187	Drain 1B Downstream of the Narrow Neck Weir	14/06/2013	14/05/2016	11.2	-	-	No – short record

A2391188	Lake Frome Outlet Drain 2km upstream Southend	26/08/2013	22/04/2017	0.5	-	-	No – short record
A2391261	Blackford Diversion Regulator	28/08/2019	27/11/2022	5.9	-	-	No – short record
A2391263	Ford crossing D/S Blackford diversion regulator	24/06/2019	12/09/2020	6.5	-	-	No – short record

Appendix C – Final calibration streamflow results

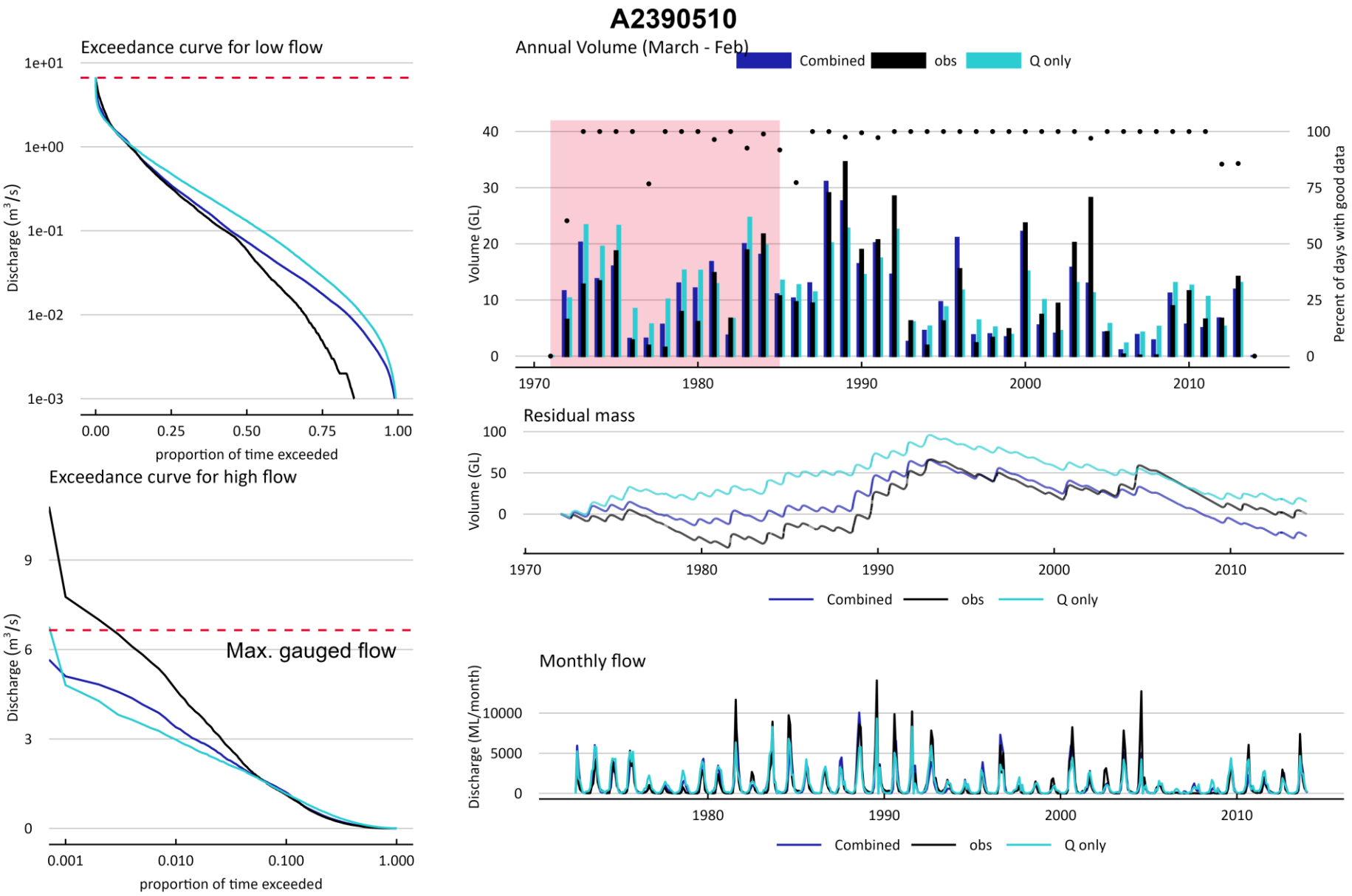

Figure C-1 Streamflow results for Drain L upstream of the Princess Highway (A2390510). See Figure 3-5 for a description of the plots.

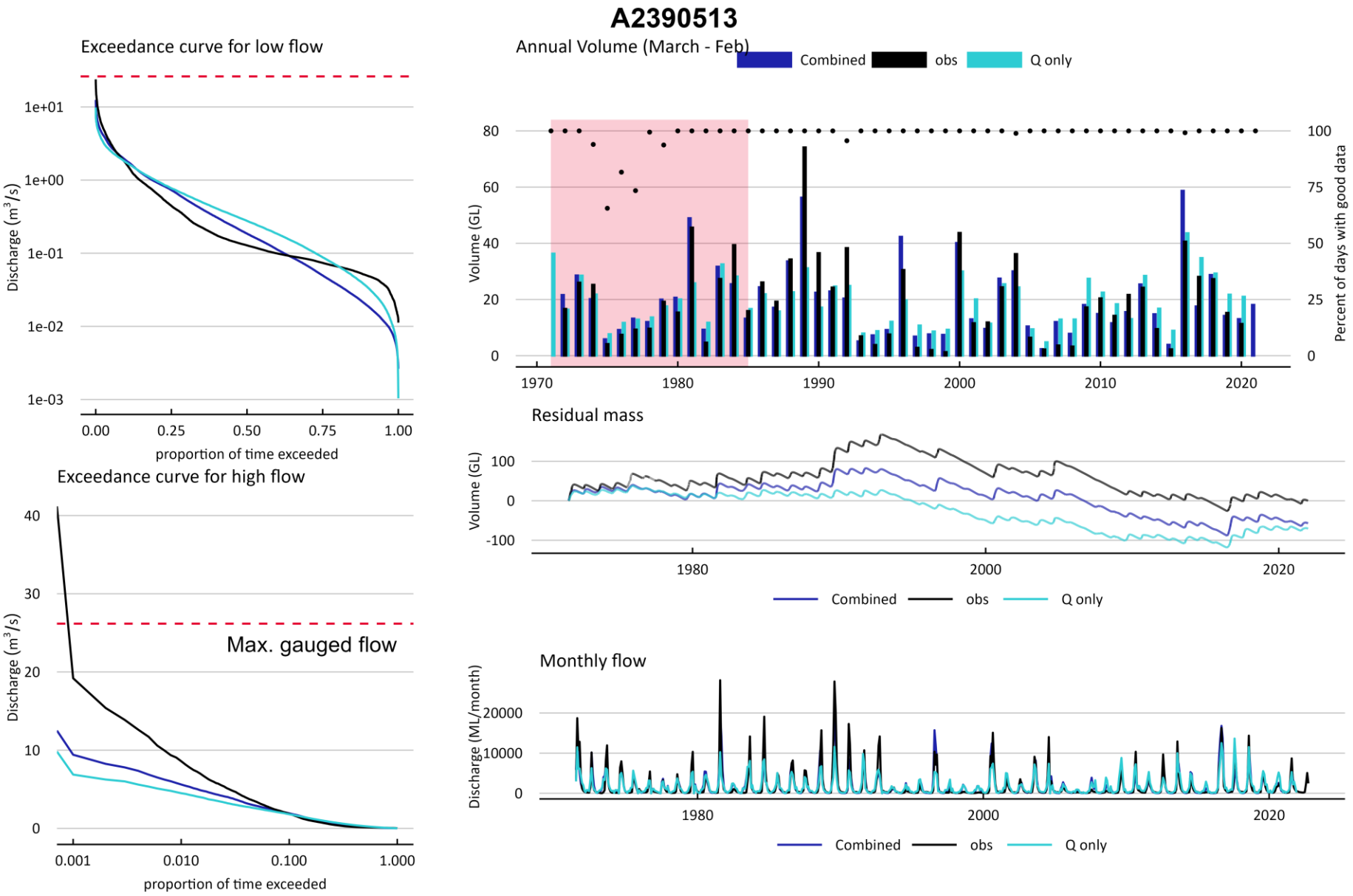

Figure C-2 Streamflow results for Reedy Creek – Mount Hope drain (A2390513). See Figure 3 9 for a description of the plots.

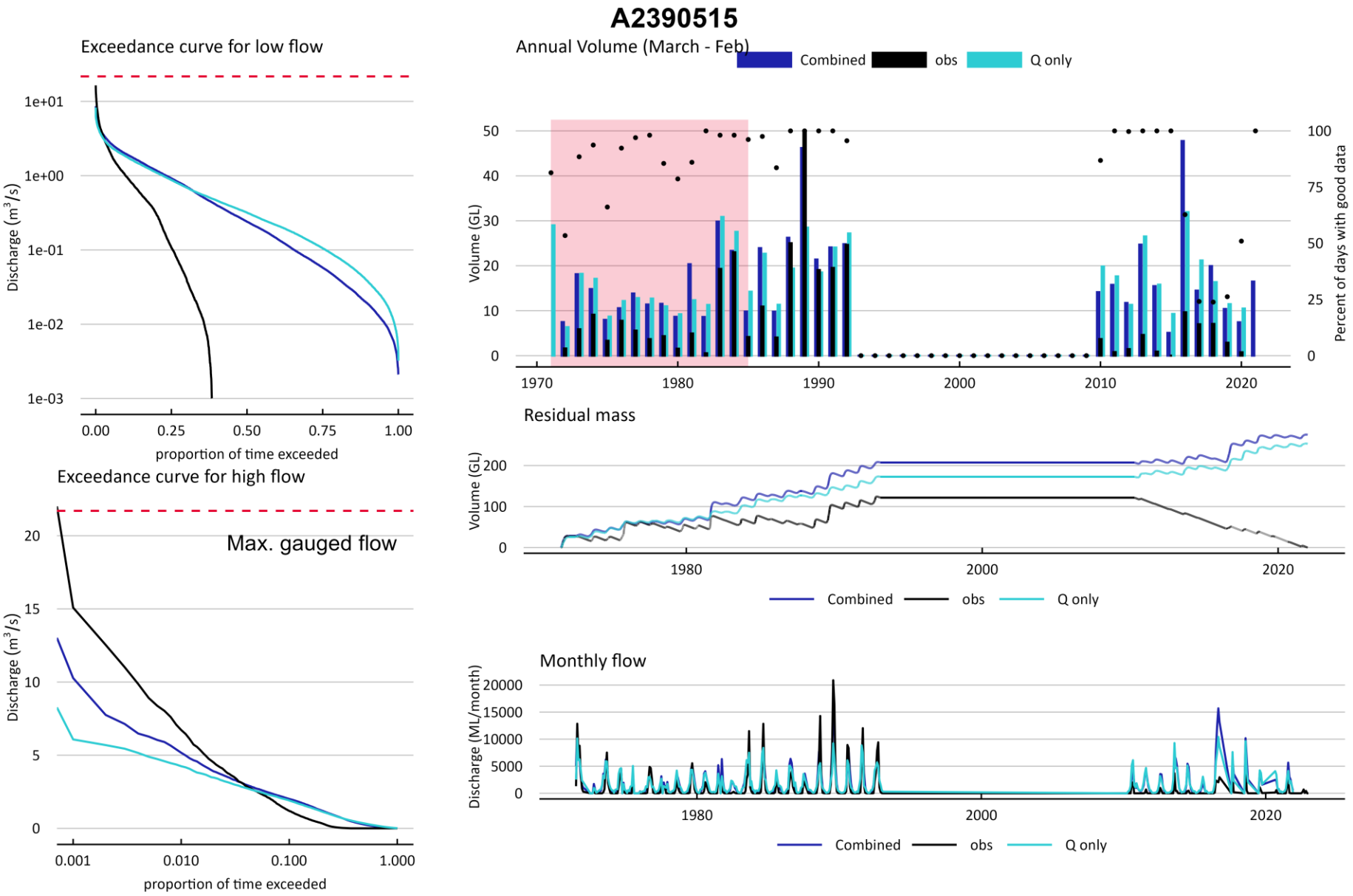

Figure C-3 Streamflow results for the Bakers Range South Drain (A2390515). See Figure 3 9 for a description of the plots.

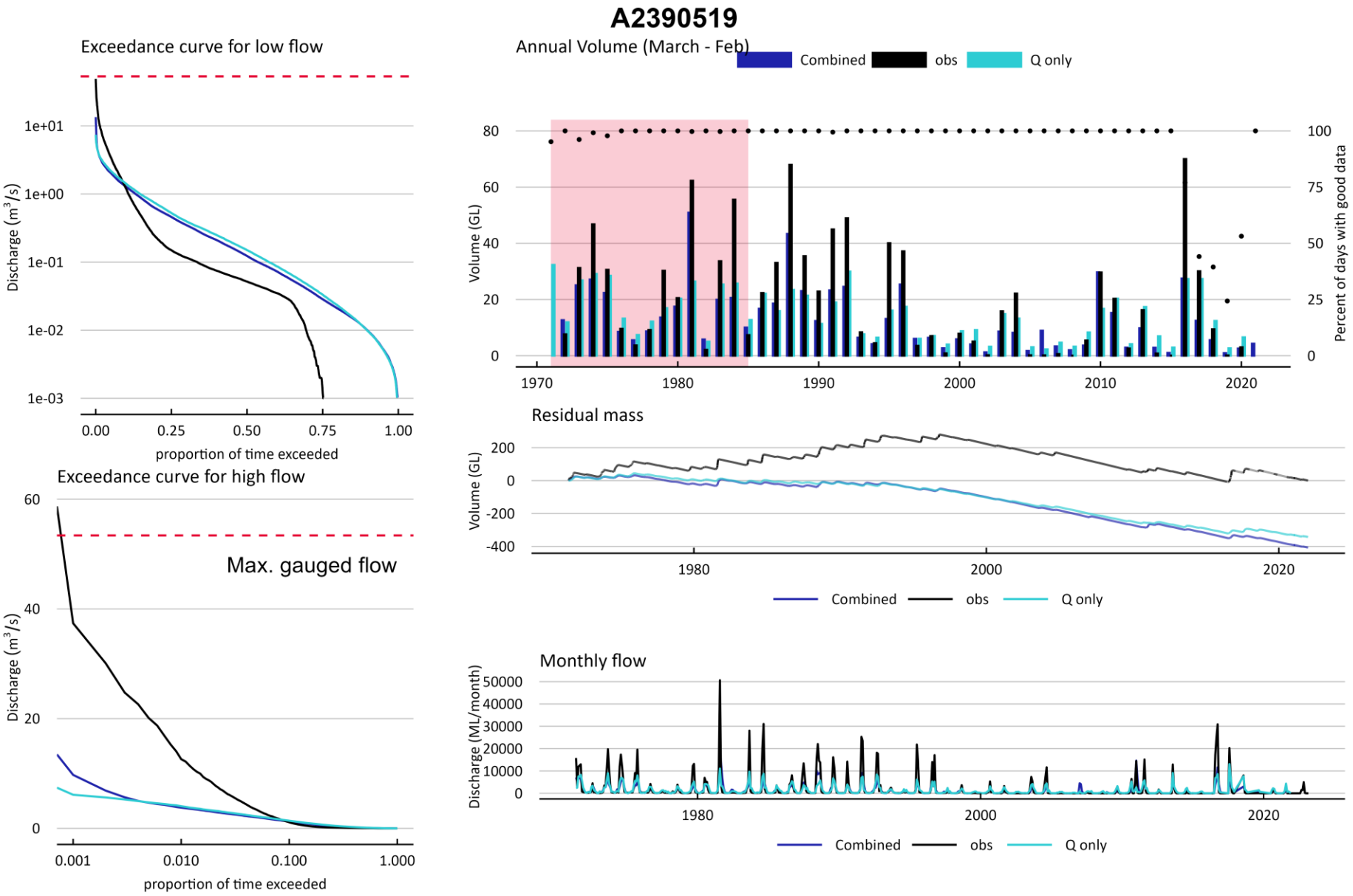

Figure C-4 Streamflow results for Mosquito Creek at Struan (A2390519). See Figure 3 9 for a description of the plots.

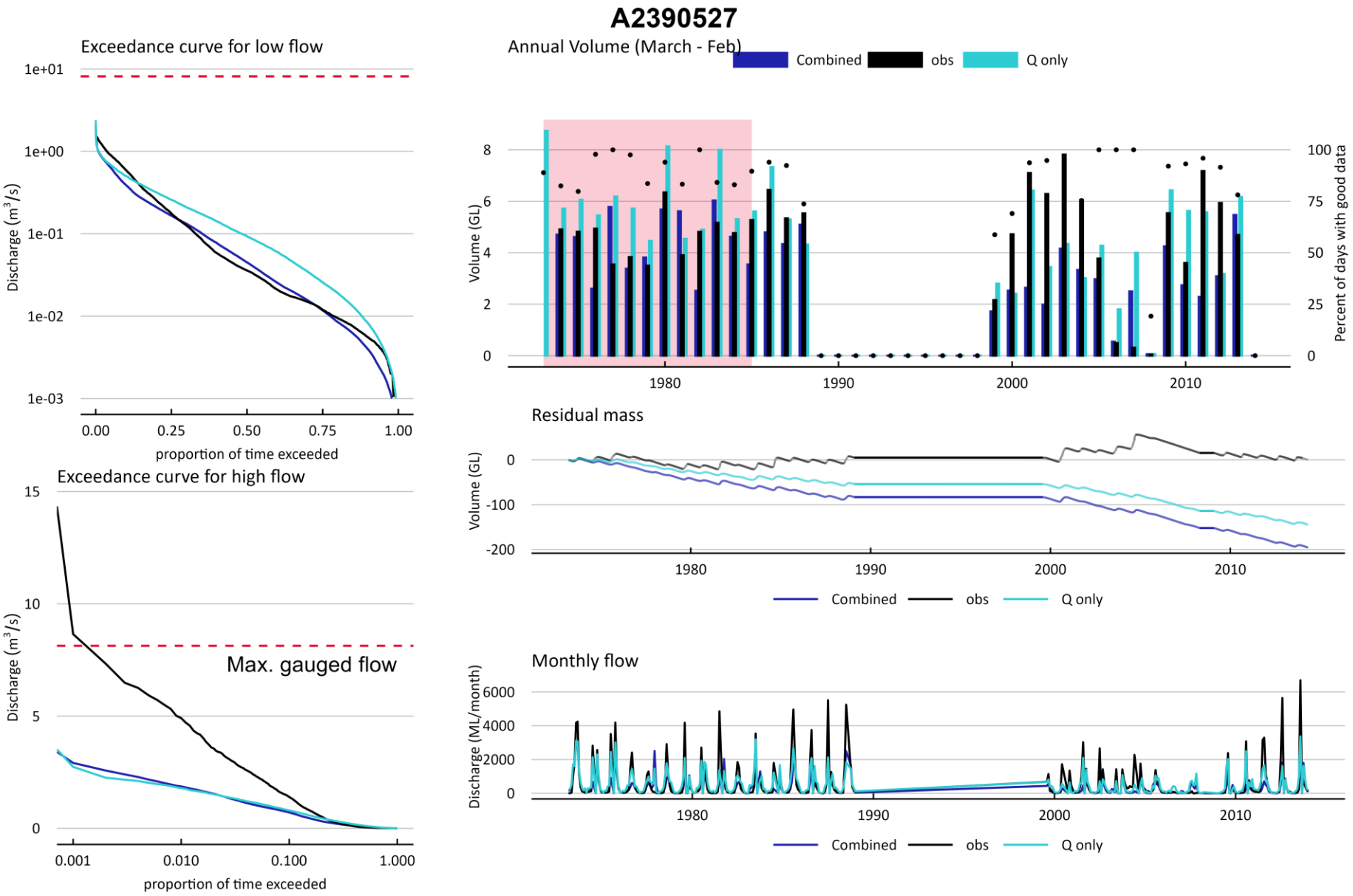

Figure C-5 Streamflow results for Wilmot Drain at 9.2km From Drain L (A2390527). See Figure 3 9 for a description of the plots.

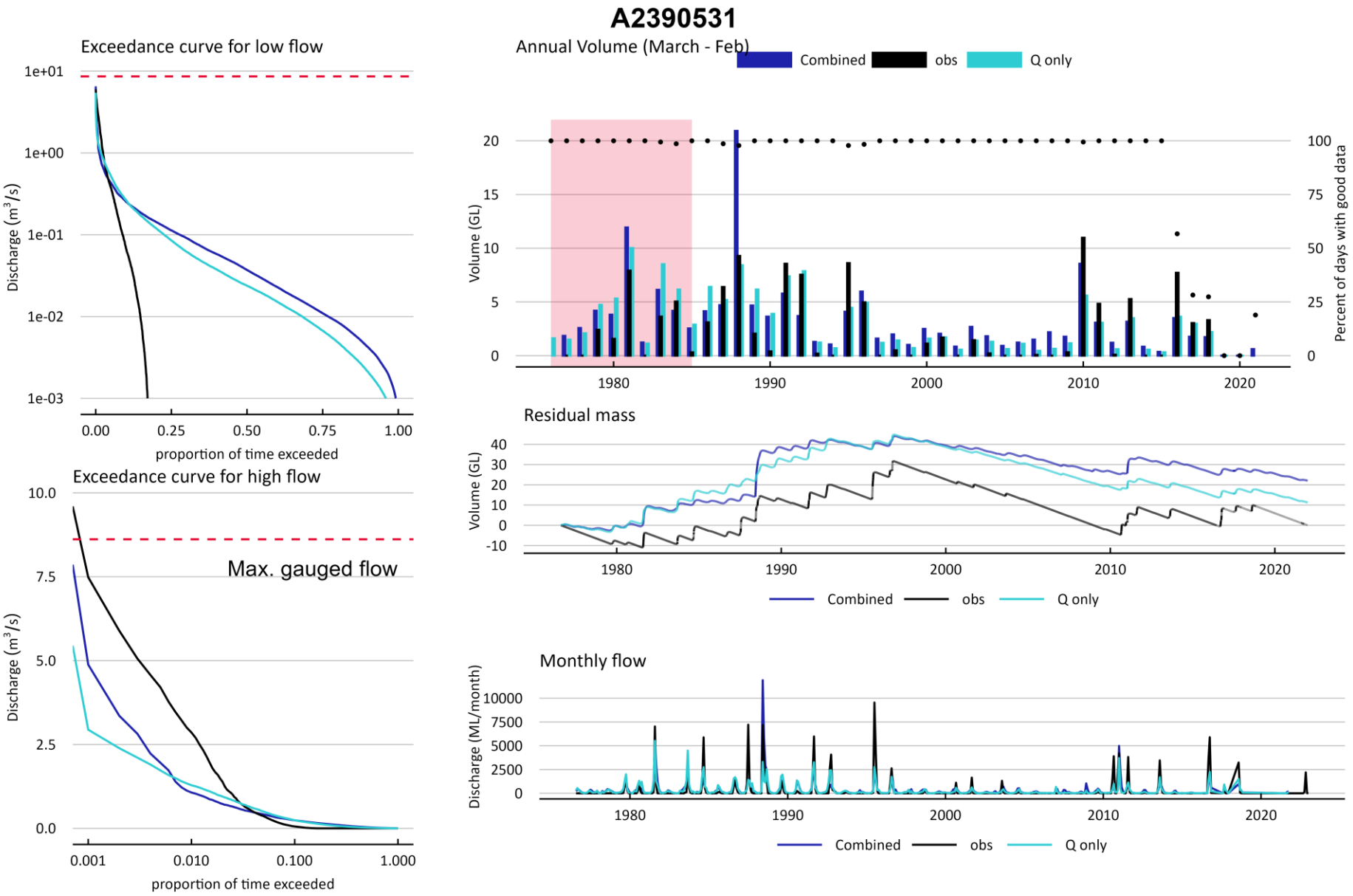

Figure C-6 Streamflow results for Morambro Creek at Bordertown-Naracoorte Road Bridge (A2390531). See Figure 3-5 for a description of the plots.

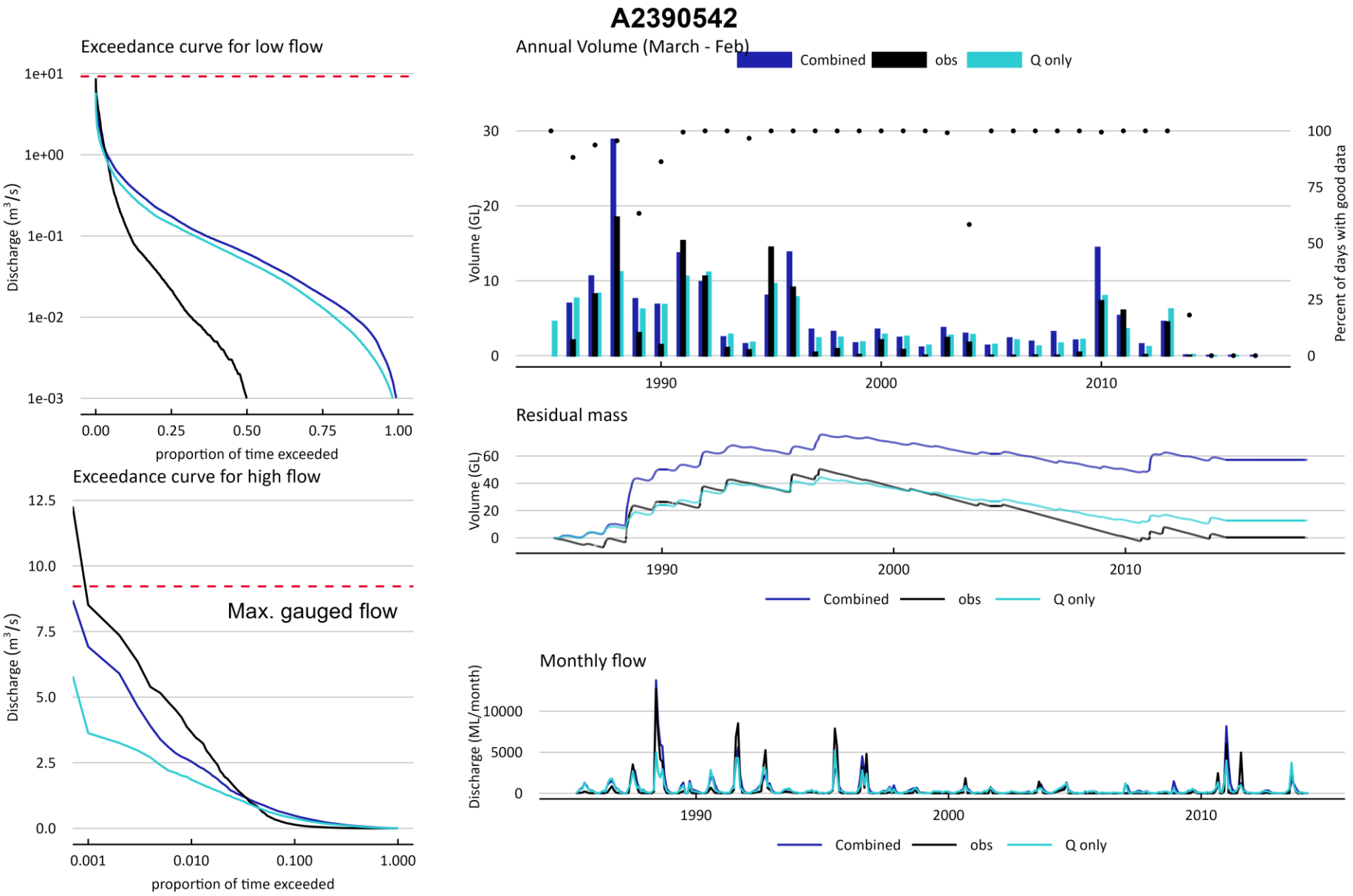

Figure C-7 Streamflow results for Naracoorte Creek at Naracoorte (A2390542). See Figure 3-5 for a description of the plots.

Appendix D – Final calibration model states results

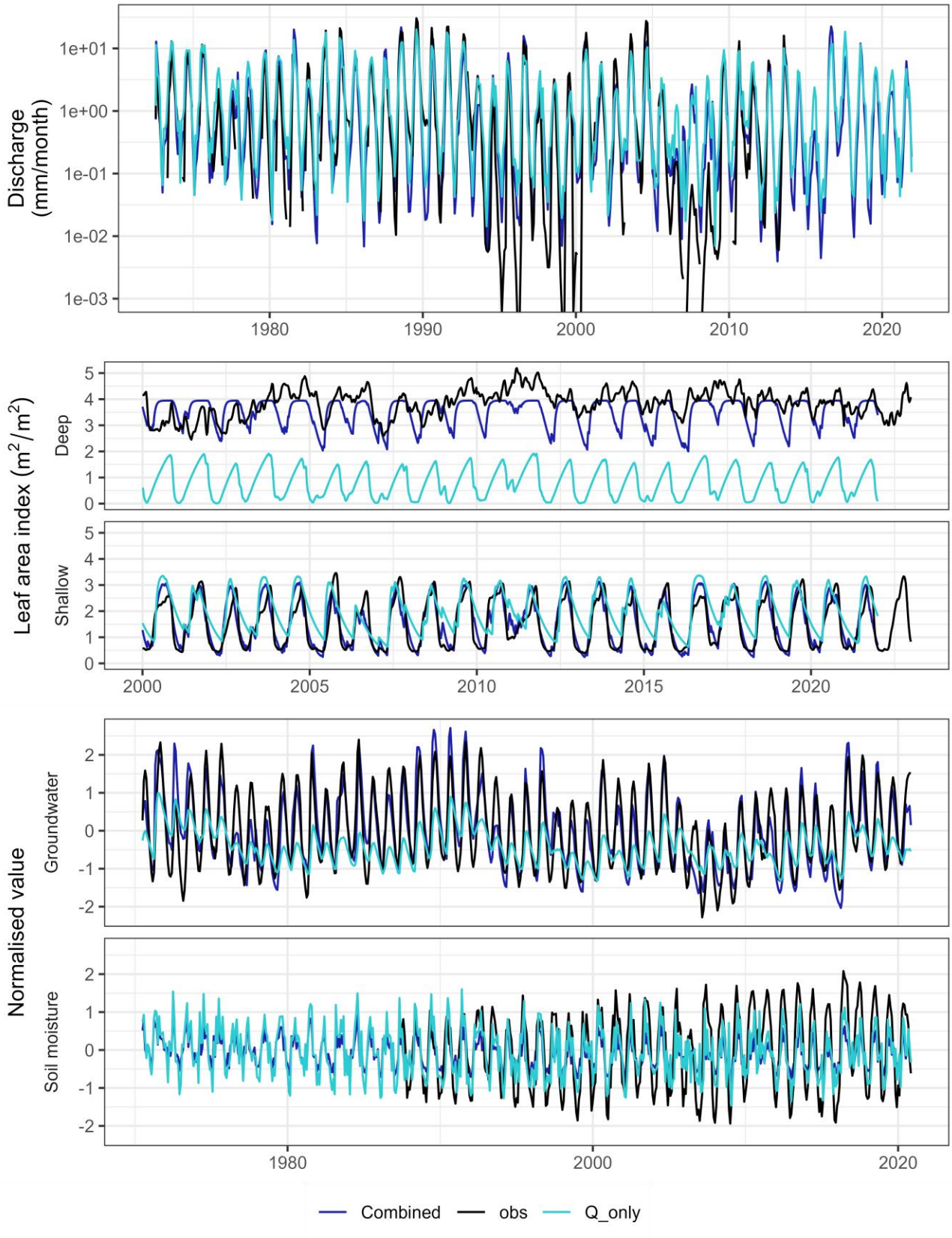

Figure D-1 Time series of streamflow and model states for Drain L upstream of the Princess Highway (A2390510). See Figure 3-6 for a description of the plots.

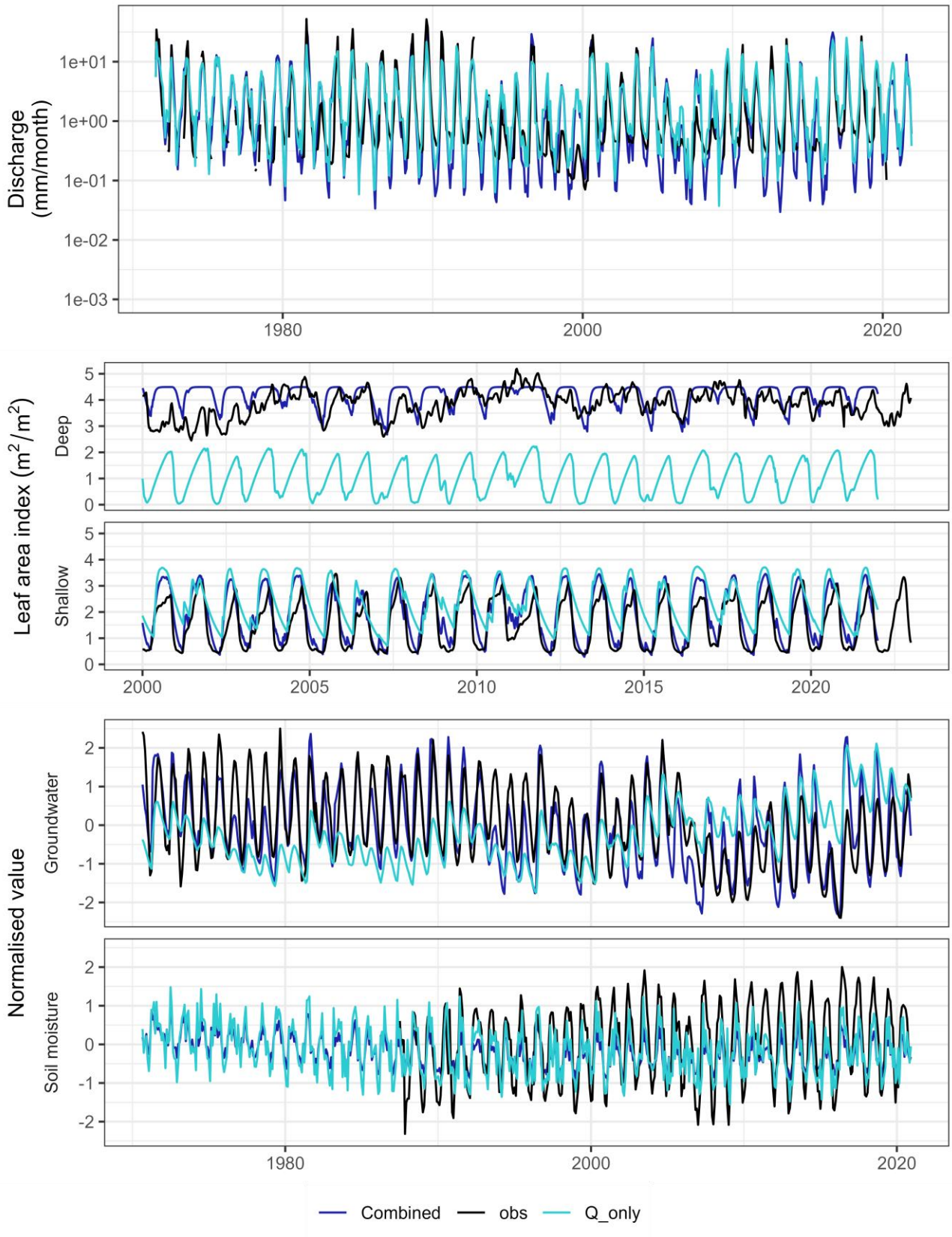

Figure D-2 Time series of streamflow and model states for Reedy Creek – Mount Hope drain (A2390513). See Figure 3-6 for a description of the plots

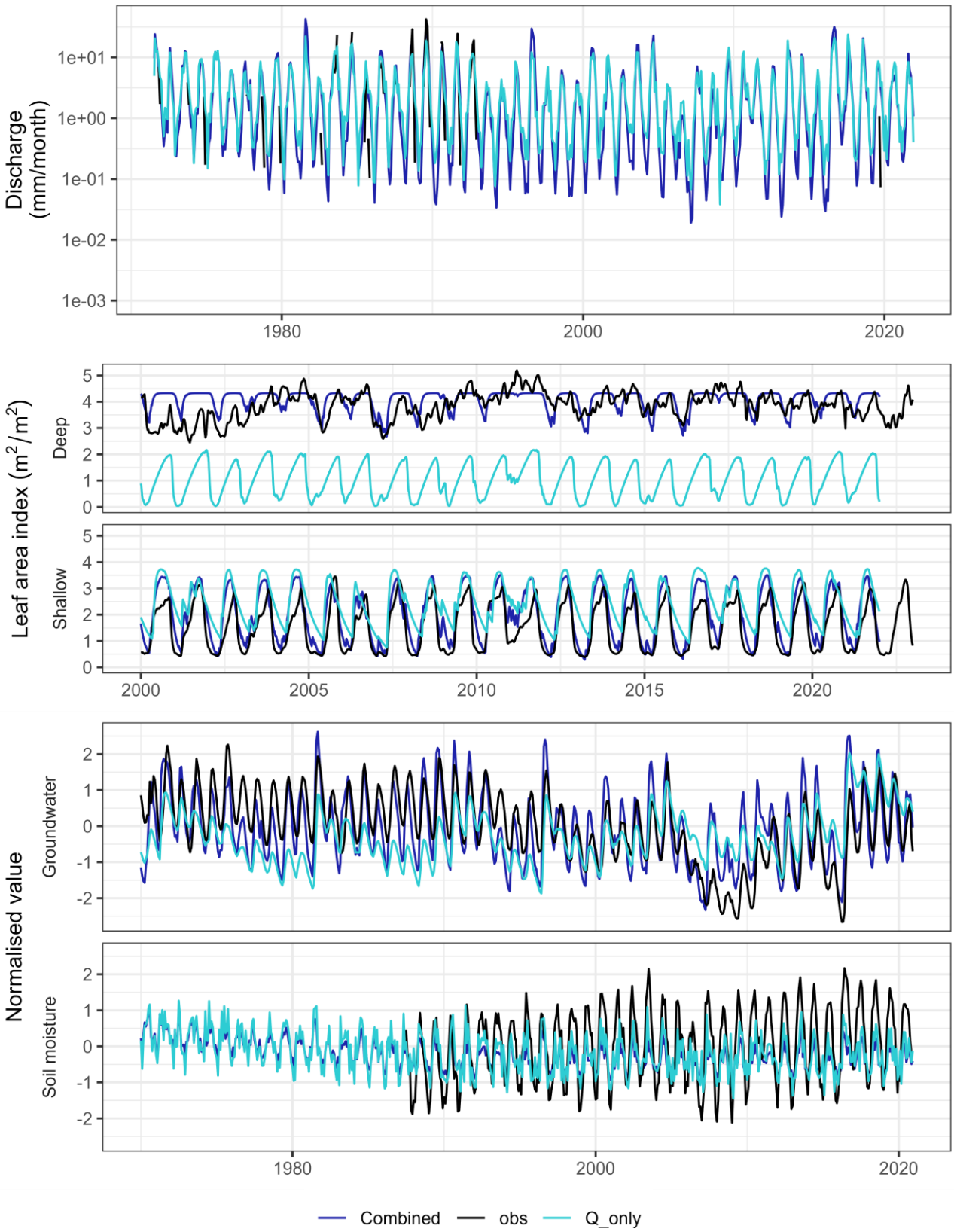

Figure D-3 Time series of streamflow and model states for the Bakers Range South Drain (A2390515). See Figure 3-6 for a description of the plots

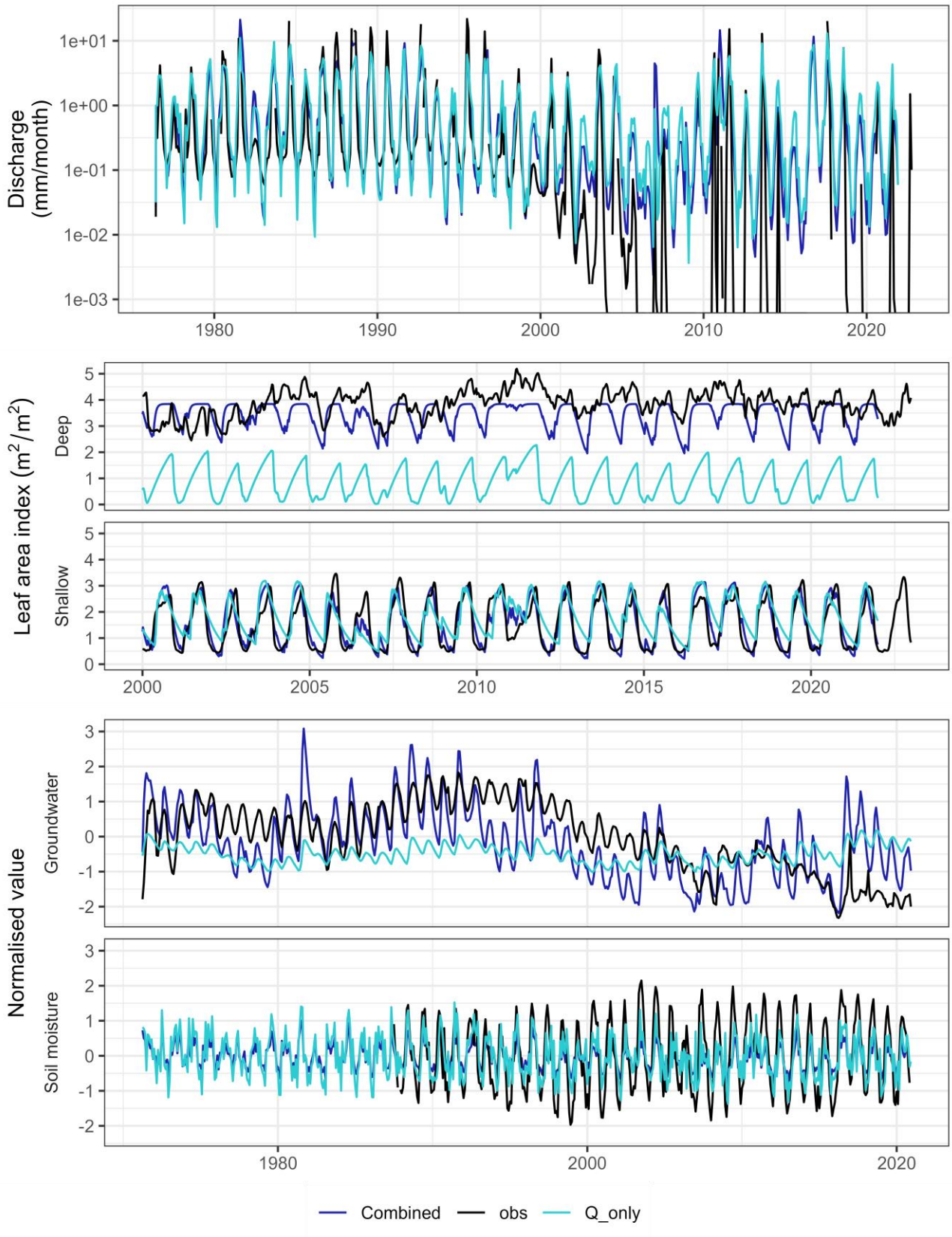

Figure D-4 Time series of streamflow and model states for Mosquito Creek at Struan (A2390519). See Figure 3-6 for a description of the plots

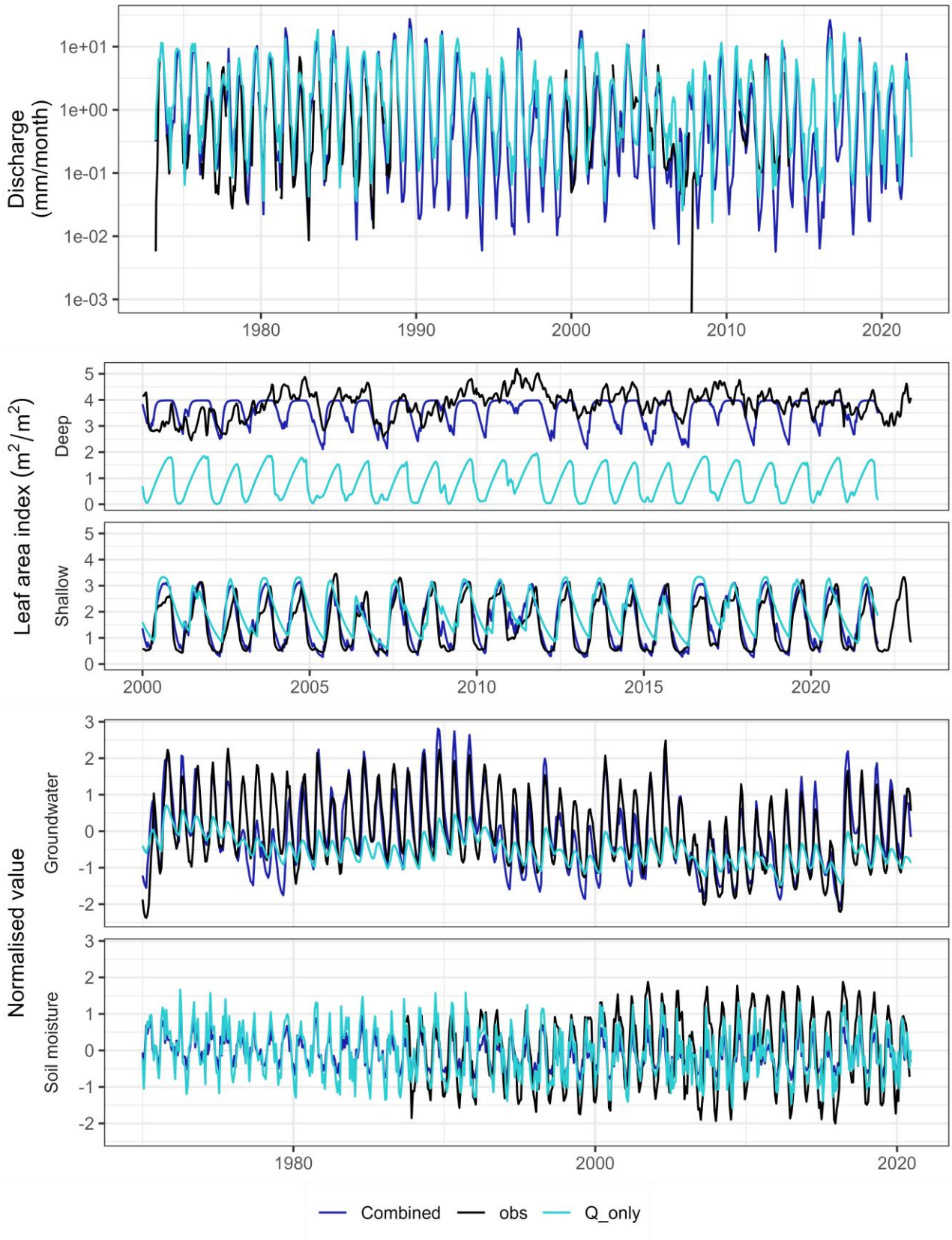

Figure D-5 Time series of streamflow and model states for Wilmot Drain at 9.2km From Drain L (A2390527). See Figure 3-6 for a description of the plots

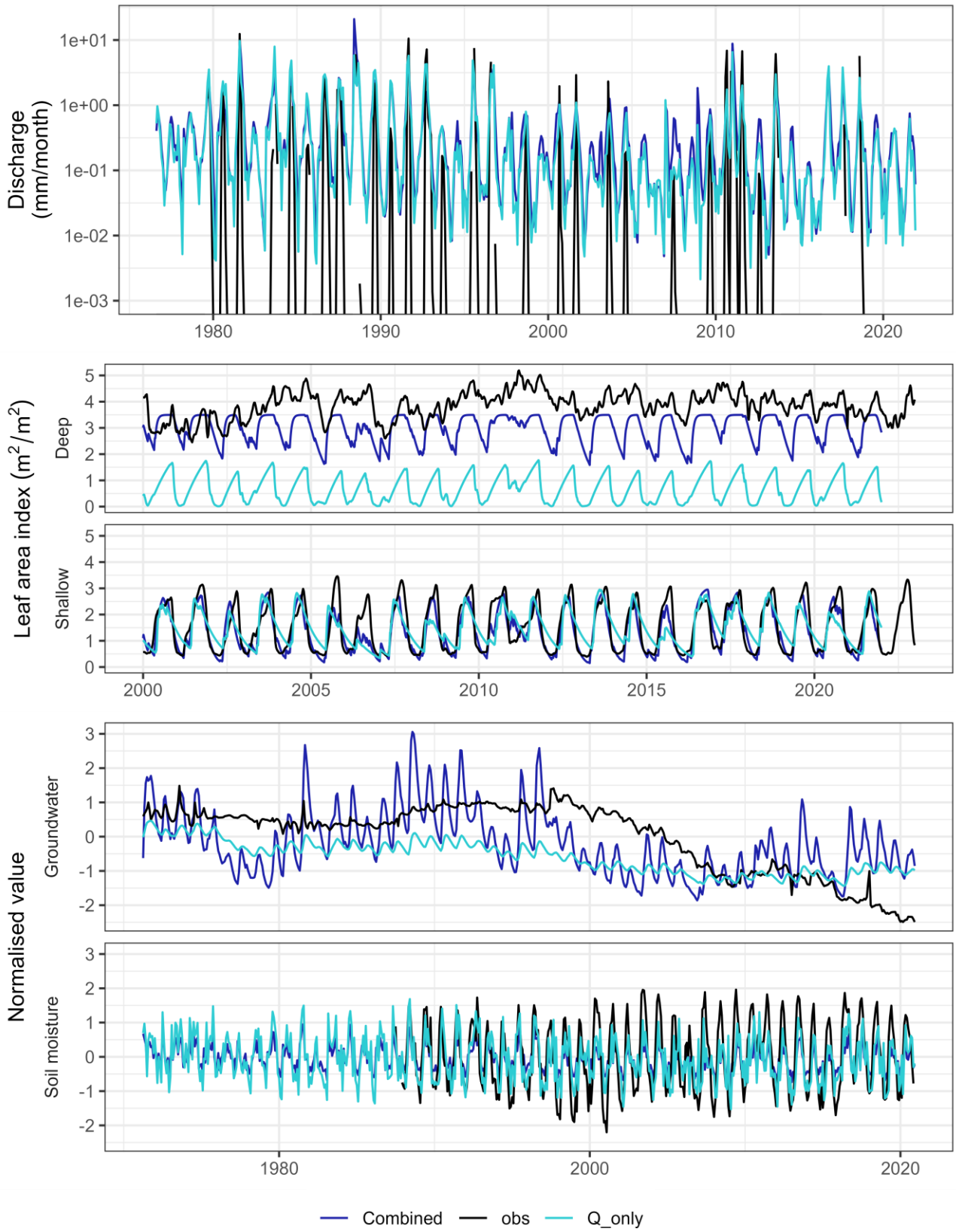

Figure D-6 Time series of streamflow and model states for Morambro Creek at Bordertown-Naracoorte Road Bridge (A2390531). See Figure 3-6 for a description of the plots

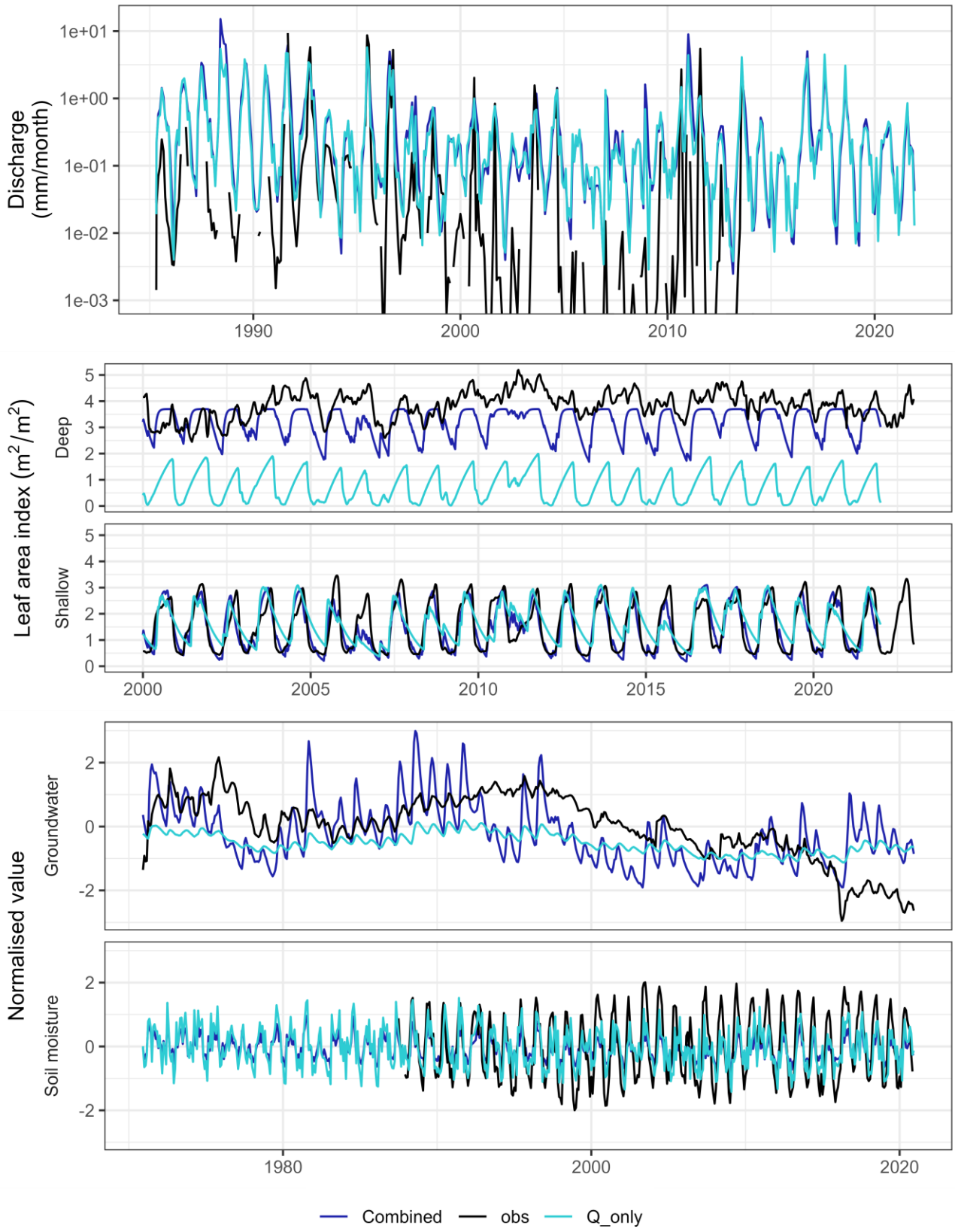

Figure D-7 Time series of streamflow and model states Naracoorte Creek at Naracoorte (A2390542). See Figure 3-6 for a description of the plots

Appendix E – Recharge trends by management zone

Zone	Groundwater data				Modelled			
	linear trend (mm/yr)	p value	Mann-Kendall statistic	p value	linear trend (mm/yr)	p value	Mann-Kendall statistic	p value
BANGHAM	-0.31	0.51	-0.14	0.37	-0.61	0.01	-0.25	0.01
BEEAMMA	0.18	0.71	0.04	0.79	-0.38	0.08	-0.17	0.09
BENARA	-0.80	0.02	-0.23	0.03	-0.06	0.61	-0.02	0.87
BLANCHE CENTRAL	-2.42	0.00	-0.40	0.00	-0.31	0.14	-0.08	0.42
BOOL	-0.70	0.18	-0.20	0.05	0.64	0.00	0.24	0.01
BOWAKA	0.32	0.24	0.12	0.27	-0.44	0.04	-0.20	0.04
BRAY	-0.40	0.17	-0.15	0.16	0.43	0.02	0.19	0.04
COLES	-1.33	0.01	-0.30	0.00	-0.43	0.03	-0.18	0.07
COMAUM	-1.51	0.00	-0.45	0.00	-0.53	0.02	-0.23	0.02
COMPTON	-0.81	0.08	-0.17	0.18	-0.05	0.80	0.01	0.95
CONMURRA	-0.09	0.77	-0.07	0.50	-0.42	0.01	-0.22	0.02
DONOVANS	0.15	0.56	0.13	0.23	-0.27	0.17	-0.13	0.17
DUFFIELD	0.25	0.18	0.17	0.13	-0.47	0.01	-0.21	0.03
FOX	-0.46	0.23	-0.14	0.17	-0.36	0.02	-0.18	0.06
FRANCES	-0.68	0.18	-0.28	0.06	-0.40	0.00	-0.31	0.00
GLEN ROY	-1.58	0.01	-0.27	0.01	-0.21	0.01	-0.30	0.00
GLENBURNIE	-0.41	0.04	-0.13	0.19	-0.54	0.06	-0.20	0.04
GREY	-1.63	0.00	-0.34	0.00	-0.11	0.53	-0.04	0.71
HACKS	-0.72	0.24	-0.13	0.21	-0.09	0.47	-0.08	0.39
HINDMARSH	-1.02	0.00	-0.30	0.00	-0.29	0.13	-0.11	0.27
HYNAM EAST	-0.91	0.03	-0.28	0.02	-0.65	0.01	-0.24	0.01
HYNAM WEST	-0.61	0.15	-0.17	0.13	-0.37	0.02	-0.20	0.03
JOANNA	-1.79	0.00	-0.35	0.00	-0.47	0.00	-0.29	0.00
JOYCE	-0.99	0.02	-0.27	0.01	-0.41	0.03	-0.19	0.05
KENNION	-1.03	0.04	-0.19	0.07	-0.32	0.03	-0.18	0.07
KILLANOOLA	-1.51	0.00	-0.31	0.00	-0.23	0.17	-0.15	0.12
KONGORONG	-0.05	0.87	0.02	0.85	-0.21	0.27	-0.06	0.53
LACEPEDE	-0.62	0.04	-0.20	0.06	-0.62	0.01	-0.24	0.01
LAKE GEORGE	-0.51	0.11	-0.15	0.16	0.34	0.00	0.33	0.00

Zone	Groundwater data				Modelled			
	linear trend (mm/yr)	p value	Mann-Kendall statistic	p value	linear trend (mm/yr)	p value	Mann-Kendall statistic	p value
LANDSEER	-0.54	0.00	-0.29	0.01	-0.22	0.28	-0.08	0.40
LOCHABER	-0.39	0.32	-0.15	0.14	-0.42	0.02	-0.19	0.05
MACDONNELL	-2.09	0.00	-0.36	0.00	-0.05	0.82	0.01	0.95
MANAGEMENT AREA 1	-1.04	0.01	-0.28	0.01	-0.35	0.03	-0.15	0.13
MANAGEMENT AREA 2A	-1.14	0.12	-0.23	0.11	-0.21	0.26	-0.06	0.56
MANAGEMENT AREA 2B	-0.73	0.02	-0.25	0.02	-0.45	0.02	-0.19	0.05
MANAGEMENT AREA 3	-0.90	0.01	-0.27	0.01	-0.31	0.02	-0.18	0.06
MANAGEMENT AREA 4	-0.54	0.09	-0.17	0.12	-0.44	0.04	-0.17	0.08
MARCOLLAT	-0.72	0.02	-0.26	0.01	-0.15	0.52	-0.05	0.63
MAYURRA	0.32	0.39	0.07	0.50	-0.11	0.49	-0.05	0.59
MINECROW	-0.78	0.01	-0.26	0.01	-0.32	0.05	-0.16	0.09
MONBULLA	-2.27	0.00	-0.32	0.00	-0.28	0.16	-0.12	0.23
MOORAK	-0.93	0.03	-0.31	0.04	-0.17	0.39	-0.07	0.48
MOUNT BENSON	-0.47	0.05	-0.31	0.01	-0.84	0.00	-0.33	0.00
MOUNT MUIRHEAD	-0.31	0.45	-0.07	0.49	-0.28	0.08	-0.14	0.13
MOYHALL	-0.97	0.05	-0.23	0.03	-0.20	0.22	-0.13	0.19
MURRABINNA	-0.78	0.00	-0.28	0.01	-0.48	0.01	-0.22	0.02
MYORA	-0.92	0.00	-0.32	0.00	-0.50	0.09	-0.16	0.10
ORMEROD	-0.92	0.12	-0.21	0.06	-0.21	0.16	-0.13	0.17
PEACOCK	-0.23	0.38	-0.11	0.30	-0.21	0.29	-0.09	0.38
RIDDOCH	0.57	0.33	0.09	0.40	-0.30	0.07	-0.15	0.11
RIVOLI BAY	-0.07	0.78	-0.04	0.69	-0.07	0.71	-0.04	0.71
ROSS	0.51	0.07	0.13	0.22	-0.11	0.59	-0.06	0.54
SHORT	-1.46	0.01	-0.26	0.01	-0.52	0.01	-0.19	0.05
SMITH	-0.80	0.02	-0.19	0.06	-0.33	0.01	-0.22	0.02
SPENCE	-0.89	0.05	-0.23	0.02	-0.33	0.09	-0.13	0.19
STEWARTS	-0.11	0.82	-0.05	0.65	-0.37	0.02	-0.23	0.02
STRUAN	-1.18	0.07	-0.23	0.04	-0.21	0.05	-0.21	0.03
SYMON	-0.53	0.17	-0.13	0.21	-0.45	0.00	-0.26	0.01
TOWNSEND	-0.15	0.68	-0.11	0.29	-0.49	0.01	-0.23	0.02
WATERHOUSE	-0.48	0.04	-0.21	0.05	0.63	0.00	0.26	0.01
WESTERN FLAT	Insufficient data				-0.579	0.004	-0.245	0.011
WOOLUMBOOL	-0.61	0.02	-0.26	0.01	-0.47	0.03	-0.18	0.06

Zone	Groundwater data				Modelled			
	linear trend (mm/yr)	p value	Mann-Kendall statistic	p value	linear trend (mm/yr)	p value	Mann-Kendall statistic	p value
YOUNG	-0.14	0.80	-0.03	0.76	-0.09	0.61	0.00	0.98
ZONE 2A	-1.08	0.00	-0.36	0.00	-0.53	0.08	-0.15	0.11
ZONE 3A	-1.19	0.01	-0.23	0.02	-0.54	0.01	-0.23	0.02
ZONE 5A	-0.01	0.99	-0.05	0.68	-0.46	0.00	-0.31	0.00

Appendix F – Water balance for each management zone

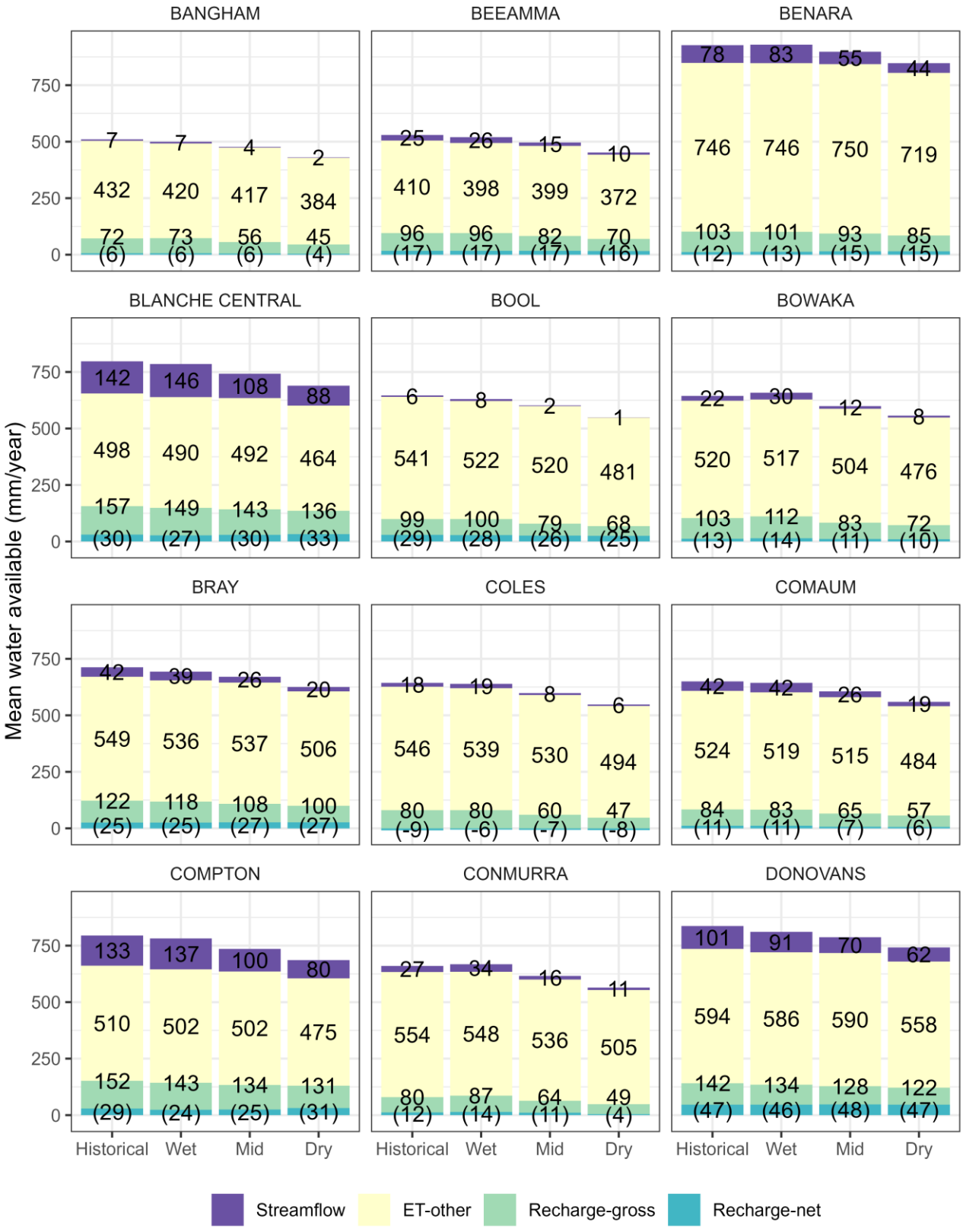

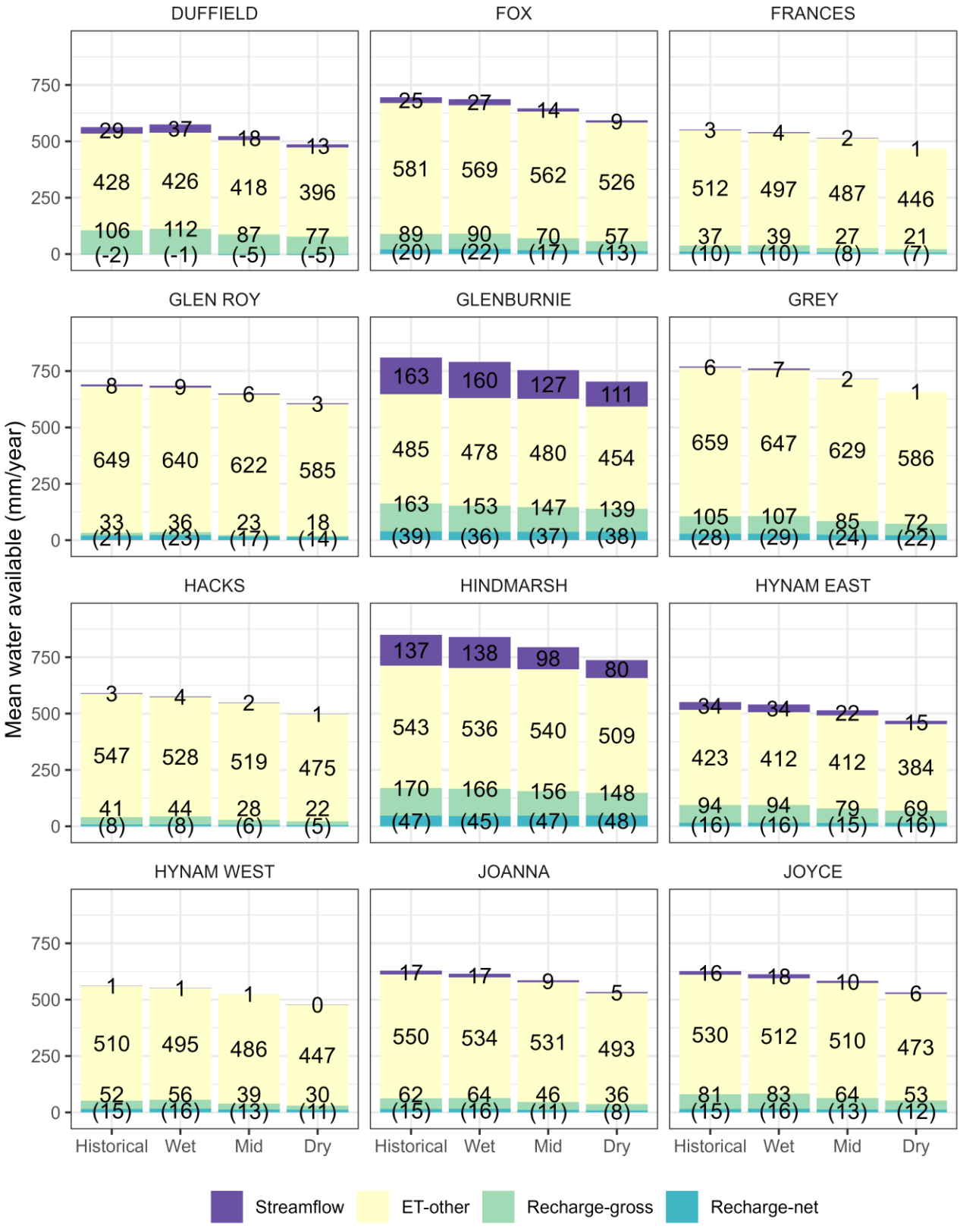
DUFFIELD
FOX
FRANCES
GLEN ROY
GLENBURNIE
GREY
HACKS
HINDMARSH
HYNAM EAST
HYNAM WEST
JOANNA
JOYCE
Mean water available (mm/year)
0
250
500
750
Historical
Wet
Mid
Dry
Streamflow
ET-other
Recharge-gross
Recharge-net

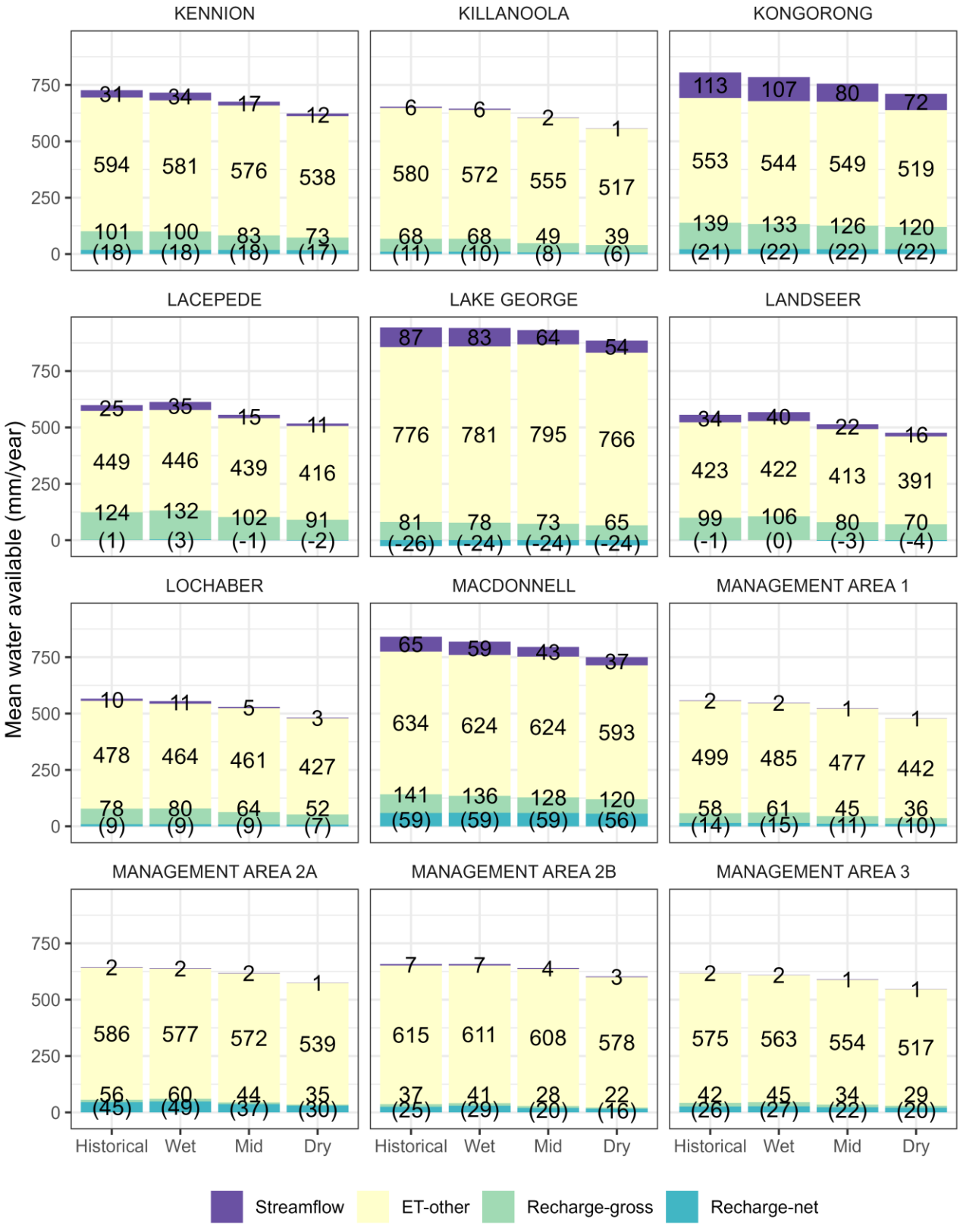
KENNION
KILLANOOLA
KONGORONG
LACEPEDE
LAKE GEORGE
LANDSEER
LOCHABER
MACDONNELL
MANAGEMENT AREA 1
MANAGEMENT AREA 2A
MANAGEMENT AREA 2B
MANAGEMENT AREA 3
Mean water available (mm/year)
0
250
500
750
Historical
Wet
Mid
Dry
Streamflow
ET-other
Recharge-gross
Recharge-net

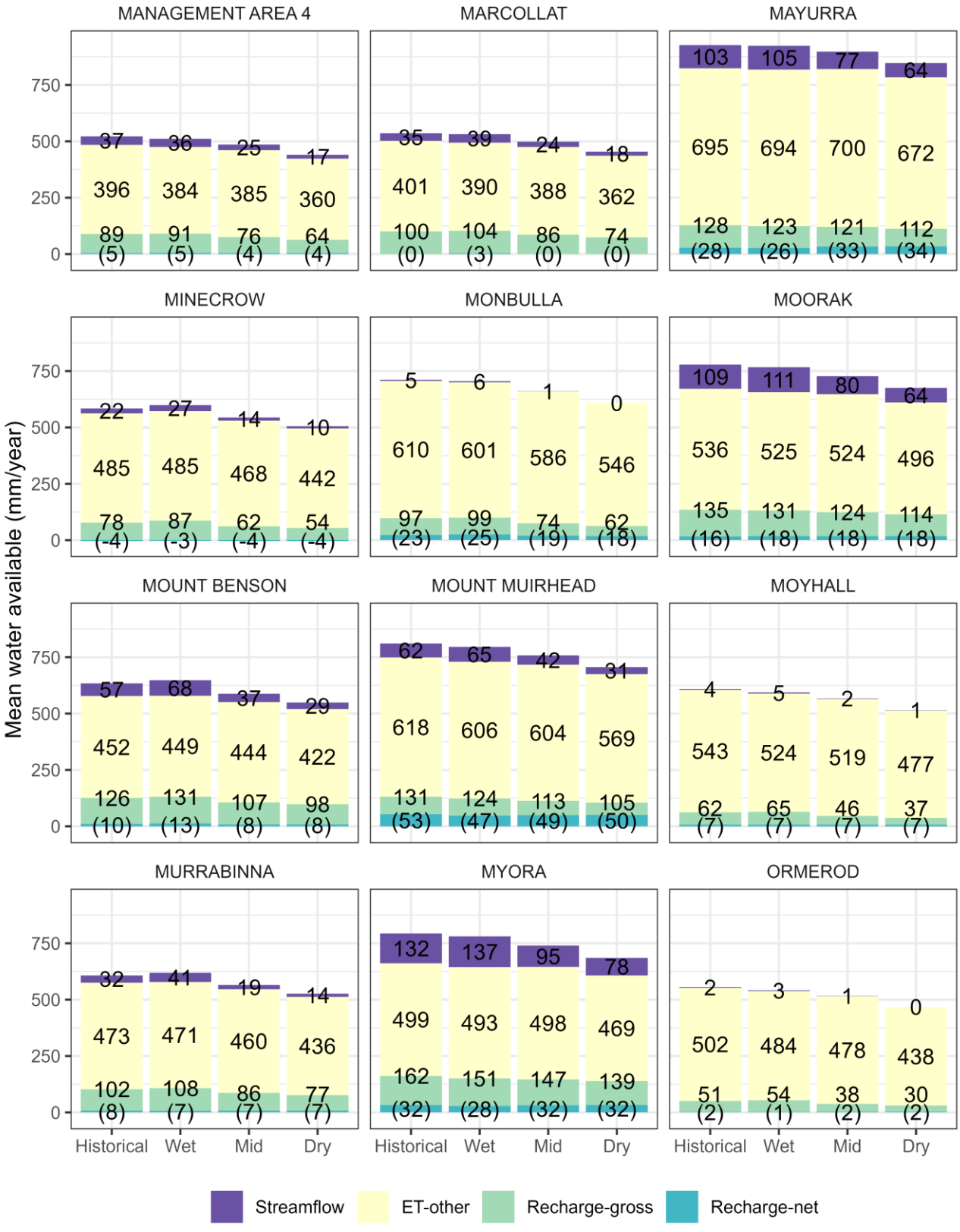
MANAGEMENT AREA 4
MARCOLLAT
MAYURRA
MINECROW
MONBULLA
MOORAK
MOUNT BENSON
MOUNT MUIRHEAD
MOYHALL
MURRABINNA
MYORA
ORMEROD
Mean water available (mm/year)
0
250
500
750
37 396 89 (5)
36 384 91 (5)
25 385 76 (4)
17 360 64 (4)
35 401 100 (0)
39 390 104 (3)
24 388 86 (0)
18 362 74 (0)
103 695 128 (28)
105 694 123 (26)
77 700 121 (33)
64 672 112 (34)
22 485 78 (-4)
27 485 87 (-3)
14 468 62 (-4)
10 442 54 (-4)
5 610 97 (23)
6 601 99 (25)
1 586 74 (19)
0 546 62 (18)
109 536 135 (16)
111 525 131 (18)
80 524 124 (18)
64 496 114 (18)
57 452 126 (10)
68 449 131 (13)
37 444 107 (8)
29 422 98 (8)
62 618 131 (53)
65 606 124 (47)
42 604 113 (49)
31 569 105 (50)
4 543 62 (7)
5 524 65 (7)
2 519 46 (7)
1 477 37 (7)
32 473 102 (8)
41 471 108 (7)
19 460 86 (7)
14 436 77 (7)
132 499 162 (32)
137 493 151 (28)
95 498 147 (32)
78 469 139 (32)
2 502 51 (2)
3 484 54 (1)
1 478 38 (2)
0 438 30 (2)
Historical
Wet
Mid
Dry
Streamflow
ET-other
Recharge-gross
Recharge-net

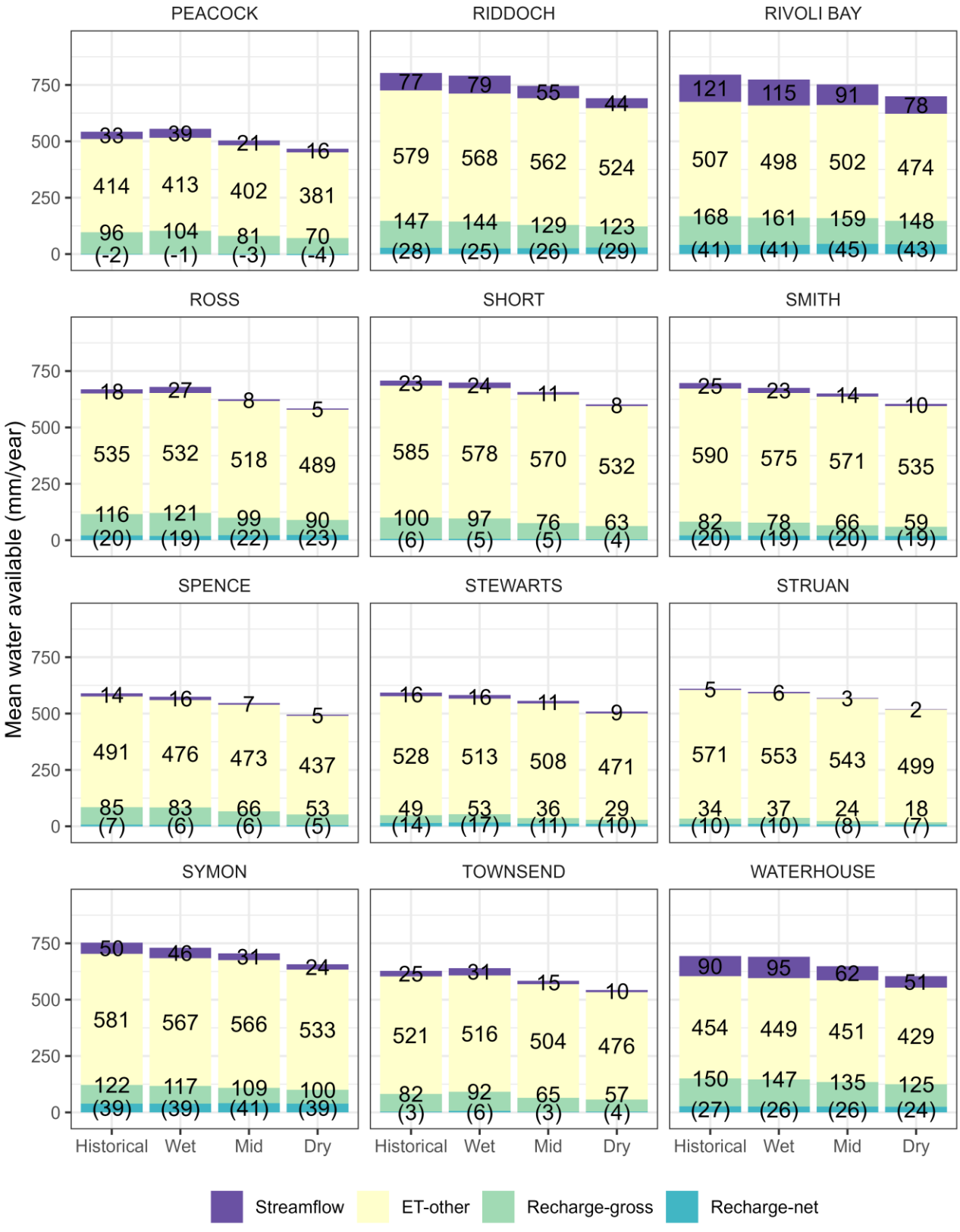
PEACOCK
RIDDOCH
RIVOLI BAY
ROSS
SHORT
SMITH
SPENCE
STEWARTS
STRUAN
SYMON
TOWNSEND
WATERHOUSE
Mean water available (mm/year)
0
250
500
750
Historical
Wet
Mid
Dry
Streamflow
ET-other
Recharge-gross
Recharge-net

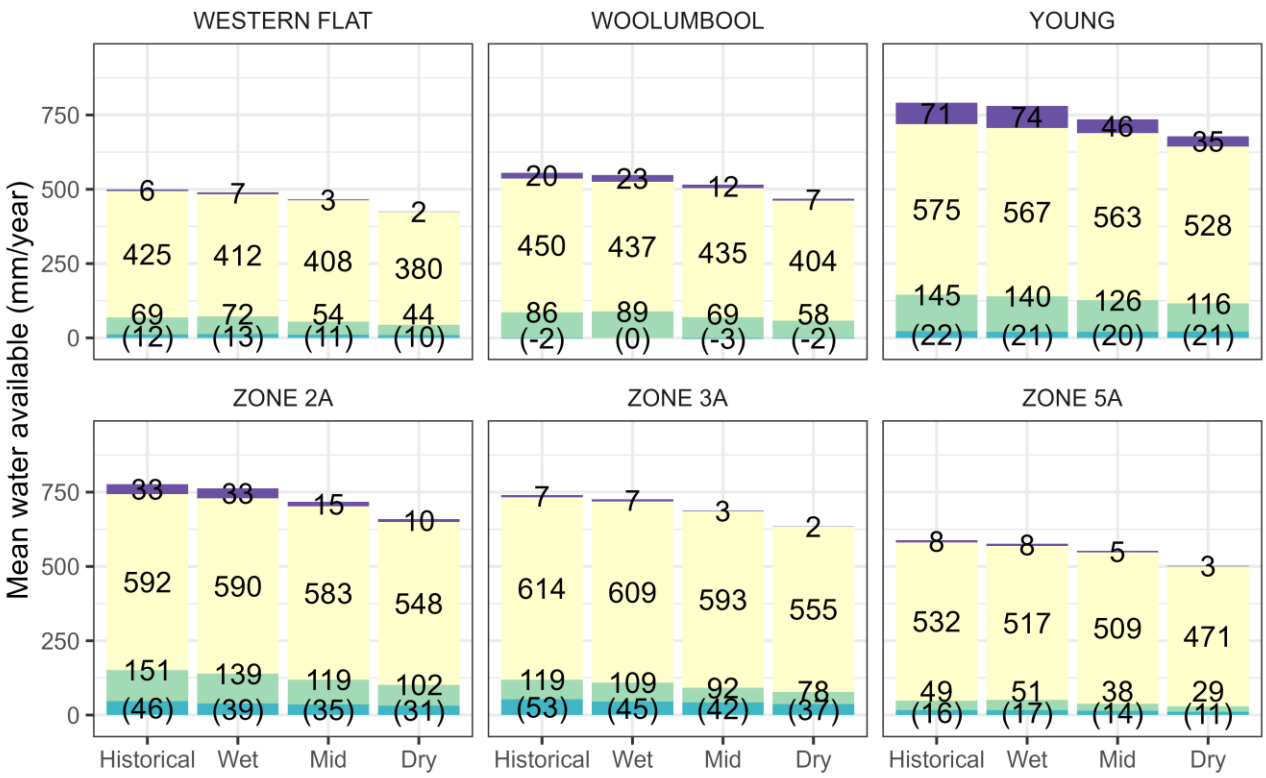
WESTERN FLAT
WOOLUMBOOL
YOUNG
ZONE 2A
ZONE 3A
ZONE 5A
Mean water available (mm/year)
750
500
250
0
6
425
69
(12)
7
412
72
(13)
3
408
54
(11)
2
380
44
(10)
20
450
86
(-2)
23
437
89
(0)
12
435
69
(-3)
7
404
58
(-2)
71
575
145
(22)
74
567
140
(21)
46
563
126
(20)
35
528
116
(21)
33
592
151
(46)
33
590
139
(39)
15
583
119
(35)
10
548
102
(31)
7
614
119
(53)
7
609
109
(45)
3
593
92
(42)
2
555
78
(37)
8
532
49
(16)
8
517
51
(17)
5
509
38
(14)
3
471
29
(11)
Historical
Wet
Mid
Dry
Streamflow
ET-other
Recharge-gross
Recharge-net

GOYDER INSTITUTE FOR WATER RESEARCH

Government of South Australia
Department for Environment and Water

CSIRO

Flinders University

THE UNIVERSITY of ADELAIDE

University of South Australia

The Goyder Institute for Water Research is a research alliance between the South Australian Government through the Department for Environment and Water, CSIRO, Flinders University, the University of Adelaide and the University of South Australia.